POLITECNICO DI MILANO

Facoltà di Ingegneria Industriale

Corso di Laurea in
Ingegneria Aeronautica

Refined finite element structural models for the vibro-acoustic response of plate-cavity systems

Relatore: Prof. Lorenzo Dozio
Co-Relatore: Prof. Erasmo Carrera

Tesi di Laurea di:
Luca ALIMONTI Matr. 712177

Anno Accademico 2009 - 2010

Ringraziamenti

Ringrazio il Prof. Gian Luca Ghiringhelli, il Prof. Alberto Guardone ed il Prof. Marco Morandini per avermi aiutato a risolvere alcuni problemi legati alla programmazione del codice a elementi finiti. In particolare un ringraziamento al Prof. Paolo Mantegazza per avermi aiutato nel momento piú difficile di questa attivitá.

Un ringraziamento sentito al Prof. Erasmo Carrera e a tutto il suo gruppo di lavoro. In particolare vorrei ringraziare Pietro Nali e Salvatore Brischetto per essere stati sempre disponibili e per avermi aiutato a comprendere la formulazione del Prof. Carrera.

Contents

List of Figures

List of Tables

Abstract

At present, numerical modeling techniques for coupled plate-cavity systems in the low-frequency range are based on deterministic approaches. The plate structure is often modeled by the finite element method and the Kirchhoff-Love or Mindlin 2-D theories are almost always assumed to describe the through-the-thickness variation of the displacement field. The simple assumptions of these plate models clearly reduce the computational effort, but can also introduce significant errors in the prediction of the dynamic response. When the analysis of a vibro-acoustic system is extended in the mid-frequency range, the contribution of the higher order modes becomes important. The characteristic wavelength of these structural modes become comparable with the plate thickness and the kinematic hypothesis of Kirchhoff-Love or Mindlin models are no more valid. Moreover, multilayered composite plate solutions has incresed rapidly over the past three decades, then the modeling of these plate structures is an important aspect. However, more accurate 2-D plate theories must be accounted to correctly reproduce the complicated effects arising in these complex structure.

The objective of the present work is the development of a refined Finite Element model for composite piezoelectric plates coupled with enclosed acoustic cavities. In the framework of the axiomatic 2-D theories, the piezo-elastic structure is described according to the Carrera's Unified Formulation. The powerful notation of this unified approach permits to obtain a wide class of refined 2-D plate theories with a unique formulation, providing an optimal tool to arbitrarily describe the complicated effects due to complex plate layouts and higher frequency ranges. The resulting structural finite element model is coupled with a standard pressure-based finite element formulation of the acoustic field. Numerical results obtained with the modal coupling reduction technique are presented for the case of plate backed by an air filled cavity. Different plate layouts, like as laminated, sandwich and piezo-embedded plates, are considered, demonstrating that a large variety of complex plate structures can be accomplished within a unified finite element formulation.

Keywords: vibroacoustic, finite element, higher order theories, multilayer composite plates, modal reduction techniques

Sommario

Le tecniche numeriche utilizzate al giorno d'oggi per la modellazione di sistemi vibroacustici costituiti da pannelli strutturali in contatto con cavitá acustiche sono principalmente ti tipo deterministico. Tra queste, l'approssimazione numerica piú utilizzata é certamente quella degli elementi finiti, la quale diventa peró inefficiente dal punto di vista computazionale quando si cerca di estendere il campo di frequenze di interesse. Infatti, in tal caso, dovrebbe essere utilizzato un numero eccessivo di elementi per ottenere il grado di accuratezza desiderato, portanto a dover risolvere un numero di equazioni troppo elevato anche per la risorse computazionali di oggi. Di conseguenza, gran parte della ricerca vibroacustica é orientata a colmare il piú possibile questa problematica che affligge i metodi deterministici come gli elementi

finiti, estendendo cosí il campo di applicazione di tali tecniche fino al cosí detto *mid-frequency range*. In effetti, in questo campo di frequenze, gli approcci energetici e statistici non sono ancora del tutto applicabili, dunque c'é grande necessitá di migliorare l'efficienza di tecniche deterministiche come quella degli elementi finiti. In questo quadro, bisogna tenere conto del fatto che estendendo il campo di frequenze trattabili da un modello a elementi finiti, possono nascere nuove problematiche legate al modello strutturale utilizzato per modellare i pannelli. Infatti, al crescere della frequenza, la lunghezza d'onda caratteristica delle componenti modali che partecipano alla risposta diminuisce, diventando confrontabile con le dimensioni della sezione del pannello. In questa situazione, modelli bidimensionali di piastra come quello di Kirchhoff-Love o Mindlin possono essere una semplificazione eccessiva, benché il loro utilizzo in diversi campi dell'ingegneria sia ormai affermato grazie all'elevato rapporto tra grado di accuratezza e onere computazionale. In effetti, quando devono essere risolti contributi ad alta frequanza, le ipotesi di queste teorie possono iniziare a vacillare e termini di ordine superiori devono essere considerati nell'approssimazione della cinematica della piastra lungo lo spessore della stessa. Inoltre l'avvento nelle industrie aeronautiche e automobilistiche di strutture composite multistarto richiede un ulteriore sforzo di modellazione. Infatti, pannelli con un elevato rapporto di ortotropia nel piano e in direzione trasversale, come nel caso di piastre multistrato e compositi tipo *sandwich*, richiedono spesso modelli strutturali piú raffinati per poter ottenere risultati numerici soddisfacenti.

L'obiettivo di questo lavoro é quello di sviluppare un modello raffinato a elementi finiti per piastre composite con comportamento piezoelettrico in contatto con cavitá acustiche. Il modello struttuarale considerato é quello della formulazione unificata proposta dal Prof. Carrera, la quale permette di ottenere una vasta gamma di teorie di piastra bidimensionali partendo da un'unica formulazione. Questo strumento puó dunque rilevarsi un importante vantaggio, potendo passare da modelli di piastra semplici a modelli piú raffinati a seconda del caso in esame. In particolare, in questo modo sará possibile trattare con un unica formulazione diverse tipologie di piastre, a partire da semplici pannelli isotropi arrivando a complesse strutture multistrato, e diversi *range* di frequenze. Il modello a elementi finiti della cavitá é invece basato sulla formulazione in pressione dell'acustica. Il modello accoppiato cosí ottenuto porta ad un sistema risolutivo non simmetrico. La soluzione é ottenuta proiettando il problema di partenza su una base formata da modi strutturali e modi acustici disaccoppiati. Questa tecnica, detta *modal coupling*, permette di ottenere buone prestazioni in termini di costo computazionale, in quanto il calcolo delle basi disaccoppiate richiede la soluzione di due problemi simmetrici e pochi modi sono sufficienti per ottenere soluzioni accurate. Purtroppo questa si rivela una tecnica efficiente solo per problemi debolmente accoppiati, i quali, tuttavia, sono i casi considerati in questo lavoro. Alcuni esempi numerici verranno presentati per mostrare come la formulazione unificata qui presentata permetta di modellare sistemi pannello-cavitá anche quando il sistema struttarale é costituito da complesse piastre composite e la forzante agisce a frequenze elevate.

Parole chiave: vibroacustica, elementi finiti, teorie di piastra di ordine elevato, piastre multistrato, riduzione modale

Introduction

Background

Whenever an elastic solid is in contact with a fluid, the structural vibrations and the acoustic pressure field in the fluid are influenced by the vibro-acoustic coupling interaction: the force loading on the structure, caused by the acoustic pressure along the fluid-structure interface, influences the structural vibrations, while at the same time the acoustic pressure field in the fluid is affected by the structural vibrations. In particular, in this work the interaction between a plate-like structure and an enclosed fluid filled cavity is considered. This problem is very important from an engineering and customer satisfaction point of view and represent a significant issue in automobile and aerospace design, where passengers comfort is an important feature. Over the last thirty years, a large amount of work has been published addressing the vibratory characteristic of structure-cavity systems and, thanks to this reaserch, the problems connected to the prediction of noise is well known. The typical vibro-acoustic behavior can be classified into three problem classes, depending on the excitation frequency. However, it is difficult to find a single prediction technique which can be applied to all the three frequency ranges.

Low-frequency range is defined as the frequency region where all the system components are small compared to the wavelength. Finite Element (FE) [5, 53] and Boundary Element (BE) [32] methods or mixed approaches (FE/BE models [46]) are tipically used for computing the system response over this range. Thanks to the long wavelength shown by structural and acoustic subsystems, low order polynomials can be selected as shape functions on the model elements providing good accuracy and efficiency. However, as the excitation frequency increases, it can be observed that the response becomes increasingly sensitive to minor structural modification, such as material properties or boundary conditions. Such a behavior is associated with the shorter structural wavelengths, resulting in high complex mode shapes. In order to adequately capture the dynamic behavior over this range, a large number of elements and an accurate structural model must be adopted. However, the use of such a deterministic approach often becomes questionable due to the large computational time required to solve the discretized coupled equations.

At very high frequencies, energy based methods have been developed. One of the most famous energy method is the Statistical Energy Analysis (SEA) [47], which describes the response of the entire system in terms of space and time averaged energy contained in each subsystem. This method requires at least two important parameters, namely the Coupling Loss Factor (CLFs), which describes the energy transfer between diffrent subsystems, and Damping Loss Factors (DLFs), which describes the energy loss and their interaction between different subsystems. The computation of these parameters is an important feature for this class of methods and experimental analysis or deterministic FE calculations must be accomplished for their accurate determination.

In mid-frequency range, none of the above mentioned techniques has been found to be adequate enough to predict the response accurately and efficiently. The use of deterministic approaches like FE method are theoretically feasible, but the computational time required to solve the coupled system of equations prohibits its use in most pratical applications. Indeed, often re-running of the deterministic models can be required, especially when optimization algorithms are used. To avoid the lack of accuracy in this frequency range, a hybrid FE-SEA method [66] has been developed. New energy based methods have been also taken in consideration for the mid/high-frequency range. In these methods the FE approach is applied on the governing differential equation in terms of averaged energy density, capturing the global response of the vibro-acoustic system with less element compared to a conventional FE analysis. Such methods are often called Energy Finite Element (EFE) methods [9].

In general, summarizing the above mentioned prediction problems in vibro-acoustic coupled analysis, the following qualitative definitions hold:

- In the low-frequency range the response spectra exhibit strong modal behavior, and a deterministic approach can lead to satisfactory results.

- In the mid-frequency range the response spectra exhibits high irregularity and single modal contributions are no more observable, due to the growing modal density and damping effect. Boundary conditions, material properties and geometry play an important role, indicating that an accurate description of the system must be accomplished.

- In the high-frequency range the response spectra are smooth, indicating very high modal density and damping effect. In this range, a detailed model description is no longer important and average techniques can give satisfactory results.

It is remarked here that a specific characterization of these frequency ranges in terms of Hz is difficult to be established because of the strong dependance from the problem type.

Once the response is computed, noise reduction strategies such as active control or passive damping can be employed to modify the system response for enhancing vibration absorption characteristics over a prescribed range of frequencies. In particular, piezoelectric inserts may be used as embedded sensors or actuators and connected to a control device. Passive piezoelectric damping [70], contrary to active control techniques, is achieved with a passive electrical network, that is directly connected to the electrodes of the piezoelectric device. With this approach the sensing element is not needed and the use of a passive network guarantees the stability of the coupled system. The control effectiveness associated with passive strategies is normally characterized by a narrowband effect, but a broadband control action can be obtained with periodic array of shunted piezoelectric patches [22]. For these reasons the modeling of piezoelectric structure is an important feature and it has been taken into account in this work.

Deterministic techniques in vibro-acoustic modeling

At this time, the main numerical prediction methods for vibro-acoustic analysis in the low/mid-frequency range are based on deterministic approaches. In particular, FE models, BE models and mixed FE/BE models are widely used. In these techniques, the continuum domain is decomposed into small elements, where the field variables are approximated by simple shape functions. As a result a substantial amount of elements must be used in order to ensure a good accuracy since a fixed number of elements per wavelenght are required to keep the prediction error within acceptable limits. Then, for low order approximating functions, which are often an efficient choice from a numerical point of view, the mesh density must be increased as the frequency increases, in order to take into account the contribution of shorter wavelenghts. The approximated model can thus become quite large, and memory and computing time limitations arise. This is a general characteristic of the most used deterministic models, and these limitations are still valid for coupled systems as well for simpler uncoupled problems. However, the looking for a compromise between accuracy level and computational effort is more important for coupled vibro-acoustic system than for uncoupled structural or acoustic problems. This is mainly due to the following considerations; first of all, the coupled system is larger than the uncoupled ones, because the structural and fluid system must be solved simultaneusly; secondly, the numerical solution procedure for coupled system can be less efficient since the coupled models can lead to unsymmetric matrices; finally, the efficiency of the modal reduction techniques is reduced for coupled system, since the modes extraction procedure is very time consuming for large and unsymmetric problem. In this framework, some solutions have been proposed in order to alleviate the computational burden, as briefly explained in the following points (see [25] for details).

- A possible choice to reduce the model size is considering a boundary formulation rather than modeling the entire continuum. However a brief comparison between BE, FE and FE/BE models partially contradicts this statement. The FE method is the most common prediction technique for solving engineering problems. Considering a weighted residual formulation or a variational approach, the governing partial differential equations are transformed into a set of algebraic equations introducing a suitable approximation of the unknowns. Therefore the continuum domain is discretized into a number of small subdomains (i.e. elements), and nodes are defined at some particular portion on each element. A local polynomial approximation of the field variables is defined on each element, and the use of Lagrangian functions permits to associate the discrete unknowns with nodal values of the approximated solution. On the other hand, BE methods are based on the direct or indirect boundary integral formulation of the considered problem. These formulations relate the distributions of the field variables in the continuum domain to the distribution of some problem related boundary variables on the boundary surface of the domain. Then, the boundary problem is transformed into a collocation or variational formulation and the boundary surface and variables are approximated by a set of shape functions, which are again locally defined. Mixed FE/BE methods employ a FE approximation of the structural subsystem and a BE description of the acoustic field. Even if mixed FE/BE methods can lead to relatively smaller model size, the computational effort required for assembly the final problem can be quite large, since the matrices in acoustic BE models are fully populated, complex, frequency dependent and, for direct methods, unsymmetric. Moreover, singular integrals must be evaluated. On the contrary, FE matrices are always symmetric, sparse, real and frequency indipendent, even if the final system can be quite larger. As a result, when comparing the total computational loads of both methods, the BE method can hardly compete with the FE method for interior acoustic problem. Therfore the FE method is usually preferred to study acoustic fields in arbitrarily complex enclosures.

- The structural FE formulation is naturally based on the displacement field as independent variable. In fluid there exist multiple choices of independent variable, e.g. fluid displacement or different scalar field such as pressure, velocity potential or displacement potential and combination of thereof. The use of fluid displacement field needs special attention to assure that the irrotational displacement field is mainteined [50]. The main advantage of this formulation is that the final system is symmetric. The disadvantage, compared to a scalar field description, is the introduction of three nodal unknowns for a 3D acoustic field, which can lead to a larger problem. On the other hand, scalar field can be used in various ways with different matrix block structures, although they all describe the same physical problem. They all automatically enforce the irrotationality of fluid motions. However, the discretized differential coupled equations yield unsymmetrical system matrices. The solution for this lack of symmetry has been given a lot of attention. The standard procedure has been to combine, in various way, the pressure and fluid displacement potential, thus achieving symmetric systems [33, 53]; in this way, more efficent solvers can be used for solving the coupled problem. On the other hand, the problem size is almost doubled. It is also possible to condense statically the two-field fluid formulations, thus producing a one-field symmetric formulation as reported in [59] and [27]. The drawback is that the resulting system yield full matrices. Another intresting symmetrization method is presented in [12]. However, at present, the most used field variables are the structual displacement and fluid pressure, which lead to the unsymmetric (u, p) formulation.

- When FE discretization of the coupled system is accomplished, very large problems are typically obtained. In order to reduce the computational effort, reduction techniqes can be adopted. In the classical modal expansion technique, the dynamic field variables are expanded in terms of the natural modes of the system. In general a relatively small truncated set of modes yields already a level of accuracy close to that of the much larger original model. In this framework, a rule of thumb states that a satisfactory prediction of the correct dynamic behavior over a certain frequency range is obtained using the modes with natural frequencies smaller than twice the upper frequency limit of the considered range. However, the application of such a technique for coupled vibro-acoustic system suffers from severe problems. Indeed, the extraction of the modes from coupled FE model is much more time consuming than from an uncoupled structural or acoustic system. Unsymmetric eigenvalue solvers, needed for the solution of the eigenvalue problem for a (u, p) formulation, have small computational efficiency with respect to the symmetric solvers. In order to alleviate the high computational resources and memory requirements, the uncoupled modal approach can be considered. In this approach a reduced basis is obtained from the uncoupled structural and acoustic modes. The uncoupled structural modes are the modes of the elastic structure without fluid pressure loading at fluid-structure interface, whereas the uncoupled acoustic modes are the cavity modes with rigid wall boundary conditions at the fluid-structure interface. Since the uncoupled modes result from symmetric problems, the computational effort for constructing the new truncated basis is much smaller than for the set of coupled modes. The efficiency of the uncoupled modal approach can be, however, significantly smaller than the efficiency of the coupled basis. This is mainly due to the inefficent way in which the displacement continuity at fluid-structure interface is approximated by the uncoupled modes. Since the uncoupled acoustic modes are calculated with rigid walled boundary conditions, the fluid displacement at fluid-structure interface is zero for each mode. In this way, any combination of the uncoupled acoustic modes violates the continuity conditions, thus to obtain an accurate local description of the fluid-structure interface a lot of high order acoustic modes must be taken into account. Consequently, the benefits of a computationally efficient truncated modal basis can be partially lost. However, it has been demonstrated [49, 68, 73] that the uncoupled modal synthesis can be successfully applied. This is particularly true in the case of weak coupled systems, where the coupling between structural and acoustic field can be partially omitted, obtaining a one-way interaction from the excited subsystem towards the other one [26, 31]. More questionable is the application of the uncoupled modal reduction technique for strong coupled systems, where the mutual interaction is no longer negligible. Despite of these difficulties, the application of some corrections to the uncoupled modal analysis formulation can lead to optimal results even in the case of strong coupled system [73]. In the last years, non modal reduction techinques have been also considered. In these methods, the reduced basis is not obtained by solving an eigenvalue problem but it is extracted using a deflation algorithm (e.g. Krylov or Lanczos iterations). The resulting orthogonal basis seems to efficiently reduce the size of both weak and strong coupled systems providing accurate solutions [36, 58].

- Finally, in order to reduce the high density mesh requirements of FE models, the developement of novels deterministic techniques with enhanced convergence rate and computational efficiency compared with the classical FE approach have been developed. Meshless techniques and spectral method may be a possible solution for shifting the pratical frequency limitation towoards the mid-frquency range. In particular the Wave Based (WB) [26] method seems to give accurate and efficient results, mainly when an hybrid approach FE/WB [34] is considered for the structural and acoustic field, respectively.

Structural model aspects

In the previous section the main challenges of the vibro-acoustic modeling have been briefly discussed. However, none has been said about the adopted structural models. At present, for what concern the coupled analysis of plate-cavity systems, which is the main problem studied in this work, simple 2-D structural theories are often used to model the kinematic behavior of the plate subsystem. Indeed Kirchhoff-Love theory (Classical Plate Theory, CPT) and Mindlin's First order Shear Deformation Theory (FSDT) are the most used models in FE analysis of plates coupled with acoustic domains. However, when the excitation frequency increases, the contribution of the shorter wavelenghts can introduce some higher order mechanisms in the plate behavior which cannot be captured by simple plate models. Moreover, the application of composite materials in aerospace and automotive vehicles has increased rapidly over the past three decades due to their high strength and low weight. Plates made of composite materials offer many advantages with respect to the metallic ones. However, a number of complicating effects arise in their modeling. In particular, the interlaminar continuity conditions and the account for higher order effects for the through-the-thickness description of displacement and stress fields are important features for these structure. Therefore, it is important to consider an accurate description of the structural behavior using an appropriate plate model, especially when the response of vibro-acoustic systems over the mid-frequency range is of interest. It is argued that this can be considered an important issue in the mid-frequency range. From this point of view, the following points, which summarized the crucial structural aspects, can be given in addition to the points outlined in the previous section.

- The most important feature which characterizes composite plates is the C_z^0 conditions [19]. Indeed, multilayerd structures can exhibit different mechanical properties in the thickness direction. For this reason, layered structure are also called transversely anisotropic. Transverse discontinous mechanical properties cause the displacement field in the thickness direction to exhibit a rapid change of the local slope at each layer interfaces. This zig-zag effect holds for the transverse stress (i.e. stress components lie on the normal plane), which must be continuous for equilibrium reasons. It is clear that the displacement and stress fields are C^0 in thickness direction. The fulfillment of these C_z^0

requirements is a crucial point in the modeling of composite structure, mainly when highly transversely anisotropic plates, like sandwich structures, are considered. When a displacement based FE structural model is used, i.e. obtained from the Principle of Virtual Displacement (PVD), only a Layer Wise (LW) description of the field variables, which provides a local description for each layer, can fulfill the displacement continuity condition. However, this condition cannot be satisfied by an Equivalent Single Layer (ESL) approach, since a global description of the multilayered plate is considered. Moreover, only considering an *a priori* modeling of the normal stress components via Reissner's Mixed Variational Theorem (RMVT) [15, 18, 20, 64, 65] an exact fulfillment of the of the continuity conditions of the stess field can be obtained.

- Another important feature involves the higher order effects arising in the displacement field in the thickness direction [10]. The in-plane anisotropy of general fiber reinforced materials and the short wavelengths considered in vibroacoustic applications can make the higher order terms necessary to describe the vibration behavior, mainly for moderately thick and very thick plates. Therefore the most used 2-D axiomatic models like as CPT and FSDT must be refined to account for this important features, leading to the so called High order Shear Deformation Theories (HSDT), like as the Reddy's Third order Shear Deformation Theory (TSDT). A comprehensive assessment of the most common axiomatic theories for multilayered composite plates is available in selected review articles [38, 52] and in the works of Reddy [61, 62, 63]. These theories, from CPT to HSDT, can be summarized as ESL theories which describe the global response of the plate expanding the in-plane variables in the thickness direction, enforcing the transverse normal stress zero condition assuming a constant value for the transversal displacement. However, as Koiter demonstrates in his lecture [40], *a refinement of Love's first approximation theory is indeed meaningless, in general, unless the effect of transverse shear and normal stress are taken into account at the same time.* Therefore, also the transversal displacement has to be assumed axiomatically varying in the thickness direction in order to consider a correct refinement of the plate kinematic model [16, 17].

All the previously mentioned composite plates features can be easily fulfilled employing the Carrera's Unified Formulation (UF) [13, 14, 28]. This formulation permits to consider a wide range of refined plate theories, accounting for ESL or LW description of the plate variables. In this way a large variety of plate structures, from simple thin isotropic plates to more complex thick sandwich composite plates, and a large frequency range in their dynamic behavior, can be considered within a unique formulation.

Objective

The aim of this work is to study the effects of structural models in the vibro-acoustic response of plate-cavity systems both for low and mid-frequency ranges. The usage of refined models for the plate structure could give the correct vibro-acoustic coupling even when shorter wavelengths become important in the dynamic response. Moreover, the refined structural model permits to adequately modeling different types of multilayered structures. The main issue of this study is that the complexity of the structural models make worse the numerical difficulties, thus the efficiency is, if possible, a more crucial aspect with respect to the approches based on CPT and FSDT models. Clearly, all these aspects cannot be studied in only one work, and the proposed objective can be hard-fought only with a long-term activity. The present work is focused on the first development of refined structural FE models for plates and on their coupling with simple pressure based acoustic FE model. Mid-frequency analysis of complex geometries couldn't have been obtained due to the huge computational effort required and the limited computing capabilities. However, accurate results can be achieved for simple geometries and for a relatively large frequency range. Hence, the main aspects of this thesis can be summarized as follows:

- Development of a deterministic FE method for piezoelectric structural acoustic analysis of plate-cavity systems which is capable to predict the harmonic response of the coupled system over a large frequency range, allowing to narrow the currently existing mid-frequency twilight zone.

- Accounting for a refined structural model using Carrera's UF: in this way a large variety of plate structure can be considered with a unique formulation, intoducing in an arbitrary manner the higher order effects induced by the high frequency modes.

- At this stage, the computational burden is partially reduced using the uncoupled modal reduction technique, even if this choice prevents the efficient simulation of strong coupled system. The linear FE approximation is considered, obtaining large sparse symmetric matrices for the structural and fluid subsystems. Therefore the eigenvalue problem can be efficiently solved for each subsystem with iterative subspace solvers.

Thesis ouline

In the first chapter the fluid-structure interaction problem is introduced; the governing differential equations are presented and the related variational principle is obtained as a starting point for the numerical approximation. In chapter 2 the UF for piezoelectric composite plates is presented and then the FE approximation for the structural and acoustic problem is introduced. In chapter 3 the uncoupled modal reduction technique adopted in this work is presented. In chapter 4 and 5 the structural FE model and the coupled FE model are validated through convergence analysis and comparisons. In chapter 6 the potentiality of the present UF are exploited in three numerical test cases. Finally, conclusions and possible future works are given.

CHAPTER 1

Piezoelectric Structural Acoustic Problem

This chapter presents the mathematical model which describes the dynamic behavior of a piezoelectric structure in contact with an acoustic domain. The aim is to introduce the reader in the framework of the fluid-structure interaction problem from a general prospective. A brief introduction to the governing differential equations is presented. Then the test-function method is applied in order to obtain the variational formulation of the coupled system. Finally, an approximation of the chosen unknown variables, that is structural displacement s_i, electric potential ψ and fluid pressure p, is introduced and the final discrete form of the coupled system is derived. In the following the variables and physical properties of the system are assumed to be space and time dependent, i.e. for instance $s_i = s_i(x_j, t)$ and $\rho_s = \rho_s(x_i, t)$. For a detailed derivation of the the classical governing equations, we refer the reader to [59] and [37] for elasticity and piezoelectric aspects, and to [57] or [45] for acoustic theory.

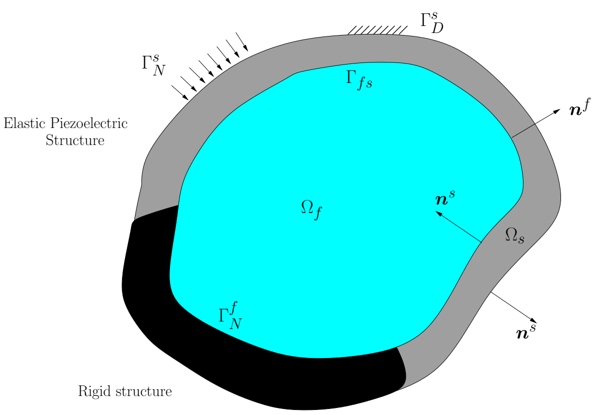

Figure 1.1: Coupled system domain.

1.1 Governing equations

In this work a linear behavior of the fluid-structure system is assumed. The structure is described by the differential equations of motion for a continuum body assuming small deformation and the electrostatic equilibrium equation within the hypotesis of linear piezoelasticity. The structure is in contact with a homegeneous, inviscid and irrotational compressible fluid. Both the fluid and the structure are modeled neglecting the gravity effects (i.e. body force).

Let us first consider the piezoelectric structure occupying the domain Ω_s (see figure 1.1). The structure is subjected to Dirichlet boundary conditions on Γ^s_D and to Neumann boundary conditions on Γ^s_N, which prescribe the displacement $\bar{s_i}$ and the surface force f_i respectively. The electric counterpart of the Dirichlet and Neumann boundaries of the structure are denoted by Γ^e_D and Γ^e_N, where the electric potential $\bar{\psi}$ and the electric charge Q are imposed, respectively. The interior fluid domain is denoted by Ω_f and Γ_{fs} is the fluid-structure interface surface. The fluid boundary Γ^f_N describes the rigid walled bounds of the fluid filled cavity, where the zero normal pressure gradient boundary condition is imposed. The linearized deformation tensor is denoted by ε_{ij} and the corresponding stress tensor by σ_{ij}. Moreover, E_i is the electric field vector and D_i denotes the electric displacement vector components. The mass density of the structure is ρ_s, whereas c_f and ρ_f are the constant speed of sound and reference mass density of the fluid. Finally n^s_i is the unit normal external to Ω_s and n^f_i is the unit normal external to Ω_f.

With this assumption, the equations that describes the elastic behavior of the structure subsystem are

$$\text{Elasticity :} \begin{cases} \sigma_{ij,j} = \rho_s \ddot{s}_i & \text{in} \quad \Omega_s \\ \sigma_{ij} n^s_j = f_i & \text{in} \quad \Gamma^s_N \\ s_i = \bar{s}_i & \text{in} \quad \Gamma^s_D \\ \sigma_{ij} n^s_j = p\, n^f_i & \text{in} \quad \Gamma_{fs}\,, \end{cases} \tag{1.1}$$

where the last boundary condition indicates the coupling with the fluid field. Moreover, the zero Neumann boundary condition is implied on the structure free-surface. Similary, the electrostatic behavior of the structure is described by the following equations

$$\text{Electrostatic :} \begin{cases} D_{i,i} = q & \text{in} \quad \Omega_s \\ D_i n^s_i = -Q & \text{in} \quad \Gamma^e_D \\ \psi = \bar{\psi} & \text{in} \quad \Gamma^e_N\,, \end{cases} \tag{1.2}$$

where there is no direct coupling with the fluid field. Again the zero Neumann boundary condition for the electric field is implied. Finally the acoustic field inside the cavity in absence of sound sources is described by the wave equation and the following boundary conditions

$$\text{Acoustic}: \begin{cases} p_{,ii} = \dfrac{1}{c_f^2}\ddot{p} & \text{in} \quad \Omega_f \\ p_{,i}n_i^f = -\rho_f \ddot{s}_i n_i^f & \text{in} \quad \Gamma_{fs} \\ p_{,i}n_i^f = 0 & \text{in} \quad \Gamma_D^f \,, \end{cases} \tag{1.3}$$

where the normal pressure gradient is related to the motion of the structure on the interface surface, describing the fluid-structure coupling term in the acoustic problem. The wave equation is obtained from the linearized version of the *Euler* equations system where a homogenous reference condition is considered. The formulation above with acoustic pressure p as indipendent variable is a choice of this work, as mentioned in the introduction chapter. The same equation (with change of dependent variable), however, holds for ρ and $v_{i,i}$; also the velocity field v_i satisfies the irrotationality conditions, so the same wave equations and the relative boundary conditions could be expressed in term of a scalar potential ϕ.

In the linear piezoelectric theory, the stress tensor σ_{ij} and the electric displacement D_i are related to the linearized strain tensor ε_{kl} and the electric field E_k through the converse and direct linear piezoelectric constitutive relations:

$$\begin{aligned} \sigma_{ij} &= c_{ijkl}\varepsilon_{kl} - e_{kij}E_k \\ D_i &= e_{ikl}\varepsilon_{kl} + \epsilon_{ik}E_k \,, \end{aligned} \tag{1.4}$$

where c_{ijkl}, e_{kij} and ϵ_{ik} denotes elastic, piezoelectric and dielectric material constants. Moreover, we have the following gradient relations between the linearized strain tensor ε_{kl} and the displacement s_k, and between the electric field E_i and the electric potential ψ:

$$\begin{aligned} \varepsilon_{ik} &= \frac{1}{2}\left(s_{k,l} + s_{l,k}\right) \\ E_k &= -\psi_{,k} \,. \end{aligned} \tag{1.5}$$

Now we can note that also the tensors σ_{ij} and D_i are a function of the derivatives of the field variables s_i and ψ.

1.2 Variational formulation

The *strong* form of the equations described in section 1.1 are expressed in terms of the chosen unknown fields of the fluid-structure system, i.e. the structural displacement s_i, the electric potential ψ and the fluid pressure p. In order to obtain the variational formulation associated with the local equations 1.1, 1.2 and 1.3, the test function method is applied. From a mathematical point of view we proceed with a generic *weak* formulation for each subsystem, introducing arbitrary weighting functions which is exactly the principal field variables that describe the evolution of the system. In this way the *weak* formulation obtained for the piezoelectric structure is equivalent to the Principle of Virtual Displacement (PVD) applied on the same system. For this reason, in this work we refer to the *weak* formulation of the piezoelectric structure such as the PVD variational formulation of the problem. This formulation differs from the Reissner's Mixed Variational Theorem (RMVT), where even the constitutive relations are modeled *a priori* introducing the stress and electric displacement components as Lagrangian multipliers, also known as secondary variables of the problem. However, in the following only the PVD statement is considered; the reader can refer to [53] or [5] for the details about variational formulations and *weak* forms.

In the following we proceed in three steps, considering firstly the system 1.1 releted to the structure, then the system 1.2 and 1.3 releted to the electric charge problem for a dielectric medium and to the acoustic cavity respectively. First, integrating over Ω_s and multiplying the dynamic equilibrium of system 1.1 by arbitrary time-indipendent test-function (or virtual displacement) δs_i, then integrating by parts and applying Green's formula, we obtain

$$\int_{\Omega_s} \delta\varepsilon_{ij}\sigma_{ij}\,\mathrm{d}V + \int_{\Omega s} \delta s_i \rho_s \ddot{s}_i\,\mathrm{d}V = \int_{\partial\Omega_s} \delta s_i \sigma_{ij} n_j^s\,\mathrm{d}s\,,$$

where $\delta\varepsilon_{ij} = \frac{1}{2}\left(\delta s_{k,l} + \delta s_{l,k}\right)$. Now distributing the right hand side integrals over the boundaries Γ_N^s and Γ_{fs} and using the boundary conditions of the system 1.1 we obtain

$$\int_{\Omega_s} \delta\varepsilon_{ij}\sigma_{ij}\,\mathrm{d}V + \int_{\Omega s} \delta s_i \rho_s \ddot{s}_i\,\mathrm{d}V = \int_{\partial\Gamma_N^s} \delta s_i f_i\,\mathrm{d}s + \int_{\partial\Gamma_{fs}} \delta s_i p\, n_i\,\mathrm{d}s\,, \tag{1.6}$$

where $n_i = n_i^f$. This is the PVD statement for the mechanical variables including the acoustic coupling term; this formulation exactly satisfy, in a *weak* sense, the *natural* boundary conditions (i.e. Neumann type) whereas the virtual displacement δs_i must be chosen according with the *essential* conditions (i.e. Dirichlet type).

Secondly, multiplying the electrostatic equilibrium of system 1.2 by $\delta\psi$, integrating over the piezoelectric continuum Ω_s, integrating by parts and applyng Green's formula as above, assuming $q = 0$ we have

$$\int_{\Omega_s} \delta E_i D_i\,\mathrm{d}V = -\int_{\partial\Omega_s} \delta\psi D_i n_i^s\,\mathrm{d}s\,.$$

Then using the Neumann boundary conditions on Γ_N^e, we obtain

$$\int_{\Omega_s} \delta E_i D_i\,\mathrm{d}V = \int_{\Gamma_N^e} \delta\psi\, Q\,\mathrm{d}s\,. \tag{1.7}$$

Again, like the elastic counterpart, this variational form satisfy the *natural* boundary conditions whereas the electric virtual displacement $\delta\psi$ must satisfy the *essential* conditions.

Finally, multiplying the wave equation of system 1.3 by δp, integrating by parts, applyng Green's formula and using the Neumann boundary condition on the fluid-structure interface surface, we obtain

$$\int_{\Omega_f} \delta p_{,i} p_{,i} \,\mathrm{d}V + \int_{\Omega_f} \frac{1}{c_f^2} \delta p\, \ddot{p} \,\mathrm{d}V = - \int_{\Gamma_{fs}} \delta p\, \rho_f \ddot{s}_i n_i \,\mathrm{d}s, \tag{1.8}$$

that satisfy the null normal pressure gradient condition along the assumed rigid wall.

Equations 1.6, 1.7 and 1.8 are the *weak* forms of the considered subsystems. The fluid-structure coupling appear evident in the terms in the right hand side of the structural and fluid equations 1.6 and 1.8. In order to obtain the final form of the variational formulation we have to take into account the constituve piezoelectric relations. Therefore, using relations 1.4 in equations 1.6 and 1.7 we finally obtain

$$\begin{cases} \int_{\Omega_s} \delta\varepsilon_{ij} c_{ijkl} \varepsilon_{kl} \,\mathrm{d}V - \int_{\Omega_s} \delta\varepsilon_{ij} e_{kij} E_k \,\mathrm{d}V \int_{\Omega s} \delta s_i \rho_s \ddot{s}_i \,\mathrm{d}V = \int_{\partial\Gamma_N^s} \delta s_i f_i \,\mathrm{d}s + \int_{\partial\Gamma_{fs}} \delta s_i p\, n_i \,\mathrm{d}s \\ \int_{\Omega_s} \delta E_i e_{ikl} \varepsilon_{kl} \,\mathrm{d}V + \int_{\Omega_s} \delta E_i \epsilon_{ik} E_k \,\mathrm{d}V = \int_{\Gamma_N^e} \delta\psi\, Q \,\mathrm{d}s \\ \int_{\Omega_f} \delta p_{,i} p_{,i} \,\mathrm{d}V + \int_{\Omega_f} \frac{1}{c_f^2} \delta p\, \ddot{p} \,\mathrm{d}V = - \int_{\Gamma_{fs}} \delta p\, \rho_f \ddot{s}_i n_i \,\mathrm{d}s. \end{cases} \tag{1.9}$$

The system of integral equations 1.9 in the field variables s_i, ψ and p is the starting point for the numerical approximation.

1.3 Numerical approximation

In order to obtain a numerical solution of the system 1.9, an approximation of the primary variable has to be considered. Therefore, let us introduce $\mathbf{U}$, $\mathbf{\Psi}$ and $\mathbf{P}$ as the vectorial unknown of the discretized problem. Thus we have

$$\begin{aligned} s_i &= \mathbf{N}_i^s \mathbf{U}\,, \\ \psi &= \mathbf{N}^\psi \mathbf{\Psi}\,, \\ p &= \mathbf{N}^p \mathbf{P}\,, \end{aligned} \tag{1.10}$$

where $\mathbf{N}_i^s$, $\mathbf{N}^\psi$ and $\mathbf{N}^p$ are generic row matrices functions of the space coordinates x_i, which interpolates the continuous unknown variables. If a FE discretization is performed, $\mathbf{U}$, $\mathbf{\Psi}$ and $\mathbf{P}$ are the nodal displacements, electric potential and pressure respectively, whereas if a Ritz method is used, the same vectorial quantities are the amplitude associated with each approximation function. In both cases the discretized unknowns are only functions of time t. Using the relations 1.10 in the system of equations 1.9 leads to the following submatrices:

$$
\begin{aligned}
\int_{\Omega_s} \delta\varepsilon_{ij} c_{ijkl} \varepsilon_{kl} \,\mathrm{d}V &= \delta\mathbf{U}^{\mathrm{T}} \mathbf{K}_{ss} \mathbf{U} \\
-\int_{\Omega_s} \delta\varepsilon_{ij} e_{kij} E_k \,\mathrm{d}V &= \delta\mathbf{U}^{\mathrm{T}} \mathbf{K}_{s\psi} \mathbf{\Psi} \\
\int_{\Omega s} \delta s_i \rho_s \ddot{s}_i \,\mathrm{d}V &= \delta\mathbf{U}^{\mathrm{T}} \mathbf{M}_{ss} \ddot{\mathbf{U}} \\
\int_{\partial\Gamma_N^s} \delta s_i f_i \,\mathrm{d}s &= \delta\mathbf{U}^{\mathrm{T}} \mathbf{F}_s \mathbf{U} \\
\int_{\partial\Gamma_{fs}} \delta s_i p\, n_i \,\mathrm{d}s &= \delta\mathbf{U}^{\mathrm{T}} \mathbf{S}_{sp} \mathbf{P} \\
\int_{\Omega_s} \delta E_i e_{kij} \varepsilon_{kl} \,\mathrm{d}V &= \delta\mathbf{\Psi}^{\mathrm{T}} \mathbf{K}_{s\psi}^{\mathrm{T}} \mathbf{U} \\
\int_{\Omega_s} \delta E_i \epsilon_{ik} E_k \,\mathrm{d}V &= \delta\mathbf{\Psi}^{\mathrm{T}} \mathbf{K}_{\psi\psi} \mathbf{\Psi} \\
\int_{\Gamma_N^e} \delta\psi\, Q \,\mathrm{d}s &= \delta\mathbf{\Psi}^{\mathrm{T}} \mathbf{F}_{\psi} \mathbf{\Psi} \\
\int_{\Omega_f} \delta p_{,i} p_{,i} \,\mathrm{d}V &= \delta\mathbf{P}^{\mathrm{T}} \mathbf{H} \mathbf{P} \\
\frac{1}{c_f^2} \int_{\Omega_f} \delta p\, \ddot{p} \,\mathrm{d}V &= \delta\mathbf{P}^{\mathrm{T}} \mathbf{Q} \ddot{\mathbf{P}} \\
\rho_f \int_{\Gamma_{fs}} \delta p\, \ddot{s}_i n_i \,\mathrm{d}s &= \delta\mathbf{U}^{\mathrm{T}} \rho_f \mathbf{S}_{sp}^{\mathrm{T}} \ddot{\mathbf{P}}
\end{aligned}
$$

where $\mathbf{M}_{ss}$ and $\mathbf{K}_{ss}$ are the mass and stiffness matrices of the structure; $\mathbf{K}_{\psi\psi}$ is the electric stiffness matrix; $\mathbf{K}_{s\psi}$ is the electromechanical coupling matrix; $\mathbf{Q}$ and $\mathbf{H}$ are the mass and stiffness matrices of the fluid; $\mathbf{S}_{sp}$ is the fluid structure coupling matrix; $\mathbf{F}_s$ and $\mathbf{F}_{\psi}$ are the applied mechanical force and charge vectors respectively. Therefore the system 1.9 can be rewritten, in discretized form, as follows:

$$\begin{bmatrix} \mathbf{M}_{ss} & 0 & 0 \\ 0 & 0 & 0 \\ -\rho_f \mathbf{S}_{sp}^{\mathrm{T}} & 0 & \mathbf{Q} \end{bmatrix} \begin{Bmatrix} \ddot{\mathbf{U}} \\ \ddot{\mathbf{\Psi}} \\ \ddot{\mathbf{P}} \end{Bmatrix} + \begin{bmatrix} \mathbf{K}_{ss} & \mathbf{K}_{s\psi} & \mathbf{S}_{sp} \\ \mathbf{K}_{s\psi}^{\mathrm{T}} & \mathbf{K}_{\psi\psi} & 0 \\ 0 & 0 & \mathbf{H} \end{bmatrix} \begin{Bmatrix} \mathbf{U} \\ \mathbf{\Psi} \\ \mathbf{P} \end{Bmatrix} = \begin{Bmatrix} \mathbf{F}_s \\ \mathbf{F}_\psi \\ 0 \end{Bmatrix}, \quad (1.11)$$

with appropriate initial conditions and *essential* boundary conditions. Using the second row of equation 1.11, the unknowns associated with the electric potential can be expressed in terms of structural displacements. Through this static condensation the unknowns of the problem are reduced to $\mathbf{U}$ and $\mathbf{P}$, obtaining an added-stiffness matrix and an added-load vector due to the electromechanical coupling. This is a classical procedure, that can reduce the problem size but, at the same time, destroyes the sparsity pattern of the system matrices. Obviously this fill-in of the matrices could be a serious drawback when a FE approximation is used; indeed in such case the sparsity property of the large FE matrices is an advantage from a numerical point of view. On the other hand, if a different approximation procedure is accounted (like as Ritz method), the static condensation can be done more easily. Then, without loss of generality, we can rearrange the equation 1.11 to obtain

$$\begin{bmatrix} \mathbf{M} & 0 \\ -\rho_f \mathbf{S}^{\mathrm{T}} & \mathbf{Q} \end{bmatrix} \begin{Bmatrix} \ddot{\tilde{\mathbf{U}}} \\ \ddot{\mathbf{P}} \end{Bmatrix} + \begin{bmatrix} \mathbf{K} & \mathbf{S} \\ 0 & \mathbf{H} \end{bmatrix} \begin{Bmatrix} \tilde{\mathbf{U}} \\ \mathbf{P} \end{Bmatrix} = \begin{Bmatrix} \mathbf{F} \\ 0 \end{Bmatrix}, \quad (1.12)$$

where, if a static condensation of the electric variables has been accounted, $\tilde{\mathbf{U}} \equiv \mathbf{U}$ and the matrix $\mathbf{K}$ and vector $\mathbf{F}$ are the structural stiffness matrix and loads with added contributes due to the electromechanical coupling, instead if no condensation has been applied $\tilde{\mathbf{U}} = \{\mathbf{U}\,\mathbf{\Psi}\}^{\mathrm{T}}$ and matrix equation 1.12 is simply a partitioning of the starting equation 1.11. The equation 1.12 is the classical discrete form of the fluid structure interaction problem, also called (u, p) formulation.

CHAPTER 2

Unified Finite Element Model

In this chapter the formulation of the piezoelectric structural acoustic problem in terms of structural displacements s_i, electric potential ψ and acoustic pressure p presented in the previous chapter will be specified for generic laminated plates made of orthotropic materials in contact with an acoustic cavity. In the first section, the material properties of a generic piezoelectric orthotropic material are presented and the constitutive relations 1.4 are expressed using the classical engineering notation. In the second section a compact form of the constitutive equations is derived, following the procedure adopted in [30] for a generic multifield problem. The kinematic assumptions introduced by the UF for the structural subsystem are described in the third section. Here it is shown how the powerful notation of the UF may lead to a widely range of 2-D plate theories. Then, in the fourth section, the FE discretization of the structural subsystem and of the fluid coupling terms is deduced in terms of fundamental nuclei, which are the lower level of the FE assembly procedure. Thus is also presented the much simpler FE discretization of the acoustic cavity. In the last section, the final form of the coupled FE equation is presented.

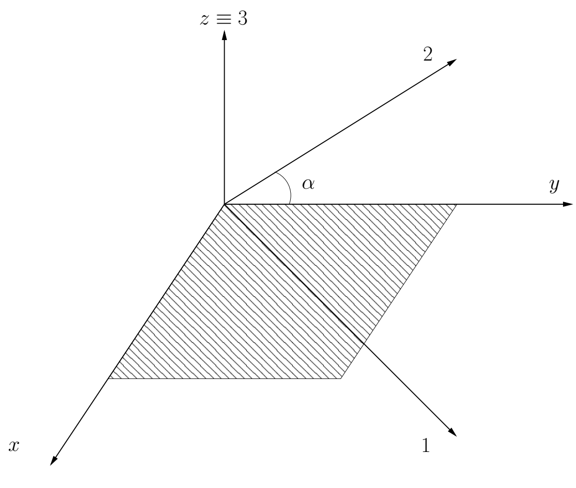

Figure 2.1: Material and plate reference systems.

2.1 Constitutive equations

Equations 1.4 are the most general form of the linear constitutive equations for a piezoelectric continuum. As stated in the previous chapter, c_{ijkl}, e_{kij} and ϵ_{ik} denotes elastic, piezoelectric and dielectric tensors. In general, they have 81, 27 and 9 material constants respectively. However, the number of indipendent components of the above tensors can be reduced thanks to the symmetry of the σ_{ij} and ε_{kl} tensors. Indeed, the former is symmetric from the momentum equation, whereas the latter is symmetric by definition. Moreover, energetic considerations, extend the symmetry of the tensor c_{ijkl} from the couples ij and kl to all the four indices. This reduces the number of indipendent material properties to 21 for c_{ijkl}. The piezoelectric e_{kij} indipendent constants becomes 18 thanks to symmmetry of indexes ij, whereas no semplification can be done for the dielectric tensor ϵ_{ik}.

With these assumptions, the constitutive equations can assume a more suitable form introducing the vector quantities $\boldsymbol{\sigma}$ and $\boldsymbol{\varepsilon}$, which contain the indipendent parameters of the related tensors. Arranging the components of the electric displacement and electric field into the vector $\boldsymbol{D}$ and $\boldsymbol{E}$ respectively, the constitutive equations 1.4 can be rewritten as

$$
\begin{aligned}
\boldsymbol{\sigma} &= \tilde{\mathrm{C}}\boldsymbol{\varepsilon} - \tilde{\boldsymbol{e}}\boldsymbol{E} \\
\boldsymbol{D} &= \tilde{\boldsymbol{e}}^{\mathrm{T}}\boldsymbol{\varepsilon} + \tilde{\boldsymbol{\epsilon}}\boldsymbol{E}\,,
\end{aligned} \tag{2.1}
$$

where the symmetric matrix $\tilde{\mathbf{C}}$ grouped the 21 indipendent elastic material properties, the matrix $\tilde{\boldsymbol{e}}$ grouped the 18 piezoelectric coefficients and finally $\tilde{\boldsymbol{\epsilon}}$ contains the 9 dielectric constants. Assumed a generic material system of reference (see figure 2.1), the terms in the introduced vectors are:

$$
\boldsymbol{\sigma} = \left\{ \begin{array}{c} \sigma_{11} \\ \sigma_{22} \\ \sigma_{33} \\ \sigma_{23} \\ \sigma_{13} \\ \sigma_{12} \end{array} \right\}, \ \boldsymbol{\varepsilon} = \left\{ \begin{array}{c} \varepsilon_{11} \\ \varepsilon_{22} \\ \varepsilon_{33} \\ \varepsilon_{23} \\ \varepsilon_{13} \\ \varepsilon_{12} \end{array} \right\}, \ \boldsymbol{D} = \left\{ \begin{array}{c} D_1 \\ D_2 \\ D_3 \end{array} \right\}, \ \boldsymbol{E} = \left\{ \begin{array}{c} E_1 \\ E_2 \\ E_3 \end{array} \right\}.
$$

Further reduction in the number of indipendent material parameters comes from the material symmetry. Indeed, elastic or piezoelectric material parameters can exhibit symmetry properties about specific directions (i.e. material planes of symmetry), and the structure of the matrices $\mathbf{C}$, $\boldsymbol{\epsilon}$ and $\boldsymbol{e}$ is modified consequently. In particular, in this work, we consider composite plates made of generic orthotropic layers. For this type of materials, three mutually orthogonal planes of symmetry exist, then the number of indipendent elastic, piezoelectric and dielectric coefficients is reduced from 21 to 9, from 18 to 5 and from 9 to 3, respectively. In this way the matrices assume the following pattern in the local material system of reference:

$$\tilde{\mathbf{C}} = \begin{bmatrix} \tilde{C}_{11} & \tilde{C}_{12} & \tilde{C}_{13} & 0 & 0 & 0 \\ \tilde{C}_{12} & \tilde{C}_{22} & \tilde{C}_{23} & 0 & 0 & 0 \\ \tilde{C}_{13} & \tilde{C}_{23} & \tilde{C}_{33} & 0 & 0 & 0 \\ 0 & 0 & 0 & \tilde{C}_{44} & 0 & 0 \\ 0 & 0 & 0 & 0 & \tilde{C}_{55} & 0 \\ 0 & 0 & 0 & 0 & 0 & \tilde{C}_{66} \end{bmatrix},$$

$$\tilde{\boldsymbol{\epsilon}} = \begin{bmatrix} \tilde{\epsilon}_{22} & 0 & 0 \\ 0 & \tilde{\epsilon}_{22} & 0 \\ 0 & 0 & \tilde{\epsilon}_{33} \end{bmatrix},$$

$$\tilde{\boldsymbol{e}} = \begin{bmatrix} 0 & 0 & \tilde{e}_{13} \\ 0 & 0 & \tilde{e}_{23} \\ 0 & 0 & \tilde{e}_{33} \\ 0 & \tilde{e}_{42} & 0 \\ \tilde{e}_{51} & 0 & 0 \\ 0 & 0 & 0 \end{bmatrix},$$

where the piezoelectric layer is assumed to be poled in the thickness direction. The non zero parameters C_{ij} can be expressed through 9 engineering constants, which are the Young's moduli E_1, E_2 and E_3, the shear moduli G_{12}, G_{13} and G_{23} and the Poisson's moduli ν_{12}, ν_{13} and ν_{23}. When there exist no preferred directions in the material properties, infinite number of planes of material symmetry are considered, and the material is assumed to be isotropic; in such case, the number of indipendent parameters reduces from 9 to 2. Indeed in this case we have $E = E_1 = E_2 = E_3$, $G = G_{12} = G_{13} = G_{23}$ and $\nu = \nu_{12} = \nu_{13} = \nu_{23}$ with

$$G = \frac{E}{2\,(1+\nu)} \,.$$

The constitutive equations 2.1 with the material matrices described above are referred to the principal material directions, indicated with pedices $1, 2$ and 3. Therefore, it is necessary to describe the same relations in the plate reference system (x, y, z), due to the fact that different layers may exhibit different material symmetry directions. As shown in figure 2.1, indicating with α the angle between the in plane material coordinates $(1, 2)$ and the plate coordinates (x, y), we can define the rotation matrices $\mathcal{R}_{6\times6}(\alpha)$ and $\mathcal{R}_{3\times3}(\alpha)$, which relate the vectorial quantities $\boldsymbol{\sigma}$, $\boldsymbol{\varepsilon}$, $\boldsymbol{D}$ and $\boldsymbol{E}$ in the material reference system with those in the plate reference system. Therefore, indicating with $\tilde{\mathbf{C}}$, $\tilde{\boldsymbol{\epsilon}}$ and $\tilde{\boldsymbol{e}}$ the material matrices in the local layer system of reference with the orthotropic pattern described above, we can obtain the quantities $\mathbf{C}$, $\boldsymbol{\epsilon}$ and $\boldsymbol{e}$ in the plate reference system performing the following transformations:

$$
\begin{aligned}
\mathbf{C} &= \mathcal{R}_{6\times 6}^{\mathrm{T}}\, \tilde{\mathbf{C}}\, \mathcal{R}_{6\times 6}\,, \\
\boldsymbol{\epsilon} &= \mathcal{R}_{3\times 3}^{\mathrm{T}}\, \tilde{\boldsymbol{\epsilon}}\, \mathcal{R}_{3\times 3}\,, \\
\boldsymbol{e} &= \mathcal{R}_{6\times 6}^{\mathrm{T}}\, \tilde{\boldsymbol{e}}\, \mathcal{R}_{3\times 3}\,,
\end{aligned}
\tag{2.2}
$$

where

$$
\mathcal{R}_{3\times 3} = \begin{bmatrix} \cos\alpha & \sin\alpha & 0 \\ -\sin\alpha & \cos\alpha & 0 \\ 0 & 0 & 1 \end{bmatrix},
$$

$$
\mathcal{R}_{6\times 6} = \begin{bmatrix}
\cos^2\alpha & \sin^2\alpha & 0 & 0 & 0 & -\sin 2\alpha \\
\sin^2\alpha & \cos^2\alpha & 0 & 0 & 0 & \sin 2\alpha \\
0 & 0 & 1 & 0 & 0 & 0 \\
0 & 0 & 0 & \cos\alpha & -\sin\alpha & 0 \\
0 & 0 & 0 & \sin\alpha & \cos\alpha & 0 \\
-\sin\alpha\cos\alpha & \sin\alpha\cos\alpha & 0 & 0 & 0 & \cos^2\alpha - \sin^2\alpha
\end{bmatrix}.
$$

2.2 Condensed notation for electromechanical problem

In this section it is shown how the geometrical and the constitutive relations can be rearranged in a more suitable form. In this way, a compact form for the electromechanical PVD is introduced. First of all, let us introduce the vector $\boldsymbol{\mathcal{U}}^k$ containing the primary unknowns of the piezo-composite plate:

$$
\boldsymbol{\mathcal{U}}^k = \left\{ \boldsymbol{s}^{k\,\mathrm{T}}\, \phi^k \right\}^{\mathrm{T}} = \left\{ u^k\, v^k\, w^k\, \psi^k \right\}^{\mathrm{T}} , \tag{2.3}
$$

where the superscript k indicates that the variables refer to the k^{th} layer of the plate, $\boldsymbol{s}$ is the vector containing the structural displacements s_i in the plate reference system and $^{\mathrm{T}}$ indicates the transposition operator. Rearranging the components of $\boldsymbol{\varepsilon}$ and $\boldsymbol{E}$, we have

$$
\boldsymbol{\varepsilon}^k = \left\{ \begin{array}{c} \varepsilon_{11} \\ \varepsilon_{22} \\ \varepsilon_{12} \\ \varepsilon_{33} \\ \varepsilon_{13} \\ \varepsilon_{23} \end{array} \right\}^k = \left\{ \begin{array}{c} \boldsymbol{\varepsilon}_p \\ \boldsymbol{\varepsilon}_n \end{array} \right\}^k, \; \boldsymbol{E}^k = \left\{ \begin{array}{c} E_{11} \\ E_{22} \\ E_{33} \end{array} \right\}^k = \left\{ \begin{array}{c} \boldsymbol{E}_p \\ E_n \end{array} \right\}^k,
$$

where subscript p denotes in-plane components, whereas subscript n refers to out-of-plane (normal) components. In the same way, the stress vector $\boldsymbol{\sigma}$ and the electrical displacement $\boldsymbol{D}$ can be rearranged to yield

$$\boldsymbol{\sigma}^k = \begin{Bmatrix} \sigma_{11} \\ \sigma_{22} \\ \sigma_{12} \\ \sigma_{33} \\ \sigma_{13} \\ \sigma_{23} \end{Bmatrix}^k = \begin{Bmatrix} \boldsymbol{\sigma}_p \\ \boldsymbol{\sigma}_n \end{Bmatrix}^k, \ \boldsymbol{D}^k = \begin{Bmatrix} D_{11} \\ D_{22} \\ D_{33} \end{Bmatrix}^k = \begin{Bmatrix} \boldsymbol{D}_p \\ D_n \end{Bmatrix}^k .$$

Then, the components of the symmetric deformation tensor collected in $\boldsymbol{\varepsilon}$ and the electric field vector $\boldsymbol{E}$ can be condensed in the same vectorial quantity $\boldsymbol{\mathcal{E}}$, which represents a generalized deformation vector. We can also rearrange the structural stress components $\boldsymbol{\sigma}$ and the electric displacement $\boldsymbol{D}$ in a generalized stress vector $\boldsymbol{\mathcal{S}}$ in the same way:

$$\boldsymbol{\mathcal{E}}^k = \begin{Bmatrix} \boldsymbol{\varepsilon}_p \\ \boldsymbol{E}_p \\ \boldsymbol{\varepsilon}_n \\ E_n \end{Bmatrix}^k = \begin{Bmatrix} \boldsymbol{\mathcal{E}}_p \\ \boldsymbol{\mathcal{E}}_n \end{Bmatrix}^k, \ \boldsymbol{\mathcal{S}}^k = \begin{Bmatrix} \boldsymbol{\sigma}_p \\ \boldsymbol{D}_p \\ \boldsymbol{\sigma}_n \\ D_n \end{Bmatrix}^k = \begin{Bmatrix} \boldsymbol{\mathcal{S}}_p \\ \boldsymbol{\mathcal{S}}_n \end{Bmatrix}^k . \tag{2.4}$$

According to this organization of the intensive and extensive variables in the vectors $\boldsymbol{\mathcal{E}}$ and $\boldsymbol{\mathcal{S}}$, respectively, the geometrical relations 1.5 can be compactly rewritten for each layer as

$$\boldsymbol{\mathcal{E}}^k = \boldsymbol{\mathcal{D}}\boldsymbol{\mathcal{U}}^k , \tag{2.5}$$

with

$$\boldsymbol{\mathcal{D}} = \begin{bmatrix} \partial_x & 0 & 0 & 0 \\ 0 & \partial_y & 0 & 0 \\ \partial_y & \partial_x & 0 & 0 \\ 0 & 0 & 0 & -\partial_x \\ 0 & 0 & 0 & -\partial_y \\ 0 & 0 & \partial_z & 0 \\ \partial_z & 0 & \partial_x & 0 \\ 0 & \partial_z & \partial_y & 0 \\ 0 & 0 & 0 & -\partial_z \end{bmatrix} = \begin{bmatrix} \boldsymbol{\mathcal{D}}_p \\ \boldsymbol{\mathcal{D}}_{n_z} + \boldsymbol{\mathcal{D}}_{n_p} \end{bmatrix} , \tag{2.6}$$

where the differential operator that acts on the out-of-plane components is splitted in two terms, one acting only with in-plane derivatives (i.e. ∂_x and ∂_y) and the other with out-of-plane derivatives (i.e. ∂_z), that is

$$
\mathcal{D}_p = \begin{bmatrix} \partial_x & 0 & 0 & 0 \\ 0 & \partial_y & 0 & 0 \\ \partial_y & \partial_x & 0 & 0 \\ 0 & 0 & 0 & -\partial_x \\ 0 & 0 & 0 & -\partial_y \end{bmatrix},
$$

$$
\mathcal{D}_{n_z} = \begin{bmatrix} 0 & 0 & \partial_z & 0 \\ \partial_z & 0 & 0 & 0 \\ 0 & \partial_z & 0 & 0 \\ 0 & 0 & 0 & -\partial_z \end{bmatrix},
$$

$$
\mathcal{D}_{n_p} = \begin{bmatrix} 0 & 0 & 0 & 0 \\ 0 & 0 & \partial_x & 0 \\ 0 & 0 & \partial_y & 0 \\ 0 & 0 & 0 & 0 \end{bmatrix}.
$$

Similarly, the constitutive relation can be rewritten in the plate reference system in the following compact form:

$$
\boldsymbol{\mathcal{S}}^k = \boldsymbol{\mathcal{C}}^k \boldsymbol{\mathcal{E}}^k \,, \tag{2.7}
$$

with

$$
\boldsymbol{\mathcal{C}}^k = \begin{bmatrix}
C_{11} & C_{12} & C_{16} & 0 & 0 & C_{13} & 0 & 0 & e_{13} \\
C_{21} & C_{22} & C_{26} & 0 & 0 & C_{23} & 0 & 0 & e_{23} \\
C_{16} & C_{26} & C_{66} & 0 & 0 & C_{36} & 0 & 0 & e_{63} \\
0 & 0 & 0 & \epsilon_{11} & \epsilon_{12} & 0 & e_{51} & e_{41} & 0 \\
0 & 0 & 0 & \epsilon_{12} & \epsilon_{22} & 0 & e_{52} & e_{42} & 0 \\
C_{13} & C_{23} & C_{36} & 0 & 0 & C_{33} & 0 & 0 & e_{33} \\
0 & 0 & 0 & e_{15} & e_{52} & 0 & C_{55} & C_{45} & 0 \\
0 & 0 & 0 & e_{41} & e_{24} & 0 & C_{45} & C_{44} & 0 \\
e_{13} & e_{23} & e_{63} & 0 & 0 & e_{33} & 0 & 0 & \epsilon_{33}
\end{bmatrix}^k = \begin{bmatrix} \boldsymbol{\mathcal{C}}^k_{pp} & \boldsymbol{\mathcal{C}}^k_{pn} \\ \boldsymbol{\mathcal{C}}^{k\,\mathrm{T}}_{pn} & \boldsymbol{\mathcal{C}}^k_{nn} \end{bmatrix}, \tag{2.8}
$$

where $\boldsymbol{\mathcal{C}}^k_{pp}$ ($\boldsymbol{\mathcal{C}}^k_{nn}$) contains the material constants that relates the in(out-of)-plane intensive variables with the in(out-of)-plane extensive variables, whereas $\boldsymbol{\mathcal{C}}^k_{pn}$ relates the in-plane with the out-of-plane ones. The matrix in equation 2.8 is obtained from a partion of the matrices $\mathbf{C}$, $\boldsymbol{\epsilon}$ and $\boldsymbol{e}$ written in the plate reference system through the coordinate transformations 2.2. Therefore equations 2.5 and 2.7 permit to express the extensive end intensive variables as a functions of $\boldsymbol{\mathcal{U}}^k$ in the plate reference system for each layer.

This formalism for the treatment of the structural variables permits to rewrite the variational formulation 1.9 in a more compact form that is useful for the introduction of the UF and for the next numerical approximation by FE method. In particular, starting from equations 1.6 1.7 and 1.8 and introducing the formalism of the vectorial notation described in this section, we have

$$
\begin{cases}
\displaystyle\int_{\Omega_s^k} \delta\boldsymbol{\mathcal{E}}^{k^{\mathrm{T}}}\boldsymbol{\mathcal{S}}^k \,\mathrm{d}V = \int_{\Omega_s^k} \delta\boldsymbol{\mathcal{U}}^{k^{\mathrm{T}}}\mathbf{f}_m^k \,\mathrm{d}V + \int_{\Gamma^k} \delta\boldsymbol{\mathcal{U}}^{k^{\mathrm{T}}}\mathbf{f}_{em}^k \,\mathrm{d}s + \int_{\Gamma_{fs}} \delta\boldsymbol{\mathcal{U}}^{\bar{k}^{\mathrm{T}}}\mathbf{f}_{sf} \,\mathrm{d}s \\
\displaystyle\int_{\Omega_f} \delta p_{,i}\, p_{,i} \,\mathrm{d}V = -\int_{\Omega_f} \frac{1}{c_f^2}\delta p\, \ddot{p} \,\mathrm{d}V - \int_{\Gamma_{fs}} \delta p\, f_{fs} \,\mathrm{d}s
\end{cases}
\tag{2.9}
$$

where

$$
\begin{aligned}
\mathbf{f}_m^k &= \left\{ \begin{array}{c} -\rho_s^k \ddot{\boldsymbol{s}}^k \\ 0 \end{array} \right\}, \\
\mathbf{f}_{em}^k &= \left\{ \begin{array}{c} \mathbf{f}^k \\ -Q^k \end{array} \right\}, \\
\mathbf{f}_{sf} &= \left\{ \begin{array}{c} p\boldsymbol{n} \\ 0 \end{array} \right\}, \\
f_{fs} &= \rho_f \left\{ \begin{array}{cc} \boldsymbol{n}^{\mathrm{T}} & 0 \end{array} \right\} \ddot{\boldsymbol{\mathcal{U}}}^{\bar{k}}
\end{aligned}
$$

are, respectively, the mechanical inertial load and the electromechanical external load on each layer, and the fluid-structure mutual loads. The summation over superscripts k is implied in system 2.9. The structural loaded area at k^{th} layer is detoted by Γ^k. It can be shown that the first term of the first equation of system 2.9 is the internal work associated with the generic orthotropic piezoelectric layer k, while the right hand side terms are the external work done for the structural variable $\boldsymbol{\mathcal{U}}$ at layer k, including the inertia of the structure and the fluid loading acting only on the displacement field $\boldsymbol{s}$. In the second equation, the left hand side term is the internal work of the acoustic cavity, while the acoustic inertial loading and the fluid-structure coupling term are on the right side. The whole system can be seen as the condition for the minimization of the total energy of the piezoelectric structural acoustic system. Finally it is noted that the fluid-structure coupling term refers only to the structural variables at layer $\bar{k}$ and then no summation has to be applied for this term; indeed, only the lamina in contact with the enclosed fluid modifies the boundary condition of the acoustic field and, analogously, the acoustic pressure works only for the displacement of the same lamina.

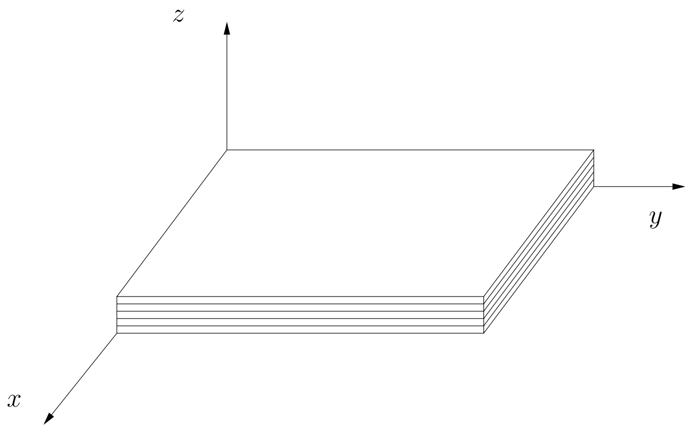

Figure 2.2: Plate reference system.

2.3 Through-the-thickness assumption for structural primary variables

In this section the UF is introduced as a powerful framework onto which a large class of 2-D axiomatic theories can be derived. The application of a 2-D model permits to express the unknown variables as a set of thickness function depending only on the thickness coordinate z and the correspondent variable depending on the in-plane plate coordinates x and y. Then, referring to the plate reference system of figure 2.2, the generic variable $g(x, y, z, t)$ and its variation $\delta g(x, y, z)$ are written according to the following expansion:

$$g(x, y, z, t) = F_\tau(z) g_\tau(x, y, t), \quad \delta g(x, y, z) = F_\tau(z) \delta g_\tau(x, y)\,, \tag{2.10}$$

with

$$\tau = 0, \cdots, N\,.$$

The variable g can be a vectorial quantity, for instance displacement $\boldsymbol{s}$, or a scalar, as the electric potential ψ. The summing convention with repeated index τ is assumed. The order of expansion goes from 1 to higher order values N and the models can be ESL or LW. In the former the expansion variables are assumed for the whole plate, and a Taylor expansion centered on the mid-plane is employed as thickness funtions $F_\tau(z)$, with z that varies from $-\frac{t}{2}$ and $\frac{t}{2}$, where t is the plate thickness, according to figure 2.3. In the latter the variables is considered indipendent in each layer and the Lagrange polynomials are assumes as thickness funtions $F(z_k)$, where z_k is the local thickness coordinate for the k^{th} layer and goes from -1 (i.e. the bottom of layer k) to 1 (i.e. the top of layer k), as it is shown in figure 2.4. In this work the fourth order is assumed as the maximum through-the-thickness expansion for LW models; indeed, due to its local description, no more orders are required in order to obtain a very accurate solution. Moreover, the huge computational effort limits the expansion order N for LW, due to the fact that, considering each layer as an indipendent subsystem, the number of unknowns depends on the number of layers. For what concern the ESL models, the order of expansion N is limited by the numerical ill-conditioning when the FE approximation is considered.

2.3.1 Mechanical variables, ESL theories

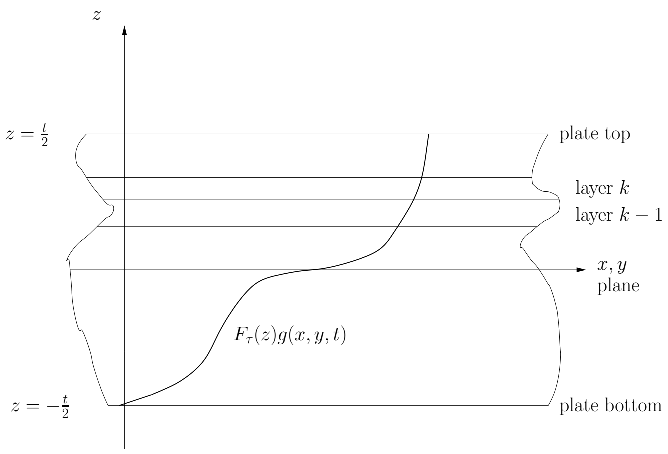

Figure 2.3: ESL model.

In this case the thickness expansion for $\boldsymbol{s}$ is obtained via Taylor polynomials, then for each scalar displacement component we have

$$\begin{aligned} u(x,y,z,t) &= F_0u_0 + F_1u_1 + \cdots + F_Nu_N = F_\tau(z)u_\tau(x,y,t)\,, \\ v(x,y,z,t) &= F_0v_0 + F_1v_1 + \cdots + F_Nv_N = F_\tau(z)v_\tau(x,y,t)\,, \\ w(x,y,z,t) &= F_0w_0 + F_1w_1 + \cdots + F_Nw_N = F_\tau(z)w_\tau(x,y,t)\,, \end{aligned}$$

with

$$F_\tau(z) = z^\tau\,.$$

Therefore the indipendent variables become the mid-plane displacements u_0, v_0 and w_0 and their high order derivatives. In vectorial notation we can rewrite as

$$\boldsymbol{s}(x,y,z,t) = F_0\boldsymbol{s}_0 + F_1\boldsymbol{s}_1 + \cdots + F_N\boldsymbol{s}_N = F_\tau(z)\boldsymbol{s}_\tau(x,y,t)\,. \tag{2.11}$$

The 2-D models obtained from 2.11 are denoted by EDN, where E indicates that an ESL approach has been employed, D indicates that the adopted variational formulation in based on displacement as primary variables (i.e. PVD) and finally N denotes the order of expansion. It is remarked here that these models do not respect the C_z^0 conditions at the layers interface, neither in term of discontinuity of the displacement slope nor in term of stress continuity.

The ED1 theory needs further comments, because it introduces a contradictory behavior for the plate structure respect to the expected 3-D solution. From equation

2.11 specified for the scalar quantities, the order of the deformations ε_{33} and ε_{11} can be easily obtained

$$\begin{aligned}\varepsilon_{11} &\propto u_{,x}N\,,\\ \varepsilon_{33} &\propto w_{,z}(N-1)\,,\end{aligned} \tag{2.12}$$

where N is again the order of the adopted theory. From the 3-D constitutive relation we have

$$\varepsilon_{33} \propto \nu\varepsilon_{11}\,, \tag{2.13}$$

indicating a physical relation between the out-of-plane deformation and the in-plane one (in this example the x-direction is considered). Now it is clear that when a first order expansion is adopted (ED1), equations 2.12 suggest that ε_{33} is null, whereas equation 2.13 says that it has at least a linear through-the-thickness variation like as ε_{11}. That contradiction originates the thickness locking effect or Poisson locking. This locking behavior holds for thin and thick plates, and can be avoided using EDN models with $N \geq 2$ or modifying the elastic coefficients of the 3-D constitutive relation introducing the $\sigma_{33} = 0$ conditions (see [21] for details). Such a modification permits to obtain the 3-D solutions in thin plate analysis. Clearly, the thickness locking does not affect classical plate theories, like as CPT, FSDT and TSDT; indeed in these cases the plane stress assumption and the assumed constant value for w in the thickness direction introduce no contradictory effects.

2.3.2 Mechanical variables, LW theories

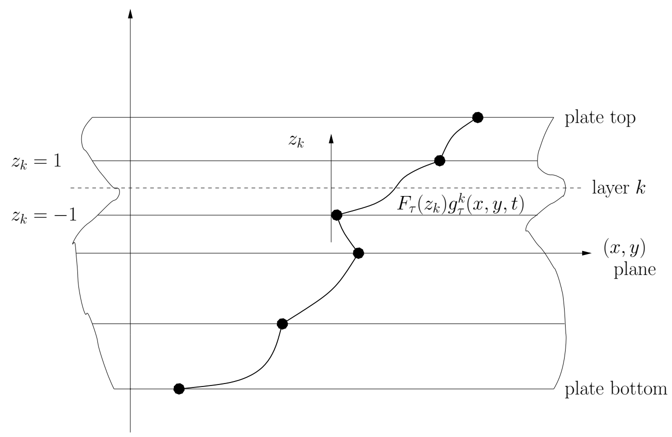

Figure 2.4: LW model.

When each layer of a multilayered structure is described as an indipendent plate, LW approach is accounted for. The displacement $\boldsymbol{s}^k$ is described for each layer, satisfying naturally the zig-zag form of displacement in transverse-anisotropy structures. The Lagrange polynomials are used for the thickness expansion obtaining

$$\boldsymbol{s}^k(x,y,z_k,t) = F_t\boldsymbol{s}_t^k + F_r\boldsymbol{s}_r^k + \cdots + F_b\boldsymbol{s}_b^k = F_\tau(z_k)\boldsymbol{s}_\tau^k(x,y,t)\,, \tag{2.14}$$

where, thanks to the properties of Lagrange polynomials, $\boldsymbol{s}_t$ is the displacement vector at the top of the considered layer, $\boldsymbol{s}_b$ is the displacement vector at the bottom of the considered layer and $\boldsymbol{s}_r$, with $r = 2, \cdots, N-1$ is the displacement vector in the points associated with the Lagrange function r. As we will see in the next sections of the present chapter, the variables at top and bottom of each layer permit to satisfy the displacement continuity at the layer interfaces. Moreover, a LW description of the plate allows easily to an accurate 3-D description of the boudary conditions, since the expansion coefficients $\boldsymbol{s}_\tau^k$ are the through-the-thickness displacements.

LDN is the notation adopted for LW models; L denotes the use of a LW description and D and N indicates again the PVD variational principle and the order of the expansion. Thanks to the piecewise constant behavior for ε_{33} when LD1 theory is adopted, no thickness locking effect are observed for transverse anisotropic plates.

2.3.3 Electrical variables, LW theories

The electric potential is modeled always as a LW variable. Then we have

$$\psi^k(x,y,z_k,t) = F_t\psi_t^k + F_r\psi_r^k + \cdots + F_b\psi_b^k = F_\tau(z_k)\psi_\tau^k(x,y,t)\,, \tag{2.15}$$

with the notation described above.

2.3.4 Condensed notation

Using the condensed structural variable $\boldsymbol{\mathcal{U}}$ introduced in section 2.2, the previous kinematic and electric axiomatic assumptions can be rearranged in order to give

$$\boldsymbol{\mathcal{U}}^k(x,y,z,t) = F_\tau(z)\boldsymbol{\mathcal{U}}_\tau^k(x,y,t)\,, \tag{2.16}$$

where, when F_τ refers to electric potential variables, a LW description is always imposed, whereas the mechanical displacements can be described as ESL or LW. Moreover, when ESL description is employed, z indicates the whole plate thickness coordinate, whereas for LW assumption, z indicates the k^{th} lamina local thickness coordinate. It is noted that the plate reference system (x, y, z), where the thickness exapansion is employed, does not necessarily coincide with the global sistem of reference (X, Y, Z) which describes the entire vibro-acoustic coupled system (see figure 2.5). This is important when the FE approximation is introduced; indeed the mechanical degrees-of-freedom must be transformed through a rotation matrix to obtain a description in terms of global coordinates.

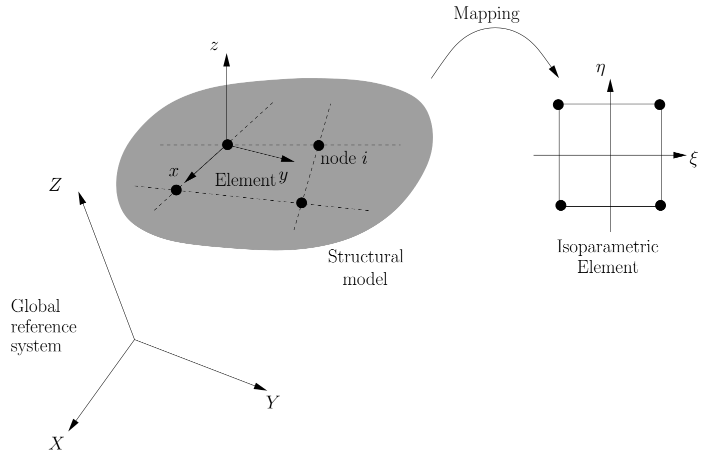

Figure 2.5: FE reference systems.

2.4 Finite Element approximation

In this section the FE approximation of the variational formulation 2.9 is considered. In the FE implementation, the unknowns can be expressed in terms of their nodal values via appropriate shape functions N_i. Thus for the structural variable $\boldsymbol{\mathcal{U}}^k_\tau$ and for the fluid scalar variable p we have

$$\boldsymbol{\mathcal{U}}^k_\tau(x,y,t) = N^s_i(x,y)\boldsymbol{\mathcal{Q}}^k_{\tau i}(t)\,, \tag{2.17}$$
$$p(x,y,z,t) = N^p_i(x,y,z)P_i(t)\,, \tag{2.18}$$

where $i = 1, \cdots, N^s_n$ for structure variables, with N^s_n denotes the number of nodes of the considered 2-D structural element, and $i = 1, \cdots, N^p_n$ for fluid variable, with N^p_n denotes the number of nodes of the considered 3-D acoustic element. From the previous condensed notation for the structure,

$$\boldsymbol{\mathcal{Q}}^k_{\tau i} = \left\{ \mathcal{Q}^k_{u_\tau i}\, \mathcal{Q}^k_{v_\tau i}\, \mathcal{Q}^k_{w_\tau i}\, \mathcal{Q}^k_{\psi_\tau i} \right\}^{\mathrm{T}}\,,$$

therefore $\boldsymbol{\mathcal{Q}}^k_{\tau i}$ contains the FE nodal values of the thickness expansion coefficients provided by UF axiomatic model for the plate subsystem. Then substituting 2.17 into 2.16 we have the final form of the approximated structural field variables in the plate element reference system of figure 2.5:

$$\boldsymbol{\mathcal{U}}^k(x,y,z,t) = F_\tau(z)N^s_i(x,y)\boldsymbol{\mathcal{Q}}^k_{\tau i}(t)\,, \tag{2.19}$$

where $k = 1, \cdots, N_{lay}$, with N_{lay} number of the plate embedded layers.

In this work the four-nodes quadrilateral element and the eight-nodes hexahedral element with isoparametric formulation are adopted for the structural and acoustic modeling, respectively. The integral terms of the FE matrices are calculated on the isoparametric element through the definition of the jacobian matrix $\mathbf{J}$ which defines the relation between the local and isoparametric element. Then, the final rotation is applied on the mechanical displacement to obtain the final equations in the global reference system (see figure 2.5).

In the following, the structural mass $\mathbf{M}$ and stiffness matrix $\mathbf{K}$, loads vector $\mathbf{F}$ and the fluid coupling matrix $\mathbf{S}$ are obtained in terms of fundamental nuclei, which are indipendent from the type and the order of the considered expansion in the thickness direction. First, the nucleus of the stiffness matrix $\mathbf{K}$ for the piezoelectric orthotropic plate modeled with the UF approach is derived; then the nucleus of the external loads vector $\mathbf{F}$ applied on the FE structure is presented. With the same approach, the inertial and fluid loads are considered, bringing to the definition of the nucleus of the mass and coupled matrices $\mathbf{M}$ and $\mathbf{S}$. Moreover, also the classical acoustic mass $\mathbf{Q}$ and stiffness $\mathbf{H}$ matrices are presented. Finally the assembling procedure from the nucleus level to the global FE matrices is described, showing the difference between the ESL and LW description. Thus, the chapter ends with the final FE matrix equation, which is formally the same as 1.12. In order to lighten the notation, in the following the dependencies of the shape functions and of the thickness functions from the x, y and z coordinates are omitted.

2.4.1 Structural stiffness matrix

Let us consider the left hand side term of the first equation of system 2.9. Using the condensed relation 2.5 and 2.7 with the partitioning presented in equations 2.4, 2.6 and 2.8, we have

$$
\begin{aligned}
\int_{\Omega_s^k} \delta\boldsymbol{\mathcal{E}}^{k^{\mathrm{T}}} \boldsymbol{\mathcal{S}}^k \,\mathrm{d}V &= \int_{\Omega_s^k} \left(\delta\boldsymbol{\mathcal{E}}_p^{k^{\mathrm{T}}} \boldsymbol{\mathcal{S}}_p^k + \delta\boldsymbol{\mathcal{E}}_n^{k^{\mathrm{T}}} \boldsymbol{\mathcal{S}}_n^k\right) \mathrm{d}V = \\
&= \int_{\Omega_s^k} \delta\boldsymbol{\mathcal{U}}^{k^{\mathrm{T}}} \Big[\boldsymbol{\mathcal{D}}_p^{\mathrm{T}} \boldsymbol{\mathcal{C}}_p^k \boldsymbol{\mathcal{D}}_p + \boldsymbol{\mathcal{D}}_p^{\mathrm{T}} \boldsymbol{\mathcal{C}}_{np}^k \left(\boldsymbol{\mathcal{D}}_{n_z} + \boldsymbol{\mathcal{D}}_{n_p}\right) + \\
&\quad + \left(\boldsymbol{\mathcal{D}}_{n_z} + \boldsymbol{\mathcal{D}}_{n_p}\right)^{\mathrm{T}} \boldsymbol{\mathcal{C}}_{np}^k \boldsymbol{\mathcal{D}}_p + \left(\boldsymbol{\mathcal{D}}_{n_z} + \boldsymbol{\mathcal{D}}_{n_p}\right)^{\mathrm{T}} \boldsymbol{\mathcal{C}}_{nn}^k \left(\boldsymbol{\mathcal{D}}_{n_z} + \boldsymbol{\mathcal{D}}_{n_p}\right)\Big] \boldsymbol{\mathcal{U}}^k \,\mathrm{d}V\,.
\end{aligned}
\tag{2.20}
$$

Introducing the through-the-thickness integrals defined as

$$
\begin{aligned}
E_{\tau s}^k &= \int_{t_k} F_\tau F_s \,\mathrm{d}z\,, \\
E_{\tau_{,z} s}^k &= \int_{t_k} F_{\tau_{,z}} F_s \,\mathrm{d}z\,, \\
E_{\tau s_{,z}}^k &= \int_{t_k} F_\tau F_{s_{,z}} \,\mathrm{d}z\,, \\
E_{\tau_{,z} s_{,z}}^k &= \int_{t_k} F_{\tau_{,z}} F_{s_{,z}} \,\mathrm{d}z\,,
\end{aligned}
$$

and defining

$$\boldsymbol{\mathcal{D}}_{n_z} F_\tau = \begin{bmatrix} 0 & 0 & 1 & 0 \\ 1 & 0 & 0 & 0 \\ 0 & 1 & 0 & 0 \\ 0 & 0 & 0 & -1 \end{bmatrix} F_{\tau,z} = \tilde{\mathbf{I}} F_{\tau,z} \,,$$

we can finally rewrite equation 2.20 as

$$\begin{aligned} \int_{\Omega_s^k} \delta \boldsymbol{\mathcal{E}}^{k^{\mathrm{T}}} \boldsymbol{\mathcal{S}}^k \,\mathrm{d}V = \delta \boldsymbol{\mathcal{Q}}_{\tau i}^{k^{\mathrm{T}}} \int_{A^k} \Big[E_{\tau s}^k \Big(& N_i^s \boldsymbol{\mathcal{D}}_p^{\mathrm{T}} \boldsymbol{\mathcal{C}}_{pp}^k \boldsymbol{\mathcal{D}}_p N_j^s + N_i^s \boldsymbol{\mathcal{D}}_p^{\mathrm{T}} \boldsymbol{\mathcal{C}}_{pn}^k \boldsymbol{\mathcal{D}}_{n_p} N_j^s + \\ & + N_i^s \boldsymbol{\mathcal{D}}_{np}^{\mathrm{T}} \boldsymbol{\mathcal{C}}_{np}^k \boldsymbol{\mathcal{D}}_p N_j^s + N_i^s \boldsymbol{\mathcal{D}}_{np}^{\mathrm{T}} \boldsymbol{\mathcal{C}}_{nn}^k \boldsymbol{\mathcal{D}}_{n_p} N_j^s \Big) + \\ & + E_{\tau_{,z} s}^k \Big(N_i^s \tilde{\mathbf{I}}^{\mathrm{T}} \boldsymbol{\mathcal{C}}_{np}^k \boldsymbol{\mathcal{D}}_p N_j^s + N_i^s \tilde{\mathbf{I}}^{\mathrm{T}} \boldsymbol{\mathcal{C}}_{nn}^k \boldsymbol{\mathcal{D}}_{n_p} N_j^s \Big) + \\ & + E_{\tau s_{,z}}^k \Big(N_i^s \boldsymbol{\mathcal{D}}_p^{\mathrm{T}} \boldsymbol{\mathcal{C}}_{pn}^k \tilde{\mathbf{I}} N_j^s + N_i^s \boldsymbol{\mathcal{D}}_{n_p}^{\mathrm{T}} \boldsymbol{\mathcal{C}}_{nn}^k \tilde{\mathbf{I}} N_j^s \Big) + \\ & + E_{\tau_{,z} s_{,z}}^k \Big(N_i^s \tilde{\mathbf{I}}^{\mathrm{T}} \boldsymbol{\mathcal{C}}_{nn}^k \tilde{\mathbf{I}} N_j^s \Big) \Big] \,\mathrm{d}s \, \boldsymbol{\mathcal{Q}}_{sj}^k = \\ & = \delta \boldsymbol{\mathcal{Q}}_{\tau i}^{k^{\mathrm{T}}} \mathbf{K}^{k\tau s i j} \boldsymbol{\mathcal{Q}}_{sj}^k \,, \end{aligned} \tag{2.21}$$

where the 4×4 stiffness nucleus $\mathbf{K}^{k\tau sij}$ for the piezoelectric structure has been defined and A^k is the reference surface area of each layer. The explicit form of $\mathbf{K}^{k\tau sij}$ is reported in Appendix A.

2.4.2 Structural external loads

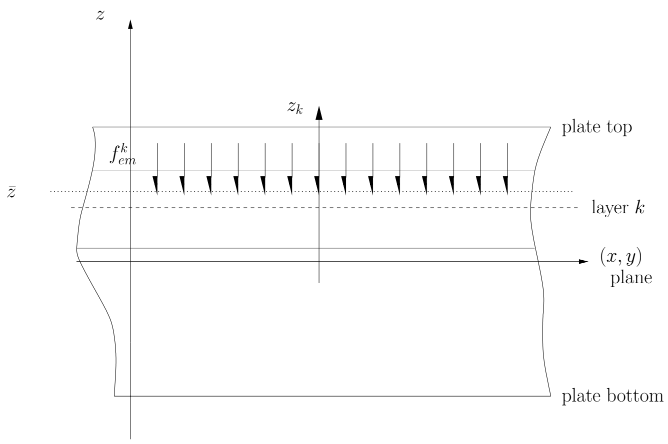

Figure 2.6: External loads on layer k.

Let us consider now the generilized electromechanical load $\mathbf{f}_{em}^k$ applied on the k^{th} layer (see figure 2.6). From right hand side of the first equation of system 2.9 we have that the work done by $\mathbf{f}_{em}^k$ is

$$\int_{\Gamma^k} \delta\boldsymbol{\mathcal{U}}^{k^{\mathrm{T}}} \mathbf{f}^k_{em}\, \mathrm{d}s \,,$$

where

$$\mathbf{f}^k_{em}(x,y) = \left\{ \begin{array}{c} f_u(x,y) \\ f_v(x,y) \\ f_w(x,y) \\ Q(x,y) \end{array} \right\} .$$

Then substituting the FE approximation of the UF variables (equation 2.19) and writing an energetically consistent load obtained interpolating the load with the same shape functions N^s_j, we obtain

$$\int_{\Gamma^k} \delta\boldsymbol{\mathcal{U}}^{k^{\mathrm{T}}} \mathbf{f}^k_{em}\, \mathrm{d}s = \delta\boldsymbol{\mathcal{Q}}^{k^{\mathrm{T}}}_{\tau i} F_\tau(\bar{z}) \int_{A^k} N^s_i N^s_j \,\mathrm{d}s\ \mathbf{a}_j \,, \tag{2.22}$$

with A_k that is the reference surface area for layer k, and the components of $\mathbf{a}_j$ are the loads evaluated on the considered element node j. Finally we can rewrite 2.22 as

$$\int_{\Gamma^k} \delta\boldsymbol{\mathcal{U}}^{k^{\mathrm{T}}} \mathbf{f}^k_{em}\, \mathrm{d}s = \delta\boldsymbol{\mathcal{Q}}^{k^{\mathrm{T}}}_{\tau i} \left\{ \begin{array}{c} F_\tau(\bar{z}) \int_{A^k} N^s_i N^s_j \,\mathrm{d}s\, f_{u\,j} \\ F_\tau(\bar{z}) \int_{A^k} N^s_i N^s_j \,\mathrm{d}s\, f_{v\,j} \\ F_\tau(\bar{z}) \int_{A^k} N^s_i N^s_j \,\mathrm{d}s\, f_{w\,j} \\ F_\tau(\bar{z}) \int_{A^k} N^s_i N^s_j \,\mathrm{d}s\, Q_j \end{array} \right\} = \delta\boldsymbol{\mathcal{Q}}^{k^{\mathrm{T}}}_{\tau i} \mathbf{F}^k_{\tau j} \,, \tag{2.23}$$

where $\mathbf{F}^k_{\tau j}$ indicates the fundamental 4×1 nuclei of the external loads, and expression 2.23 indicates the energetically equivalent work done by the distributed load $\mathbf{f}^k_{em}$ on the layer k. Clearly, if no loads are applied on k^{th} lamina, expression 2.23 is null and no contribution on the external work is given by the considered layer. Finally, considering the case of a concentrated load $\mathbf{f}^k_{em}(\bar{x},\bar{y})$ when the application point coincides with the node i of the finite element model (i.e. $(\bar{x},\bar{y}) = (x_i, y_i)$), the work done on the layer k is simply

$$\int_{\Gamma^k} \delta\boldsymbol{\mathcal{U}}^{k^{\mathrm{T}}} \mathbf{f}^k_{em}\, \delta(x-\bar{x}, y-\bar{y})\, \mathrm{d}s = \delta\boldsymbol{\mathcal{Q}}^{\mathrm{T}}_{\tau i} F_\tau(\bar{z}) \mathbf{f}^k_{em_i} \,,$$

where $\mathbf{f}^k_{em_i}$ is the load applied on the i^{th} node on the k^{th} layer, and $\delta(x-\bar{x}, y-\bar{y})$ is the Dirac's delta function. This term is non null only if the load is applied on the considered node i.

2.4.3 Structural mass matrix

The virtual work done by the inertial loads of the k^{th} layer for the structural variables $\boldsymbol{\mathcal{U}}^k$ can be rewritten as

$$\int_{\Omega_s^k} \delta \boldsymbol{\mathcal{U}}^{k^{\mathrm{T}}} \mathbf{f}_m^k \,\mathrm{d}s = \int_{\Omega_s^k} \delta \boldsymbol{\mathcal{U}}^{k^{\mathrm{T}}} \rho_s^k \hat{\mathbf{I}} \ddot{\boldsymbol{\mathcal{U}}}^k \,\mathrm{d}s\,, \tag{2.24}$$

where we have introduced the $\hat{\mathbf{I}}$ matrix defined as

$$\hat{\mathbf{I}} = \begin{bmatrix} 1 & 0 & 0 & 0 \\ 0 & 1 & 0 & 0 \\ 0 & 0 & 1 & 0 \\ 0 & 0 & 0 & 0 \end{bmatrix}\,,$$

and it shows that no mass is associated with electrical degree of freedom (an electrostatic approximation is adopted for the electrical problem). Again, using the FE approximation 2.19, we finally obtain

$$\begin{aligned} \int_{\Omega_s^k} \delta \boldsymbol{\mathcal{U}}^{k^{\mathrm{T}}} \mathbf{f}_m^k \,\mathrm{d}s &= \delta \boldsymbol{\mathcal{Q}}_{\tau i}^{k^{\mathrm{T}}} E_{\tau s}^k \int_{A^k} N_i^s \rho_s^k \hat{\mathbf{I}} N_j^s \,\mathrm{d}s \ddot{\boldsymbol{\mathcal{Q}}}_{sj}^k = \\ &= \delta \boldsymbol{\mathcal{Q}}_{\tau i}^{k^{\mathrm{T}}} \mathbf{M}^{k\tau sij} \ddot{\boldsymbol{\mathcal{Q}}}_{sj}^k\,, \end{aligned} \tag{2.25}$$

where it has been introduced the 4×4 mass matrix nucleus $\mathbf{M}^{k\tau sij}$.

2.4.4 Fluid-Strucure coupling matrix

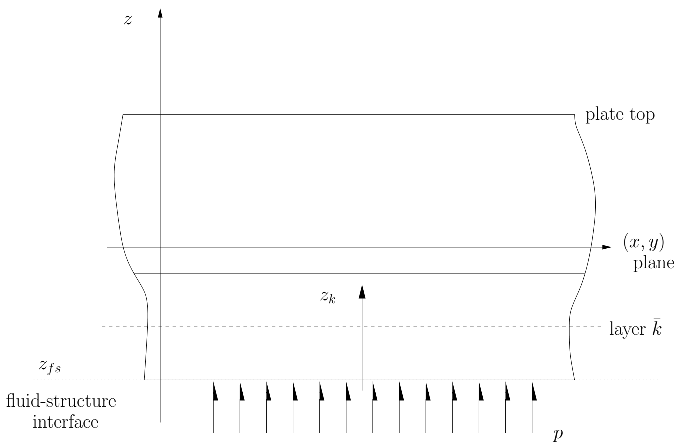

Figure 2.7: Acoustic load.

Let us consider the work done by the fluid (see figure 2.7) on the structural variables. Again, using the FE approximation 2.19 we have

$$
\begin{aligned}
\int_{\Gamma_{fs}} \delta \boldsymbol{\mathcal{U}}^{\bar{k}^{\mathrm{T}}} \mathbf{f}_{sf}\, \mathrm{d}s &= \delta \boldsymbol{\mathcal{Q}}_{\tau i}^{\bar{k}^{\mathrm{T}}} F_\tau(z_{fs}) \int_{A^{\bar{k}}} N_i^s N_j^p\, \mathrm{d}s \left\{ \begin{array}{c} \boldsymbol{n} \\ 0 \end{array} \right\} P_j = \\
&= \delta \boldsymbol{\mathcal{Q}}_{\tau i}^{\bar{k}^{\mathrm{T}}} \left\{ \begin{array}{c} F_\tau(z_{fs}) \int_{A^{\bar{k}}} N_i^s N_j^p\, n_x\, \mathrm{d}s \\ F_\tau(z_{fs}) \int_{A^{\bar{k}}} N_i^s N_j^p\, n_y\, \mathrm{d}s \\ F_\tau(z_{fs}) \int_{A^{\bar{k}}} N_i^s N_j^p\, n_z\, \mathrm{d}s \\ 0 \end{array} \right\} P_j = \\
&= \boldsymbol{\mathcal{Q}}_{\tau i}^{\bar{k}^{\mathrm{T}}} \mathbf{S}^{\bar{k}\tau ij} P_j \,,
\end{aligned}
\tag{2.26}
$$

where 4×1 the fluid coupling nucleus is $\mathbf{S}^{\bar{k}\tau ij}$ obtained. It is remarked that in equation 2.26 the acoustic shape functions N_j^p are evalueted at the fluid structure interface, i.e. on the reference plane A^k (see figure 2.8). Moreover, with the same procedure it can be demonstrated that the work made by the structure on the fluid is

$$
\int_{\Gamma^{fs}} \delta p\, f_{fs}\, \mathrm{d}s = \delta P_i\, \rho_f \mathbf{S}^{\bar{k}\tau ij^{\mathrm{T}}} \ddot{\boldsymbol{\mathcal{Q}}}_{\tau j}^{\bar{k}} \,, \tag{2.27}
$$

where the 1×4 transpose coupling matrix nucleus is obtained. A careful analysis of the nucleus pattern show that the fluid pressure works only for the machanical structural degrees-of-freedom, as expected.

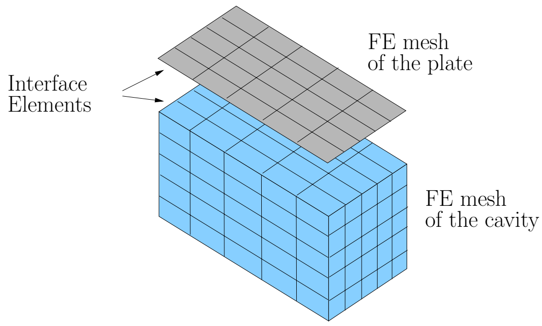

Figure 2.8: Acoustic-structure interface of a simple plate-cavity FE model.

2.4.5 Fluid stiffness and mass matrices

Concerning the fluid internal work and inertial load of system 2.9, using the FE interpolation of the fluid variable p (equation 2.18), we obtain the acoustic stiffness matrix

$$
\int_{\Omega^f} \delta p_{,l}\, p_{,l}\, \mathrm{d}V = \delta P_i \int_{\Omega^f} N_{i,l}^p N_{j,l}^p\, \mathrm{d}V\, P_j = \delta P_i \mathrm{H}^{ij} P_j \,, \tag{2.28}
$$

and the acoustic mass matrix

$$
\frac{1}{c_f^2} \int_{\Omega^f} \delta p\, \ddot{p}\, \mathrm{d}V = \delta P_i\, \frac{1}{c_f^2} \int_{\Omega^f} N_i^p N_j^p\, \mathrm{d}V\, \ddot{P}_j = \delta P_i \mathrm{Q}^{ij} \ddot{P}_j \,, \tag{2.29}
$$

2.5 Assembly procedure and final form of the coupled equations

In this section the assembly procedure for the FE matrices obtained in the previous section is presented. First of all, substituting the relations 2.21, 2.25, 2.27, 2.23, 2.28 and 2.29 into the variational formulation 2.9, we obtain the following equations for the arbitrary virtual displacement $\delta \boldsymbol{\mathcal{Q}}^k_{\tau i}$ and δP_l:

$$\begin{cases} \delta \boldsymbol{\mathcal{Q}}^k_{\tau i} & : \ \mathbf{M}^{k\tau sij} \ddot{\boldsymbol{\mathcal{Q}}}^k_{sj} + \mathbf{K}^{k\tau sij} \boldsymbol{\mathcal{Q}}^k_{sj} - \mathbf{S}^{\bar{k}\tau im} P_m = \mathbf{F}^{k\tau ij} \\ \delta P_l & : \ \mathrm{Q}^{lm} \ddot{P}_m + \mathrm{H}^{lm} P_m + \rho_f \mathbf{S}^{\bar{k}slj^{\mathrm{T}}} \boldsymbol{\mathcal{Q}}^k_{sj} = \mathbf{0} \end{cases} \tag{2.30}$$

where

$$\begin{aligned} \tau, s &= 1, \cdots, N\,, \\ k &= 1, \cdots, N_{lay}\,, \\ i, j &= 1, \cdots, N^s_n\,, \\ l, m &= 1, \cdots, N^p_n\,. \end{aligned}$$

It is remarked that $\mathbf{S}^{\bar{k}\tau im}$ (and its transpose in the fluid equation) is non null only for $k = \bar{k}$ and for fluid and structure nodes i and m that belong on the interface finite elements. Moreover, the term $\mathbf{F}^{k\tau ij}$ is non null only if the considered layer k is mechanically or electrically (or both) loaded. The system 2.30 is the starting point for the assembly procedure. Indeed, in addition to the classical FE assembly on the nodes ij and lm of the structural and fluid elements, the matrices that pre- or post-multiply the structural unknown $\boldsymbol{\mathcal{Q}}$ (or its variation) must be assembled on the indexes τ, s and k. It is noted that the fundamental nuclei appear in system 2.30 do not depend on the adopted LW or ESL theory; indeed, even if the correct thickness integrals must be used, no formally dependencies are observed. Moreover, pure mechanical cases can be easily modeled considering only the mechanical partition of each nucleus, obtaining a 3×3 stiffness and mass nucleus and 3×1 loads nuclei. On the other hand, the assembly procedure on the index k makes the difference between the ESL and LW description of the multilayered plate.

Indexes τ and s indicates which coefficient of the UF expansion is considered. This layer level assembly does not depend on the assumed kinematic description (ESL or LW). Given the expansion order N, the degrees-of-freedom for the k^{th} layer and node i (or j) are:

$$\boldsymbol{\mathcal{Q}}^k_i = \left\{ \ \boldsymbol{\mathcal{Q}}^{k^{\mathrm{T}}}_{1i} \quad \boldsymbol{\mathcal{Q}}^{k^{\mathrm{T}}}_{2i} \quad \cdots \quad \boldsymbol{\mathcal{Q}}^{k^{\mathrm{T}}}_{Ni} \ \right\}^{\mathrm{T}}\,. \tag{2.31}$$

Then the assembly on the multilayered level has to be performed. In the following the index k is assumed varying from the top layer (denoted by $k = 1$) to the bottom one (denoted by $k = N_{lay}$). For ESL theories, the degrees-of-freedom of each layer are the same and they refer to the description of an equivalent single layer plate. Then we have

$$\mathcal{Q}_i = \mathcal{Q}_i^1 = \mathcal{Q}_i^2 = \cdots = \mathcal{Q}_i^{N_{lay}}, \tag{2.32}$$

consequently the contribution of the mass and stiffness matrices and of the load vectors of each layers are added together. On the other hand, the assembly procedure at multilayer level for LW theory makes it possible to fulfill the C_z^0 continuity for the displacement field. Indeed the assembled unknown vector on multilayer level for LW models is

$$\mathcal{Q}_i = \left\{ \cdots \quad \mathcal{Q}_{ti}^{k^{\mathrm{T}}} \quad \mathcal{Q}_{ri}^{k^{\mathrm{T}}} \quad \mathcal{Q}_{bi}^{k^{\mathrm{T}}} = \mathcal{Q}_{ti}^{k-1^{\mathrm{T}}} \quad \mathcal{Q}_{ri}^{k-1^{\mathrm{T}}} \quad \cdots \right\}^{\mathrm{T}}, \tag{2.33}$$

with $r = 1, \cdots, N-1$ and the variables associated with $\tau = 1$ or $\tau = N$ are replaced with subscripts t and b indicating the top and the bottom of each layer. Therefore, only the mass, stiffness and load contributions from the top and the bottom of two adiacent layer are added together. A clear example of an ESL and LW mass or stiffness matrix assembly is reported in figure 2.9. In case of a mixed description of the UF variables, like as the electromechanical case with an ESL description for the displacement $\boldsymbol{s}$ and a LW model for the electric potential ψ, we have that the mechanical variables are assembled as 2.32 and electric degrees-of-freedom as 2.33. In this way, the assembled unknown vector at node level is:

$$\mathcal{Q}_i = \left\{ \boldsymbol{\mathcal{M}}_i^{1^{\mathrm{T}}} = \boldsymbol{\mathcal{M}}_i^{2^{\mathrm{T}}} = \cdots = \boldsymbol{\mathcal{M}}_i^{N_{lay}^{\mathrm{T}}} \quad \cdots \quad \Big| \quad \cdots \quad \mathcal{Z}_{ti}^k \quad \mathcal{Z}_{ri}^k \quad \mathcal{Z}_{bi}^k = \mathcal{Z}_{ti}^{k-1} \quad \mathcal{Z}_{ri}^{k-1} \quad \cdots \right\}^{\mathrm{T}}, \tag{2.34}$$

where $\boldsymbol{\mathcal{M}}$ indicates the mechanical degrees-of-freedom and $\mathcal{Z}$ the electrical ones; threfore the following partitioning has been assumed:

$$\mathcal{Q}_{\tau i}^k = \left\{ \boldsymbol{\mathcal{M}}_{\tau i}^{k^{\mathrm{T}}} \quad \mathcal{Z}_{\tau i}^k \right\}^{\mathrm{T}}.$$

Finally the classical FE global assembly must be performed, eliminating also the indexes ij and lm. Assuming the following organization for the system unknowns

$$\begin{aligned} \mathcal{Q} &= \left\{ \mathcal{Q}_1^{\mathrm{T}} \quad \cdots \quad \mathcal{Q}_{N_n^s}^{\mathrm{T}} \right\}^{\mathrm{T}}, & (2.35)\\ \mathbf{P} &= \left\{ P_1 \quad \cdots \quad P_{N_n^p} \right\}^{\mathrm{T}}, & (2.36) \end{aligned}$$

the system 2.30 leads to the following coupled problem

$$\begin{bmatrix} \mathbf{M} & 0 \\ -\rho_f \mathbf{S}^{\mathrm{T}} & \mathbf{Q} \end{bmatrix} \begin{Bmatrix} \ddot{\mathcal{Q}} \\ \ddot{\mathbf{P}} \end{Bmatrix} + \begin{bmatrix} \mathbf{K} & \mathbf{S} \\ 0 & \mathbf{H} \end{bmatrix} \begin{Bmatrix} \mathcal{Q} \\ \mathbf{P} \end{Bmatrix} = \begin{Bmatrix} \mathbf{F} \\ 0 \end{Bmatrix}, \tag{2.37}$$

which is formally the same (u, p) system presented at the end of the Chapter 1, and the same considerations about the condensation of the electrical degrees-of-freedom are still valid. The matrix equation 2.37 with the related Dirichlet boundary conditions on the structural variables $\boldsymbol{\mathcal{Q}}$, describes the coupled pizoelectric structural acoustic system. In this work the eigenvalue problem and the frequency response analysis associated with equation 2.37 is considered. It is anticipated here that solving this coupled large unsymmetric system is a cumbersome task; in the next chapter the method adopted in this work is presented.

A FE code based on the formulation presented in this chapter has been implemented. In particular, even if a structural FE code based on the UF was available at the Department of Aerospace Engineering of Politecnico di Torino, a new code has been written in order to efficiently solve large static and dynamic problems containing the computational time and memory requirements. A FE acoustic codes has been written too, and coupled with the structural model. A brief overview of the important programming details are reported in Appendix B.

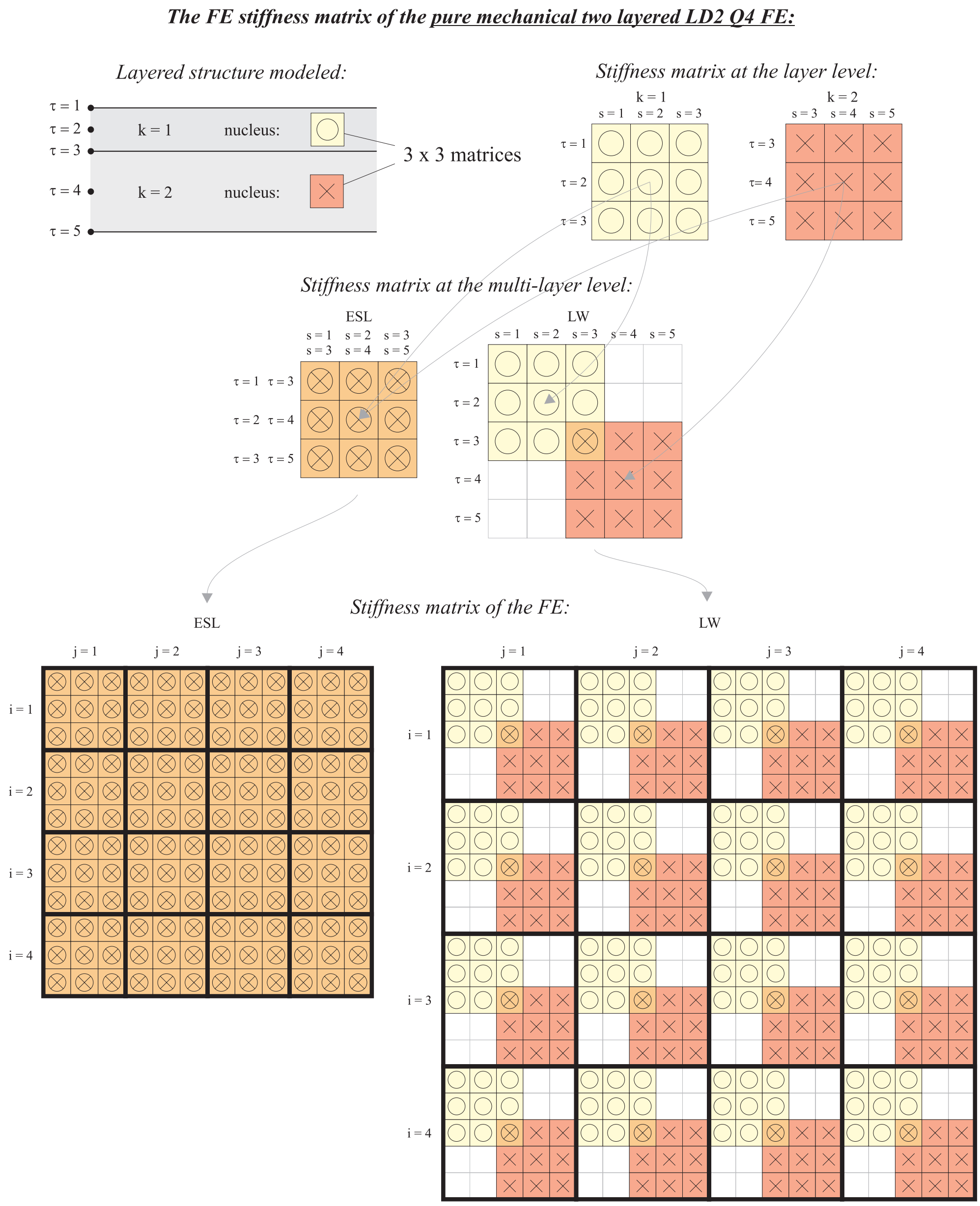

Figure 2.9: Example of the assembly procedure from nucleus to element level for a four-node quadrilateral element.

CHAPTER 3

Modal Coupling Method

The system 2.37 decribing the dynamic behavior of the plate-cavity system is analyzed in the frequency domain in order to obtain the transfer functions relative to the desired system outputs. Typically, the output parameters considered in vibro-acoustic analysis are both local and global. The former refers to structural displacement or acoustic pressure at specific points, whereas the latter refers to energy parameters such as the structural kinetic energy and the fluid potential energy. Direct resolution of the forced system 2.37 is time consuming. To alleviate this problem, modal approach are often used. Unfortunately, the coupled eigenproblem is large and unsymmetric, thus the computationl time needed to extract the modal basis may be significant.

As it has been pointed out in the introduction of this work, alternative approaches to the non-symmetric (u, p) formulation have been developed. Even if different strategies can lead to a symmetric problem, the final system of equations can be twice or more the dimension of system 2.37. A widely used technique in the acoustic-structure interaction problem is based on the use of the uncoupled modal basis. In this approach, the in vacuo structure modes and the rigid walled cavity modes are considered in order to obtain a new basis to describe the coupled problem. In this way, two smaller and symmetric eigenvalue problems must be solved. Moreover, only few eigenvalue-eigenvector pairs are needed from the large FE structural and acoustic models, then iterative solvers can be succesfully utilized, obtaining a further reduction of the computational effort. Unfortunately, there is no reliable criterion for chosing the number of kept modes for each subsystem; indeed, the uncoupled basis does not decouple the fluid-structure system, then, theoretically, all the subsystem modes are coupled together because of the matrix $\mathbf{S}$. The poor efficiency of the uncoupled modal basis in reducing coupled model size is due to the fact that the modes of the uncoupled acoustic model do not fulfill the continuity condition at the plate interface; therefore, for an accurate representation of the near-field effect in the vicinity of the fluid-plate coupling interface, a possible large number of high order modes in acoustic modal basis is required. This is always true when strong coupled system is considered, whereas the modal basis approach can lead to satisfactory results in terms of accuracy and computational efficiency in case of weak coupled system. For instance, in figures 3.1 and 3.2 a simple isotropic plate coupled with an air filled cavity is considered. The first non null coupled mode (the system has a zero frequency eigenvalue due to the presence of a rigid cavity mode) is computed with an uncoupled modal basis considering 6 structural modes and 8 cavity modes (figure 3.1) and considering 20 structural modes and 60 cavity modes (figure 3.2). It is clear that, even if the natural frequency is almost the same, 8 acoustic modes are a poor basis to reproduce correctly the continuity condition at the fluid-structure interface, demonstrating that even a poor basis can lead to a correct prediction of the global behavior but a larger basis must be accounted for an accurate local description of the system. In the next two sections the construction of the modal basis and the form of the reduced coupled system are presented.

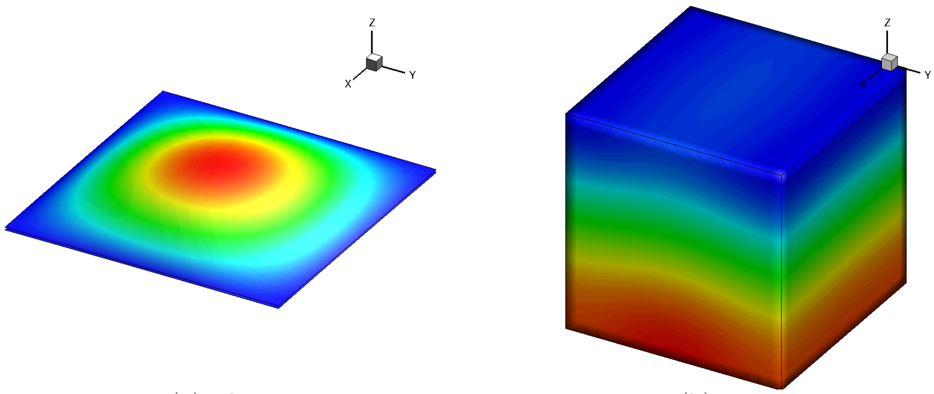

(a) plate (b) cavity

Figure 3.1: First non null coupled mode ($\omega = 50.13$ Hz) calculated with the modal coupling method with 6 structural modes and 8 acoustic modes.

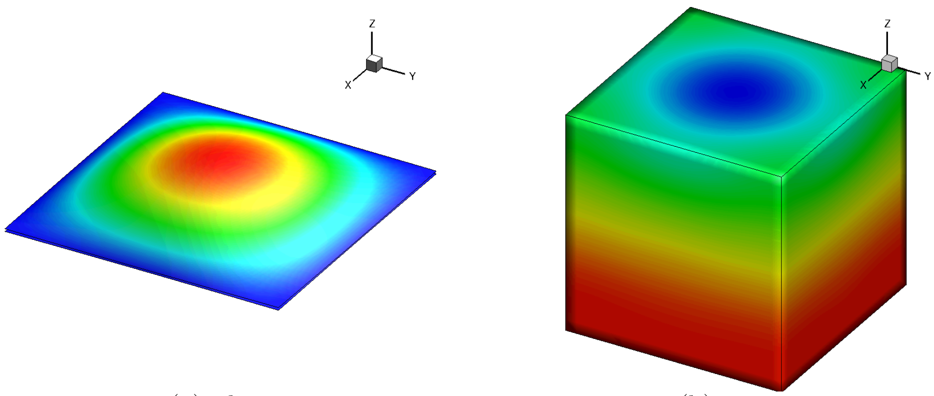

(a) plate (b) cavity

Figure 3.2: First non null coupled mode ($\omega = 50.03$ Hz) calculated with the modal coupling method with 20 structural modes and 60 acoustic modes.

3.1 The uncoupled basis

Using the notation adopted for the submatrices of the system 2.37, the eigenvalue problems relative to the uncoupled subsystems are

$$
\begin{aligned}
(\mathbf{K}-\omega_s^2\mathbf{M})\bar{\boldsymbol{\mathcal{Q}}} &= 0\,,\\
(\mathbf{H}-\omega_p^2\mathbf{Q})\bar{\mathbf{P}} &= 0\,,
\end{aligned}
$$

where ω_s and ω_p are the structural and acoustic uncoupled natural frequencies, and $\bar{\boldsymbol{\mathcal{Q}}}$ and $\bar{\mathbf{P}}$ are the relative eigenvectors. Arranging the first n_s eigenvectors $\bar{\boldsymbol{\mathcal{Q}}}$ in the basis matrix $\mathbf{X}_s$, and the first n_p eigenvectors $\bar{\mathbf{P}}$ in the basis matrix $\mathbf{X}_p$, the structural and acoustic degrees-of-freedom can be expressed as a linear combination of their respective eigenvectors:

$$
\boldsymbol{\mathcal{Q}} = \mathbf{X}_s\boldsymbol{\eta}_s\,, \tag{3.1}
$$

$$
\mathbf{P} = \mathbf{X}_p\boldsymbol{\eta}_p\,, \tag{3.2}
$$

where η_s and η_p represents the modal unknowns (i.e. modal amplitudes). Clearly, if $\boldsymbol{\mathcal{Q}}$ ($\mathbf{P}$) is a vector of lenght N_n^s (N_n^p) and $\mathbf{X}_s$ ($\mathbf{X}_p$) is a $N_n^s \times n_s$ ($N_n^p \times n_p$) basis, then $\boldsymbol{\eta}_s$ ($\boldsymbol{\eta}_p$) is a vector of n_s (n_p) modal unknowns. In a more compact form, relations 3.1 and 3.2 can be rewritten as

$$
\left\{ \begin{array}{c} \boldsymbol{\mathcal{Q}} \\ \mathbf{P} \end{array} \right\} = \left[\begin{array}{cc} \mathbf{X}_s & 0 \\ 0 & \mathbf{X}_p \end{array} \right] \left\{ \begin{array}{c} \boldsymbol{\eta}_s \\ \boldsymbol{\eta}_p \end{array} \right\}. \tag{3.3}
$$

3.2 Reduced model

Relation 3.3 is the coordinates transformation that permits to describe the problem in terms of the smaller modal unknown. Considering a normalization with respect to the corresponding mass matrix for the computed eigenvectors, substituting the relation 3.3 in equation 2.37 and pre-mutiplying by the transpose of the uncoupled basis matrix, we obtain

$$
\left[\begin{array}{cc} \mathbf{I}_s & 0 \\ -\rho_f \mathbf{X}_p^{\mathrm{T}}\mathbf{S}^{\mathrm{T}}\mathbf{X}_s & \mathbf{I}_p \end{array} \right] \left\{ \begin{array}{c} \ddot{\boldsymbol{\eta}}_s \\ \ddot{\boldsymbol{\eta}}_p \end{array} \right\} + \left[\begin{array}{cc} \mathbf{D}_s & \mathbf{X}_s^{\mathrm{T}}\mathbf{S}\mathbf{X}_p \\ 0 & \mathbf{D}_p \end{array} \right] \left\{ \begin{array}{c} \boldsymbol{\eta}_s \\ \boldsymbol{\eta}_p \end{array} \right\} = \left\{ \begin{array}{c} \mathbf{X}_s^{\mathrm{T}}\mathbf{F} \\ 0 \end{array} \right\}, \tag{3.4}
$$

where $\mathbf{I}_s$ and $\mathbf{I}_p$ are identity matrices of dimensions $n_s \times n_s$ and $n_p \times n_p$ respectively, when $\mathbf{D}_s$ and $\mathbf{D}_p$ are diagonal matrices such that

$$
\begin{aligned}
\mathbf{D}_s &= \left[\begin{array}{ccc} \omega_{s_1}^2 & \cdots & 0 \\ 0 & \ddots & 0 \\ 0 & \cdots & \omega_{s_{n_s}}^2 \end{array} \right] = \mathrm{Diag}\left(\omega_{s_i}^2\right)\,,\\
\mathbf{D}_p &= \left[\begin{array}{ccc} \omega_{p_1}^2 & \cdots & 0 \\ 0 & \ddots & 0 \\ 0 & \cdots & \omega_{p_{n_p}}^2 \end{array} \right] = \mathrm{Diag}\left(\omega_{p_i}^2\right)\,,
\end{aligned}
$$

and $\mathbf{X}_s^{\mathrm{T}}\mathbf{F}$ is the structural load vectror projected in the structural modal basis. The off diagonal elements account for the cross coupling between structural and fluid kept modes, constituting a $n_s \times n_p$ (and its transpose) submatrix $\tilde{\mathbf{S}} = \mathbf{X}_s^{\mathrm{T}}\mathbf{S}\mathbf{X}_p$. According to this modal reduction, the forced response of the coupled system 3.4 in the frequency domain is

$$\left(\begin{bmatrix} \mathbf{D}_s & \tilde{\mathbf{S}} \\ 0 & \mathbf{D}_p \end{bmatrix} + j\omega \begin{bmatrix} \mathbf{C}_s & 0 \\ 0 & \mathbf{C}_p \end{bmatrix} - \omega^2 \begin{bmatrix} \mathbf{I}_s & 0 \\ -\rho_f \tilde{\mathbf{S}}^{\mathrm{T}} & \mathbf{I}_p \end{bmatrix}\right) \begin{Bmatrix} \boldsymbol{\eta}_p \\ \boldsymbol{\eta}_s \end{Bmatrix} = \begin{Bmatrix} \tilde{\mathbf{F}} \\ \mathbf{0} \end{Bmatrix}, \quad (3.5)$$

where $\tilde{\mathbf{F}} = \mathbf{X}_s^{\mathrm{T}}\mathbf{F}$, j is the imaginary unit and the diagonal matrix $\mathbf{C}_s$ and $\mathbf{C}_p$ indicates that a modal damping has been taken into account. In particular we have

$$\begin{aligned} \mathbf{C}_s &= \begin{bmatrix} 2\xi_{s_1}\omega_{s_1} & \cdots & 0 \\ 0 & \ddots & 0 \\ 0 & \cdots & 2\xi_{s_{n_s}}\omega_{s_{n_s}} \end{bmatrix} = \mathrm{Diag}\left(2\xi_{s_i}\omega_{s_i}\right) \\ \mathbf{C}_p &= \begin{bmatrix} 2\xi_{p_1}\omega_{p_1} & \cdots & 0 \\ 0 & \ddots & 0 \\ 0 & \cdots & 2\xi_{pn_p}\omega_{p_{n_p}} \end{bmatrix} = \mathrm{Diag}\left(2\xi_{p_i}\omega_{p_i}\right). \end{aligned}$$

The undamped case of equation 3.5 with no applied force is the free response associated with the reduced coupled preblem. Although the obtained eigenvalue problem is still unsymmentric, real eigenvalue and eigenvector couples exist, as demonstrated in [68].

3.3 Energy response parameters

As it is mentioned above, in addition to local parameters, also global idexes are used to analyzed the response of the coupled system. For what concern the acoustic pressure response, the mean-square pressure E_p^f is introduced. Using the FE approximation presented in chapter 2 and introducing the uncoupled modal basis, the mean-square pressure can be expressed as

$$E_p^f = \frac{1}{2}\frac{1}{\Omega_f}\int_{\Omega_f} |p|^2 \,\mathrm{d}V = \frac{1}{2}\frac{c_f^2}{\Omega_f}\boldsymbol{\eta}_p^*\boldsymbol{\eta}_p \quad (3.6)$$

where * denotes che complex conjugate operator of the vector. In some textbook the mean-square pressure is denoted by $\langle p^2 \rangle$; here it is indicated with E_p^f because the expression 3.6 indicates the fluid potential energy for less than a scale factor depending on the fluid properties. Analogously, the kinetic energy of the general orthotropic multilayered plate per unit of volume is

$$E_k^s = \frac{1}{2}\frac{\omega^2}{\Omega_s}\int_{\Omega_s} \rho_s |\boldsymbol{s}|^2 \,\mathrm{d}V = \frac{1}{2}\frac{\omega^2}{\Omega_s}\boldsymbol{\eta}_s^* \boldsymbol{\eta}_s \tag{3.7}$$

thanks to the fact that no mass is associated with the electric degrees-of-freedom. When the embedded layers has the same mass density ρ_s or the plate is isotropic, the specific kinetic energy can be easily computed dividing E_k^s by ρ_s.

CHAPTER 4

Structural Model Validation

This chapter discusses the validation of the structural FE code written to implement the UF presented in chapter 2. The chapter is formally subdivided into three parts; in the first, some preliminary assessments are given to analyze the convergence behaviour of the method; in the second part, some literature benchmarks are given in order to validate the accuracy of the present formulation; finally, some benchmarks are proposed and discussed in order to demonstrate the capabilities of these refined models in predicting higher order modes. According to the aim of the present work, this chapter verifies the capabilities of the present structural model to correctly reproduce the dynamic response of plate structures with different layouts. An extensive validation of the structural FE model is required to guarantee the correct formulation of the structural-acoustic coupling.

The notation assumed for the plate geometry, for the boundary conditions and for the nondimensional parameters used for representing the numerical results are now introduced. First, classical boundary constraints are considered in this work, i.e. simply supported, clamped and free edge conditions. On the generic plate edge at $x = const$, if a simply supported condition (S) is assumed, we have:

$$w = 0,\ v = 0\,,$$

then only the motion normal toi the edge is permitted. The clamped (C) condition assumes that:

$$u = 0,\ w = 0,\ v = 0\,,$$

therefore no displacement of the boundary is permitted. Finally, the completely free condition implies no constraints on the displacement field. For the electric boundary conditions, in an open circuit (OC) condition, the plate is assumed to be grounded along its edges, then

$$\psi = 0\,,$$

whereas in short circuit (SC) condition, also the top and the bottom of the plate are grounded.

Concerning the geometry of the plate, generic quadrilateral forms are considered in the present analysis. In principle, more geomtries could be treated with the adoption of an isoparamentric formulation. However quadrilateral plates are one of the most interesting case in the analysis of acoustic cavities. With the notation depicted in figure 4.1, the boundary condition, for instance, SFCF denotes a quadrilateral plate with edges 1, 2, 3 and 4 having the simply supported, free, clamped and free boundary condition, respectively. When the adopted plate geometry, materials and layouts with its own boundary condition are such that $xz-$ and $yz-$plane are symmetry planes, the classification of the vibration modes into distinct symmetry classes are assumed. Namely, doubly symmetric modes (SS), symmetric-antisymmetric modes (SA), antisymmetric-symmetric modes (AS) and doubly antisymmetric modes (AA). In this way only one quarter of the plate can be analyzed, reducing the computational effort. Typically this classification is adopted in the related literature to sort the modes of isotropic plates with symmetric boundary conditions. In this work we have taken advantage from material and edge constraints symmetries even in case of cross-ply composite plates. Furthermore if also the $xy-$plane is a symmetry plane, symmetric and antisymmetric modes in the thickness direction will be introduced.

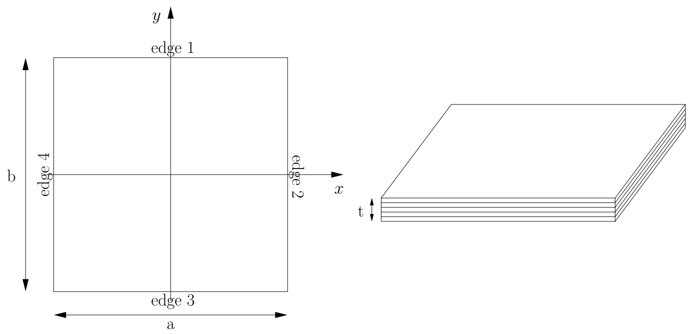

Figure 4.1: Geometry of a rectangular plate.

The following nondimensional frequency parameters are introduced:

- for isotropic plates:

$$\lambda = \omega \frac{b^2}{\pi^2} \sqrt{\frac{\rho t}{D}} \tag{4.1}$$

- for laminated plates:

$$\lambda = \omega b \sqrt{\frac{\rho^{(1)}}{E_2^{(1)}}} \tag{4.2}$$

- for sandwich plates:

$$\lambda = \omega b \sqrt{\left(\frac{\rho}{E_2}\right)_{(f)}} \tag{4.3}$$

where,

$$D = \frac{Et^3}{12\left(1-\nu^2\right)} \tag{4.4}$$

is the flexural rigidity of the isotropic plate. The apices (1) in laminated plates indicates that the properties are referred to the bottom layer, while pedix (f) for sandwich plates is referred to the material properties of the face skins.

In the cases presented below, the results obtained with LD models are limited to fourth order due to the huge computational effort when laminated structures are considered. Despite this limit, it will be clear that LD4 theory can provide a very accurate solution, capturing the 3-D elastic behavior even of complex plate structures. On the other hand, the maximum order of ED models is limited by ill-conditioning issues arising when the order of the adopted theory increases. Moreover, the cases analyzed in this work suggest that ill-conditioning for ED models depends on the thickness ratio and with less emphasis on the structural problem. This misbehavior should not astonish the reader; indeed when plate-like structure are modeled as a 3-D continuum (or quasi-3-D as the present ESL and LW models) some numerical problems arise in the thin plate anlysis, as also mentioned in [76]. Probably the ill-conditioning is due to the Taylor expansion used to describe the through-the-thickness displacement field. Fortunately this limit does not prevent the accuracy of these models as long as the global displacement field assumption is still valid.

In the next three sections the case of electromechanical PVD without fluid coupling will be approached deeply for generic quadrilateral plates with different boundary conditions in order to demonstrate the capabilities of ED and LD theories in predicting high frequency vibrating modes for isotropic and composite plates. For each of these layouts, convergence studies and a numerical validations are presented. Finally a brief comparison between EDN and LDN theories is presented, with the aim of giving a generic view of the benefits and drawbacks of these axiomatic theories with different plate layouts. The material properties adopted in the following analysis are reported in appendix C. Finally, for what concern the FE integration scheme, the selective integration [5, 53] is employed for the adopted isoparametric quadratic element.

4.1 Convergence study

In this section, some suggestive analysis are presented to demonstrate the convergence rate and the numerical stability of the present method. The convergence behavior of several natural frequencies λ are examinated varying different parameters. In particular, in the next sections the effect of the order N, of the adopted theory (LW or ESL), of the thickness ratio, of the boundary constraints, and the effect of the lamination lay-up are briefly presented. We assume that the selected cases are good candidate to demonstrate the numerical properties and accuracy of the present method. The convergence tables are reported for convenience in appendix D, whereas the convergence patterns of the first bending modes varying the aforementioned parameters are reported graphically. In these figures, the percentage error $\varepsilon = \frac{\lambda-\lambda_{conv}}{\lambda_{conv}} \times 100$ with respect to the assumed converged solution and the number of elements n_x, n_y are reported along the y and x axis, respectively. In this convergence study only squared plates are considered. The mesh sizes of the assumed converged solutions are 120×120 and 60×60 for isotropic and laminated plates respectively.

4.1.1 Effect of the adopted theory

In this section the effects of the adopted theory in terms of order N of the through-the-thickness expansion and in terms of the adopted kinematic assumptions (LW or ESL) are presented for isotropic and laminated square plates. In figure 4.2(a) the convergence of the first bending mode of a simply supported isotropic plates with $\nu = 0.3$ and $\frac{t}{b} = 0.1$ is monitored for ED2 and ED3 solutions. The convergence behavior for ED2 and LD1 solutions of a multilayered square plate are reported in figures 4.2(b) and 4.2(c). The former referers to a clamped plate made of material 2 (see appendix C) with lamination sequence 0°/90°/0° and $\frac{t}{b} = 0.01$. The latter is an electromechanical plate made of a cross-ply 0°/90°/0° core of material 2 bonded by two PZT-4 layers. The thickness ratio is $\frac{t}{b} = 0.02$ and the relative thickness of the mechanical and piezoelectric layers are $\frac{t_m}{t} = \frac{11}{45}$ and $\frac{t_p}{t} = \frac{2}{15}$ respectively. The plate is assumed to be clamped and electrically grounded along its edge and OC configuration is considered. From these figures it can be pointed out that the order N and the through-the-thickness assumptions do not affect the convergence behavior. A monotonic downward convergence is always observed.

4.1.2 Effect of the thickness ratio

In this section the effect of the thickness ratio on the convergence pattern is analyzed. In figures 4.3(a) and 4.3(b) the same isotropic and laminated plates described above (see section 4.1.1) are considered for two thickness ratio, $\frac{t}{b} = 0.1$ and $\frac{t}{b} = 0.01$. In figures 4.3(c) and 4.3(d) a fully clamped sandwich plates with lamination sequence 0°/90°/core/0°/90° and made of material 4 with a soft core of material 5, is considered varying the thickness ratio $\frac{t}{b}$ and the relative core-to-faces thickness ratio $\frac{t_c}{t_f}$.

Figures 4.3(a) and 4.3(b) show that, as the thickness ratio decreases, the convergence becomes slower for both ESL and LW theories, with the consequence that a larger number of elements must be accounted to reach the desired accuracy. This behavior, which is more effective for higher order modes (see tables D.1-D.7 and D.8-D.25), is observed also using a Ritz method for 3-D elasticity, as mentioned in [44] and [76]. The same conclusions can be made for a sandwich plates when ESL assumptions are adopted (see figure 4.3(c)). On the contrary, the LW description leads to an opposite behavior (i.e. convergence becomes faster as the thickness ratio decreases). This fact show how the zig-zag form of the displacement field in the through-the-thickness direction become an important aspect when highly transversely isotropic plates, are considered. The ESL description cannot see, from a global point of view, the difference between laminated and sandwich plates, then the same effects are observed varying the thickness ratio. However, when a consistent LW description of the sandwich plate is considered, a different behavior is obtained. The same effect is observed for the LD solution when the relative thickness ratio

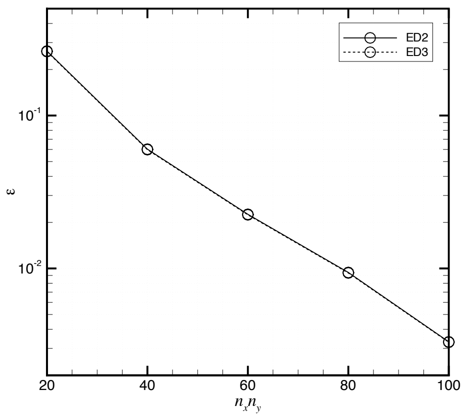

(a) isotropic plate

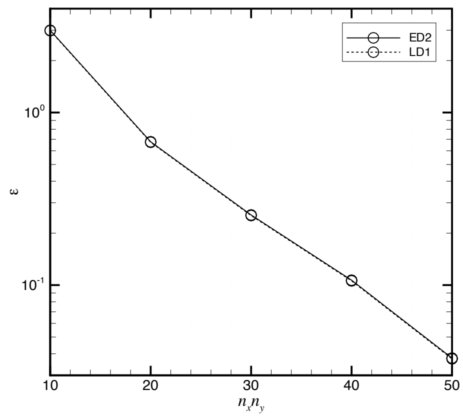

(b) laminated plate

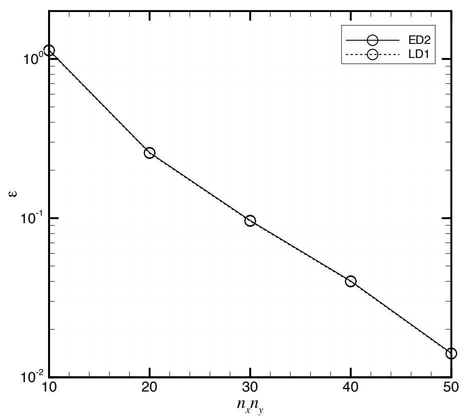

(c) piezoelectric plate

Figure 4.2: Effect of the order N and of the kinematic assumption on the convergence of the first bending mode for different plate layouts.

$\frac{t_c}{t_f}$ increases (see figure 4.3(d)), whreas no substantial change in the convergence pattern is observed for the ED solution.

It is anticipated here that, as it is shown by convergence tables D.26-D.34, an ESL description for sandwich plates cannot lead to satisfactory results, mainly when thick plates with soft are considered.

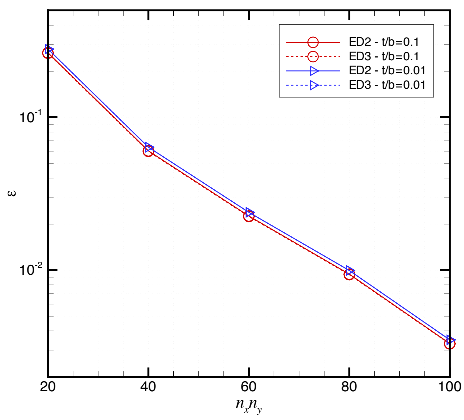

(a) isotropic plate

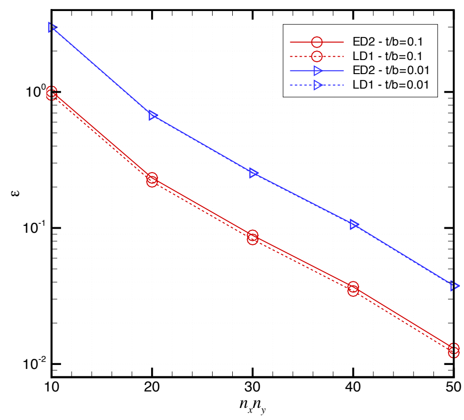

(b) laminated plate

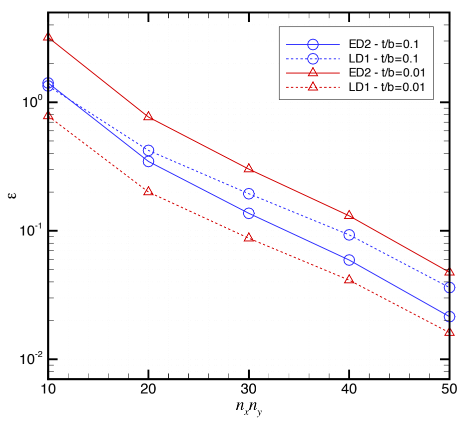

(c) sandwich plate

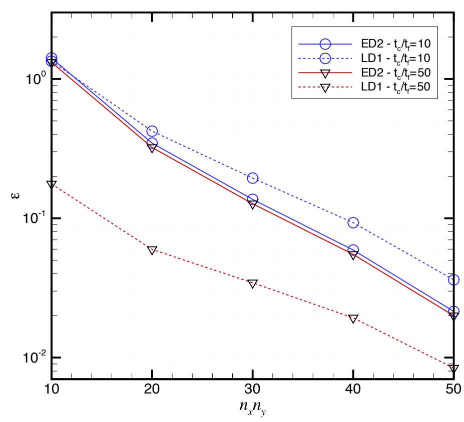

(d) sandwich plate

Figure 4.3: Effect of the thickness ratio on the convergence of the first bending mode for different plate layouts.

4.1.3 Effect of the boundary conditions

In this section the effect of the mechanical and electric boundary conditions is analyzed. In figures 4.4(a), 4.4(b) and 4.4(c), the convergence of the first bending mode for the same isotropic, laminated and piezoelectric plates introduced in section 4.1.1 are analyzed varying the boundary constraints. The thickness ratio of the laminated plate is $\frac{t}{b} = 0.1$, whereas the same values reported in 4.1.1 are used for the isotropic and piezoelectric cases. Figure 4.4(c) show that no differences are observed when OC or SC electric boundary conditions are considered, whereas from figure 4.4(a) and 4.4(b) it can be argued that a slower convergence is observed when mechanical clamped conditions are accounted. Sure enough, when some edge is clamped, more elements are needed to correctly reproduce the modal form due to the high gradients in the wave-form. However, the monotonic downward convergence is still observed.

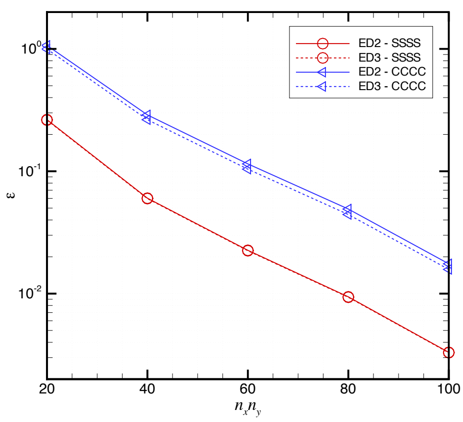

(a) isotropic plate

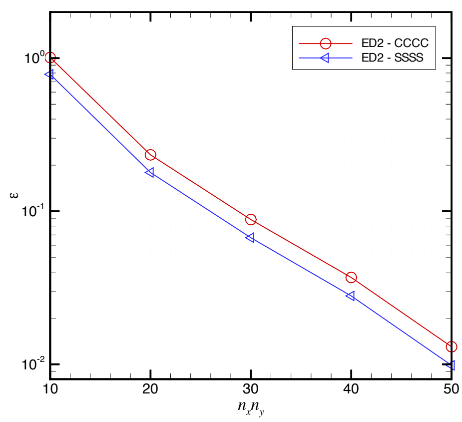

(b) laminated plate

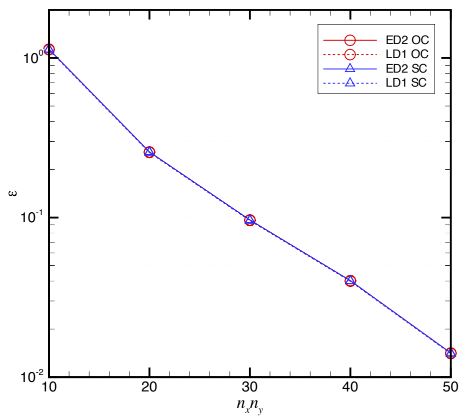

(c) piezoelectric plate

Figure 4.4: Effect of the boundary conditions on the convergence of the first bending mode for different plate layouts.

4.1.4 Effect of lamination lay-up

Finally, in this section the effect of the lamination scheme on the convergence pattern is analyzed. The three-layered plate presented in section 4.1.1 with $\frac{t}{b} = 0.1$ is considered as the starting layout. Then several lamination schemes is considered varying the simmetry, the number of the layers and the plies angle. The convergence table D.8-D.25 are difficult to comment due to the differences in the eigenvectors wave-form; however, the first bending mode is still comparable, and figure 4.5 shows that a slightly slower convergence is observed for unsymmetric layouts and for angle-ply schemes.

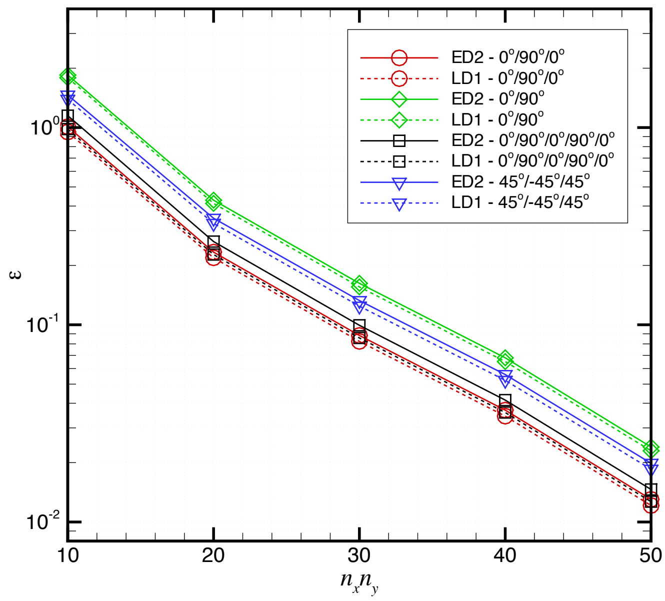

Figure 4.5: Effect of the lamination scheme on the convergence of the first bending mode for different lamination schemes, $\frac{t}{b} = 0.1$.

4.2 Validation

In order to evaluate the accuracy of the present method in predicting the natural frequencies of various types of plates, some benchmarks available in the open literature are presented. The accuracy is examined for plates with various thickness ratios, layouts and boundary conditions. We argue that the selected cases demonstrate the numerical accuracy of the present method.

4.2.1 Literature review

In this section a brief review of the relevant literature is provided with emphasis on the works selected for the validation of the present FE structural model.

Despite the pratical importance of elastic vibration solution of plate structures, exact 3-D elasticity solutions are limited only to few cases with simple geometry and boundary conditions ([54, 71, 72]). In the other cases, approximate methods must be used. The Ritz method [41] is one of the most efficient method for the analysis of structure. The Ritz procedure is well established, but convergence, accuracy and stability of the solution depends greatly on the choice of the admissible functions. Mainly we put our attention on the works of Liew et al. [44] and Zhou et al. [76]; in the former vibration analysis of thick isotropic plates subject to generic boundary conditions is performed using a 3-D Ritz formulation for the continuum with polynomial functions, whereas in the latter, the same analysis is presented using Chebyshev polynomials as admissible functions in the Ritz method. Moreover, in the last decade, the DQ method, originated by Bellman and his co-workers [6], has demonstrated its good performance in terms of convergence speed, accuracy and computational effort in the 3-D elasticity [42, 43]. In particular we consider the works of Chen and Lue [23] and of Lu et al. [48] as good references for a validation purpose for laminated plates. It should be remarked that the FE method is the most flexible method, in handling arbitrary geometry, boundary conditions and layouts, but the numerical efficiency is reduced with respect to Ritz and DQ method.

Concerning the case of sandwich plates, difficuties arise due to the high transversely orthotropy. To the best author knowledge, accurate 3-D Ritz or DQ solutions for this kind of structures are not present in the related literature. On the other hand, assumptions on the through-the-thickness displacement field, like as ESL or LW, are often introduced. The ESL models, even when higher order expansion is adopted, fail to reproduce the correct static and dynamic response of sandwich structures. In the last decade the works of Carrera [11, 29] and Rao and his colleagues [60] have shown the inaccuracy of ESL theories, especially when soft core sandwiches are considered. This kind of plate are widely used in the modern aerospace structure, and in many cases foam-type core is employed to optimize the response of the vibro-acoustic coupled systems. For this reason, some refined models which can predict the response of this kind of structures have been developed. In particular, the RMVT-based LW solutions in [60] and [29] can be considered as the reference due to their consistent description of the 3-D displacement field (a complete fulfillment of the C_z^0 conditions is provided). The theories obtained with this approach will be indicated as LM theories. On the other hand, more practically solutions have been developed, such as FE models based on higher order theories or other different approaches. For example in the work of Zhen et al. [75], the author proposes a FE model based on higher order expansion in the thickness direction with global and local terms, in order to account the continuity conditions for the displacements and for the in-plane stresses. A different model is adopted by Wang et al. in [74]; in this work the author proposes a different through-the-thickness kinematic assumption for the face skin and for the core.

In addition to these difficulties in obtaining reference solutions for pure mechanical problems, in the case of piezoelectric structures also the coupling with the electrostatic field must be solved. Modeling and analysis of laminated plates with piezoelectric layers have reached a relative maturity as attested by the numerous reviews and surveys, like as, for instance, [69] and [7]. 3-D exact solution of the piezoelastic coupled problem is reported in [35] for laminated plates with simple boundary conditions. Moreover, a careful analysis of the relevant literature indicates that approximate theories were often used; these mainly differs by the simplifying axiomatic assumptions concerning the piezoelectric effect representation, i.e. the direction of electric field and/or displacement and the through-the-thickness distibutions of the mechanical displacement and electric potential. Theoretically, at least quadratically variation of the electric potential in the thickness direction may provide a correct representation of the electromechanical coupling [69]. However, simplified theory can led to satisfactory results if thin plates are considered.

In order to provide an accurate validation of the present FE model, a lot of attention must be used to select the reference solutions among the open literature. In particular, considering generic layouts and boundary constraints, Ritz and DQ methods can be considered the best accuracy level. However when these solutions are hardly applicable, especially in case of sandwich and piezoelectric plate, RMVT solutions can be considered accurate enough for the present validation. In this cases, when simply supported boundary conditions are given, analytical Navier-type solutions are available. Following these criteria, the selected reference solutions are:

- for isotropic plates the 3-D Ritz solutions of [44] and [76],
- for laminated plates the 3-D DQ solutions of [23] and [48],
- for sandwich plates the analytical LM solutions of [60], the analytical solutions of [74] and the experimental results of [51],
- for piezoelectric plates the exact 3-D solutions of [35] and the LM solutions of [8].

It is remarked that, only the Ritz method applied to the 3-D elasticity provides an upper bound solution.

4.2.2 Results

The first three frequency parameters for each symmetry class for a rectangular isotropic plate with various boundary conditions and different thickness ratio $\frac{t}{b}$ computed using the present UF are given in tables 4.1-4.3 and compared with other published Ritz solutions. The ED3 and ED4 solutions are assumed as the optimal models to obtain the desired accuracy and to limit the computational effort when thin and thick plates respectively are considered. This choice is large justified by the result reported in tables D.1-D.7. From tables 4.1-4.3 it can be pointed out that the present method could be quite accurate with respect to the 3-D reference solution. In particular the results show that the accuracy of the present FE solution tends to get worse when the plates become thinner. For example from table 4.1 it can be seen that in case of moderately thick and thick plates ($\frac{t}{b} = 0.2,\ 0.1$) the present solutions are in very good agreement with the reference ones, whereas the accuracy undergoes a little worsening in case of thin plates ($\frac{t}{b} = 0.01$). The same tendencies can be shown in tables 4.2-4.3, and it could be a consequence of the higher dense mesh needed when the plate become thinner, as we have pointed out in the convergence study (see section 4.1.2). In this case the FE solution suffers the worst convergence rate and the locking behaviour in comparison with the Ritz method, therefore the accuracy deteriorates. This tendency is emphasized in the case of high aspect ratio, due to the worst spatial resolution in the stretched direction, since the same number of elements is used for the rectangular plates.

In figures 4.6(a), 4.6(b) and 4.6(c) the comparison between the ED4 solution and that is reported in [76] is presented in terms of percentage error Δ for more than 50 frequency parameters for an isotropic square plate. It is clear that the error tends to increase with the mode number (i.e. the frequency value), showing that higher order effect become more and more important. Furthermore, figures 4.6(a), 4.6(b) and 4.6(c) also show that some frequency parameters are in very good agreement (the error is nearly null) with the reference values; these frequencies correspond to the symmetric modes in the thickness direction.

In table 4.4 the first three frequency parameters corresponding to the first two wave numbers are compared to those reported in [23] for a simply supported laminated plate with two different layout. The convergent LD solution shows very good agreement with the reference value, whereas the performance of the ED theory deteriorates for wave numbers couple greater than $(1, 1)$, probably due to the moderately high value of $\frac{t}{b}$. Moreover, the ill-conditioning prevents to reach a more accurate solution for the ED models. In table 4.5 the first three mode numbers in the simply supported direction (i.e. x direction in figure 4.1) for a symmetrical laminated square plate with different constraints on the other edge pair are compared with the solution reported in [23]. It can pointed out that the accuracy of the ED and LD solutions is not affected by the boundary conditions. Finally the first frequency parameter of an angle-ply plate with simply supported and clamped conditions is compared with the solutions reported in [48]. The table 4.6 shows that the accuracy of both ED and LD theories deteriorates with angle-ply plates. However, it is remarked here that DQ solutions do not provide an upper bound for the present FE solution.

In table 4.7 the case of a simply supported square sandwich plate with face sheets made of material 4 and a soft core of material 5 is considered. The results are compared with the reference LM solution of [60] and with the solution presented in [74]. The table shows a good agreement of the LD solution with the reference values, confirming the fact that a LW description can predict the correct response of the plate. The ED solution is not reported here for its large errors and its inaccurate description of the displacement field. Inaccuracy of global models is shown in figure 4.7, where two higher order ED solutions are compared with the accurate LD4 solution; one can see that, even if an apparent convergence of the ED solution in terms of eigenvalue λ to the LD4 one is observed as the order increases, the computed displacement field is non physical.

In table 4.8 the present LD3 solution is compared with the theoretical and experimental results reported in [51], where a sandwich plate with honeycomb core and two identical aluminium face sheets is considered (see tables C.2 for material properties and geometry). The table shows again the accuracy of the present method.

Finally in table 4.9, the present ED and LD electromechanical solutions are compared with those reported in [8] and [35]. In the former exact analitical 3-D

Table 4.1: Frequency parameters for an isotropic plate with SSSS boundary conditions, $\nu = 0.3$.

			mode number											
$\frac{a}{b}$	$\frac{t}{b}$	Solution method	SS-1	SS-2	SS-3	SA-1	SA-2	SA-3	AS-1	AS-2	AS-3	AA-1	AA-2	AA-3
1	0.01	Present ED3 (120×120)	1.9995	9.9898	9.9898	4.9971	12.978	16.973	4.9971	12.978	16.973	7.9914	19.954	19.954
		3-D Ritz [44]	1.9993	9.9826	9.9826	4.9956	12.971	16.950	4.9956	12.971	16.950	7.9888	19.930	19.930
		3-D Ritz [76]	1.9993	9.9826	9.9826	-	-	-	-	-	-	-	-	-
	0.1	Present ED4 (120×120)	1.9344	8.6669	8.6669	4.6234	6.5236	10.884	4.6234	6.5236	10.884	7.1048	13.048	13.048
		3-D Ritz [44]	1.9342	8.6617	8.6617	4.6222	6.5234	10.879	4.6222	6.5234	10.879	7.1030	13.047	13.047
	0.2	Present ED4 (120×120)	1.7759	4.6130	6.6899	3.2618	3.8999	7.2945	3.2618	3.8999	7.2945	5.6534	6.5241	6.5241
		3-D Ritz [44]	1.7758	4.6127	6.6868	3.2617	3.8991	7.2934	3.2617	3.8991	7.2934	5.6524	6.5234	6.5234
		3-D Ritz [76]	1.7758	4.6127	6.6868	-	-	-	-	-	-	-	-	-
2	0.01	Present ED3 (120×120)	1.2498	3.2499	7.2547	1.9997	5.0013	9.9900	4.2483	6.2460	10.246	4.9973	7.9952	12.999
		3-D Ritz [44]	1.2497	3.2482	7.2408	1.9993	4.9956	9.9826	4.2468	6.2432	10.232	4.9956	7.9888	12.971
	0.1	Present ED4 (120×120)	1.2238	3.0841	6.5106	1.9346	4.6269	6.5236	3.2618	3.9727	5.6806	4.6235	6.5241	7.1075
		3-D Ritz [44]	1.2237	3.0825	6.5003	1.9342	4.6222	6.5234	3.2617	3.9715	5.6785	4.6222	6.5234	7.1031
	0.2	Present ED4 (120×120)	1.1556	2.7208	3.6469	1.7760	3.2618	3.9023	1.6309	3.4118	4.6656	3.2621	3.8999	5.6549
		3-D Ritz [44]	1.1555	2.7197	3.6467	1.7758	3.2617	3.8991	1.6309	3.4110	4.6644	3.2617	3.8991	5.6524

Table 4.2: Frequency parameters for an isotropic plate with CFCF boundary conditions, $\nu = 0.3$.

			mode number											
$\frac{a}{b}$	$\frac{t}{b}$	Solution method	SS-1	SS-2	SS-3	SA-1	SA-2	SA-3	AS-1	AS-2	AS-3	AA-1	AA-2	AA-3
1	0.01	Present ED3 (120×120)	2.2484	4.4061	12.165	6.2010	8.8526	18.172	2.6739	8.0647	12.823	6.8013	12.559	20.789
		3-D Ritz [44]	2.2482	4.4083	12.153	6.1972	8.8531	18.171	2.6743	8.0653	12.813	6.7985	12.560	20.754
	0.1	Present ED4 (120×120)	2.1043	3.9229	9.7328	5.3864	7.3583	10.634	2.4481	5.9498	6.9693	5.8276	10.072	10.963
		3-D Ritz [44]	2.1050	3.9234	9.7276	5.3859	7.3581	10.636	2.4489	5.9500	6.9678	5.8272	10.070	10.961
	0.2	Present ED4 (120×120)	1.8007	3.1922	5.8794	4.1108	5.3319	5.4665	2.0375	2.9770	5.4346	4.4128	5.4834	6.5934
		3-D Ritz [44]	1.7996	3.1909	5.8790	4.1062	5.3313	5.4625	2.0363	2.9770	5.4325	4.4084	5.4824	6.5929
2	0.01	Present ED3 (120×120)	0.5590	2.7680	3.0312	1.5421	4.0167	5.0218	0.9095	3.6663	6.6570	2.0847	5.7068	7.8149
		3-D Ritz [44]	0.5589	2.7687	3.0281	1.5411	4.0182	5.0121	0.9099	3.6643	6.6554	2.0845	5.6985	7.8148
	0.1	Present ED4 (120×120)	0.5486	2.6073	2.8295	1.4803	3.6565	4.5353	0.8670	2.6554	3.3588	1.9563	5.0729	5.2170
		3-D Ritz [44]	0.5492	2.6076	2.8300	1.4811	3.6575	4.5324	0.8677	2.6560	3.3596	1.9573	5.0707	5.2162
	0.2	Present ED4 (120×120)	0.5222	2.3072	2.4187	1.3369	2.6553	3.0723	0.7885	1.3289	2.8102	1.7136	2.6088	4.0499
		3-D Ritz [44]	0.5224	2.3071	2.4174	1.3367	2.6556	3.0720	0.7884	1.3291	2.8090	1.7135	2.6083	4.0462

Table 4.3: Frequency parameters for an isotropic plate with CCCC boundary conditions $\nu = 0.3$.

$\frac{a}{b}$	$\frac{t}{b}$	Solution method	mode number											
			SS-1	SS-2	SS-3	SA-1	SA-2	SA-3	AS-1	AS-2	AS-3	AA-1	AA-2	AA-3
1	0.01	Present ED3 (120×120)	3.6497	13.327	13.391	7.4392	16.696	21.305	7.4392	16.696	21.305	10.959	24.478	24.581
		3-D Ritz [44]	3.6429	13.315	13.379	7.4352	16.682	21.266	7.4352	16.682	21.266	10.953	24.441	24.543
	0.1	Present ED4 (120×120)	3.3205	10.503	10.603	6.3459	12.521	12.710	6.3459	12.521	12.710	8.9037	14.872	17.288
		3-D Ritz [44]	3.3215	10.498	10.598	6.3457	12.522	12.706	6.3457	12.522	12.706	8.9030	14.870	17.275
		3-D Ritz [76]	3.3176	10.488	10.587	6.3389	12.518	12.695	6.3389	12.518	12.695	8.8943	14.870	17.261
	0.2	Present ED4 (120×120)	2.7280	7.3344	7.4355	4.7774	6.2747	8.7088	4.7774	6.2747	8.7088	6.4250	7.4382	9.1364
		3-D Ritz [44]	2.7261	7.3241	7.4249	4.7725	6.2735	8.6980	4.7725	6.2735	8.6980	6.4185	7.4370	9.1342
		3-D Ritz [76]	2.7241	7.3208	7.4211	4.7696	6.2722	8.6944	4.7696	6.2722	8.6944	6.4152	7.4369	9.1323
2	0.01	Present ED3 (120×120)	2.4936	4.5423	8.8593	3.2287	6.4275	11.821	6.4879	8.4402	12.538	7.2055	10.215	15.403
		3-D Ritz [44]	2.4933	4.5396	8.8403	3.2278	6.4186	11.781	6.4836	8.4348	12.519	7.2010	10.205	15.364
	0.1	Present ED4	2.3251	4.1002	7.5506	2.9715	5.6531	8.4150	5.6225	7.1312	10.128	6.1821	8.4588	11.803
		3-D Ritz [44]	2.3261	4.1014	7.5448	2.9728	5.6514	8.4158	5.6221	7.1317	10.124	6.1823	8.4577	11.803
		3-D Ritz [76]	2.3231	4.0954	7.5332	2.9688	5.6437	8.4139	5.6157	7.1234	10.111	6.1753	8.4480	11.801
	0.2	Present ED4 (120×120)	1.9763	3.3365	5.7090	2.4853	4.2111	4.4390	4.2810	5.3399	5.6329	4.6806	5.9100	6.2271
		3-D Ritz [44]	1.9751	3.3346	5.7012	2.4842	4.2111	4.4350	4.2764	5.3356	5.6317	4.6763	5.9089	6.2218
		3-D Ritz [76]	1.9735	3.3318	5.6969	2.4841	4.2104	4.4315	4.2736	5.3324	5.6304	4.6734	5.9082	6.2182

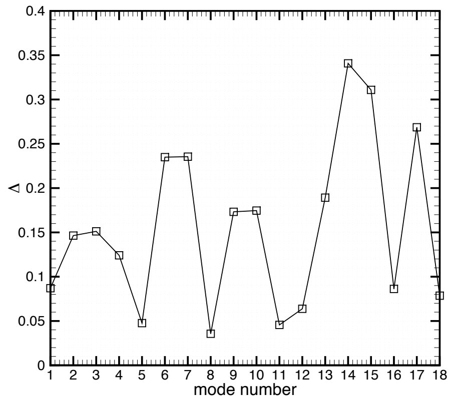

(a) SS modes

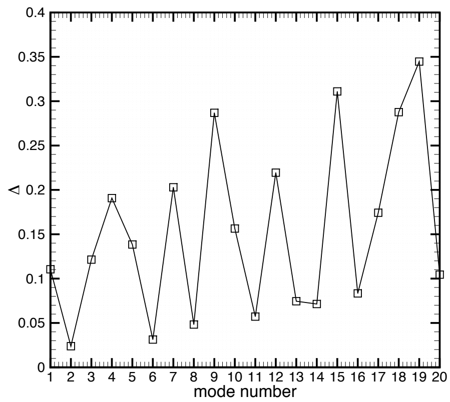

(b) SA modes

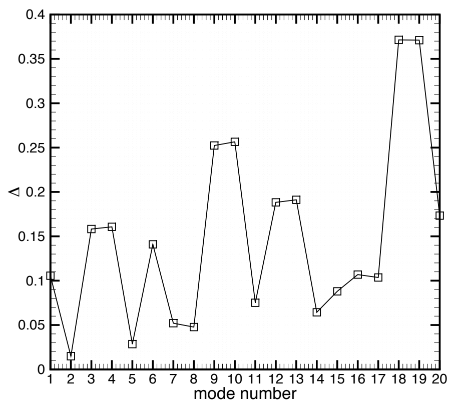

(c) AA modes

Figure 4.6: Isotropic clamped plates with $\frac{t}{b} = 0.1$ and $\nu = 0.3$. On the y axis is reported the percentage error Δ of the present ED4 solution with respect to [76].

Table 4.4: Comparison of the first 3 frequency parameters $\bar{\lambda} = \lambda \frac{t}{b}$ corresponding to several low-order modes for SSSS square laminated plates of material 3, $\frac{t}{b} = 0.1$.

Lamina scheme	Mode (n, m)	Solution method	mode number 1	2	3
$0°/90°/0°$	1,1	3-D DQ [23]	0.06715	0.50350	0.63776
		Present LD4 (60×60)	0.06716	0.50355	0.63782
		Present ED7 (60×60)	0.06750	0.50412	0.63851
	1,2	3-D DQ [23]	0.12811	0.68880	0.95017
		Present LD4 (60×60)	0.12822	0.68893	0.95050
		Present ED7 (60×60)	0.12889	0.68966	0.95455
	2,1	3-D DQ [23]	0.17228	0.58375	1.17826
		Present LD4 (60×60)	0.17230	0.58380	1.17824
		Present ED7 (60×60)	0.17427	0.58430	1.18274
	2,2	3-D DQ [23]	0.20807	0.97523	1.20362
		Present LD4 (60×60)	0.20812	0.97553	1.20363
		Present ED7 (60×60)	0.21021	0.97957	1.20639
$0°/90°/0°/90°$	1,1	3-D DQ [23]	0.06621	0.54596	0.59996
		Present LD4 (60×60)	0.06623	0.54602	0.60001
		Present ED7 (60×60)	0.06679	0.54664	0.60061
	1,2/2,1	3-D DQ [23]	0.15203	0.63883	1.07656
		Present LD4 (60×60)	0.15206	0.63888	1.07653
		Present ED7 (60×60)	0.15473	0.63945	1.08126
	2,2	3-D DQ [23]	0.20848	1.06252	1.15535
		Present LD4 (60×60)	0.20856	1.06273	1.15606
		Present ED7 (60×60)	0.21263	1.06703	1.16060

Table 4.5: Comparison of the fundamental frequency parameter $\bar{\lambda} = \lambda \frac{b}{t}$ for the first three mode number (m) of a $0°/90°/0°$ SSSS square laminated plate of material 2, $\frac{t}{b} = 0.1$.

m	Solution method	Boundary condition type CSCS	CSSS	CSFS
1	3-D DQ [23]	19.809	17.195	7.256
	Present LD4 (40×40)	19.820	17.205	7.299
	Present ED7 (40×40)	19.830	17.213	7.304
2	3-D DQ [23]	25.085	23.289	16.998
	Present LD4 (40×40)	25.109	23.319	17.015
	Present ED7 $(40 \times 40$	25.152	23.362	17.068
3	3-D DQ [23]	36.908	35.877	31.929
	Present LD4 (40×40)	37.033	36.011	32.057
	Present ED7 (40×40)	37.182	36.162	32.225

Table 4.6: Comparison of the fundamental frequency parameter $\bar{\lambda} = \lambda \frac{b}{t}$ for an angle-ply $45°/-45°$ square laminated plate of material 2.

BC type	Solution method	$\frac{t}{b}$ = 0.1	$\frac{t}{b}$ = 0.05
CCCC	3-D DQ [48]	16.9980	20.8797
	FE [48]	17.4509	21.1185
	Present LD4 (40×40)	17.2799	21.0548
	Present ED7 (40×40)	17.2916	21.0621
SSSS	3-D DQ [48]	14.2123	16.7141
	FE [48]	14.4099	16.7329
	Present LD4 (40×40)	14.3240	16.6624
	Present ED7 (40×40)	14.3727	16.7106

Table 4.7: Comparison of the fundamental frequency parameter $\bar{\lambda} = \lambda \frac{b}{t}$ for several wave number for a $0°/90°$/core/$0°/90°$ plate with soft core. LD4 and LD3 are use for thick and thin plate respectively.

	m	n	Solution type: Present LD	Analytic [74]	Analytic LM [60]
$\frac{t}{b} = 0.01$					
	1	1	11.9479	11.9401	11.8593
	1	2	23.4259	23.4017	23.3419
	1	3	36.2033	36.1434	36.1150
	2	2	30.9694	30.9432	30.8647
	2	3	41.4951	41.4475	41.3906
	3	3	49.8090	49.7622	49.7091
$\frac{t}{b} = 0.1$					
	1	1	1.8492	1.8480	1.8470
	1	2	3.2234	3.2196	3.2182
	1	3	5.2360	5.2234	5.2286
	2	2	4.2945	4.2894	4.2882
	2	3	6.1071	6.0942	6.0901
	3	3	7.6959	7.6762	7.6721

Table 4.8: Comparison of the first 6 frequencies [Hz] for a sandwich plate with honeycomb core.

mode number	[51] Experiment	[51] Analysis	Present LD3 (60×60)
1	-	23	23.02
2	45	44	44.15
3	69	71	69.76
4	78	80	79.27
5	92	91	90.24
6	125	126	124.36

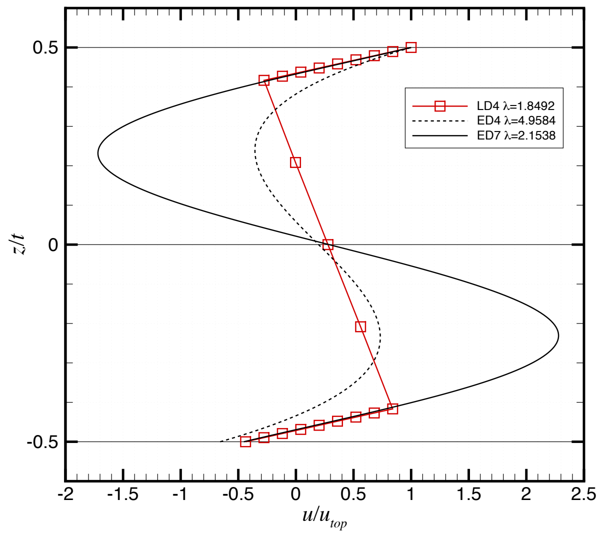

Figure 4.7: LD4 and two ED solution for the plate layout considered in the validation case. The displacement u refers to the $y = 0$ and $x = \frac{a}{2}$ coordinates.

solutions are presented, whereas in the latter an LM model is used. Despite of the limits due to computational effort of the present LD theories, the results appear to be in good agreement with the reference ones. However, more accurate solutions can be obtained with smaller mesh size. Morover, no substantial differences in the accuracy are observed varying the electrical boudary conditions; indeed, very similar results are obtained for OC and SC conditions.

Table 4.9: Comparison of the first 5 frequency $\bar{\lambda} = \omega a^2 \sqrt{\rho} \frac{1}{2\pi t 10^3}$ corresponding to several low-order modes for SSSS square laminated plates bonded by two PZT-4 layers, $\frac{t}{b} = 0.02$.

		mode number				
BC	Solution method	1	2	3	4	5
OC	3-D exact [35]	245.942	-	-	-	-
	LM [8]	245.937	559.406	691.731	965.191	1091.003
	Present ED4 (30×30)	246.398	562.766	696.129	971.939	1106.863
	Present LD3 (30×30)	246.251	561.951	695.095	969.956	1103.547
SC	3-D exact [35]	245.941	-	-	-	-
	LM [8]	245.936	559.402	691.727	956.179	1090.983
	Present ED4 (30×30)	246.394	562.729	696.116	971.876	1106.700
	Present LD3 (30×30)	246.251	561.945	695.091	969.942	1103.523

4.3 Comparison among different UF theories

In this section the capabilities of the UF formulation are exploited in solving the free vibrations problem of plate-like structure. In particular, several different theories are compared to find out how to obtain the best compromise between accuracy and computational effort. Note that the present section has not to be considered as guideline for the free vibration analysis of every type of plate structure; indeed the present FE method is not suitable for this kind of study due to its computational inefficiency respect to other numerical method. Moreover only a few representative number of parameters are considered in the following. It should be clear that the present structural model could be used for several accurate analysis in the framework of structural mechanics. However this is not the aim of this work, thus only few pure structural case are studied.

In the following isotropic, laminated, sandwich and piezoelectric plate cases are presented in indipendent sections.

4.3.1 Isotropic plates

In this section isotropic square plates with FE mesh size 120×120 are considered. Figures 4.8 and 4.9 show the percentage error $\Delta = \frac{\lambda - \lambda_{ref}}{\lambda_{ref}} \times 100$ of several higher order theories obtained by the present UF for the first 40 modes of a simply supported and clamped plates with different thickness ratio. The ED3 and ED4 solutions are assumed as the reference ones for thin and thick plates respectively; section 4.2 and tables D.1-D.7 clearly justified this assumption. Firstly, figures 4.8(a) and 4.9(a) reveal that the accuracy depends on the mode type for both simply supported and clamped edges; indeed when symmmetrical modes appear in the considered portion of spectrum, higher order effects are not relevant for such modes, then low order models could provide the same accuracy as the reference model, explaining the local minimum of the error in thick plates cases. On the other hand, the same figures show that for non-symmetric modes the error gets larger as the frequency increases, demonstarting that the higher order effect get prominent when the local wave-form becomes comparable with the dimensions of the plate sections. Despite that, as shown in figures 4.8(b) and 4.9(b), when thin plate are taken into account, this high frequency effect becomes less prominent and the accuracy is not compromised even if low order theories are considered. This effect can be shown also in figure 4.10, where the thruogh-the-thickness displacement u is reported along the y axis for thin and thick simply supported plates for two different bending modes; it is clear that, for thick plates, the higher is the wave number the more is the warping of the section. However, no differences are observed in the case of thin plates, demonstrating the small percentage error accomplished by the simplest plate theory.

In addition to higher order effects, also the quasi-3-D description of the displacement field is an important feature of the CUF models. Indeed the CPT and the FSDT (and also the Reddy's TSDT) neglect the through-the-thickness variation of the transversal displacement w. Modeling this kinematic aspect could be important in predicting natural frequencies associated with symmetric modes in the thickness direction; in fact, in some cases, the vertical displacement could get prominent for this kind of modes, becoming a prevalently thickness modes. A careful scrunity of tables D.1-D.7 and figures 4.8 and 4.9 reveal that symmetric modes appear in the low portion of the spectrum when the thickness ratio increases; in particular moving from thin to moderately thick and thick plates the symmetric modes increases from none to up to ten in the considered portion of spectrum. However, considering the simply supported case, the observed symmetric modes are almost always membranal modes (i.e. prevalently in-plane motion), then the assumption of zero transversal displacement could be accurate enough. On the contrary, when clamped edges are considered, the symmetric modes are also thickness modes, probably due to the in-plane constaints along the plate edges, then through-the-thickness variation of w should be taken into account. In tables D.1-D.7 symmetric modes with thickness variation are characterized by the fact that, differently from symmetric modes with prevalently in-plane displacement, higher order terms improve the accuracy of the associated frequency parameter. For example, in figure 4.11 the first thickness mode for a clamped plate is reported.

Finally, it could be observed that low order theories could provide a good accuracy in the eigenfrequency analysis of isotropic plates when small thickness ratio are considered, and no missing frequencies due to kinematic model assumptions should be observed in a large portion of the spectrum if CPT or FSDT are used (i.e. no prevalently thickness modes appear). However, when the plate become thicker, high order effects have to be considered and thickness modes become important, especially for clamped plates. From this point of view, the UF can provide a large variety of theories and then some combinations of the patrameters (such as $\frac{t}{b}$) and larger frequency range could be solved correctly.

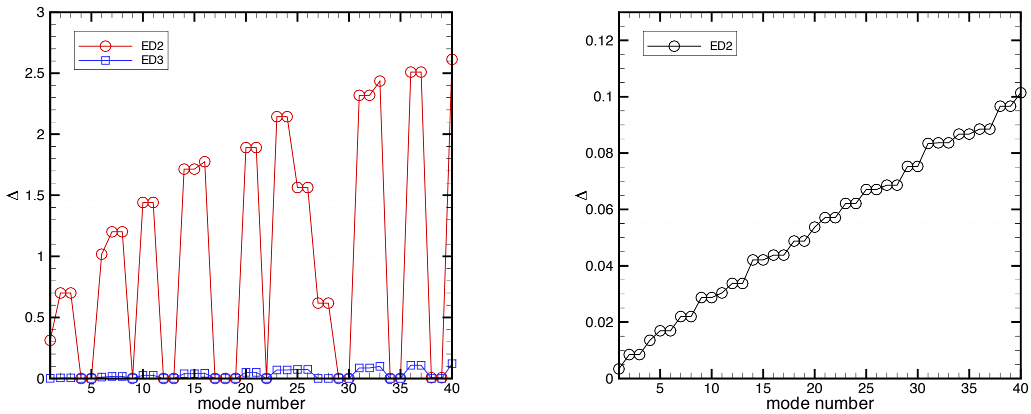

(a) $\frac{t}{b} = 0.1$ (b) $\frac{t}{b} = 0.01$

Figure 4.8: Effect of the thickness ratio on the accuracy of several ED theories. On the y axis is reported the percentage error Δ respect to ED4 and ED3 for thick and thin plate respectively. Simply supported plate with $\nu = 0.3$.

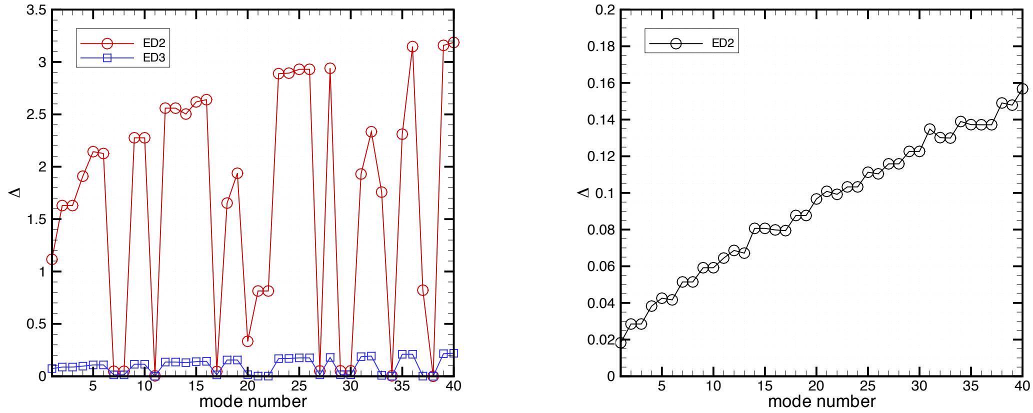

(a) $\frac{t}{b} = 0.1$ (b) $\frac{t}{b} = 0.01$

Figure 4.9: Effect of the thickness ratio on the accuracy of several ED theories. On the y axis is reported the percentage error Δ respect to ED4 and ED3 for thick and thin plate respectively. Clamped plate with $\nu = 0.3$.

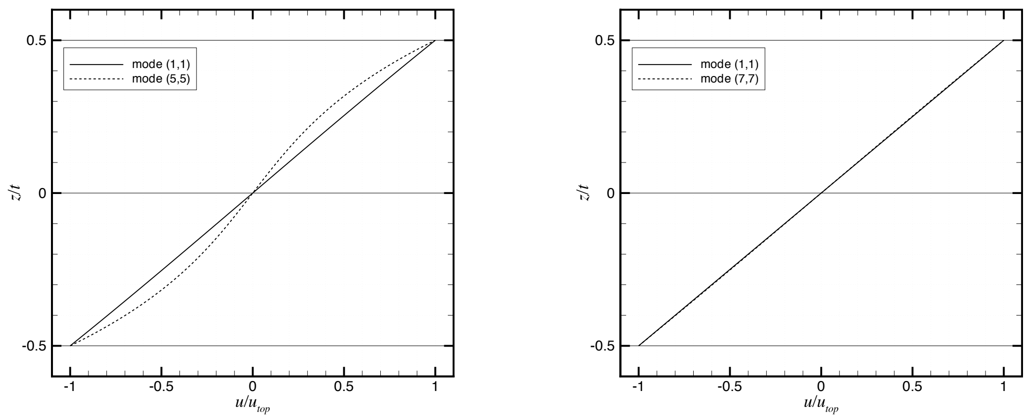

(a) $\frac{t}{b} = 0.1$ (b) $\frac{t}{b} = 0.01$

Figure 4.10: Effect of the high frequencies on the through-the-thickness displacement u. Isotropic plates with simply supported edge is considered. The displacement u refers to the $y = 0$ and $x = \frac{a}{2}$ coordinates.

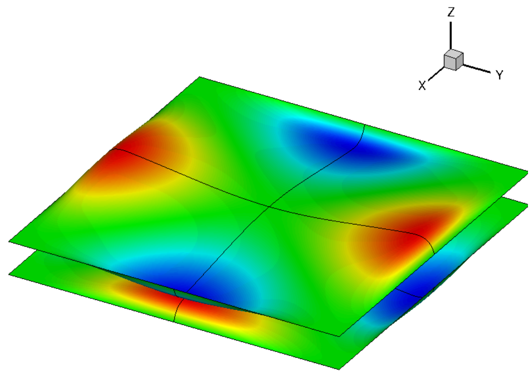

Figure 4.11: First symmetric mode. Isotropic plate with $\frac{t}{b} = 0.1$ and clamped edge.

4.3.2 Laminated plates

In this section laminated plates are considered. In the following anlysis we consider the LD3 and LD4 solution as the reference ones and Δ indicates again the relative percentage error. This choice is largely justified by the previous validation (see 4.2).

The thickness ratio $\frac{t}{b}$ and the ply number are considered as varying parameters in order to understand the efficiency of some theories obtained by the present UF. Such a parametric study is not the aim of this work, thus only a representative number of cases is analysed in order to obtain a first understanding of the correct use (in terms of accuracy and computational effort) of the present theories; indeed the computational effort is an important feature especially when acoustic coupling is accounted in the elastic problem.

Figures 4.12(a)-4.12(b) show the effect of increasing the number of layers in the accuracy of some ED and LD theories. A clamped cross-ply square plate symmetrically laminated with FE mesh size 60×60, made of material 2 and $\frac{t}{b} = 0.1$ is considered; the starting lay-up scheme is $0°/90°/0°$. First, figures 4.12(a)-4.12(b) show a strong dependance of the accuracy with the mode number. This behavior is partially inhibited increasing the number of layers, probably because the material difference between x and y directions is reduced by the averaging effect induced when the number of layers become large. After this clarification, the same figures show the effect of increasing the plies number for the ED and LD theories. Thanks to its local description of the plate, LD theories show a clear behavior: as the number of layers increases, the local plies thickness decreases, then the error of LD solutions tends to decrease for all the observed modes. For what concern the ED models, the error in the selected frequency range seems to remains the same on average; moreover, except for the ED2 theory, the error seems to assume a more constant value showing a less dependence on the mode number. This observation does not demonstrate the superiority of the LD theories with respect to ED ones; indeed, even if the LD error decreases and ED remains approximately the same, the problem size of a LD theory increase whereas the ED one remains the same. Moreover, a careful scrunity of figures 4.12(a) and 4.12(b) reveals that the odd orders are much more effective then the even ones for ESL analysis of a simmetrically laminated plate. In figures 4.13(a) and 4.13(b) the same parameter is studied for a thinner plate. In this case the mode dependance of the error become less evident, and it is clearly visible the tendency of the error to get larger as the mode number increases. Above that, the previous analysis is still valid, even more evident for a cross-ply plate with $\frac{t}{b} = 0.01$. Therefore, for what concern the efficient use of these theories, figures 4.12-4.13 show that the LW modeling of the plate is not necessary in the considered frequency range. Indeed, assuming an accuracy limit of 0.5% the ED7 theory (24 degrees-of-freddom per node) is more efficient then LD3 (30 and 66 degrees-of-freddom per node for three- and seven-layered laminate) for thick plates, and ED3 (12 degrees-of-freddom per node) is more efficient then LD1 (12 and 24 degrees-of-freddom per node for three- and nine-layered laminate) for thin plates.

In figures 4.14 the displacement field in the thickness direction for the first bending mode is shown for the previously analyzed layout; the fact that ED theories work well as the layer number increases and the plate become thinner (considering a real application case) is confirmed by the tendency of the section to warping less. Of course the warping increases with the modes number and then the error tends to raise, as shown in figure 4.15, requiring higher order terms in the thickness direction for a more accurate solution. This observation demonstrates the clear tendency of the error to increase as the frequency increase (figure 4.13(a)-4.13(b)): the thinner is the plate the more are the higher order effect as the frequency increases, whereas, for a thick plates, even at low frequencies the section warping plays an important role.

The 3-D description of the plate structure could play an important role when symmetric modes in thickness direction is considered. Actually, the through-the-thickness variation of the displacement w is prominent when the symmetric mode is predominantly a thickness mode. Tables D.8-D.25 show that symmetric modes are observed even in the low portion of the spectrum when thick plate are considered, whereas they move to high frequencies when the plate becomes thinner. Furthermore, for a given thickness ratio, the simply support condition moves the symmetric modes at low frequency due to the unconstrained in-plane displacement along the plate edge. Even the material properties play an important role in the position of these modes in the frequency spectrum. In the analyzed cases with clamped edges, the observed symmetric modes are predominantly in-plane modes, then no 3-D description is required to capturing them with good accuracy. Otherwise, considering a simply supported cross-ply plates of material 3 (the validation case of table 4.4), several modes with significant displacement in the thickness direction (figure 4.16) are observed under the fiftieth mode.

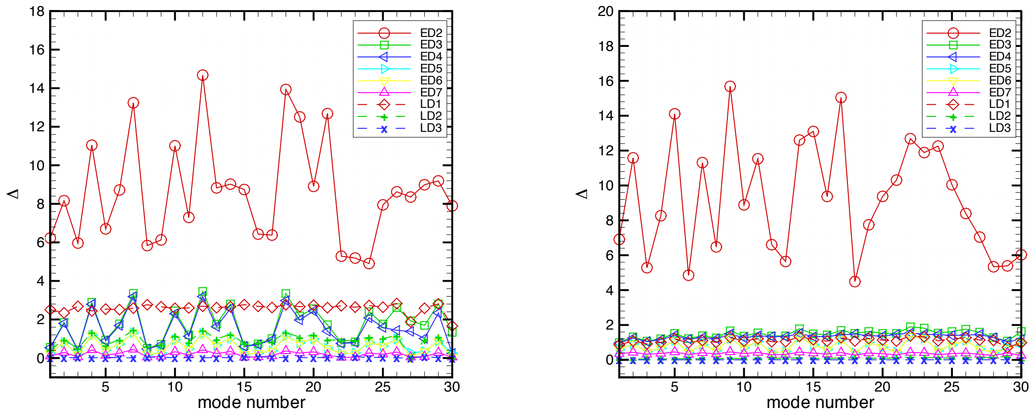

(a) $0°/90°/0°$ (b) $0°/90°/0°/90°/0°/90°/0°$

Figure 4.12: Effect of the layer number on the accuracy of ED and LD theories. On the y axis is reported the percentage error Δ respect to LD4. Clamped cross-ply symmetrically laminated plate with $\frac{t}{b} = 0.1$.

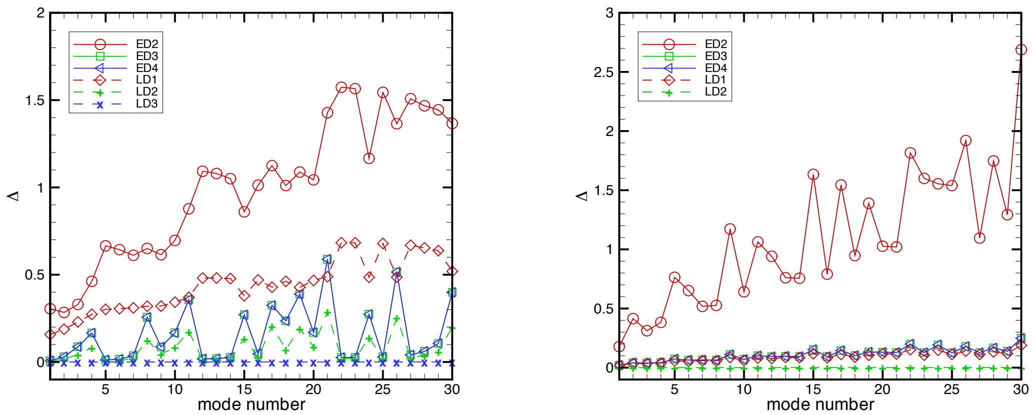

(a) $0°/90°/0°$ (b) $0°/90°/0°/90°/0°/90°/0°/90°/0°$

Figure 4.13: Effect of the layer number on the accuracy of ED and LD theories. On the y axis is reported the percentage error Δ respect to LD4 and LD3 for three-layered and nine-layered plate respectively. Clamped cross-ply symmetrically laminated plate with $\frac{t}{b} = 0.01$.

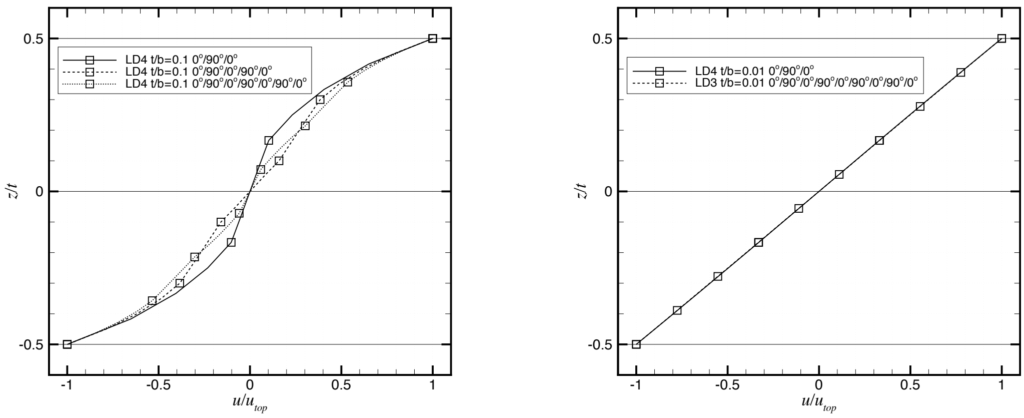

(a) $\frac{t}{b} = 0.1$ (b) $\frac{t}{b} = 0.01$

Figure 4.14: Effect of the layer number on the section warping of a cross-ply symmetrically laminated plate with clamped edge. The displacement u refers to the $y = 0$ and $x = \frac{a}{2}$ coordinates. Symbols are reported only at interfaces between adiacent layers.

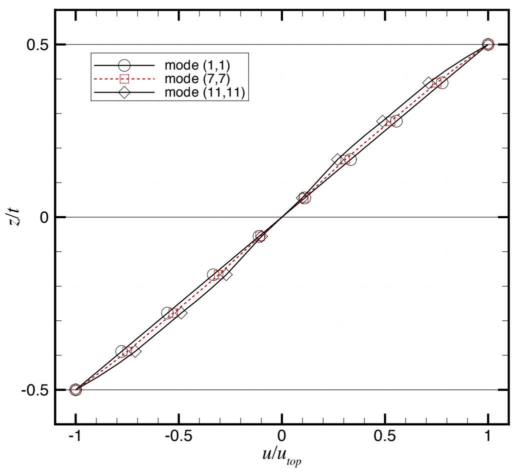

Figure 4.15: Effect of the high frequencies on the through-the-thickness displacement field. nine-layered laminated plate with simply supported edge is considered. The displacement u refers to the $y = 0$ and $x = \frac{a}{2}$ coordinates. Symbols are reported only at interfaces between adiacent layers.

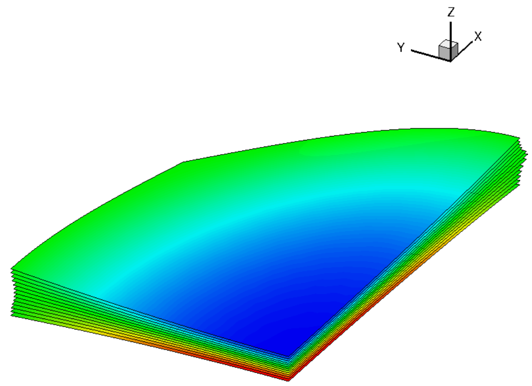

Figure 4.16: Symmetric mode. Only one quarter of the SS mode is reported.

4.3.3 Sandwich plates

As demonstrated in sections 4.1 and 4.2, ED theories are not appropiate to correctly describe the dynamic response of sandwich plates. Then, only LD results are considered and discussed here.

In figures 4.17 and 4.18 the error Δ with respect to the LD3 and LD4 solutions for the cases considered in the convergence section are presented. The considered mesh size is 60×60. It can be shown that the error increases at higher frequencies; in particular, a clear tendency is shown in the thin plate case ($\frac{t}{b} = 0.01$) and for higher core-to-face thickness ratio ($\frac{t_c}{t_f} = 50$), whereas the thick plate case with $\frac{t_c}{t_f} = 10$ has a less different trend due to the symmetric modes (mainly tickness modes) presented in the second half of the considered frequency range. Figures 4.17 and 4.18 show the effect of the two considered parameters $\frac{t}{b}$ and $\frac{t_c}{t_f}$ on the accuracy of the LD models; figure 4.17(b) demonstrates that for thinner plates even the LD1 model provides a very accurate solution, although some higher order effects appears as the modes number increases. On the other hand, the relative thickness ratio $\frac{t_c}{t_f}$ seems to have no substantial effect on the accuracy of the first 15 frequencies (4.18), whereas a different tendency is observed for the higher portion of the spectrum due to the vanishing of the symmetrical modes in the thickness direction.

Figure 4.19(b) shows the through-the-thickness variation of the u component of the displacement field for two different modes when a simply supported plate with soft core is considered (see section 4.2). The two displacements refer to the first ($m = 1$ and $n = 1$) and twentieth ($m = 7$ and $n = 7$) mode of the SS class respectively, and they confirm that no higher order effects are observed in the considered frequency range when a thin ($\frac{t}{b} = 0.01$) soft core is considered. Moreover it can be pointed out that as the mode number increases the discontinuities due to inhomogeneous material properties in thickness direction get more important. Otherwise, when a thicker plate is considered ($\frac{t}{b} = 0.1$), the high order terms plays an important role as the considered frequency range increases (see figure 4.19(a)).

This confirms the previous accuracy analysis.

The last two examples show how a LW description which can take into account the non-linear effects in the displacement field of the core is really important in modeling sandwich plates. Indeed, considering the through-the-thickness variation of the normal displacement component could be a fundamental feature when soft cores are taken. Especially when the thickness ratio $\frac{t}{b}$ assumes relatively high values (in the order of 10^{-1}), the symmetric modes in the thickness direction are always predominantly thickness modes and populates the low portion of the spectrum (see tables D.26-D.34). However, when the plate becomes thinner or the core becomes thicker respect to the skin faces, the thickness modes move to higher frequency values. In the case of $\frac{t}{b} = 0.01$ no symmetric modes are observed in the frequency range where the present FE analysis is still accurate; whereas the increase of the $\frac{t_c}{t_f}$ moves the first thickness modes to the twenty-third modes of the SS class. In figure 4.20 the first thickness modes of a thick sandwich plate ($\frac{t}{b} = 0.1$) is reported.

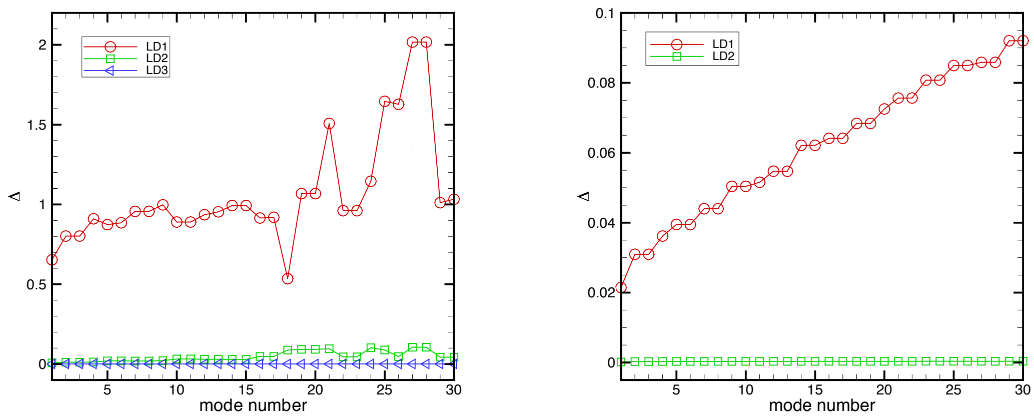

(a) $\frac{t}{b} = 0.1$

(b) $\frac{t}{b} = 0.01$

Figure 4.17: Effect of the thickness ratio $\frac{t}{b}$ on the accuracy of LD theories. On the y axis is reported the percentage error Δ with respect to LD4 and LD3 for thick and thin plate respectively. Clamped sandwich plate with stacking sequence $0°/90°/\text{core}/0°/90°$ and $\frac{t_c}{t_f} = 10$ is considered.

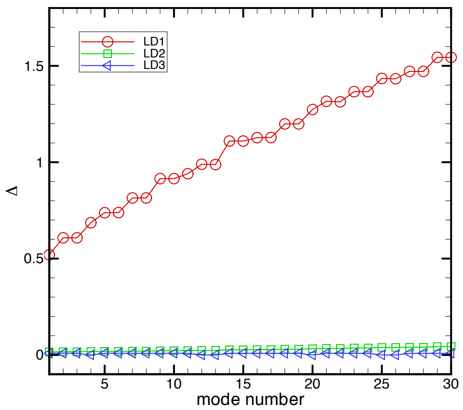

Figure 4.18: Effect of the relative thickness ratio $\frac{t_c}{t_f}$ on the accuracy of LD theories. On the y axis is reported the percentage error Δ with respect to LD4. Clamped sandwich plate with stacking sequence $0°/90°$/core/$0°/90°$, $\frac{t}{b} = 0.1$ and $\frac{t_c}{t_f} = 50$ is considered.

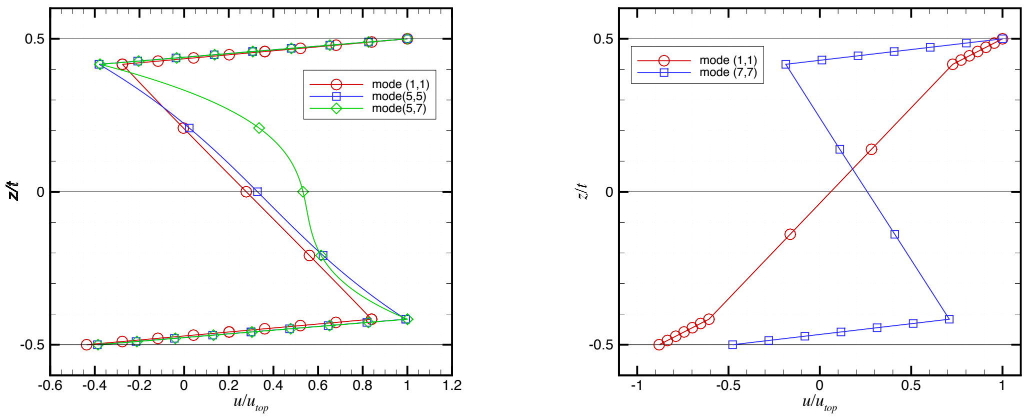

(a) $\frac{t}{b} = 0.1$ and $\frac{t_c}{t_f} = 10$

(b) $\frac{t}{b} = 0.01$ and $\frac{t_c}{t_f} = 10$

Figure 4.19: Effect of the high frequencies on the through-the-thickness displacement u. The displacement u refers to the $y = 0$ and $x = \frac{a}{2}$ coordinates. Simply supported sandwich plate with stacking sequence $0°/90°$/core/$0°/90°$ is considered.

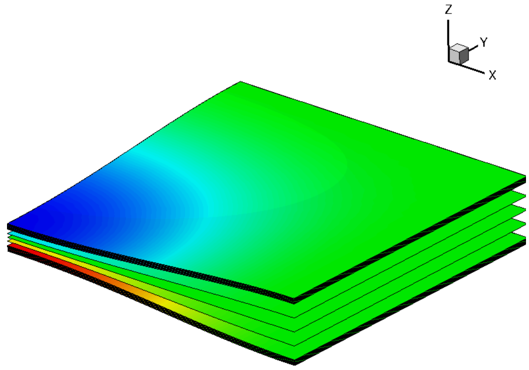

Figure 4.20: Symmetric mode. Only one quarter of the SS mode is reported.

4.3.4 Laminated plates with piezoelectric materials

Finally,the electromechanical models obtained with the present UF are compared considering the plate lay-up of section 4.2. However, due to the huge memory requirements of the high order LD theories, a complete comparison can be enstablished only over a restricted frequency range. In particular the first 10 modes are considered, and the accuracy of the ED and LD theories is compared with respect to the LD3 solutions. The effect of the electric boundary conditions OC and SC on the accuracy is also shown.

In figures 4.21(a) and 4.21(b) nothing new, compared to the previous considerations about laminated plates, appears. A stronger dependance of ED theories from the mode number with respect to LD models is still observable. Moreover, the electric boundary conditions seem to not affect the accuracy: only slightly larger errors are observed for the ED2 solutions when the OC electric condition is considered.

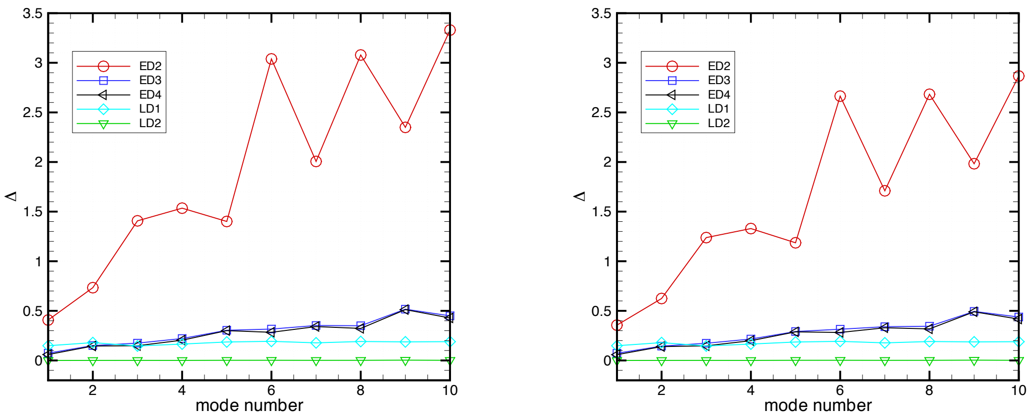

(a) $\frac{t}{b} = 0.02$, OC

(b) $\frac{t}{b} = 0.02$, SC

Figure 4.21: Effect of the electric boundary conditions on the accuracy of LD and ED theories. On the y axis is reported the percentage error Δ respect to LD3 solution. Simply supported plate with stacking sequence PZT/0°/90°/0°/PZT is considered.

CHAPTER 5

Fluid-Structure Interaction Validation

This chapter deals with the validation of the whole structural-acoustic FE code considering the acoustic FE and the fluid structure coupling. The organization is the following: in the first section, the acoustic elements are validated for a simple geometry, where analytical solution is known; in the second section, the vibro-acoustic response of the fluid loaded plate is compared with cases available in the open literature in terms of frequency response functions (FRFs). The second section of this chapter is prominent in this work and it is dual-purpose; indeed, not only the validation of the interface elements is considered, but also the modal coupling approach is studied in order to find the convergence behavior of this approach.

5.1 Acoustic model validation

Let us consider the case of a rectangular rigid walled cavity. In this simple case, the analytical solution of the eigenvalue problem is known; in particular, if the cavity has dimensions $a \times b \times c$, the natural circular frequencies of the acoustic system are given by:

$$\omega_{ijk} = \sqrt{c_f^2 \left[\left(\frac{i\pi}{a} \right)^2 + \left(\frac{j\pi}{b} \right)^2 + \left(\frac{k\pi}{c} \right)^2 \right]}. \tag{5.1}$$

The first 10 frequencies of a $0.6 \times 0.4 \times 0.5$ m^3 cavity are reported in table 5.1, and compared with FE solutions with increasing number of elements in each directions. The convergence pattern is reported in figure 5.1 for three representative modes. Table 5.1 and figure 5.1 show the monotonic downward convergence behavior of the 8-nodes hexahedral element considered in this work. Moreover the results appear in good agreement with the analytical solutions. Finally in figure 5.2 three eigenvectors are shown.

5.2 Coupling validation

In this section the coupled model presented in chapter 2 is validated. Only the mechanical case is considered, since, to the best author knowledge, no reference

Table 5.1: First ten natural frequencies [Hz] for the rigid walled $0.6 \times 0.4 \times 0.5$ m^3 cavity

		mode number									
$(n_x \times n_y \times n_z)$	n_{dof}	1	2	3	4	5	6	7	8	9	10
$(5 \times 5 \times 5)$	216	290.56	348.67	435.83	453.86	523.81	558.14	609.58	629.24	702.25	731.49
$(10 \times 10 \times 10)$	1331	287.01	344.41	430.52	448.32	517.41	551.33	581.11	621.57	675.51	697.33
$(20 \times 20 \times 20)$	9261	286.13	343.35	429.19	446.95	515.82	549.63	574.02	619.65	668.87	688.82
$(40 \times 40 \times 40)$	68921	285.91	343.09	428.86	446.60	515.43	549.21	572.25	619.17	667.22	686.71
exact (equation 5.1)	-	285.83	343.00	428.75	446.49	515.29	549.07	571.67	619.01	666.67	686.00

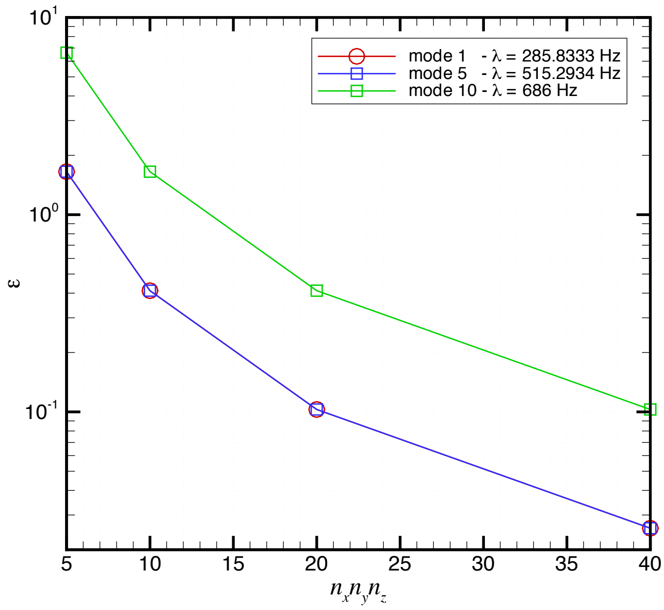

Figure 5.1: Space convergence of three modes for the $0.6 \times 0.4 \times 0.5$ m^3 cavity. The relative percentage error ε with respect to the exact solution 5.1 is reported on the y axis.

electromechanical cases are available in the literature. Despite that, the electromechanical coupling is a structural feature and does not directly interact with the vibro-acoustic coupling; indeed, it is remarked that the problem can be always expressed in terms of displacement $\boldsymbol{s}$ and pressure p only, via static condensation of the electric degrees-of-freedom.

In the following, the modal coupling solution method is validated considering two test cases; the first is referred to a weak coupled system, whereas the second is a strong coupled case. As it is stated in the introduction chapter, the weak or strong coupling is an important feature of a vibro-acoustic system, mainly when the uncoupled modal basis are used to reduce the problem size. For this reason, it is often desiderable to know before hand whether a system is weakly or strongly coupled. Despite a dimensionless quantity is defined by Atalla [4] to classify the vibro-acoustic system in weakly or strongly coupled, in [26] it is noted that this measure is not fully comprehensive, since it takes into account only the mass properties of the structure and acoustic bulk stiffness. However, as it is noted in [39], the coupling between structural and acoustic subsystems is a more complex function of the mass properties, geometry and excitation frequency. However, even if it is in generally difficult to classify vibro-acoustic systems for their coupling behavior, the following classification for simple geometries, like those considered in these works, holds: whenever an heavy fluid fluid, like as water, is contact with a structure, a strong coupling behavior is observed, whereas when the cavity is filled by a lightweight fluid, like as air, a weak coupling is obtained. For this reason, two cases are considered in the

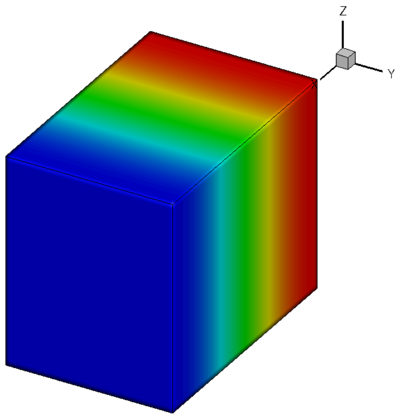

(a) mode 1

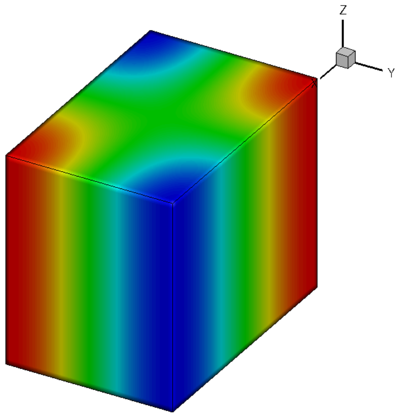

(b) mode 5

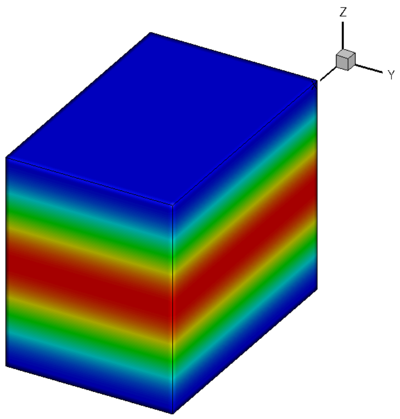

(c) mode 10

Figure 5.2: Some representative eigenvectors for the $0.6 \times 0.4 \times 0.5$ m^3 cavity. Mesh size $40 \times 40 \times 40$.

following, consisting in an isotropic plate backed by a rigid walled cavity filled with air and water. Unfortunately, no similar cases with composite plates are founded in literature.

5.2.1 Weak coupling case

The case presented here is also considered in [58]. The test structure (see figure 5.3) is a square simply supported 1×1 m^2 aluminium plate with thickness $t = 0.01\,\mathrm{m}$, backed by a rigid walled cubic cavity of dimensions $1 \times 1 \times 1\,\mathrm{m}^3$. The mechanical properties of the plate structure are as follows: Young's modulus $E = 70\,\mathrm{GPa}$, mass density $\rho_s = 2700\,\frac{\mathrm{Kg}}{\mathrm{m}^3}$ and Poisson's ratio $\nu = 0.35$. The cubic cavity is filled with air with the following properties: speed of sound $c_f = 343\,\frac{\mathrm{m}}{\mathrm{s}}$ and mass density $\rho_f = 1.2\,\frac{\mathrm{Kg}}{\mathrm{m}^3}$. A constant amplitude mechanical excitation of $1\,\mathrm{N}$ over the frequencies of $0 - 300\,\mathrm{Hz}$, is applied on the FE structural node denoted by point A, with coordinates $(0.25\,\mathrm{m}, 0.35\,\mathrm{m})$. The following system outputs are considered: acoustic pressure at point B of coordinates $(0.75\,\mathrm{m}, 0.25\,\mathrm{m}, 0.75\,\mathrm{m})$ and at point C $(0.75\,\mathrm{m}, 0.25\,\mathrm{m}, 0.95\,\mathrm{m})$, the plate specific kinetic energy $\frac{E_k^s}{\rho_s}$ and the acoustic mean-square pressure E_p^f. The convergence of the modal coupled method is analyzed by increasing the number of the structural and acoustic modes retained in the reduced basis. In particular the modes included in the range of f_{max}, $1.5f_{max}$, $2f_{max}$ and almost $3f_{max}$ with $f_{max} = 300\,\mathrm{Hz}$ are considered. A FE mesh of $20 \times 20 \times 20$ is used, and the ED2 theory is adopted.

Figure 5.4 shows the convergence of the pressure response at point B increasing the number of the structural and acoustic modes of the reduced model. The reference solution refers to the full coupling case reported in [58], where no damping effect is considered. It can be observed that a good accuracy is obtained with only 10 structural modes and 20 acoustic modes, which are the uncoupled modes included in the $0 - 1.5f_{max}$ frequency range. A fully convergent solution is achieved if all the uncoupled modes in the frequency range below $3f_{max}$ are retained. Small differences are observed with respect to the reference solution, because the fully coupled solution is obtained with a different structural model. In particular, the present structural element leads to slightly overestimation of some resonance peaks, probably due to the performance of the selective integration adopted to avoide shear locking effects. It also can be observed that the resonance peaks are obtained with good accuracy even considering only the modes below f_{max}, whereas the convergence of the anti-resonance peaks appears slower.

Figure 5.5 shows the convergence of the pressure response at point C, which is near the plate-fluid interface. At this point no reference solutions are available, so the number of modes needed to achieve a fully convergent solution in the previous case (point B, $n_s = 20$ and $n_p = 60$) is assumed as the reference basis. The convergence appears slightly slower for the acoustic pressure near the plate surface, confirming the fact that more acoustic modes are required to obtain an accurate local description of the fluid-structure interface.

Finally in figure 5.6 the convergence of the energetic parameters is analyzed.

The convergence of the structural kinetic energy and of the fluid potential energy appears to be faster then that observed for the local response, confirming the fact that when global response parameters are considered the modal coupling technique provides good accuracy and efficienty.

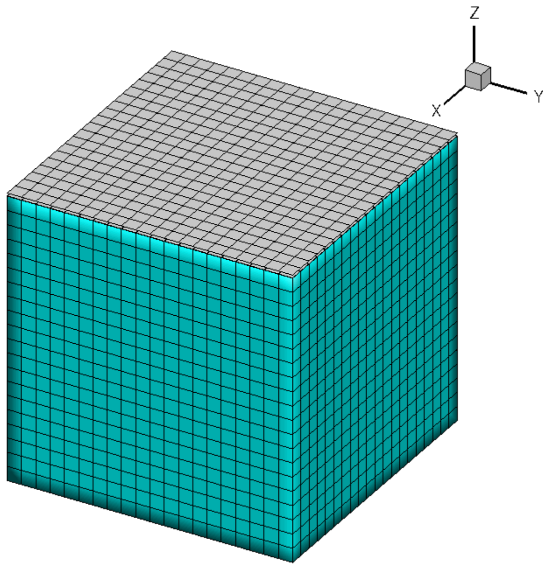

Figure 5.3: FE model for weakly coupled validation case.

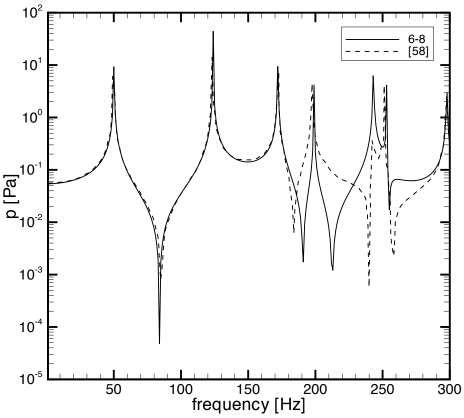

(a) $n_s = 6$, $n_p = 8$

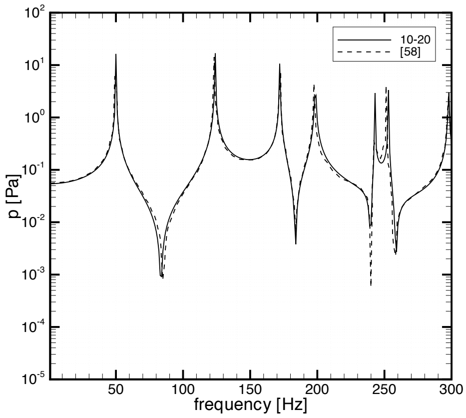

(b) $n_s = 10$, $n_p = 20$

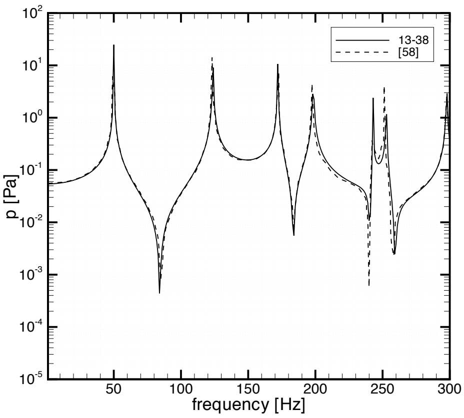

(c) $n_s = 13$, $n_p = 38$

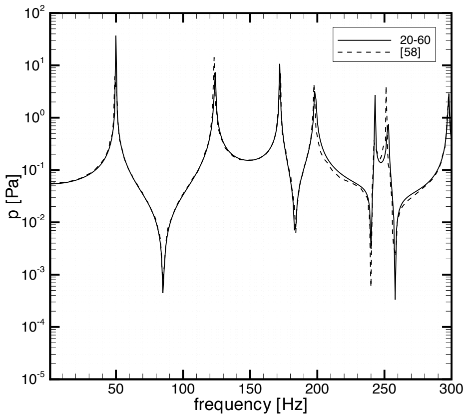

(d) $n_s = 20$, $n_p = 60$

Figure 5.4: Pressure response at point B. Convergence of the modal coupling reduction technique with respect to the full coupling solution of [58].

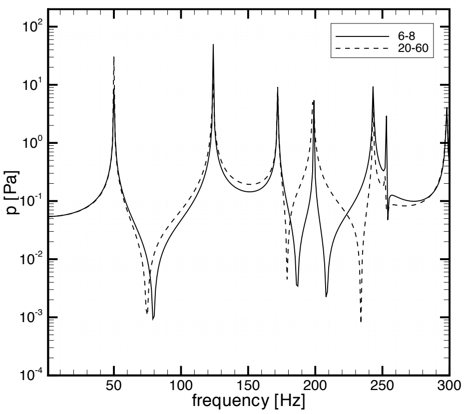

(a) $n_s = 6$, $n_p = 8$

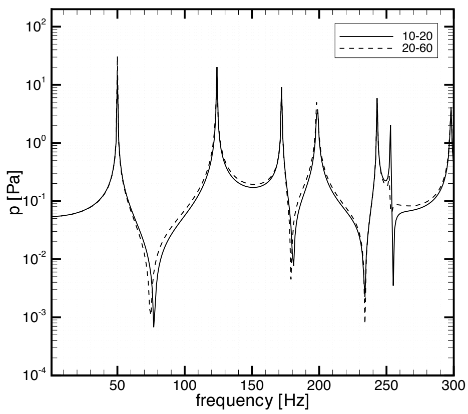

(b) $n_s = 10$, $n_p = 20$

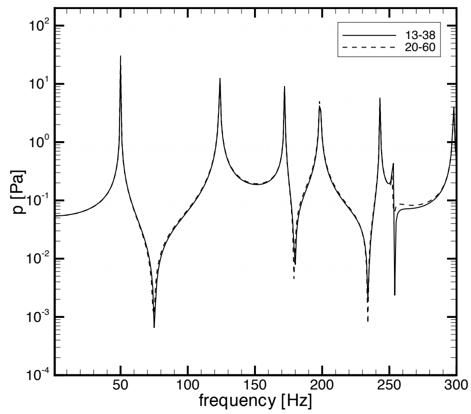

(c) $n_s = 13$, $n_p = 38$

Figure 5.5: Pressure response at point C. Convergence of the modal coupling reduction technique with respect to the assumed converged solution.

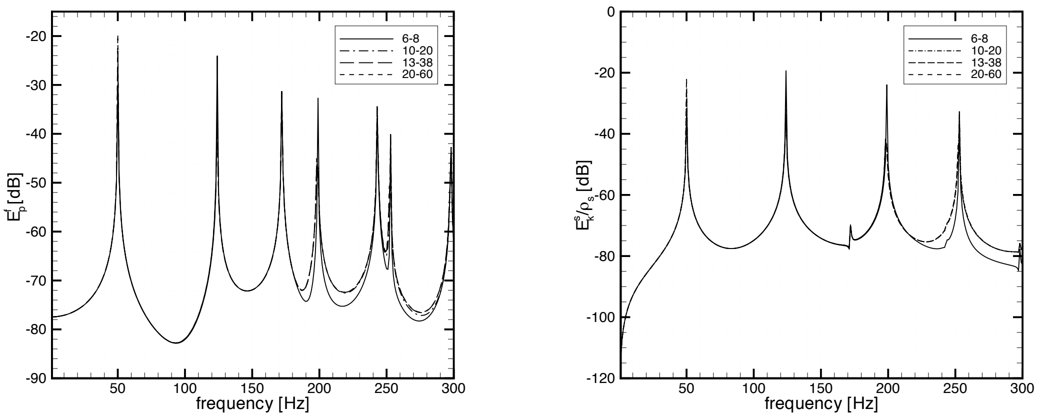

(a) mean-square pressure

(b) structural specific kinetic energy

Figure 5.6: Response in terms of global parameters. Convergence of the modal coupling reduction technique with respect to the assumed converged solution.

5.2.2 Strong coupling case

A simply supported plate backed by a water filled cavity is considered as the validation case for strong coupling. The cavity-plate system has the following dimensions (see figure 5.7): 0.29 m in x direction, 0.35 m in y direction, 0.14 m deep with a 1.5 mm thick aluminium plate. The mechanical propertise are: Young's modulus $E = 72\,\mathrm{GPa}$, mass density $\rho_s = 2700\,\frac{\mathrm{Kg}}{\mathrm{m}^3}$ and Poisson's ratio $\nu = 0.33$. The cavity is filled with water with the following properties: speed of sound $c_f = 1500\,\frac{\mathrm{m}}{\mathrm{s}}$ and mass density $\rho_f = 1000\,\frac{\mathrm{Kg}}{\mathrm{m}^3}$. The plate is discretized using 20×20 structural elements and the cavity with $20 \times 20 \times 10$ acoustic elements. Again, the ED2 theory is considered. The coupled system is excited using a constant force of 1 N over the entire range of $0 - 600\,\mathrm{Hz}$. The force is applied on plate point A $(0.039\,\mathrm{m}, 0.272\,\mathrm{m})$. The system outputs are: colocated mid-plane transverse displacement w_0, acoustic pressure at point B of coordinates $(0.135\,\mathrm{m}, 0.175\,\mathrm{m}, 0.07\,\mathrm{m})$, the plate specific kinetic energy $\frac{E_k^s}{\rho_s}$ and the acoustic mean-square pressure E_p^f. The convergence of the modal coupled method is analyzed by increasing the number of the structural and acoustic modes of the reduced basis. In particular, the number of uncoupled modes varies from $n_s = 50$ and $n_p = 50$ to $n_s = 1000$ and $n_p = 1000$. The description of this case can also be found in [58] and [73]. The fully coupled solution reported in [58] is assumed as the reference for the local transfer functions. No damping is accounted in the present analysis.

In figure 5.8 the convergence of the pressure FRF at point B is studied. As expected, a fully converged solution is hard to be established even considering a large number of uncoupled modes. In particular, it is observed that only considering almost 1000 structural modes and 1000 acoustic modes gives rather satisfactory results. However, only the modal contributions below 300 Hz seems to be converged. The same consideration can be made for figure 5.9, where the mid-plane structural displacement at point A is considered as system output. Again the FRF is far from convergence for the frequencies above 250 Hz, even if the resonance peaks are in good agreement with those reported in [58] up to 500 Hz. Finally in figure 5.10 the global system response in evaluated in terms of specific structural kinetic energy and mean-square pressure. It is confirmed that, also form an energetic point of view, the solution with 1000 acoustic modes and 1000 structural modes provides a good approximation of the dynamic system response only in the low frequency range. Clearly, this fact confirms the poor accuracy of the modal coupling method when strong coupled systems are considered. However, more accurate and efficient solution can be obtained via uncoupled basis if static corrections are accounted for. These techniques are beyond the scope of this work and in the last part of this dissertation, where numerical examples are presented, only weak coupled system are considered. The reader can refer to [73] and [49] for more information about static correction techniques.

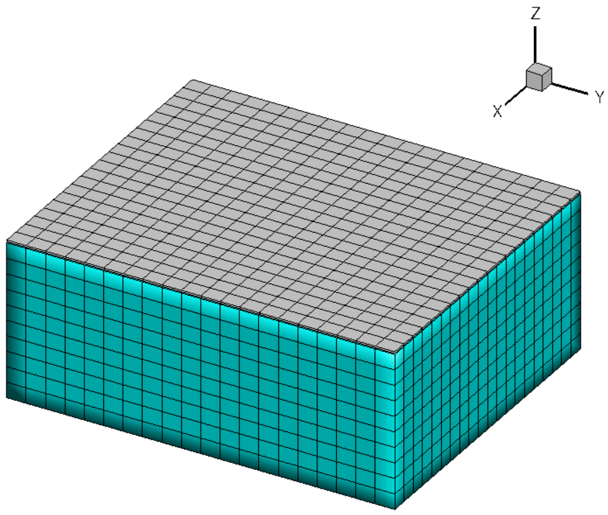

Figure 5.7: FE model for strongly coupled validation case.

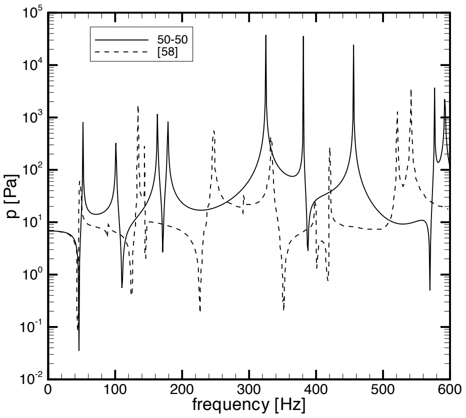

(a) $n_s = 50$, $n_p = 50$

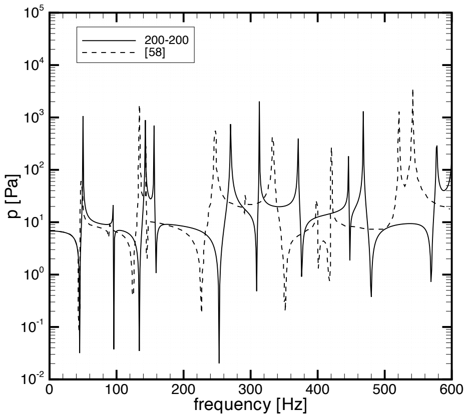

(b) $n_s = 200$, $n_p = 200$

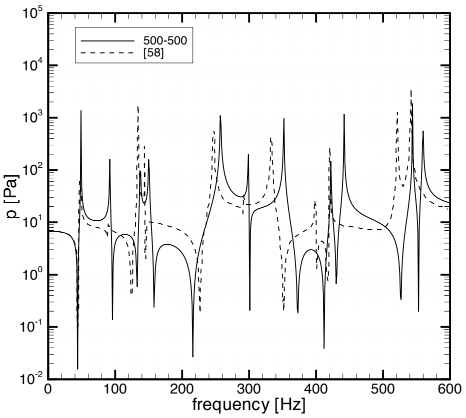

(c) $n_s = 500$, $n_p = 500$

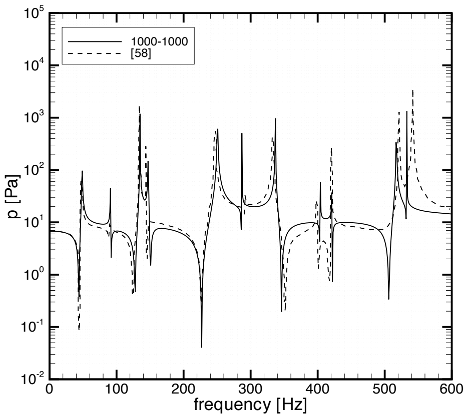

(d) $n_s = 1000$, $n_p = 1000$

Figure 5.8: Pressure response at point B. Convergence of the modal coupling reduction technique with respect to the full coupling solution of [58].

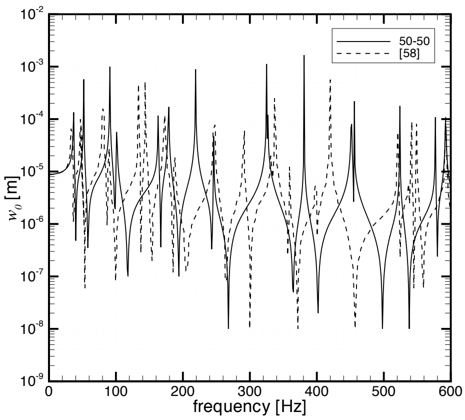

(a) $n_s = 50$, $n_p = 50$

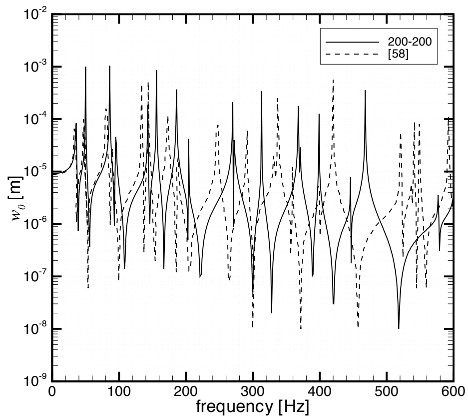

(b) $n_s = 200$, $n_p = 200$

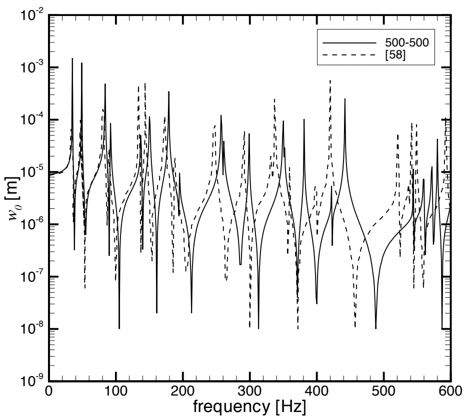

(c) $n_s = 500$, $n_p = 500$

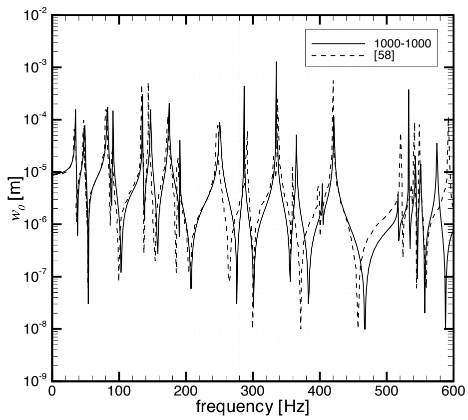

(d) $n_s = 1000$, $n_p = 1000$

Figure 5.9: Structural displacement response at point A. Convergence of the modal coupling reduction technique with respect to the full coupling solution of [58].

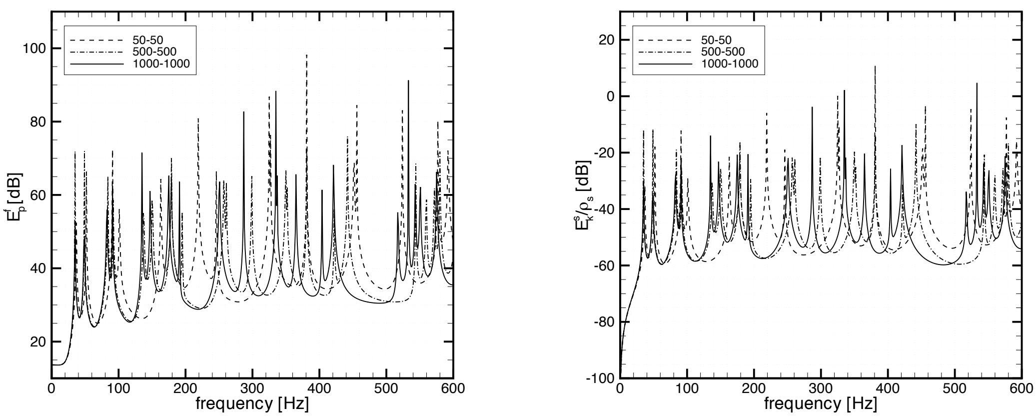

(a) mean-square pressure (b) structural specific kinetic energy

Figure 5.10: Response in terms of global parameters. Convergence of the modal coupling reduction technique.

CHAPTER 6

Numerical Results

In order to illustrate the applicability of the present FE model for vibro-acoustic application, the UF is applied to different cavity-backed plate systems. Thanks to the unified approach, a large variety of plate structures can be analyzed. The FE model has been validated in case of simple isotropic plates in the previous chapter. In the present chapter, more complex cases such as laminated and sandwich plates are considered. Moreover, both mechanical and electromechanical structural systems are taken into account.

The method adopted for the solution of the coupled piezoelectric structural acoustic system is the modal coupling method, which has been discussed deeply in chapter 5. Due to the bad efficiency and accuracy of this solution method in the case of strong coupled systems, only air filled cavity cases (i.e. weak coupling cases) are presented. Moreover, comparisons between LW and ESL description and between different order theories represent an important focus of this chapter. Therefore, in order to find out the effect of considering higher order theories, thin and thick plates cases are both considered. The features of the LW description connected to the use of Lagrange polynomials are also exploited, providing a more accurate description of the boundary constraints.

In the next sections, three numerical cases are presented. Two cases consist of pure mechanical structures; in section 6.1 the vibro-acoustic response of a thin laminated plate coupled with a shallow cavity is analyzed, whereas in section 6.3 a sandwich plate with soft core is considered. In section 6.2 an electromechanical thick plate case is presented. For each of these cases, the frequency response of the coupled system is analyzed in terms of local and global parameters. The FRFs obtained with different structural models are compared also in terms of relative error. Clearly, due to the presence of resonance and anti-resonance peaks, the local error between two FRFs may be large even if the considered solutions are in good agreement. However, even if the local error could be misleading, at the same time it can be a simple tool to analyze qualitatively how the structural model refinement effects depend on the frequency.

6.1 Test case 1

A thin laminated simply supported plate is considered as the first numerical case. The plate structure has dimensions $0.6 \times 0.4\,\mathrm{m}^2$ and the shallow cavity is $0.1\,\mathrm{m}$ deep (see figure 6.1). The multilayered structure consists of nine layers in symmetric cross-ply configuration with lamination scheme $[(0°/90°)_4/0°]$. The plate thickness is $t = 3\,\text{mm}$, and each lamina is $0.\bar{3}\,\text{mm}$ thick. The Gr-Ep reinforced fiber is considerd, and the material properties are reported in appendix C. The cavity is air filled with speed of sound $c_f = 343\,\frac{\text{m}}{\text{s}}$ and mass density $\rho_f = 1.2\,\frac{\text{Kg}}{\text{m}^3}$. The plate is excited by a 1 N force applied at structural node A $(0.13\,\text{m}, 0.053\,\text{m})$ at the top of the plate in transversal direction. The frequency range of interest is $0 - 2\,\text{KHz}$, i.e. $f_{max} = 2\,\text{KHz}$. The system outputs are: structural mid-plane transversal displacement w_0 at point B of coordinates $(0.52\,\text{m}, 0.313\,\text{m})$, acoustic pressure at point C of coordinates $(0.346\,\text{m}, 0.186\,\text{m}, 0.07\,\text{m})$, the plate kinetic energy E_k^s and the acoustic mean-square pressure E_p^f. A FE mesh of $90 \times 60 \times 10$ is kept. The thin multilayerd plates allow to use ESL theories, as we see in chapter 4; in particular ED2 and ED3 solution are compared. The modal coupling technique is used considering acoustic and structural modes below $3f_{max}$. The uncoupled modes included in the frequency range $0 - 2\,\text{KHz}$ are 41 cavity modes and 42 structural modes. Finally a modal damping factor $\xi_s = \xi_f = 0.01$ is assumed.

In figures 6.2 and 6.3 the FRFs of pressure and displacement outputs obtained using ED2 and ED3 models are presented with the relative error. It is clear that no substantial difference appears between ED2 and ED3 solutions; however, even if the two FRFs almost coincides, the error shows a growing tendence as the frequency increases. Moreover, this tendency appear more regular for the displacement output. This results are in agreement with the analysis reported in chapter 4, where it has been shown that for thin laminated plates with high number of layers, no substantial differences among various plate theories appear in the free response untill up to 30 natural frequencies. Although, the higher order effects get more important in the high frequency range and affect both the displacement and the acoustic field.

In figures 6.4 and 6.5 the structural kinetic energy and the acoustic mean-square pressure are reported. It can be oserved that the growing tendency shown by the error of the local parameters (i.e. pressure p and displacement w_0) is less pronounced for the global parameters. Indeed, the error of the structural and fluid energy seems to reach a constant maximum value.

Clearly, for the considered structure a low order theory can lead to sufficient accuracy in the selected frequency range, and no more refined models are needed. Moreover, figures 6.2, 6.3, 6.4 and 6.5 show that at high frequencies the damping effects and the growing modal density become important. Despite of the simple damping model used here, no clear modal contributes are observed above 1500 KHz and this effect is more pronounced when global parameters are observed.

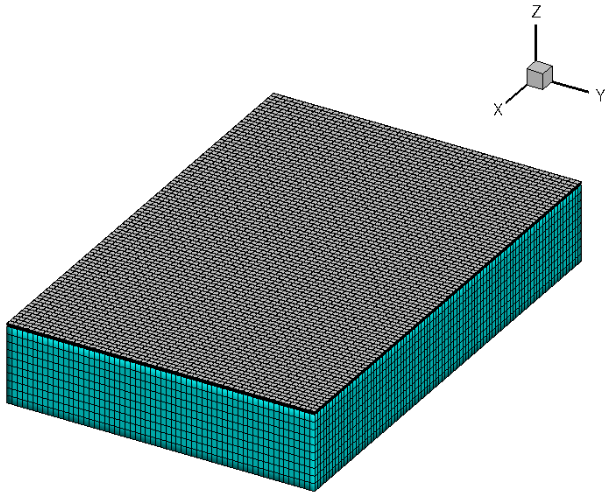

Figure 6.1: FE model for test case 1.

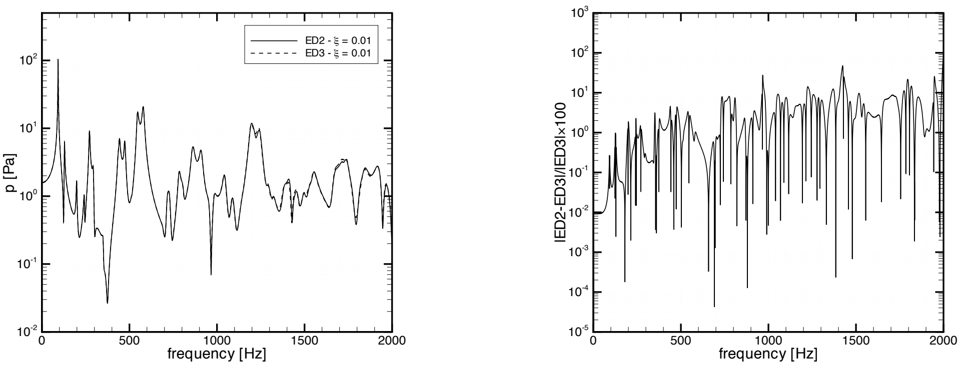

(a) FRF

(b) error

Figure 6.2: Pressure response at point C and percentage error between ED2 and ED3.

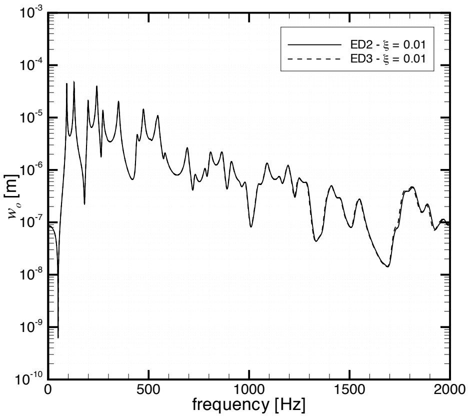

(a) FRF

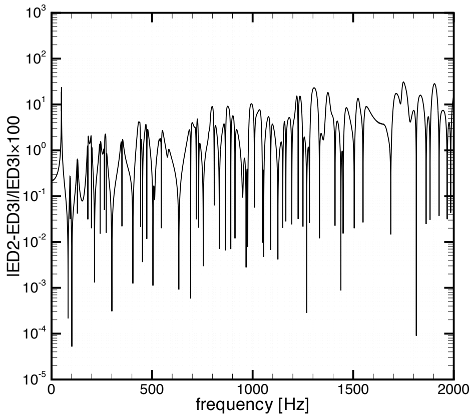

(b) error

Figure 6.3: Structural displacement response at point B and percentage error between ED2 and ED3.

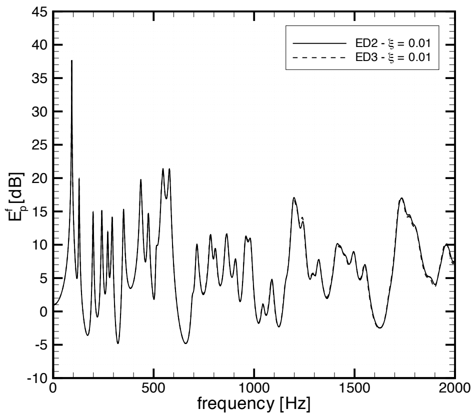

(a) FRF

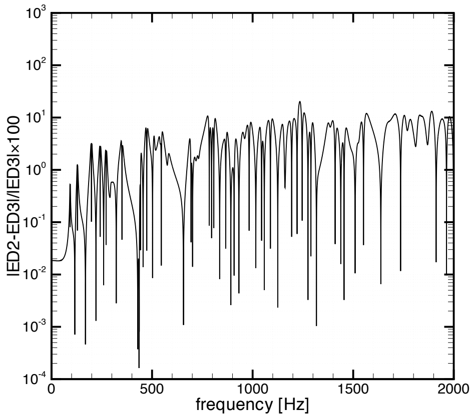

(b) error

Figure 6.4: Response in terms of fluid potential energy and percentage error between ED2 and ED3.

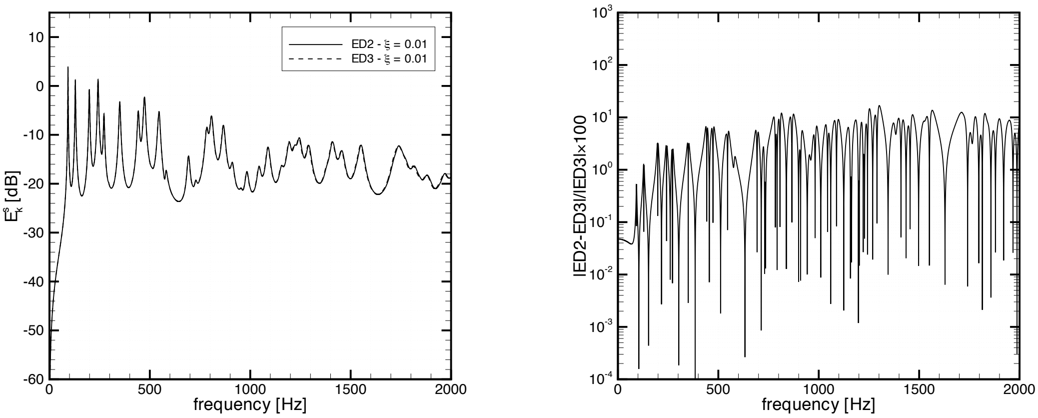

(a) FRF

(b) error

Figure 6.5: Response in terms of structural kinetic energy and percentage error between ED2 and ED3.

6.2 Test case 2

A thick laminated simply supported plate bonded by two piezoelectric layers is considered as the second numerical case. The plate structure has dimensions $1.2 \times 0.8\,\mathrm{m}^2$ and the shallow cavity is 0.2 m deep (see figure 6.6). The multilayered structure is made of 3 layers in symmetric cross-ply configuration with lamination scheme $0°/90°/0°$. The plate thickness is $t = 24\,\mathrm{mm}$, the Gr-Ep layers are 6.4 mm thick, whereas the PZT-4 top and bottom layers are 2.4 mm thick. Material properties are reported in appendix C. The plate is electrically grounded along its edge and only the OC case is considered. The cavity is air filled with speed of sound $c_f = 343\,\frac{\mathrm{m}}{\mathrm{s}}$ and mass density $\rho_f = 1.2\,\frac{\mathrm{Kg}}{\mathrm{m}^3}$. The plate is excited by a 1 N force applied at structural node A $(0.268\,\mathrm{m}, 0.108\,\mathrm{m})$ at the top of the plate in transversal direction. The frequency range of interest is $0 - 1\,\mathrm{KHz}$, i.e. $f_{max} = 1\,\mathrm{KHz}$. The system outputs are: structural mid-plane transversal displacement w_0 at point B of coordinates $(1.038\,\mathrm{m}, 0.63\,\mathrm{m})$, acoustic pressure at point C of coordinates $(0.684\,\mathrm{m}, 0.376\,\mathrm{m}, 0.13\,\mathrm{m})$, the plate kinetic energy E_k^s and the acoustic mean-square pressure E_p^f. A FE mesh of $45 \times 30 \times 10$ is used. The plates structure is modeled with ED2 and LD2 theories. The fully converged solution with the modal coupling technique is reached with considering acoustic and structural modes below $3f_{max}$. The uncoupled modes included in the frequency range $0-1\,\mathrm{KHz}$ are 41 cavity modes and 10 structural modes. Finally a modal damping factor $\xi_s = \xi_f = 0.01$ is assumed.

Figures 6.7 and 6.8 show the local response of the plate and cavity subsystems in terms of their own primary variables. Thanks to the low modal density in the considered frequency range, every single modal contribution is clear visible, mostly for what concern the structural response; here, due to the weak coupling between fluid and structure, only the 10 natural frequencies controlled by the plate vibrations are visible. (For more informations about the definition of plate- and cavity-controlled modes in coupled vibro-acoustic systems see [56] and [55]). The effect of the refined LD2 model with respect to the ED2 solution is evident for the plate displacement w_0; in fact, figure 6.8 shows that the FRF response of the refined LW model appears shifted toward low frequencies, due to the overstiffness exhibited by the ED2 solution. As it can seen, the error after 400 Hz may be important.

The differences between LW and ESL solution get more prominent if we consider the pressure response in figure 6.7. For instance, let us focus on the frequency range between 550 and 750 Hz. The natural frequencies of the coupled system over this frequency range are reported in table 6.1. Here, only the mode 22 is controlled by the plate vibrations, whereas the other natural frequencies are related to cavity-controlled modes. It is evident that the structural model refinement obtained using the LD2 theory is effective only for the mode 22, whereas the natural frequencies controlled by the acoustic cavity remain almost the same. This is also observed on the entire frequency range of interest. Therefore, in the pressure response, the refinement obtained for the plate-controlled modal contributions is combined with the unchanged cavity modal contributions, leading to a more complex behavior than the shifted effect observed for the displacement response. Indeed, table 6.1 and figure 6.7, show that the contributions from modes 22, 23, 24, 25, 26 lead to a single resonance peak when ED2 theory is adopted, whereas the LD2 theory shows the presence of two different peaks thanks to the refinement obtained for the predominantly structural mode 22. Consequently, also the amplitude of the two peaks is reduced. A similar case is observed between 800 and 900 Hz and between 950 and 1000 Hz; in the first case the refined LW theory shows different amplitude for resonance and anti-resonance peaks due to the different combination of the local modal contributions, whereas in the second case a larger amplitude resonance peak is obtained. Even if the error seems to grow as the frequency increases, high frequency analysis are difficult to be established due to the high computational effort (LD2 theory has 44 degrees-of-freedom per node). However the effect of the damping factor and of the raising modal density could modify this tendency.

The same consideration can be made for figures 6.9 and 6.10, where global response parameters are presented. Again, large differences are shown for the frequency range $600 - 1000$ Hz.

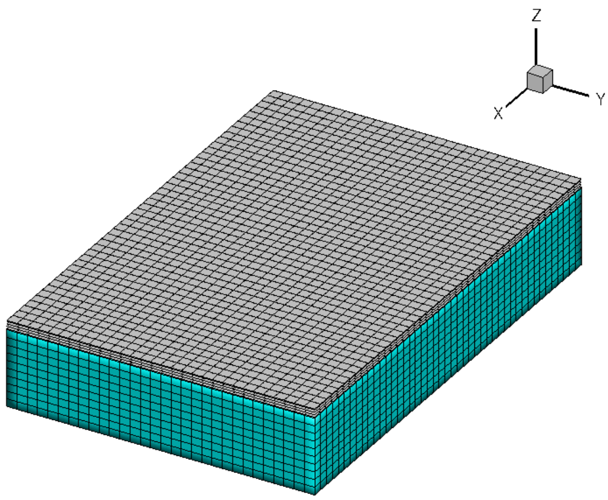

Figure 6.6: FE model for test case 2.

Table 6.1: Natural frequencies of the coupled system in the frequency range $550-750$ Hz.

	Frequency [Hz]	
mode	ED2	LD2
17	573.72	573.68
18	607.39	607.37
19	612.13	612.05
20	645.77	645.73
21	661.45	661.44
22	689.68	668.22
23	706.89	706.55
24	716.5	716.38
25	718.05	717.96
26	739.13	718.89
27	749.49	749.48

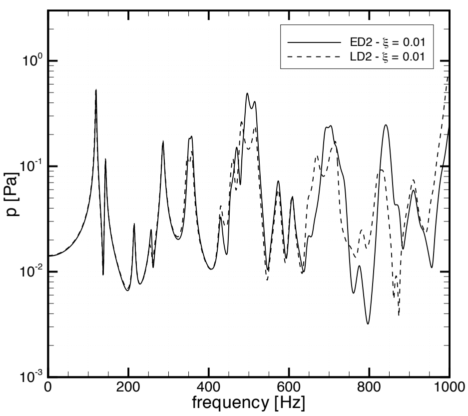

(a) FRF

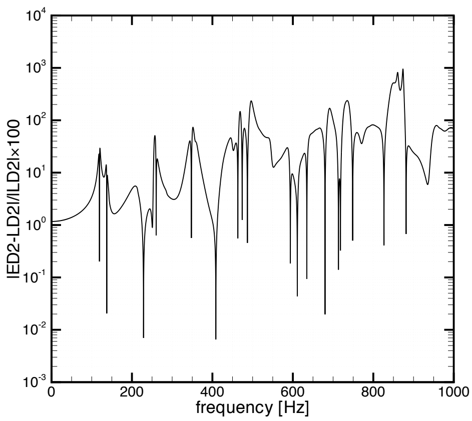

(b) error

Figure 6.7: Pressure response at point C and percentage error between ED2 and LD2.

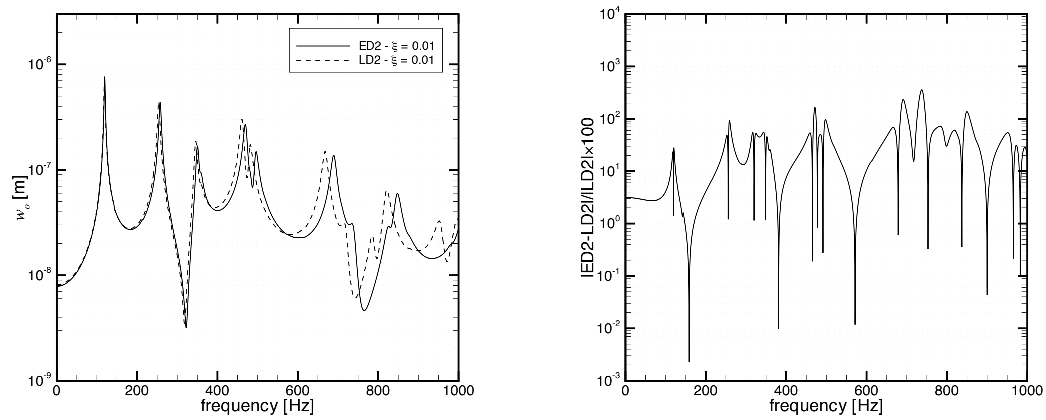

(a) FRF (b) error

Figure 6.8: Structural displacement response at point B and percentage error between ED2 and LD2.

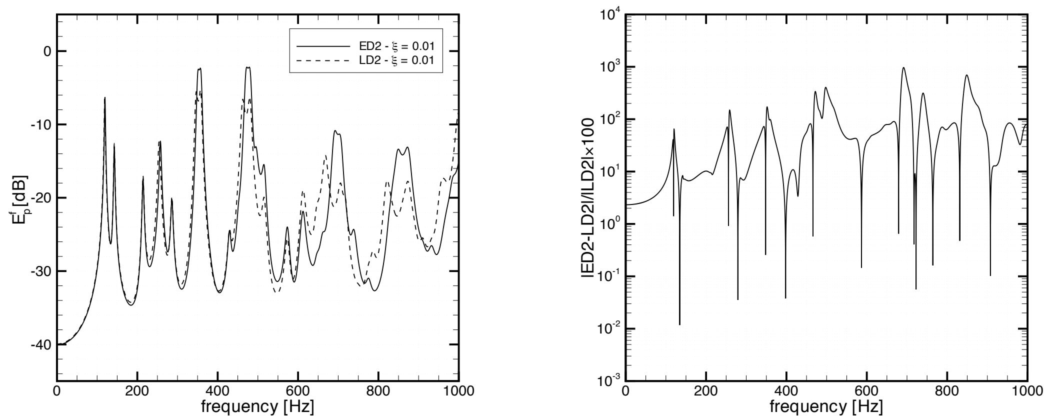

(a) FRF (b) error

Figure 6.9: Response in terms of fluid potential energy and percentage error between ED2 and LD2.

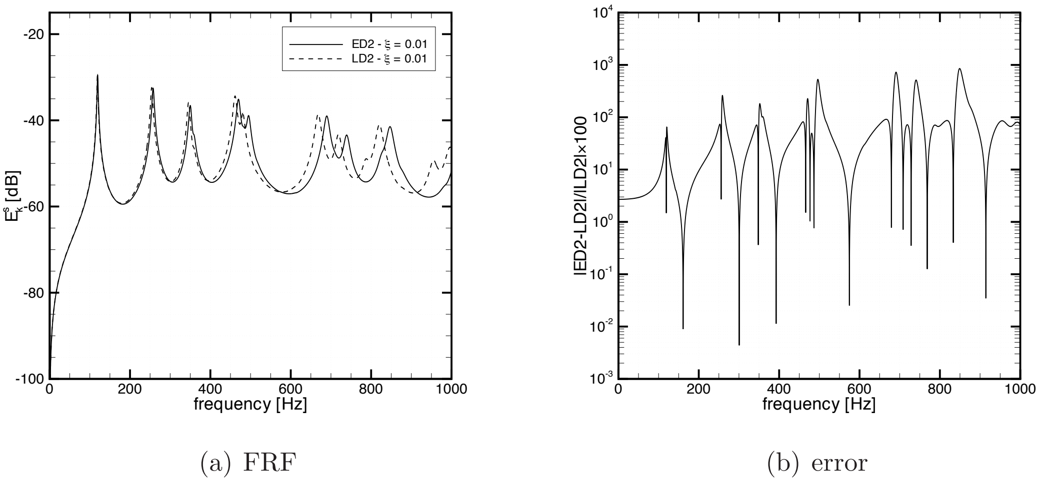

Figure 6.10: Response in terms of structural kinetic energy and percentage error between ED2 and LD2.

6.3 Test case 3

A sandwich-like composite plate is considered as the last numerical case. The plate structure has the dimensions $0.6 \times 0.4\,\mathrm{m}^2$ and the cavity is $0.5\,\mathrm{m}$ deep (see figure 6.11). The composite structure is made of two-layered Gr-Ep skins with lamination scheme $90°/0°$ and a soft core made of material 5. The plate thickness is $t = 12\,\mathrm{mm}$, the face skins layers are $0.5\,\mathrm{mm}$ thick and the core thickness is $10\,\mathrm{mm}$. Again, material properties are reported in appendix C. The cavity is air filled with speed of sound $c_f = 343\,\frac{\mathrm{m}}{\mathrm{s}}$ and mass density $\rho_f = 1.2\,\frac{\mathrm{Kg}}{\mathrm{m}^3}$. The plate is excited by a 1N force applied at the top of structural node A of coordinates $(0.13\,\mathrm{m}, 0.053\,\mathrm{m})$ at the top of the plate in transversal direction. The frequency range of interest is $0 - 1\,\mathrm{KHz}$, i.e. $f_{max} = 1\,\mathrm{KHz}$. The system outputs are: colocated structural transversal displacement w at core-skin top interface, acoustic pressure at point B of coordinates $(0.346\,\mathrm{m}, 0.186\,\mathrm{m}, 0.325\,\mathrm{m})$, the plate kinetic energy E_k^s and the acoustic mean-square pressure E_p^f. A FE mesh of $90 \times 60 \times 20$ is kept. The LW description of the sandwich plates allow to take advantage from the use of Lagrangian polynomials; two slighty different boundary condition sets are compared. In the first case a fully clamped condition is considered (denoted by BC1), whereas in the second case (denoted by BC2) the tranversal displacement is free on the bottom skin which interact with the fluid. A fully converged solution is reached considering an uncoupled modal basis obtained with the acoustic and structural modes below $3f_{max}$. The uncoupled modes included in the frequency range $0-1\,\mathrm{KHz}$ are 25 cavity modes and 44 structural modes. Finally a modal damping factor $\xi_s = \xi_f = 0.01$ is assumed.

In figure 6.13 the colocated structural displacement at the core-skin top interface is presented. It can be observed that a shifting effect occurs when the second set of boundary conditions is considered. Indeed, the modified clamped condition are less constraining, then a shifting effect towards lower frequencies is expected. On the other hand, larger error are observed in figure 6.12, where the FRF in terms of pressure at point B is presented. Unlike the previously analyzed piezoelectric case, the high modal density exhibited in the second half of the considered frequency range makes it difficult to comment the differences between the two sets of boundary conditions in terms of modal contributions. However, a careful scrunity of table 6.2, where the coupled natural frequencies in the range $600 - 800\,\mathrm{Hz}$ are reported, show that a slightly different set of structural constraints has effect on both the modes controlled by the structural and cavity vibrations. Indeed, five cavity modes are observed over this range, but only two of these natural frequencies are not affected by the second set of boundary conditions (modes 44 and 33).

Although a larger difference between the two set of constraints is expected as the frequency increases, i.e. when shorter wavelengths appear, the high modal density and the accounted damping effect tend to contain this effect. This is more clear observing the global parameters in figures 6.14 and 6.15, where single modal contributions are not yet observable above $600\,\mathrm{Hz}$, mainly considering the response in terms of structural kinetic energy. In fact, in this case, the error even seems to decrese at higher frequencies.

Finally it can be pointed out that a poor description of the boundary conditions can potentially lead to significant error at high frequencies range, but the high modal density and the dissipation of the system could contain the error, mainly for what concern the energy parameters.

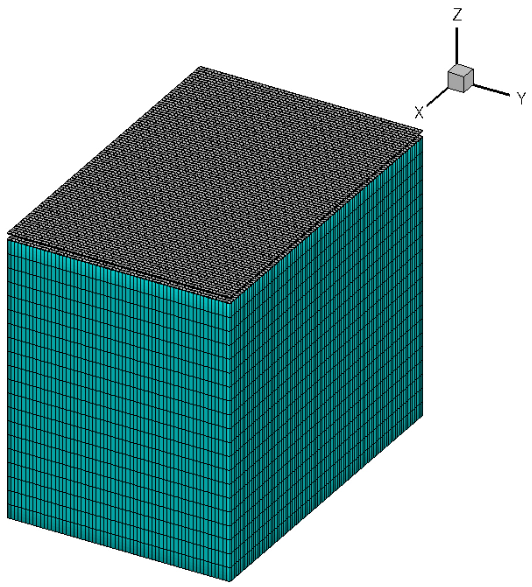

Figure 6.11: FE model for test case 3.

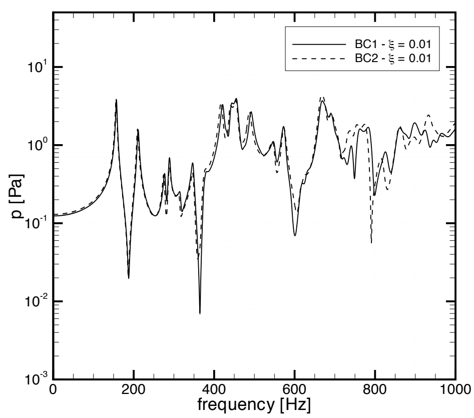

(a) FRF

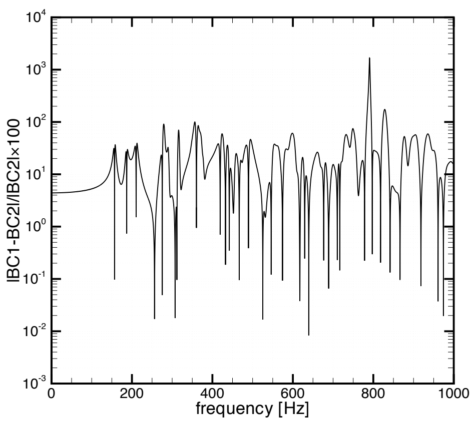

(b) error

Figure 6.12: Pressure response at point B and percentage error between BC1 and BC2.

Table 6.2: Natural frequencies of the coupled system in the frequency range $600-800$ Hz.

	Frequency [Hz]	
mode	BC1	BC2
26	617.45	613.72
27	621.21	615.78
28	627.91	623.08
29	629.56	626.31
30	666.47	664.54
31	678.51	671.71
32	679.23	675.76
33	691.51	691.11
34	702.76	696.47
35	714.12	711.77
36	722.87	718.85
37	739.01	731.15
38	739.92	731.72
39	745.51	742.56
40	758.77	752.35
41	786.51	777.17
42	790.181	783.28
43	794.3	786.89
44	794.92	794.85

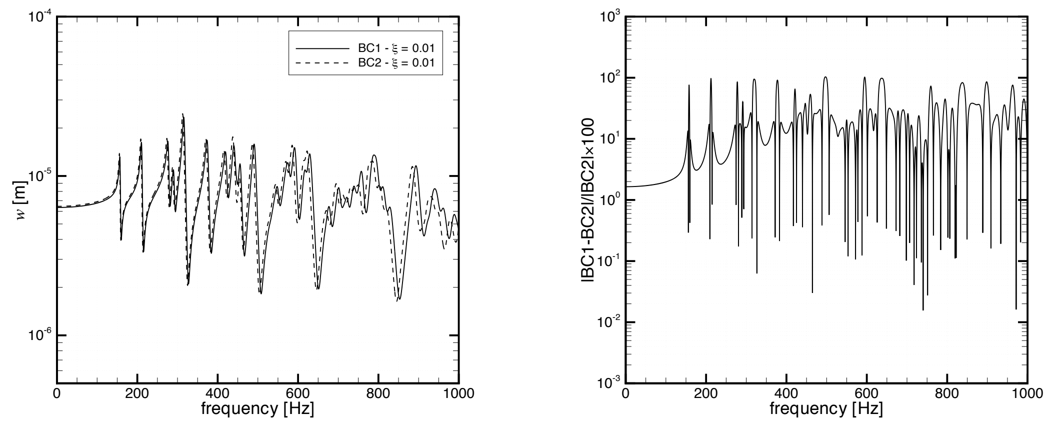

(a) FRF

(b) error

Figure 6.13: Structural displacement response at point B and percentage error between BC1 and BC2.

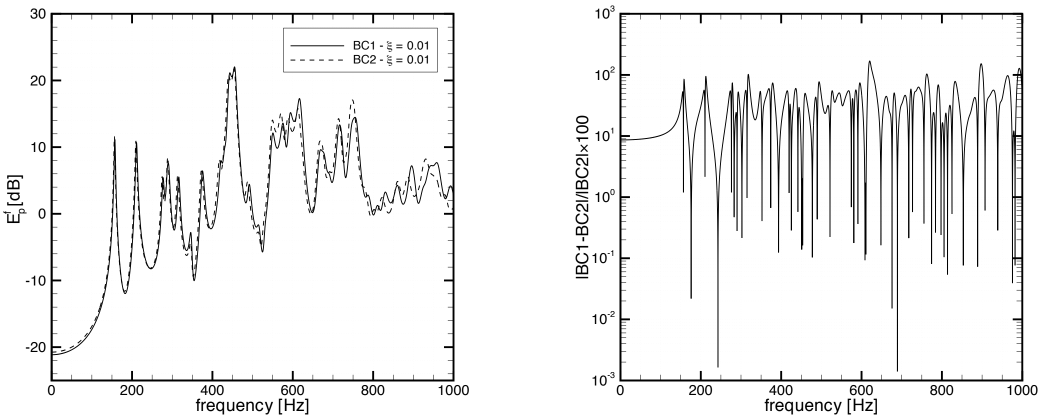

(a) FRF (b) error

Figure 6.14: Response in terms of fluid potential energy and percentage error between BC1 and BC2.

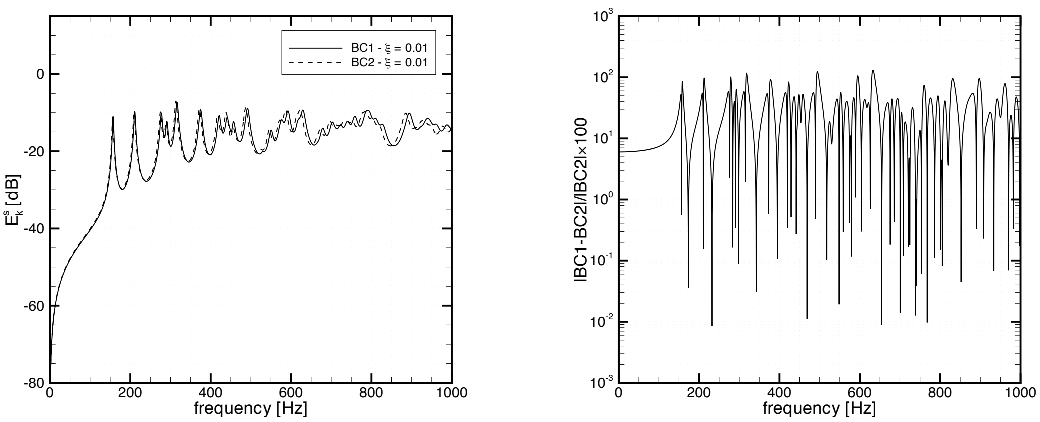

(a) FRF (b) error

Figure 6.15: Response in terms of structural kinetic energy and percentage error between BC1 and BC2.

Conclusions and future works

In this work the Carrera's UF has been extended in the framework of vibro-acoustic coupling, providing a powerful and accurate tool for the frequency analysis of plate-cavity systems. The main focus of this work lies on the formulation of the vibro-acoustic coupling for composite plates with piezoelectric layers in contact with enclosed acoustic cavity and its FE code developing. Shorter wavelength frequency range has been considered, in order to estimate the higher order effects of the through-the-thickness assumptions for the structural variables on the coupled system behavior.

The need for high computational efficiency in the deterministic vibro-acoustic analysis has been a crucial point in this work. The structural FE code has been written in order to contain the computational effort when large model size must be considered in mid-frequency analysis. The sparsity pattern of the FE matrices and the high efficiency of the iterative solvers for large and sparse problems have been exploited in order to reduce the memory requirements and the computational time. The performance of the developed structural FE code has been demonstrated in chapter 4, where a convergence analysis and a careful validation have been considered for mechanical and electromechanical rectangular plates with different layouts and boundary conditions. Moreover, the flexibility of the FE model permits to consider more generic plate configurations, for instance mixed boundary conditions and skewed plates, providing an efficient tool for static and dynamic structural analysis. The present structural model has been coupled with a pressure-based FE formulation for the acoustic cavity, leading to the unsymmetric (u, p) formulation of the vibro-acoustic problem. The drawbacks related with the lack of symmetry in the final, large, set of equations has been limited using the uncoupled modal technique to reduce the problem size. The uncoupled basis have been extracted with efficient iterative solver from the uncoupled symmetric structural and acoustic problem, and the final reduced size model has been easily solved by dense solver. The accuracy of the coupled model and the efficiency of the solution procedure have been validated in chapter 5, where it has been shown that the modal coupling solution can be efficiently used in case of weakly coupled systems. In such cases, this techniques provides an optimal reduction of the computational burden since only few uncoupled modes must be considered in the reduced basis to obtain the desired accuracy, mainly when energetic parameters are of interest. More difficult is the application of the uncoupled modal reduction in case of strong coupling.

In chapter 6 the vibro-acoustic FE code has been used in order to presenting three representative benchmarks of plate-cavity systems. Here the fundamental features of the UF has been exploited. Indeed, the unified approach has permitted to consider different plate layouts, i.e. laminated, sandwich and piezo-embedded plates, different kinematic assumptions, i.e. ESL and LW descriptions, and different high order refinements with a unique FE formulation. In this way the effects of these models on the accuracy of the vibro-acoustic response have been evalueted. As expected, the high order effects observed for pure structural case (section 4.3) also affect the fluid-structure coupling behavior (sections 6.1 and 6.2). In particular, it has been observed that no higher order theories are required when thin isotropic plates or thin multulayered plates with many layers are considered (sections 4.3 and 6.1). However, higher order terms must be taken into account as the frequency and/or the thickness ratio increases (sections 4.3 and 6.2). Moreover, it has been observed that the modes controlled by plate vibrations seem to be more sensitive to the plate theory refinements than those controlled by the cavity vibrations (section 6.2). In section 4.2 it has been shown that a refined LW description is strictly recommended when high transversely isotropic plates are considered. Besides, it has been shown how the LW description can be exploited to provide a better approximation of the boundary conditions, and that two slightly different sets of boundary conditions can lead to different dynamic behaviors of the vibro-acoustic system, mainly as the frequency increases. It has to be said that, even if all the considered refinements seem to have more prominent effect over higher frequency ranges, the raising modal density and the damping dissipation effect could contain, or even reduce, this tendency, mainly for what concern the global response of the coupled system.

The above conclusions are valid for the simple coupled systems and the frequency range considered in this work. Indeed, the modal coupling approach has not permitted to analyze strong coupled system, i.e. water filled cavity, complex geometry or double panel configurations. Moreover, the limited computational facilities has not permitted to consider more complex or larger models. More general analysis and a complete extension of the frequency range towards the intrinsic limit of the deterministic approaches could be obtained only with the following modeling and numerical improvements.

- Even if a unified formulation is powerful tool providing an arbitrary accurate analysis of a widely variety of plate configurations, the UF can hardly provide a computationally efficient model. The recovery of simple plate theories, such as CPT or FSDT, can be obtained with the introduction of penalty functions [21]. However, in this way only an approximation of these simple theories can be obtained. On the other hand, a generalized approach to the UF could be studied in order to freely choose the orders of each variables regardless of the the orders used for the thickness expansion of the other variables. In this way all classical ESL models could be obtained, as shown in [24]. Moreover, a different expansion could be used for different layers, providing an accurate description only where it is necessary. This type of approach could lead to a significant reduction of the computational effort: for instance, a sandwich plate could be modeled with higher order expansion terms only in the core region, whereas a Kirchhoff model could be used for the plate faces.

- In order to extend the applicability of the present FE approach to the mid-frequency range, all the numerical aspects presented in the introduction chapter should be studied. A fully coupled solution of the unsymmetric eigenvalue problem using iterative solvers should be developed, providing the truncated basis for the modal analysis. Moreover, also the static corrections for the uncoupled modal reduction strategy and non modal approaches should be considered. In this way, a large variety of solution procedure could be used depending on the considered problem. Although the FE model efficiency reduces as the frequency increases, leading to excessively large problems, more accurate and efficient numerical approximation techniques can be hardly compete with the great flexibility of the FE approach. Indeed, even if meshless and spectral methods show excellent convergence properties, they are not capable, at they current stage of development, of combining three important aspects, i.e. enhanced computational efficiency together with the general applicability with respect to geometrical complexibility and the ability to account for mutual fluid-structure coupling effect. However the hybrid approach proposed by Desmet [34], which combine the FE approach for the structural modeling with the efficient WB prediction technique for the acoustic field, seems to obtain satisfactory results. From this point of view, an extension of the present formulation accounting for the coupling between the unified FE structural model and the WB approach for the acoustic field could be a very interesting study.

APPENDIX A

Explicit form of the stiffness nucleus

In this appendix the explicit form for the UF stiffness nucleus is presented. In order to lighten the notation, the following integral operator is introduced:

$$\int_{\Omega_s^k} (\cdot)\,\mathrm{d}s = \triangleleft (\cdot) \triangleright$$

where $(\cdot)$ indicates the generic shape functions products on which the integral operator must be applied. The element by element explicit form of the 4×4 stiffness nucleus $\mathbf{K}^{k\tau sij}$ is:

$$\begin{aligned}
\mathbf{K}^{k\tau sij}(1,1) &= E^k_{\tau s}C^k_{11} \triangleleft N_{i,x}N_{j,x} \triangleright + E^k_{\tau s}C^k_{16} \triangleleft N_{i,x}N_{j,y} \triangleright + E^k_{\tau s}C^k_{16} \triangleleft N_{i,y}N_{j,x} \triangleright + E^k_{\tau s}C^k_{66} \triangleleft N_{i,y}N_{j,y} \triangleright + E^k_{\tau,z\,s,z}C^k_{55} \triangleleft N_iN_j \triangleright \\
\mathbf{K}^{k\tau sij}(1,2) &= E^k_{\tau s}C^k_{12} \triangleleft N_{i,x}N_{j,y} \triangleright + E^k_{\tau s}C^k_{16} \triangleleft N_{i,x}N_{j,x} \triangleright + E^k_{\tau s}C^k_{26} \triangleleft N_{i,y}N_{j,y} \triangleright + E^k_{\tau s}C^k_{66} \triangleleft N_{i,y}N_{j,x} \triangleright + E^k_{\tau,z\,s,z}C^k_{45} \triangleleft N_iN_j \triangleright \\
\mathbf{K}^{k\tau sij}(1,3) &= E^k_{\tau,z\,s}C^k_{55} \triangleleft N_iN_{j,x} \triangleright + E^k_{\tau,z\,s}C^k_{45} \triangleleft N_iN_{j,y} \triangleright + E^k_{\tau s,z}C^k_{13} \triangleleft N_{i,x}N_j \triangleright + E^k_{\tau s,z}C^k_{36} \triangleleft N_{i,y}N_j \triangleright + \\
\mathbf{K}^{k\tau sij}(1,4) &= E^k_{\tau,z\,s}e^k_{51} \triangleleft N_iN_{j,x} \triangleright + E^k_{\tau,z\,s}e^k_{52} \triangleleft N_iN_{j,y} \triangleright + E^k_{\tau s,z}e^k_{13} \triangleleft N_{i,x}N_j \triangleright + E^k_{\tau s,z}e^k_{63} \triangleleft N_{i,y}N_j \triangleright + \\
\mathbf{K}^{k\tau sij}(2,1) &= E^k_{\tau s}C^k_{12} \triangleleft N_{i,y}N_{j,x} \triangleright + E^k_{\tau s}C^k_{16} \triangleleft N_{i,x}N_{j,x} \triangleright + E^k_{\tau s}C^k_{26} \triangleleft N_{i,y}N_{j,y} \triangleright + E^k_{\tau s}C^k_{66} \triangleleft N_{i,x}N_{j,y} \triangleright + E^k_{\tau,z\,s,z}C^k_{45} \triangleleft N_iN_j \triangleright \\
\mathbf{K}^{k\tau sij}(2,2) &= E^k_{\tau s}C^k_{22} \triangleleft N_{i,y}N_{j,y} \triangleright + E^k_{\tau s}C^k_{26} \triangleleft N_{i,y}N_{j,x} \triangleright + E^k_{\tau s}C^k_{26} \triangleleft N_{i,x}N_{j,y} \triangleright + E^k_{\tau s}C^k_{66} \triangleleft N_{i,x}N_{j,x} \triangleright + E^k_{\tau,z\,s,z}C^k_{44} \triangleleft N_iN_j \triangleright \\
\mathbf{K}^{k\tau sij}(2,3) &= E^k_{\tau,z\,s}C^k_{45} \triangleleft N_iN_{j,x} \triangleright + E^k_{\tau,z\,s}C^k_{44} \triangleleft N_iN_{j,y} \triangleright + E^k_{\tau s,z}C^k_{36} \triangleleft N_{i,x}N_j \triangleright + E^k_{\tau s,z}C^k_{23} \triangleleft N_{i,y}N_j \triangleright + \\
\mathbf{K}^{k\tau sij}(2,4) &= E^k_{\tau,z\,s}e^k_{41} \triangleleft N_iN_{j,x} \triangleright + E^k_{\tau,z\,s}e^k_{24} \triangleleft N_iN_{j,y} \triangleright + E^k_{\tau s,z}e^k_{63} \triangleleft N_{i,x}N_j \triangleright + E^k_{\tau s,z}e^k_{23} \triangleleft N_{i,y}N_j \triangleright + \\
\mathbf{K}^{k\tau sij}(3,1) &= E^k_{\tau s,z}C^k_{55} \triangleleft N_{i,x}N_j \triangleright + E^k_{\tau s,z}C^k_{45} \triangleleft N_{i,y}N_j \triangleright + E^k_{\tau,z\,s}C^k_{13} \triangleleft N_iN_{j,x} \triangleright + E^k_{\tau,z\,s}C^k_{36} \triangleleft N_iN_{j,y} \triangleright + \\
\mathbf{K}^{k\tau sij}(3,2) &= E^k_{\tau s,z}C^k_{45} \triangleleft N_{i,x}N_j \triangleright + E^k_{\tau s,z}C^k_{44} \triangleleft N_{i,y}N_j \triangleright + E^k_{\tau,z\,s}C^k_{36} \triangleleft N_iN_{j,x} \triangleright + E^k_{\tau,z\,s}C^k_{23} \triangleleft N_iN_{j,y} \triangleright + \\
\mathbf{K}^{k\tau sij}(3,3) &= E^k_{\tau s}C^k_{55} \triangleleft N_{i,x}N_{j,x} \triangleright + E^k_{\tau s}C^k_{45} \triangleleft N_{i,x}N_{j,y} \triangleright + E^k_{\tau s}C^k_{45} \triangleleft N_{i,y}N_{j,x} \triangleright + E^k_{\tau s}C^k_{44} \triangleleft N_{i,y}N_{j,y} \triangleright + E^k_{\tau,z\,s,z}C^k_{33} \triangleleft N_iN_j \triangleright \\
\mathbf{K}^{k\tau sij}(3,4) &= E^k_{\tau s}e^k_{51} \triangleleft N_{i,x}N_{j,x} \triangleright + E^k_{\tau s}e^k_{52} \triangleleft N_{i,x}N_{j,y} \triangleright + E^k_{\tau s}e^k_{41} \triangleleft N_{i,y}N_{j,x} \triangleright + E^k_{\tau s}e^k_{42} \triangleleft N_{i,y}N_{j,y} \triangleright + E^k_{\tau,z\,s,z}e^k_{33} \triangleleft N_iN_j \triangleright \\
\mathbf{K}^{k\tau sij}(4,1) &= E^k_{\tau s,z}e^k_{51} \triangleleft N_{i,x}N_j \triangleright + E^k_{\tau s,z}e^k_{52} \triangleleft N_{i,y}N_j \triangleright + E^k_{\tau,z\,s}e^k_{13} \triangleleft N_iN_{j,x} \triangleright + E^k_{\tau,z\,s}e^k_{63} \triangleleft N_iN_{j,y} \triangleright + \\
\mathbf{K}^{k\tau sij}(2,4) &= E^k_{\tau s,z}e^k_{41} \triangleleft N_{i,x}N_j \triangleright + E^k_{\tau s,z}e^k_{24} \triangleleft N_{i,y}N_j \triangleright + E^k_{\tau,z\,s}e^k_{63} \triangleleft N_iN_{j,x} \triangleright + E^k_{\tau,z\,s}e^k_{23} \triangleleft N_iN_{j,y} \triangleright + \\
\mathbf{K}^{k\tau sij}(3,4) &= E^k_{\tau s}e^k_{51} \triangleleft N_{i,x}N_{j,x} \triangleright + E^k_{\tau s}e^k_{52} \triangleleft N_{i,y}N_{j,x} \triangleright + E^k_{\tau s}e^k_{41} \triangleleft N_{i,x}N_{j,y} \triangleright + E^k_{\tau s}e^k_{42} \triangleleft N_{i,y}N_{j,y} \triangleright + E^k_{\tau,z\,s,z}e^k_{33} \triangleleft N_iN_j \triangleright \\
\mathbf{K}^{k\tau sij}(1,1) &= E^k_{\tau s}\epsilon^k_{11} \triangleleft N_{i,x}N_{j,x} \triangleright + E^k_{\tau s}\epsilon^k_{12} \triangleleft N_{i,x}N_{j,y} \triangleright + E^k_{\tau s}\epsilon^k_{12} \triangleleft N_{i,y}N_{j,x} \triangleright + E^k_{\tau s}\epsilon^k_{22} \triangleleft N_{i,y}N_{j,y} \triangleright + E^k_{\tau,z\,s,z}\epsilon^k_{33} \triangleleft N_iN_j \triangleright
\end{aligned}$$

APPENDIX B

Programming details

A FORTRAN code based on the FE formulation described chapter 2 has been developed. The code is subdivided into four upper level modules, which manage the pre-processing and post-processing routines, the matrices assembly procedure and the solver. The pre-processing module creates the FE data structure given the mesh obtained with an external software. The post-processing module, similary, interfaces the solution data structure with an external visualization softaware. Independent modules are accounted for uncoupled structural, uncoupled acoustic and coupled structural-acoustic problems. Clearly, the heart of the code are the assembly routines and the solver; indeed, as remarked in the introduction chapter, the memory requirements and the computing time are the two major important aspects for a FE approximation of the fluid-structure coupling. Therefore, an efficient way for the matrix storage and for limiting the computational time has been taken into account. In particular, sparse storage schemes have been used for the FE matrices allocation, and efficient iterative solvers have been chosen to extract the truncated uncoupled modal basis. These efficient solutions has permitted to run the present FE code on a 2.8 GHz Intel *core 2 Duo* processor with a 4 GB ram. In figure B.1 the simplified organization of the developed FE code is depicted, and the available analysis are also reported. It is remarked that the coupled analysis provided by the developed code are based on the modal coupling technique presented in chapter 3.

B.1 Sparse matrix storage

When large sparse matrices must be stored, like as in the FE codes, a great save of memory can be obtained storing only the non null elements of the considered matrix. One of the difficulties in sparese matrix computations is the variety of matrices that are encountered in pratical applications. The purpose of each of these schemes is to gain efficiency both in terms of memory utilization and arithmetic operations. As a result many different ways of storing sparse matrices have been developed to take advantage of the structure of the matrices or the specificity of the problem from which they arise. For example, when regulary structured matrices, simple vectors can be utilized for storing diagonal terms. However, if the matrix is not regulary structured, more generic scheme must be adopted; from this point of view, the one of the most common storage scheme in use today is the Compressed Sparse Row (CSR) format. In this scheme all non zero entries are stored row by row in a one-dimensional array A together with an array JA containing their column indices and a poiter array which contains the addresses in A and JA of the beginning of each row. Also the Coordinate (COO) format is one of the most used schemes. In COO format the non null entries are stored with their row and column indices. However the efficiency is slightly reduced with respect to the CSR format. For these reasons, the CSR format is the storage schemes selected for the present FE code. The SPARSKIT2 library [3] has been also used to manage simple linear algebra operations for sparse matrices in an efficient way.

B.2 Iterative solver

As an alternative to direct solution method used for dense matrix problems, the iterative solvers, which are based on working with sequences of orthogonal vectors, are the most effective iterative procedures for solving large sparse matrix problems. In this context, the *Scalable Library for Eigenvalue Problem Computations* (SLEPc) [2], based on the *Portable Extensive Toolkit for Scientific Computation* (PETSc) [1] linear and non-linear algebra package, has been selected as the solver library in the present FE code. SLEPc focuses on the solution of eigenvalue problem in which the matrices are large and sparse, and only methods that preserve sparsity are considered. Most eigensolvers provided by SLEPc perform a Rayleigh-Ritz projection for extracting the spectral approximations, that is, they project the problem onto a low-dimansional subspace that is built appropriately. Starting from this general idea, eigensolvers differ from each other in whic subspace is used, how it is built and other convergence and storage requirements improving. For a detailed and comprehensive description of these methods, the reader can refer to [67].

Even if, in contrast to direct solvers, the performance of these iterative methods is highly problem-dependent and the convergence may deteriorate under certain conditions, they provide an efficient solution for the uncoupled modal extraction. Indeed, as explained in chapter 3, the structural and acoustic eigenvalue problems are separately solved and no numerical difficulties arise for the uncoupled spectral analysis with iterative methods. In this way the reduced basis can be efficiently calculated, and the modal coupling matrix $\tilde{\mathbf{S}}$ can be easily computed. Clearly the reduced problem does not have the memory requirements of the starting large FE model, then the FRF analysis can be easily computed in a MATLAB environment.

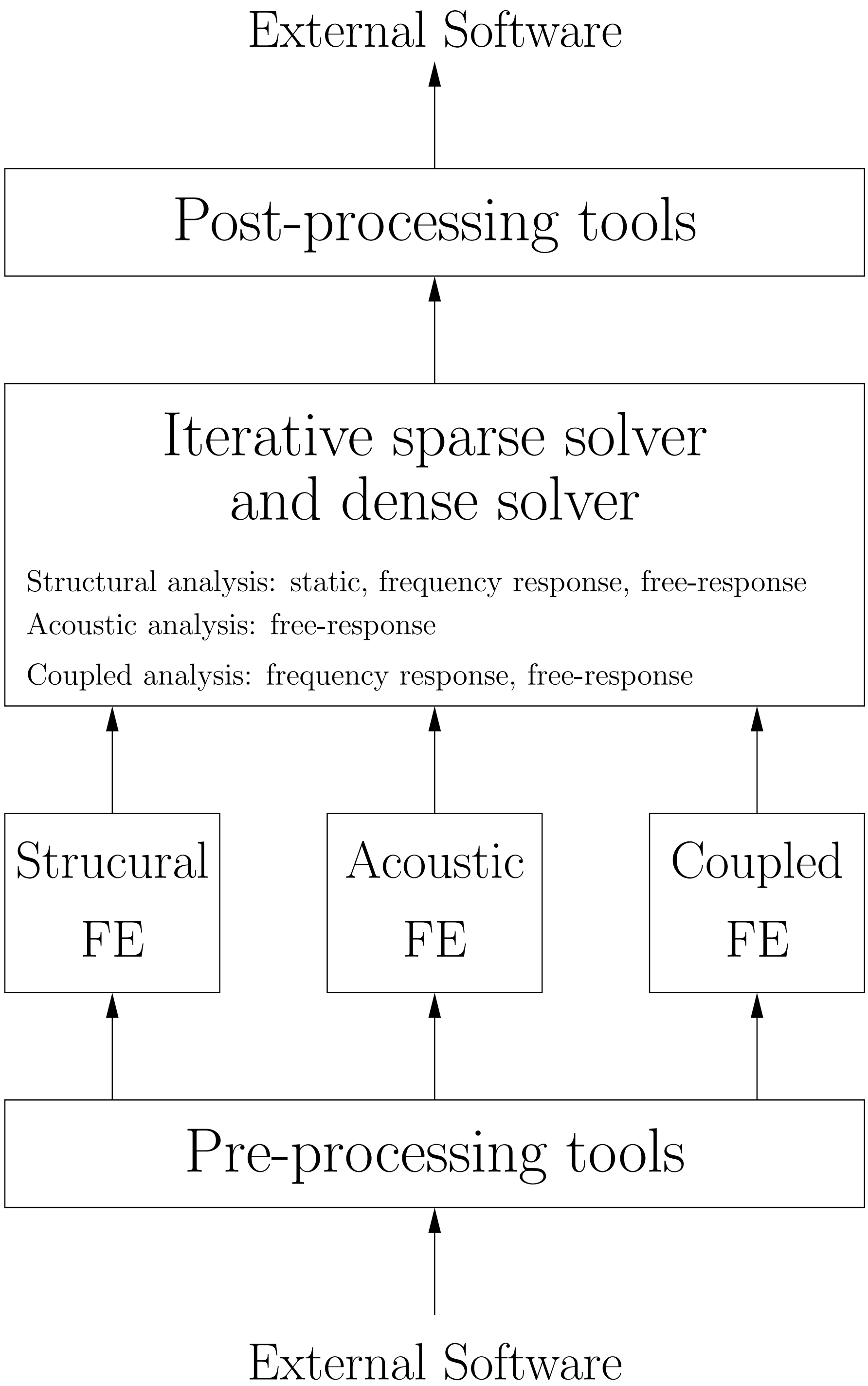

Figure B.1: Organization of the developed FE code.

Materials propeties

In this Appendix, the physical properties of the materials used in chapters 4 and 6 are reported in tabular form. In table C.1 the mechanical properties of four orthotropic materials and of a soft core are reported. In table C.2, the properties of the sandwich-type plate used in [51] for experimental analysis are listed. Finally, in tables C.3 and C.4, the properties of the *Graphite-Epoxy* and PZT-4 materials are reported.

Table C.1: Materials adopted in the present work.

	materials number				
	1	2	3	4	5
E_1 [GPa]	25	40	25.1	131	0.00689
E_2 [GPa]	1	1	25.1	10.34	0.00689
E_3 [GPa]	1	1	0.75	10.34	0.00689
G_{12} [GPa]	0.5	0.6	1.36	6.895	0.00345
G_{13} [GPa]	0.5	0.6	1.2	6.205	0.00345
G_{23} [GPa]	0.2	0.5	0.47	6.895	0.00345
ν_{12} [-]	0.25	0.25	0.036	0.22	0
ν_{13} [-]	0.25	0.25	0.25	0.22	0
ν_{23} [-]	0.25	0.25	0.171	0.49	0
ρ [Kg/m^3]	1000	1000	1000	1627	0.097

Table C.2: Materials adopted for the honeycomb plate with dimensions $a = 1.83$ m and $b = 1.22$ m. Values from [60].

	face sheets	core
E_1 [GPa]	68.984	0
E_2 [GPa]	68.984	0
E_3 [GPa]	68.984	0.1379
G_{12} [GPa]	25.924	0
G_{13} [GPa]	25.924	0.13445
G_{23} [GPa]	25.924	0.05171
ν_{12} [-]	0.3	0
ν_{13} [-]	0.3	0
ν_{23} [-]	0.3	0
ρ [Kg/m^3]	2768	121.8
t [mm]	0.4064	6.35

Table C.3: Graphite-Epoxy material properties. $\epsilon_0 = 8.8510^{-12}$ [F/m].

E_1 [GPa]	132.38
E_2 [GPa]	10.76
E_3 [GPa]	10.76
G_{12} [GPa]	5.65
G_{13} [GPa]	5.65
G_{23} [GPa]	3.61
ν_{12} [-]	0.24
ν_{13} [-]	0.24
ν_{23} [-]	0.49
ρ [Kg/m^3]	1578
ϵ_{11}/ϵ_0 [-]	3.5
ϵ_{22}/ϵ_0 [-]	3.0
ϵ_{33}/ϵ_0 [-]	3.0

Table C.4: PZT-4 material properties. $\epsilon_0 = 8.8510^{-12}$ [F/m].

E_1 [GPa]	81.3
E_2 [GPa]	81.3
E_3 [GPa]	64.5
G_{12} [GPa]	30.6
G_{13} [GPa]	25.6
G_{23} [GPa]	25.6
ν_{12} [-]	0.33
ν_{13} [-]	0.43
ν_{23} [-]	0.43
ρ [Kg/m^3]	7600
e_{31} [Kg/m^2]	7.209
e_{32} [Kg/m^2]	7.209
e_{33} [Kg/m^2]	15.08
e_{24} [Kg/m^2]	12.322
e_{15} [Kg/m^2]	12.322
ϵ_{11}/ϵ_0 [-]	1475
ϵ_{22}/ϵ_0 [-]	1475
ϵ_{33}/ϵ_0 [-]	1300

APPENDIX D

Convergence tables

In this Appendix, the convergence tables referred to the numerical cases presented in section 4.1 are reported. In the following, the superscript ^{s} indicates that the assumed convergent frequency parameter is associated with a symmetric mode in the thickness direction.

Table D.1: Convergence of the first 10 frequency parameters λ for the SS modes of a SSSS isotropic square plate with $\nu = 0.3$. Only ED theories are considered.

			mode number									
$\frac{t}{b}$	$(n_x \times n_y)$, N	n_{dof}	SS-1	SS-2	SS-3	SS-4	SS-5	SS-6	SS-7	SS-8	SS-9	SS-10
0.01	(10×10), 2	1089	2.0051	10.2532	10.2532	18.4188	28.0665	28.0665	36.0558	36.0558	53.3102	58.4811
	(20×20), 2	3969	2.0008	10.0503	10.0503	18.0647	26.4106	26.4106	34.3538	34.3538	50.4982	51.6172
	(30×30), 2	8649	2.0000	10.0135	10.0135	18.0003	26.1215	26.1215	34.0548	34.0548	50.0021	50.4867
	(40×40), 2	15129	1.9997	10.0007	10.0007	17.9779	26.0215	26.0215	33.9513	33.9513	49.8302	50.1003
	(50×50), 2	23409	1.9996	9.9948	9.9948	17.9675	25.9755	25.9755	33.9036	33.9036	49.7509	49.9231
	(60×60), 2	33489	1.9995	9.9915	9.9915	17.9618	25.9505	25.9505	33.8777	33.8777	49.7080	49.8273
	(60×60), 3	44652	1.9995	9.9898	9.9898	17.9564	25.9392	25.9392	33.8584	33.8584	49.6665	49.7856
	(60×60), 4	55815	1.9995	9.9898	9.9898	17.9564	25.9391	25.9391	33.8584	33.8584	49.6665	49.7856
0.1	(10×10), 2	1089	1.9455	8.9628	8.9628	9.2469	14.8197	15.5827	20.8253	20.8253	20.8512	20.8512
	(20×20), 2	3969	1.9416	8.8143	8.8143	9.2308	14.6240	15.5733	19.9470	19.9470	20.6843	20.6843
	(30×30), 2	8649	1.9409	8.7872	8.7872	9.2279	14.5879	15.5715	19.7897	19.7897	20.6535	20.6535
	(40×40), 2	15129	1.9406	8.7778	8.7778	9.2268	14.5753	15.5709	19.7350	19.7350	20.6427	20.6427
	(50×50), 2	23409	1.9405	8.7734	8.7734	9.2263	14.5694	15.5706	19.7098	19.7098	20.6377	20.6377
	(60×60), 2	33489	1.9404	8.7710	8.7710	9.2261^s	14.5662	15.5705^s	19.6961	19.6961	20.6350^s	20.6350^s
	(60×60), 3	44652	1.9344	8.6683	8.6683	9.2261^s	14.3182	15.5703^s	19.2880	19.2880	20.6350^s	20.6350^s
	(60×60), 4	55815	1.9344	8.6669	8.6669	9.2261^s	14.3122	15.5703^s	19.2738	19.2738	20.6350^s	20.6350^s

Table D.2: Convergence of the first 10 frequency parameters λ for the AS modes of a SSSS isotropic square with $\nu = 0.3$ (SA modes are identical). Only ED theories are considered.

			mode number									
$\frac{t}{b}$	$(n_x \times n_y)$, N	n_{dof}	AS-1	AS-2	AS-3	AS-4	AS-5	AS-6	AS-7	AS-8	AS-9	AS-10
0.01	(10×10), 2	1089	5.0492	13.2669	17.8227	25.9129	31.0154	41.4204	43.3872	49.2799	61.3224	65.3011
	(20×20), 2	3969	5.0092	13.0456	17.1648	25.1482	29.3793	37.8633	41.3744	45.7568	54.5451	61.7999
	(30×30), 2	8649	5.0019	13.0054	17.0474	25.0109	29.0933	37.2585	41.0185	45.1550	53.4284	61.0284
	(40×40), 2	15129	4.9993	12.9914	17.0067	24.9631	28.9944	37.0505	40.8951	44.9478	53.0467	60.7620
	(50×50), 2	23409	4.9982	12.9849	16.9879	24.9410	28.9489	36.9549	40.8382	44.8525	52.8716	60.6393
	(60×60), 2	33489	4.9975	12.9814	16.9777	24.9291	28.9242	36.9031	40.8074	44.8009	52.7769	60.5728
	(60×60), 3	44652	4.9971	12.9785	16.9728	24.9186	28.9101	36.8802	40.7794	44.7672	52.7302	60.5114
	(60×60), 4	55815	4.9971	12.9785	16.9728	24.9186	28.9101	36.8802	40.7794	44.7672	52.7302	60.5114
0.1	(10×10), 2	1089	4.6990	6.5301	11.2266	14.4233	14.6680	19.5466	19.7518	22.5008	23.8712	24.6483
	(20×20), 2	3969	4.6656	6.5251	11.0829	14.0111	14.6070	19.1787	19.6155	21.7014	23.6076	24.5825
	(30×30), 2	8649	4.6595	6.5242	11.0565	13.9367	14.5958	19.1111	19.5903	21.5577	23.5592	24.5703
	(40×40), 2	15129	4.6573	6.5238	11.0473	13.9107	14.5918	19.0874	19.5815	21.5077	23.5422	24.5661
	(50×50), 2	23409	4.6563	6.5237	11.0431	13.8987	14.5900	19.0765	19.5775	21.4846	23.5344	24.5641
	(60×60), 2	33489	4.6558	6.5236	11.0408	13.8922	14.5890^s	19.0706	19.5752^s	21.4721	23.5301^s	24.5630^s
	(60×60), 3	44652	4.6236	6.5236	10.8866	13.6633	14.5890^s	18.6832	19.5752^s	21.0035	23.5301^s	24.5615^s
	(60×60), 4	55815	4.6234	6.5236	10.8839	13.6580	14.5890^s	18.6703	19.5752^s	20.9854	23.5301^s	24.5615^s

Table D.3: Convergence of the first 10 frequency parameters λ for the AA modes of a SSSS isotropic square plate with $\nu = 0.3$. Only ED theories are considered.

			mode number									
$\frac{t}{b}$	$(n_x \times n_y)$, N	n_{dof}	AA-1	AA-2	AA-3	AA-4	AA-5	AA-6	AA-7	AA-8	AA-9	AA-10
0.01	(10×10), 2	1089	8.0821	20.8086	20.8086	33.3377	44.3215	44.3215	56.4908	56.4908	78.9750	82.8227
	(20×20), 2	3969	8.0128	20.1486	20.1486	32.2044	40.8135	40.8135	52.7334	52.7334	70.6883	70.6883
	(30×30), 2	8649	8.0001	20.0306	20.0306	32.0009	40.2166	40.2166	52.0864	52.0864	68.7621	68.7621
	(40×40), 2	15129	7.9956	19.9896	19.9896	31.9302	40.0113	40.0113	51.8633	51.8633	68.1085	68.1085
	(50×50), 2	23409	7.9936	19.9707	19.9707	31.8976	39.9169	39.9169	51.7606	51.7606	67.8095	67.8095
	(60×60), 2	33489	7.9924	19.9604	19.9604	31.8798	39.8657	39.8657	51.7050	51.7050	67.6480	67.6480
	(60×60), 3	44652	7.9914	19.9537	19.9537	31.8627	39.8390	39.8390	51.6602	51.6602	67.5716	67.5716
	(60×60), 4	55815	7.9914	19.9537	19.9537	31.8627	39.8390	39.8390	51.6602	51.6602	67.5715	67.5715
0.1	(10×10), 2	1089	7.2433	13.1005	13.1005	16.3875	16.3875	18.6227	23.7686	26.5247	26.5247	29.4016
	(20×20), 2	3969	7.1922	13.0602	13.0602	16.0129	16.0129	18.4937	23.3125	26.2011	26.2011	27.9375
	(30×30), 2	8649	7.1828	13.0528	13.0528	15.9450	15.9450	18.4700	23.2276	26.1413	26.1413	27.6764
	(40×40), 2	15129	7.1795	13.0502	13.0502	15.9213	15.9213	18.4617	23.1978	26.1205	26.1205	27.5857
	(50×50), 2	23409	7.1780	13.0490	13.0490	15.9103	15.9103	18.4578	23.1841	26.1108	26.1108	27.5439
	(60×60), 2	33489	7.1772	13.0483^s	13.0483^s	15.9044	15.9044	18.4557^s	23.1766	26.1055^s	26.1055^s	27.5212
	(60×60), 3	44652	7.1056	13.0483^s	13.0483^s	15.6170	15.6170	18.4557^s	22.6478	26.1055^s	26.1055^s	26.8317
	(60×60), 4	55815	7.1048	13.0483^s	13.0483^s	15.6093	15.6093	18.4557^s	22.6254	26.1055^s	26.1055^s	26.7956

Table D.4: Convergence of the first 10 frequency parameters λ for the SS modes of an isotropic square plate with $\frac{t}{b} = 0.1$ and different boundary conditions ($\nu = 0.3$). Only ED theories are considered.

			mode number									
B.C.	$(n_x \times n_y)$, N	n_{dof}	SS-1	SS-2	SS-3	SS-4	SS-5	SS-6	SS-7	SS-8	SS-9	SS-10
CFCF	(10×10), 2	1089	2.1516	3.9868	10.2942	11.7526	11.8158	12.2031	18.3854	18.8542	19.4289	22.0151
	(20×20), 2	3969	2.1306	3.9703	10.0222	11.5477	11.7807	11.9845	18.1491	18.6200	19.5350	21.2062
	(30×30), 2	8649	2.1260	3.9667	9.9704	11.5097	11.7737	11.9426	18.1031	18.5741	19.5546	21.0076
	(40×40), 2	15129	2.1242	3.9653	9.9520	11.4963	11.7712	11.9276	18.0867	18.5575	19.5614	20.9380
	(50×50), 2	23409	2.1234	3.9646	9.9433	11.4901	11.7700	11.9206	18.0791	18.5496	19.5646	20.9057
	(60×60), 2	33489	2.1229	3.9643	9.9386	11.4868	11.7693^s	11.9167	18.0749	18.5452^s	19.5663	20.8881^s
	(60×60), 3	44652	2.1057	3.9244	9.7431	11.3365	11.6744	11.7683^s	17.6892	18.5448^s	19.5663	20.3291^s
	(60×60), 4	55815	2.1043	3.9229	9.7328	11.3329	11.6636	11.7678^s	17.6732	18.5446^s	19.5663	20.2957^s
CCCC	(10×10), 2	1089	3.3934	11.0514	11.1585	16.8300	20.8573	22.8884	22.9489	23.7563	25.9166	26.9070
	(20×20), 2	3969	3.3673	10.8045	10.9062	16.5526	20.6944	21.8530	21.9093	23.6233	25.6716	26.1024
	(30×30), 2	8649	3.3614	10.7574	10.8580	16.4990	20.6635	21.6644	21.7197	23.5979	25.6258	25.9531
	(40×40), 2	15129	3.3592	10.7406	10.8409	16.4798	20.6526	21.5984	21.6533	23.5889	25.6098	25.9006
	(50×50), 2	23409	3.3581	10.7328	10.8328	16.4709	20.6475	21.5678	21.6226	23.5847	25.6023	25.8762
	(60×60), 2	33489	3.3576	10.7285	10.8284	16.4660	20.6448^s	21.5512	21.6059	23.5824^s	25.5983	25.8630
	(60×60), 3	44652	3.3229	10.5147	10.6145	16.0848	20.6370^s	20.9814	21.0340	23.5737^s	25.1604	25.3217
	(60×60), 4	55815	3.3205	10.5034	10.6030	16.0639	20.6338^s	20.9461	20.9983	23.5704^s	25.1134	25.2731

Table D.5: Convergence of the first 10 frequency parameters λ for the SA modes of an isotropic square plate with $\frac{t}{b} = 0.1$ and different boundary conditions ($\nu = 0.3$). Only ED theories are considered.

			mode number									
B.C.	$(n_x \times n_y)$, N	n_{dof}	SA-1	SA-2	SA-3	SA-4	SA-5	SA-6	SA-7	SA-8	SA-9	SA-10
CFCF	(10×10), 2	1089	5.5973	7.5783	10.6929	13.8047	14.4568	15.9245	17.6642	18.0382	23.2120	25.1396
	(20×20), 2	3969	5.5012	7.5059	10.6536	13.7293	14.2671	15.3338	17.1652	17.9348	22.8185	24.6147
	(30×30), 2	8649	5.4819	7.4912	10.6452	13.7149	14.2310	15.2243	17.0722	17.9145	22.7424	24.5124
	(40×40), 2	15129	5.4750	7.4858	10.6420	13.7098	14.2182	15.1857	17.0394	17.9071	22.7154	24.4757
	(50×50), 2	23409	5.4716	7.4833	10.6404	13.7074	14.2122	15.1677	17.0241	17.9036	22.7028	24.4584
	(60×60), 2	33489	5.4698	7.4818	10.6395^s	13.7061^s	14.2090	15.1579	17.0158	17.9017^s	22.6959	24.4489^s
	(60×60), 3	44652	5.3909	7.3632	10.6359^s	13.7051^s	13.9628	14.7976	16.6059	17.8986^s	22.1381	24.2152
	(60×60), 4	55815	5.3864	7.3583	10.6344^s	13.7047^s	13.9547	14.7781	16.5852	17.8973^s	22.1097	24.1894
CCCC	(10×10), 2	1089	6.5648	12.5724	13.2989	16.6298	20.9105	21.4696	24.4590	25.3447	29.8490	30.5366
	(20×20), 2	3969	6.4780	12.5380	13.0709	16.0755	20.7502	21.0101	23.5285	25.1201	28.1158	29.7608
	(30×30), 2	8649	6.4604	12.5311	13.0269	15.9727	20.7204	20.9230	23.3582	25.0771	27.8030	29.6133
	(40×40), 2	15129	6.4540	12.5287	13.0111	15.9365	20.7101	20.8922	23.2985	25.0620	27.6939	29.5612
	(50×50), 2	23409	6.4510	12.5276	13.0038	15.9197	20.7052	20.8778	23.2708	25.0549	27.6435	29.5370
	(60×60), 2	33489	6.4493	12.5270^s	12.9997	15.9106	20.7026^s	20.8700	23.2557	25.0511^s	27.6161	29.5238
	(60×60), 3	44652	6.3515	12.5227^s	12.7250	15.5345	20.3406	20.7018^s	22.6334	25.0418^s	26.8298	28.6888
	(60×60), 4	55815	6.3459	12.5210^s	12.7104	15.5135	20.3091	20.7015^s	22.5938	25.0381^s	26.7736	28.6277

Table D.6: Convergence of the first 10 frequency parameters λ for the AS modes of an isotropic square plate with $\frac{t}{b} = 0.1$ and different boundary conditions ($\nu = 0.3$). Only ED theories are considered.

			mode number									
B.C.	$(n_x \times n_y)$, N	n_{dof}	AS-1	AS-2	AS-3	AS-4	AS-5	AS-6	AS-7	AS-8	AS-9	AS-10
CFCF	(10×10), 2	1089	2.4990	5.9803	7.1194	10.7126	14.7366	17.5305	18.1649	19.8730	22.6031	23.1079
	(20×20), 2	3969	2.4805	5.9584	7.0621	10.4547	14.5446	17.0124	17.9532	19.7187	21.5456	22.6874
	(30×30), 2	8649	2.4763	5.9536	7.0511	10.4055	14.5074	16.9174	17.9122	19.6894	21.3523	22.6070
	(40×40), 2	15129	2.4747	5.9518	7.0472	10.3878	14.4940	16.8843	17.8975	19.6790	21.2845	22.5785
	(50×50), 2	23409	2.4739	5.9509	7.0454	10.3796	14.4878	16.8689	17.8906	19.6741	21.2531	22.5653
	(60×60), 2	33489	2.4735	5.9504^s	7.0444	10.3751	14.4844	16.8606	17.8868^s	19.6714^s	21.2360	22.5581
	(60×60), 3	44652	2.4495	5.9499^s	6.9711	10.1669	14.1838	16.5815	17.8864^s	19.6684^s	20.6621	22.0510
	(60×60), 4	55815	2.4481	5.9498^s	6.9693	10.1567	14.1713	16.5728	17.8863^s	19.6672^s	20.6287	22.0276
CCCC	(10×10), 2	1089	6.5648	12.5724	13.2989	16.6298	20.9105	21.4696	24.4590	25.3447	29.8490	30.5366
	(20×20), 2	3969	6.4780	12.5380	13.0709	16.0755	20.7502	21.0101	23.5285	25.1201	28.1158	29.7608
	(30×30), 2	8649	6.4604	12.5311	13.0269	15.9727	20.7204	20.9230	23.3582	25.0771	27.8030	29.6133
	(40×40), 2	15129	6.4540	12.5287	13.0111	15.9365	20.7101	20.8922	23.2985	25.0620	27.6939	29.5612
	(50×50), 2	23409	6.4510	12.5276	13.0038	15.9197	20.7052	20.8778	23.2708	25.0549	27.6435	29.5370
	(60×60), 2	33489	6.4493	12.5270^s	12.9997	15.9106	20.7026^s	20.8700	23.2557	25.0511^s	27.6161	29.5238
	(60×60), 3	44652	6.3515	12.5227^s	12.7250	15.5345	20.3406	20.7018^s	22.6334	25.0418^s	26.8298	28.6888
	(60×60), 4	55815	6.3459	12.5210^s	12.7104	15.5135	20.3091	20.7015^s	22.5938	25.0381^s	26.7736	28.6277

Table D.7: Convergence of the first 10 frequency parameters λ for the AA modes of an isotropic square plate with $\frac{t}{b} = 0.1$ and different boundary conditions ($\nu = 0.3$). Only ED theories are considered.

B.C.	$(n_x \times n_y)$, N	n_{dof}	mode number AA-1	AA-2	AA-3	AA-4	AA-5	AA-6	AA-7	AA-8	AA-9	AA-10
CFCF	(10×10), 2	1089	6.0396	10.3561	11.0299	13.2676	16.2907	19.7100	19.9823	20.5541	24.0324	25.3488
	(20×20), 2	3969	5.9507	10.2716	10.9797	13.1963	15.7224	19.2613	19.5539	20.4025	23.6578	25.0024
	(30×30), 2	8649	5.9328	10.2548	10.9700	13.1814	15.6168	19.1776	19.4734	20.3744	23.5829	24.9384
	(40×40), 2	15129	5.9263	10.2487	10.9666	13.1757	15.5795	19.1482	19.4450	20.3645	23.5560	24.9159
	(50×50), 2	23409	5.9232	10.2458	10.9650	13.1729	15.5622	19.1345	19.4317	20.3599	23.5435	24.9054
	(60×60), 2	33489	5.9215	10.2442	10.9642^s	13.1713^s	15.5527	19.1271	19.4245	20.3574^s	23.5366^s	24.8996^s
	(60×60), 3	44652	5.8321	10.0777	10.9632^s	13.1691^s	15.1786	18.7504	18.9599	20.3564^s	23.5349^s	24.8967^s
	(60×60), 4	55815	5.8276	10.0719	10.9629^s	13.1683^s	15.1592	18.7356	18.9373	20.3561^s	23.5343^s	24.8955^s
CCCC	(10×10), 2	1089	9.2186	14.9520	18.3586	18.3661	18.5547	25.5451	27.1585	27.8455	31.0773	31.2103
	(20×20), 2	3969	9.1097	14.8910	17.8851	18.0563	18.2847	25.0095	26.7936	27.4957	29.4999	29.6192
	(30×30), 2	8649	9.0876	14.8796	17.7954	17.9632	18.2703	24.9070	26.7263	27.4310	29.2147	29.3311
	(40×40), 2	15129	9.0796	14.8757	17.7638	17.9303	18.2652	24.8706	26.7028	27.4084	29.1151	29.2306
	(50×50), 2	23409	9.0758	14.8738	17.7490	17.9150	18.2628	24.8537	26.6919	27.3980	29.0691	29.1840
	(60×60), 2	33489	9.0737	14.8728^s	17.7410	17.9066	18.2615^s	24.8445	26.6860^s	27.3923^s	29.0441	29.1588
	(60×60), 3	44652	8.9123	14.8724^s	17.3124	17.4709	18.2556^s	24.1783	26.6852^s	27.3914^s	28.2155	28.3203
	(60×60), 4	55815	8.9037	14.8722^s	17.2883	17.4460	18.2532^s	24.1350	26.6849^s	27.3911^s	28.1549	28.2583

Table D.8: Convergence of the frequency parameters λ for the first 12 modes of a CCCC square laminated plate with $\frac{t}{b} = 0.1$ and stacking sequence $0°/90°/0°$. Material 2 is used.

			mode number											
theory	$(n_x \times n_y)$, N	n_{dof}	1	2	3	4	5	6	7	8	9	10	11	12
ED	(10×10), 2	1089	2.2765	3.2248	4.3823	4.9301	5.0171	6.2124	6.9552	7.2637	7.4552	8.0989	8.2364	9.5974
	(20×20), 2	3969	2.2590	3.1410	4.3115	4.7117	4.8514	6.0000	6.7227	6.7371	7.0913	7.6820	7.9101	9.0256
	(30×30), 2	8649	2.2557	3.1260	4.2984	4.6584	4.8366	5.9618	6.5964	6.6968	7.0581	7.5846	7.8720	8.7838
	(40×40), 2	15129	2.2545	3.1208	4.2938	4.6400	4.8314	5.9485	6.5529	6.6826	7.0463	7.5509	7.8584	8.7008
	(50×50), 2	23409	2.2540	3.1184	4.2917	4.6315	4.8290	5.9423	6.5329	6.6761	7.0409	7.5353	7.8521	8.6626
	(60×60), 2	33489	2.2537	3.1171	4.2905	4.6269	4.8277	5.9390	6.5220	6.6726	7.0379	7.5269	7.8487	8.6420
	(60×60), 3	44652	2.1334	2.9349	4.0661	4.2872	4.5670	5.5596	5.9527	6.3362	6.6791	6.9463	7.4030	7.7963
	(60×60), 4	55815	2.1329	2.9335	4.0651	4.2830	4.5651	5.5550	5.9428	6.3344	6.6765	6.9360	7.3977	7.7765
	(60×60), 5	66978	2.1271	2.9049	4.0560	4.2166	4.5426	5.5025	5.8354	6.3159	6.6499	6.8452	7.3497	7.6324
	(60×60), 6	78141	2.1271	2.9048	4.0560	4.2163	4.5425	5.5023	5.8347	6.3158	6.6498	6.8447	7.3495	7.6310
	(60×60), 7	89304	2.1238	2.8902	4.0512	4.1842	4.5308	5.4766	5.7853	6.3076	6.6371	6.8023	7.3263	7.5677
LD	(10×10), 1	1452	2.1956	3.0360	4.2496	4.5834	4.7305	5.8140	6.6908	6.7699	7.0365	7.5301	7.7229	8.9588
	(20×20), 1	5292	2.1797	2.9686	4.1786	4.3370	4.6607	5.6482	6.0746	6.5451	6.8615	7.0792	7.5594	8.0670
	(30×30), 1	11532	2.1767	2.9565	4.1654	4.2940	4.6475	5.6181	5.9698	6.5038	6.8282	7.0012	7.5259	7.8594
	(40×40), 1	20172	2.1757	2.9523	4.1608	4.2791	4.6428	5.6075	5.9338	6.4894	6.8165	6.9743	7.5140	7.7885
	(50×50), 1	31212	2.1752	2.9503	4.1587	4.2723	4.6407	5.6027	5.9172	6.4827	6.8110	6.9619	7.5085	7.7561
	(60×60), 1	44652	2.1749	2.9493	4.1575	4.2686	4.6395	5.6000	5.9082	6.4791	6.8081	6.9551	7.5054	7.7385
	(60×60), 2	78141	2.1307	2.9088	4.0693	4.2221	4.5553	5.5153	5.8436	6.3440	6.6770	6.8594	7.3759	7.6442
	(60×60), 3	111630	2.1221	2.8822	4.0504	4.1672	4.5259	5.4640	5.7599	6.3077	6.6345	6.7815	7.3177	7.5367
	(60×60), 4	148840	2.1217	2.8818	4.0490	4.1667	4.5246	5.4628	5.7594	6.3047	6.6316	6.7803	7.3151	7.5359

Table D.9: Convergence of the frequency parameters λ for modes 13-24 of a CCCC square laminated plate with $\frac{t}{b} = 0.1$ and stacking sequence $0°/90°/0°$. Material 2 is used.

theory	$(n_x \times n_y)$, N	n_{dof}	mode number 13	14	15	16	17	18	19	20	21	22	23	24
ED	(10 × 10), 2	1089	9.7405	9.8978	10.4047	10.4226	10.8943	11.4105	11.7609	11.8388	12.5774	12.7559	12.7971	12.9938
	(20 × 20), 2	3969	9.2310	9.2405	9.4924	9.7534	10.0998	10.9865	11.1342	11.5465	11.8052	11.8136	11.9977	12.1098
	(30 × 30), 2	8649	9.1478	9.1583	9.4145	9.5528	10.0343	10.8362	11.0622	11.1389	11.6356	11.7547	11.7989	11.8419
	(40 × 40), 2	15129	9.1154	9.1326	9.3872	9.4837	10.0109	10.7836	10.9992	11.0359	11.5735	11.6327	11.7873	11.7967
	(50 × 50), 2	23409	9.1004	9.1207	9.3745	9.4519	10.0000	10.7593	10.9351	11.0235	11.5448	11.5767	11.7620	11.7957
	(60 × 60), 2	33489	9.0923	9.1142	9.3676	9.4347	9.9940	10.7460	10.9004	11.0167	11.5292	11.5463	11.7482	11.7952^{s}
	(60 × 60), 3	44652	8.5018	8.5942	8.6689	8.9296	9.4897	9.7473	9.8999	10.3743	10.4085	11.0530	11.2621	11.5142
	(60 × 60), 4	55815	8.4910	8.5741	8.6665	8.9264	9.4840	9.7128	9.8794	10.3627	10.3740	11.0501	11.2584	11.4789
	(60 × 60), 5	66978	8.4112	8.4465	8.6321	8.8871	9.4296	9.5409	9.7655	10.2163	10.2843	10.9931	11.1987	11.3360
	(60 × 60), 6	78141	8.4108	8.4454	8.6317	8.8868	9.4294	9.5386	9.7647	10.2145	10.2841	10.9923	11.1980	11.3346
	(60 × 60), 7	89304	8.3734	8.3886	8.6179	8.8699	9.4046	9.4668	9.7135	10.1481	10.2476	10.9702	11.1737	11.2732
LD	(10 × 10), 1	1452	9.2647	9.5270	9.6560	9.8568	10.0536	10.8172	10.8516	11.8075	12.1776	12.4972	12.5471	12.5472
	(20 × 20), 1	5292	8.6663	8.8489	9.0058	9.2313	9.7461	10.1421	10.2651	10.6029	10.8847	11.5588	11.7234	11.7746
	(30 × 30), 1	11532	8.6084	8.6808	8.9101	9.1509	9.6811	9.9022	10.0195	10.5387	10.5735	11.3743	11.5611	11.6915
	(40 × 40), 1	20172	8.5879	8.6233	8.8768	9.1226	9.6579	9.7792	9.9768	10.4672	10.5159	11.3101	11.5044	11.6088
	(50 × 50), 1	31212	8.5784	8.5969	8.8614	9.1096	9.6471	9.7229	9.9571	10.4190	10.5048	11.2805	11.4781	11.5709
	(60 × 60), 1	44652	8.5732	8.5826	8.8530	9.1025	9.6412	9.6925	9.9464	10.3929	10.4987	11.2644	11.4638	11.5504
	(60 × 60), 2	78141	8.4373	8.4633	8.6809	8.9344	9.4753	9.5573	9.7928	10.2371	10.3288	11.0672	11.2708	11.3660
	(60 × 60), 3	111630	8.3573	8.3613	8.6202	8.8700	9.3999	9.4329	9.6908	10.1172	10.2364	10.9765	11.1781	11.2463
	(60 × 60), 4	148840	8.3549	8.3600	8.6146	8.8647	9.3949	9.4319	9.6884	10.1158	10.2317	10.9670	11.1690	11.2439

Table D.10: Convergence of the frequency parameters λ for modes 25-36 of a CCCC square laminated plate with $\frac{t}{b} = 0.1$ and stacking sequence $0°/90°/0°$. Material 2 is used.

			mode number											
theory	$(n_x \times n_y)$, N	n_{dof}	25	26	27	28	29	30	31	32	33	34	35	36
ED	(10×10), 2	1089	13.0478	13.3747	13.6096	13.6372	13.8177	13.8458	14.0731	14.5050	14.5774	15.1413	15.4787	15.5154
	(20×20), 2	3969	12.4590	12.5275	12.5865	13.0877	13.2733	13.6905	14.2495	14.4056	14.4463	14.4616	14.5821	14.6899
	(30×30), 2	8649	12.3313	12.4721	12.5182	12.8077	13.1669	13.6182	13.6668	14.1225	14.1419	14.1997	14.3071	14.3521
	(40×40), 2	15129	12.2858	12.4302	12.5149	12.7103	13.1274	13.4019	13.6586	13.9277	14.0357	14.1251	14.2106	14.3094
	(50×50), 2	23409	12.2646	12.4105	12.5134	12.6653	13.1087	13.3028	13.6547	13.8383	13.9866	14.0902	14.1660	14.2890
	(60×60), 2	33489	12.2530	12.3997	12.5125^s	12.6409	13.0985	13.2492	13.6526^s	13.7899	13.9600	14.0712	14.1418	14.2777
	(60×60), 3	44652	11.5512	11.7137	11.7709	11.7950^s	12.3323	12.4428	12.5124^s	12.9629	13.2817	13.4395	13.4603	13.6350
	(60×60), 4	55815	11.5307	11.5794^s	11.7073	11.7161	12.2766	12.3090^s	12.4318	12.9280	13.2258	13.4197	13.4574	13.4654^s
	(60×60), 5	66978	11.4222	11.5282	11.5794^s	11.6376	12.1024	12.3090^s	12.3425	12.7929	13.0642	13.3064	13.3729	13.4654^s
	(60×60), 6	78141	11.4218	11.5250	11.5535^s	11.6371	12.0997	12.2846^s	12.3422	12.7920	13.0621	13.3061	13.3715	13.4428^s
	(60×60), 7	89304	11.3730	11.4503	11.5535^s	11.6068	12.0292	12.2846^s	12.3025	12.7334	12.9957	13.2559	13.3385	13.4428^s
LD	(10×10), 1	1452	12.5681	12.7375	12.7933	13.1440	13.3330	13.3522	13.6295	13.7888	13.9184	14.1274	15.1837	15.4117
	(20×20), 1	5292	11.8061	11.9327	12.1110	12.4985	12.6549	12.7776	13.1509	13.3340	13.6636	13.7482	13.9985	14.1903
	(30×30), 1	11532	11.7107	11.7684	11.9787	12.0720	12.4894	12.6310	12.6715	13.1570	13.5727	13.6403	13.6465	13.8745
	(40×40), 1	20172	11.6758	11.7663	11.8756	11.9319	12.4559	12.4862	12.6324	13.0940	13.4284	13.6073	13.6321	13.7646
	(50×50), 1	31212	11.6595	11.7653	11.7861	11.9100	12.3760	12.4847	12.6140	13.0647	13.3624	13.5886	13.6283	13.7139
	(60×60), 1	44652	11.6505	11.7379	11.7647^s	11.8981	12.3330	12.4839^s	12.6039	13.0487	13.3268	13.5782	13.6263^s	13.6864
	(60×60), 2	78141	11.4665	11.5482^s	11.5502	11.7075	12.1281	12.2795^s	12.4103	12.8384	13.0982	13.3729	13.4381^s	13.4744
	(60×60), 3	111630	11.3555	11.4165	11.5481^s	11.6071	11.9977	12.2794^s	12.2970	12.7114	12.9673	13.2445	13.3509	13.4380^s
	(60×60), 4	148840	11.3511	11.4153	11.5481^s	11.5984	11.9961	12.2794^s	12.2889	12.7072	12.9649	13.2368	13.3360	13.4380^s

Table D.11: Convergence of the frequency parameters λ for the first 12 modes of a CCCC square laminated plate with $\frac{t}{b} = 0.01$ and stacking sequence $0°/90°/0°$. Material 2 is used.

			mode number											
theory	$(n_x \times n_y)$, N	n_{dof}	1	2	3	4	5	6	7	8	9	10	11	12
ED	(10×10), 2	1089	0.4255	0.5221	0.7846	1.1755	1.2240	1.2900	1.3722	1.7301	2.1578	2.4156	2.4442	2.4634
	(20×20), 2	3969	0.4159	0.5031	0.7138	1.0638	1.1057	1.1523	1.2745	1.5174	1.5569	1.9151	2.1484	2.1807
	(30×30), 2	8649	0.4141	0.4997	0.7023	1.0305	1.0935	1.1397	1.2578	1.4785	1.4850	1.8436	2.0451	2.1042
	(40×40), 2	15129	0.4135	0.4985	0.6983	1.0192	1.0893	1.1354	1.2521	1.4527	1.4740	1.8200	1.9936	2.0891
	(50×50), 2	23409	0.4132	0.4980	0.6965	1.0141	1.0873	1.1334	1.2494	1.4410	1.4690	1.8093	1.9705	2.0822
	(60×60), 2	33489	0.4131	0.4977	0.6955	1.0113	1.0863	1.1323	1.2480	1.4347	1.4663	1.8036	1.9582	2.0784
	(60×60), 3	44652	0.4119	0.4964	0.6938	1.0083	1.0792	1.1252	1.2408	1.4291	1.4586	1.7941	1.9481	2.0563
	(60×60), 4	55815	0.4119	0.4964	0.6938	1.0083	1.0792	1.1252	1.2408	1.4291	1.4586	1.7941	1.9480	2.0563
LD	(10×10), 1	1452	0.4248	0.5214	0.7831	1.1705	1.2190	1.2843	1.3668	1.7215	2.1383	2.3970	2.4251	2.4422
	(20×20), 1	5292	0.4153	0.5025	0.7129	1.0613	1.1015	1.1482	1.2704	1.5124	1.5504	1.9069	2.1347	2.1669
	(30×30), 1	11532	0.4135	0.4992	0.7015	1.0283	1.0895	1.1358	1.2540	1.4731	1.4805	1.8366	2.0336	2.0912
	(40×40), 1	20172	0.4129	0.4980	0.6976	1.0172	1.0853	1.1315	1.2483	1.4477	1.4696	1.8134	1.9831	2.0764
	(50×50), 1	31212	0.4126	0.4975	0.6958	1.0122	1.0834	1.1296	1.2457	1.4362	1.4647	1.8029	1.9605	2.0695
	(60×60), 1	44652	0.4125	0.4972	0.6948	1.0094	1.0824	1.1285	1.2442	1.4300	1.4620	1.7972	1.9483	2.0658
	(60×60), 2	78141	0.4118	0.4963	0.6935	1.0075	1.0792	1.1251	1.2406	1.4272	1.4580	1.7926	1.9445	2.0562
	(60×60), 3	111630	0.4118	0.4963	0.6932	1.0067	1.0791	1.1250	1.2404	1.4254	1.4573	1.7911	1.9411	2.0560
	(60×60), 4	148840	0.4118	0.4963	0.6932	1.0067	1.0791	1.1250	1.2404	1.4254	1.4573	1.7911	1.9411	2.0560

Table D.12: Convergence of the frequency parameters λ for modes 13-24 of a CCCC square laminated plate with $\frac{t}{b} = 0.01$ and stacking sequence $0°/90°/0°$. Material 2 is used.

theory	$(n_x \times n_y)$, N	n_{dof}	mode number											
			13	14	15	16	17	18	19	20	21	22	23	24
ED	(10×10), 2	1089	2.5285	2.7471	3.2645	3.6521	3.8529	4.2725	4.2840	4.3232	4.4055	4.4367	4.7408	5.5294
	(20×20), 2	3969	2.2054	2.2601	2.4215	2.4894	2.7071	3.0323	3.1593	3.2612	3.5347	3.5596	3.6170	3.7310
	(30×30), 2	8649	2.1370	2.2150	2.3408	2.3680	2.6267	2.7344	2.9787	3.0168	3.4198	3.4461	3.5047	3.5544
	(40×40), 2	15129	2.1219	2.1996	2.2932	2.3497	2.5997	2.6415	2.8909	2.9706	3.3810	3.3983	3.4077	3.4666
	(50×50), 2	23409	2.1151	2.1925	2.2719	2.3413	2.5873	2.6004	2.8520	2.9497	3.3298	3.3632	3.3901	3.4367
	(60×60), 2	33489	2.1113	2.1886	2.2604	2.3367	2.5776	2.5815	2.8312	2.9385	3.2935	3.3536	3.3806	3.4173
	(60×60), 3	44652	2.0892	2.1664	2.2472	2.3144	2.5572	2.5617	2.8116	2.9131	3.2662	3.3025	3.3294	3.3871
	(60×60), 4	55815	2.0892	2.1664	2.2472	2.3144	2.5572	2.5617	2.8116	2.9131	3.2662	3.3025	3.3294	3.3871
LD	(10×10), 1	1452	2.5087	2.7247	3.2316	3.5832	3.7828	4.2178	4.2283	4.2657	4.3277	4.3758	4.6709	5.4221
	(20×20), 1	5292	2.1906	2.2463	2.4072	2.4737	2.6908	3.0024	3.1372	3.2311	3.5011	3.5259	3.5831	3.6965
	(30×30), 1	11532	2.1240	2.2021	2.3284	2.3548	2.6121	2.7126	2.9565	2.9982	3.3889	3.4152	3.4737	3.5162
	(40×40), 1	20172	2.1093	2.1870	2.2818	2.3369	2.5857	2.6220	2.8710	2.9531	3.3510	3.3648	3.3777	3.4366
	(50×50), 1	31212	2.1025	2.1800	2.2609	2.3286	2.5734	2.5819	2.8330	2.9327	3.2983	3.3336	3.3605	3.4132
	(60×60), 1	44652	2.0988	2.1762	2.2497	2.3241	2.5598	2.5675	2.8127	2.9218	3.2630	3.3242	3.3512	3.3943
	(60×60), 2	78141	2.0890	2.1662	2.2442	2.3139	2.5542	2.5575	2.8061	2.9107	3.2564	3.3023	3.3292	3.3826
	(60×60), 3	111630	2.0888	2.1659	2.2412	2.3133	2.5489	2.5557	2.8008	2.9082	3.2471	3.3017	3.3285	3.3779
	(60×60), 4	148840	2.0888	2.1659	2.2412	2.3133	2.5489	2.5557	2.8008	2.9082	3.2471	3.3017	3.3285	3.3779

Table D.13: Convergence of the frequency parameters λ for modes 25-36 of a CCCC square laminated plate with $\frac{t}{b} = 0.01$ and stacking sequence $0°/90°/0°$. Material 2 is used.

			mode number											
theory	$(n_x \times n_y)$, N	n_{dof}	25	26	27	28	29	30	31	32	33	34	35	36
ED	(10×10), 2	1089	6.4164	6.5333	6.8468	6.8894	6.8896	6.9168	6.9259	6.9939	7.3735	7.5240	8.7202	9.1336
	(20×20), 2	3969	3.8165	3.9356	4.0718	4.2592	4.2745	4.7163	4.7953	5.2624	5.2816	5.3243	5.3711	5.4075
	(30×30), 2	8649	3.5547	3.6160	3.7607	3.8059	4.1021	4.2507	4.5163	4.5306	4.6941	5.0186	5.0407	5.0875
	(40×40), 2	15129	3.4730	3.5768	3.6108	3.7618	4.0448	4.1110	4.2679	4.4451	4.4533	4.8852	4.9373	4.9602
	(50×50), 2	23409	3.4491	3.5448	3.5592	3.7417	4.0187	4.0497	4.1603	4.3481	4.4078	4.7868	4.9003	4.9201
	(60×60), 2	33489	3.4397	3.5101	3.5493	3.7308	4.0047	4.0173	4.1036	4.2932	4.3874	4.7351	4.8803	4.8887
	(60×60), 3	44652	3.3884	3.4807	3.4980	3.6791	3.9519	3.9789	4.0622	4.2500	4.3316	4.6843	4.7823	4.8056
	(60×60), 4	55815	3.3883	3.4807	3.4980	3.6791	3.9519	3.9789	4.0622	4.2500	4.3316	4.6842	4.7822	4.8055
LD	(10×10), 1	1452	6.1685	6.2827	6.5905	6.7487	6.7511	6.7820	6.7934	6.8452	7.1970	7.2456	8.3919	9.0693
	(20×20), 1	5292	3.7818	3.8997	4.0156	4.2034	4.2341	4.6573	4.7451	5.1942	5.2131	5.2553	5.2703	5.3378
	(30×30), 1	11532	3.5280	3.5848	3.7227	3.7739	4.0674	4.2096	4.4535	4.4898	4.6317	4.9579	4.9798	5.0264
	(40×40), 1	20172	3.4485	3.5467	3.5774	3.7311	4.0118	4.0745	4.2143	4.3988	4.4083	4.8302	4.8789	4.9017
	(50×50), 1	31212	3.4195	3.5134	3.5295	3.7114	3.9865	4.0152	4.1103	4.2986	4.3708	4.7354	4.8429	4.8661
	(60×60), 1	44652	3.4104	3.4797	3.5200	3.7008	3.9728	3.9837	4.0556	4.2455	4.3510	4.6855	4.8235	4.8440
	(60×60), 2	78141	3.3881	3.4717	3.4975	3.6782	3.9500	3.9710	4.0473	4.2359	4.3280	4.6716	4.7819	4.8052
	(60×60), 3	111630	3.3874	3.4629	3.4966	3.6768	3.9477	3.9631	4.0331	4.2223	4.3239	4.6591	4.7807	4.8040
	(60×60), 4	148840	3.3874	3.4629	3.4966	3.6768	3.9477	3.9631	4.0331	4.2223	4.3239	4.6591	4.7806	4.8039

Table D.14: Convergence of the frequency parameters λ for the first 12 modes of a SSSS square laminated plate with $\frac{t}{b} = 0.1$ and stacking sequence $0°/90°/0°$. Material 2 is used.

theory	$(n_x \times n_y)$, N	n_{dof}	mode number 1	2	3	4	5	6	7	8	9	10	11	12
ED	(10×10), 2	1089	1.5365	2.3281	2.4435	2.4435	4.0739	4.0835	4.4297	4.9473	4.9473	5.5297	6.5996	6.8083
	(20×20), 2	3969	1.5272	2.2833	2.4360	2.4360	3.8598	4.0040	4.3709	4.8870	4.8870	5.3821	5.9661	6.5845
	(30×30), 2	8649	1.5255	2.2752	2.4346	2.4346	3.8206	3.9911	4.3598	4.8758	4.8758	5.3551	5.8575	6.5434
	(40×40), 2	15129	1.5249	2.2723	2.4341	2.4341	3.8071	3.9866	4.3558	4.8719	4.8719	5.3457	5.8202	6.5290
	(50×50), 2	23409	1.5246	2.2710	2.4339	2.4339	3.8008	3.9845	4.3540	4.8701	4.8701	5.3414	5.8030	6.5223
	(60×60), 2	33489	1.5245	2.2703	2.4337^s	2.4337^s	3.7974	3.9834	4.3530	4.8692^s	4.8692^s	5.3390	5.7937	6.5187
	(60×60), 3	44652	1.4713	2.1926	2.4337^s	2.4337^s	3.5980	3.7413	4.1095	4.8692^s	4.8692^s	5.0305	5.3637	6.1098
	(60×60), 4	55815	1.4713	2.1923	2.4337^s	2.4337^s	3.5965	3.7407	4.1086	4.8692^s	4.8692^s	5.0281	5.3580	6.1082
	(60×60), 5	66978	1.4708	2.1800	2.4337^s	2.4337^s	3.5453	3.7405	4.1026	4.8692^s	4.8692^s	4.9937	5.2504	6.1035
	(60×60), 6	78141	1.4708	2.1800	2.4337^s	2.4337^s	3.5452	3.7405	4.1026	4.8692^s	4.8692^s	4.9937	5.2500	6.1034
	(60×60), 7	89304	1.4705	2.1733	2.4337^s	2.4337^s	3.5190	3.7397	4.0986	4.8692^s	4.8692^s	4.9754	5.1988	6.1006

Table D.15: Convergence of the frequency parameters λ for modes 13-24 of a SSSS square laminated plate with $\frac{t}{b} = 0.1$ and stacking sequence $0°/90°/0°$. Material 2 is used.

			mode number											
theory	$(n_x \times n_y)$, N	n_{dof}	13	14	15	16	17	18	19	20	21	22	23	24
ED	(10×10), 2	1089	6.9811	7.5196	7.5727	7.5727	7.6403	9.0479	9.2671	9.6724	9.7333	10.1012	10.2784	10.3794
	(20×20), 2	3969	6.8102	7.0514	7.3681	7.3681	7.4884	8.3995	8.7449	9.1625	9.1953	9.3158	9.8029	9.8947
	(30×30), 2	8649	6.7776	6.9697	7.3305	7.3305	7.4572	8.1738	8.6849	9.0091	9.0684	9.2365	9.7399	9.8052
	(40×40), 2	15129	6.7662	6.9416	7.3173	7.3173	7.4461	8.0965	8.6637	8.9452	9.0355	9.2088	9.7175	9.7739
	(50×50), 2	23409	6.7609	6.9286	7.3112	7.3112	7.4409	8.0610	8.6539	8.9158	9.0204	9.1959	9.7070	9.7595
	(60×60), 2	33489	6.7580	6.9216	7.3079^s	7.3079^s	7.4381	8.0418	8.6485	8.9000	9.0121	9.1889	9.7013	9.7517^s
	(60×60), 3	44652	6.3545	6.4333	6.9974	7.2985	7.3079^s	7.3079^s	8.0736	8.1311	8.5024	8.6871	9.1744	9.3196
	(60×60), 4	55815	6.3525	6.4264	6.9936	7.2840	7.3079^s	7.3079^s	8.0651	8.1150	8.4998	8.6840	9.1695	9.2901
	(60×60), 5	66978	6.3414	6.3447	6.9666	7.1208	7.3079^s	7.3079^s	7.9753	7.9974	8.4793	8.6623	9.0858	9.1350
	(60×60), 6	78141	6.3411	6.3446	6.9666	7.1197	7.3079^s	7.3079^s	7.9744	7.9973	8.4791	8.6621	9.0836	9.1349
	(60×60), 7	89304	6.2998	6.3398	6.9517	7.0471	7.3079^s	7.3079^s	7.9112	7.9636	8.4718	8.6534	8.9981	9.1189

Table D.16: Convergence of the frequency parameters λ for modes 25-36 of a SSSS square laminated plate with $\frac{t}{b} = 0.1$ and stacking sequence $0°/90°/0°$. Material 2 is used.

			mode number											
theory	$(n_x \times n_y)$, N	n_{dof}	25	26	27	28	29	30	31	32	33	34	35	36
ED	(10×10), 2	1089	10.3794	11.0145	11.2500	11.8148	12.5769	12.6013	12.6979	12.7233	12.8440	13.3360	13.3633	13.3723
	(20×20), 2	3969	9.8947	10.5206	10.7624	11.0562	11.6572	11.7631	11.7822	11.8703	12.2066	12.2331	12.4820	12.4820
	(30×30), 2	8649	9.8052	10.3833	10.6583	10.6978	11.3104	11.5832	11.7113	11.7762	12.1011	12.1039	12.3068	12.3068
	(40×40), 2	15129	9.7739	10.3355	10.5224	10.6742	11.1917	11.5204	11.6556	11.7741	12.0580	12.0626	12.2457	12.2457
	(50×50), 2	23409	9.7595	10.3134	10.4601	10.6631	11.1373	11.4914	11.6298	11.7731	12.0366	12.0446	12.2174	12.2174
	(60×60), 2	33489	9.7517^s	10.3014	10.4264	10.6571	11.1079	11.4757	11.6159	11.7726^s	12.0250	12.0347	12.2021^s	12.2021^s
	(60×60), 3	44652	9.4877	9.7517^s	9.7517^s	9.9952	10.0237	10.9189	11.0679	11.1304	11.1962	11.3929	11.4581	11.7726^s
	(60×60), 4	55815	9.4700	9.7517^s	9.7517^s	9.9639	10.0141	10.9157	11.0641	11.0973	11.1774	11.3413	11.4526	11.5570^s
	(60×60), 5	66978	9.3525	9.7517^s	9.7517^s	9.7813	9.9485	10.8681	10.9374	11.0169	11.0700	11.1167	11.3972	11.5570^s
	(60×60), 6	78141	9.3520	9.7517^s	9.7517^s	9.7795	9.9485	10.8674	10.9362	11.0163	11.0698	11.1134	11.3968	11.5312^s
	(60×60), 7	89304	9.2979	9.7020	9.7517^s	9.7517^s	9.9175	10.8524	10.8671	11.0003	11.0210	11.0245	11.3753	11.5311^s

Table D.17: Convergence of the frequency parameters λ for the first 12 modes of a CCCC square laminated plate with $\frac{t}{b} = 0.1$ and stacking sequence $0°/90°$. Material 2 is used.

theory	$(n_x \times n_y)$, N	n_{dof}	mode number 1	2	3	4	5	6	7	8	9	10	11	12
ED	(10×10), 2	1089	1.8978	3.4043	3.4043	4.4407	5.5049	5.5270	6.1957	6.1957	7.5015	8.0395	8.0395	8.4679
	(20×20), 2	3969	1.8714	3.3080	3.3080	4.3276	5.2250	5.2449	5.9567	5.9567	7.2420	7.4056	7.4056	7.9352
	(30×30), 2	8649	1.8665	3.2904	3.2904	4.3063	5.1747	5.1941	5.9121	5.9121	7.1906	7.2933	7.2933	7.8382
	(40×40), 2	15129	1.8647	3.2842	3.2842	4.2988	5.1571	5.1764	5.8965	5.8965	7.1724	7.2543	7.2543	7.8044
	(50×50), 2	23409	1.8639	3.2813	3.2813	4.2954	5.1490	5.1682	5.8893	5.8893	7.1639	7.2364	7.2364	7.7887
	(60×60), 2	33489	1.8634	3.2797	3.2797	4.2935	5.1446	5.1638	5.8853	5.8853	7.1593	7.2266	7.2266	7.7802
	(60×60), 3	44652	1.8441	3.2301	3.2301	4.2256	5.0445	5.0626	5.7765	5.7765	7.0239	7.0559	7.0559	7.6104
	(60×60), 4	55815	1.8085	3.1583	3.1583	4.1372	4.9296	4.9477	5.6571	5.6571	6.8867	6.9017	6.9017	7.4565
	(60×60), 5	66978	1.7988	3.1391	3.1391	4.1123	4.8993	4.9175	5.6233	5.6233	6.8461	6.8617	6.8617	7.4137
	(60×60), 6	78141	1.7981	3.1378	3.1378	4.1108	4.8975	4.9157	5.6216	5.6216	6.8442	6.8595	6.8595	7.4115
	(60×60), 7	89304	1.7967	3.1356	3.1356	4.1082	4.8950	4.9133	5.6187	5.6187	6.8411	6.8571	6.8571	7.4087
LD	(10×10), 1	1089	1.8773	3.3566	3.3566	4.3819	5.4193	5.4415	6.1101	6.1101	7.4032	7.9142	7.9142	8.3479
	(20×20), 1	3969	1.8519	3.2633	3.2633	4.2724	5.1446	5.1645	5.8755	5.8755	7.1468	7.2851	7.2851	7.8188
	(30×30), 1	8649	1.8472	3.2463	3.2463	4.2518	5.0953	5.1148	5.8320	5.8320	7.0963	7.1743	7.1743	7.7231
	(40×40), 1	15129	1.8455	3.2403	3.2403	4.2446	5.0781	5.0975	5.8167	5.8167	7.0785	7.1359	7.1359	7.6898
	(50×50), 1	23409	1.8447	3.2375	3.2375	4.2413	5.0702	5.0895	5.8096	5.8096	7.0702	7.1182	7.1182	7.6744
	(60×60), 1	33489	1.8443	3.2360	3.2360	4.2394	5.0659	5.0852	5.8058	5.8058	7.0656	7.1086	7.1086	7.6660
	(60×60), 2	55815	1.8336	3.2104	3.2104	4.2040	5.0150	5.0335	5.7498	5.7498	6.9971	7.0199	7.0199	7.5781
	(60×60), 3	78141	1.7956	3.1339	3.1339	4.1062	4.8932	4.9114	5.6169	5.6169	6.8395	6.8565	6.8565	7.4079
	(60×60), 4	100467	1.7954	3.1331	3.1331	4.1051	4.8913	4.9096	5.6148	5.6148	6.8368	6.8529	6.8529	7.4043

Table D.18: Convergence of the frequency parameters λ for modes 13-24 of a CCCC square laminated plate with $\frac{t}{b} = 0.1$ and stacking sequence $0°/90°$. Material 2 is used.

			mode number											
theory	$(n_x \times n_y)$, N	n_{dof}	13	14	15	16	17	18	19	20	21	22	23	24
ED	(10×10), 2	1089	8.4937	9.3841	9.3841	10.7923	10.9464	10.9537	11.2137	11.2137	11.7661	11.7881	12.7026	12.7026
	(20×20), 2	3969	7.9556	8.9536	8.9536	9.7410	9.7479	10.1649	10.1649	10.3800	10.9578	10.9734	12.1407	12.1407
	(30×30), 2	8649	7.8577	8.8674	8.8674	9.5292	9.5359	9.9761	9.9761	10.2844	10.7989	10.8134	11.8482	11.8482
	(40×40), 2	15129	7.8235	8.8369	8.8369	9.4561	9.4628	9.9107	9.9107	10.2499	10.7430	10.7571	11.7264	11.7264
	(50×50), 2	23409	7.8077	8.8227	8.8227	9.4225	9.4291	9.8805	9.8805	10.2337	10.7171	10.7311	11.6703	11.6703
	(60×60), 2	33489	7.7992	8.8150	8.8150	9.4042	9.4108	9.8642	9.8642	10.2249	10.7030	10.7169	11.6399	11.6399
	(60×60), 3	44652	7.6264	8.6311	8.6311	9.1433	9.1491	9.6086	9.6086	10.0094	10.4483	10.4591	11.2680	11.2680
	(60×60), 4	55815	7.4748	8.4695	8.4695	8.9622	8.9688	9.4315	9.4315	9.8312	10.2650	10.2797	11.0792	11.0792
	(60×60), 5	66978	7.4323	8.4210	8.4210	8.9157	8.9224	9.3825	9.3825	9.7755	10.2104	10.2253	11.0302	11.0302
	(60×60), 6	78141	7.4302	8.4189	8.4189	8.9132	8.9199	9.3801	9.3801	9.7732	10.2080	10.2230	11.0271	11.0271
	(60×60), 7	89304	7.4275	8.4159	8.4159	8.9109	8.9176	9.3775	9.3775	9.7702	10.2051	10.2201	11.0244	11.0244
LD	(10×10), 1	1089	8.3751	9.2639	9.2639	10.6641	10.7866	10.7946	11.0640	11.0640	11.6224	11.6477	12.5656	12.5656
	(20×20), 1	3969	7.8403	8.8329	8.8329	9.5807	9.5880	10.0123	10.0123	10.2435	10.8055	10.8232	11.9810	11.9810
	(30×30), 1	8649	7.7436	8.7476	8.7476	9.3704	9.3776	9.8248	9.8248	10.1481	10.6472	10.6636	11.6556	11.6556
	(40×40), 1	15129	7.7099	8.7175	8.7175	9.2980	9.3050	9.7599	9.7599	10.1138	10.5916	10.6076	11.5340	11.5340
	(50×50), 1	23409	7.6944	8.7035	8.7035	9.2646	9.2717	9.7300	9.7300	10.0977	10.5659	10.5817	11.4781	11.4781
	(60×60), 1	33489	7.6859	8.6958	8.6958	9.2466	9.2536	9.7138	9.7138	10.0889	10.5519	10.5676	11.4478	11.4478
	(60×60), 2	55815	7.5962	8.6030	8.6030	9.1070	9.1135	9.5779	9.5779	9.9829	10.4208	10.4345	11.2404	11.2404
	(60×60), 3	78141	7.4269	8.4154	8.4154	8.9132	8.9200	9.3797	9.3797	9.7707	10.2072	10.2226	11.0318	11.0318
	(60×60), 4	100467	7.4232	8.4113	8.4113	8.9073	8.9141	9.3738	9.3738	9.7654	10.2010	10.2163	11.0230	11.0230

Table D.19: Convergence of the frequency parameters λ for modes 25-36 of a CCCC square laminated plate with $\frac{t}{b} = 0.1$ and stacking sequence $0^\circ/90^\circ$. Material 2 is used.

			mode number											
theory	$(n_x \times n_y)$, N	n_{dof}	25	26	27	28	29	30	31	32	33	34	35	36
ED	(10×10), 2	1089	13.0103	13.0103	13.4992	13.4992	13.4998	13.7993	14.0294	14.2559	14.2559	14.3788	14.3836	14.5517
	(20×20), 2	3969	12.2004	12.2004	12.5384	12.5459	13.0280	13.0280	13.1914	13.1914	13.5214	13.6481	13.8383	14.1540
	(30×30), 2	8649	12.0005	12.0005	12.2142	12.2225	12.9113	12.9113	13.0181	13.0181	13.4986	13.5138	13.8323	13.9227
	(40×40), 2	15129	11.9495	11.9495	12.1021	12.1104	12.8141	12.8141	13.0148	13.0148	13.4425	13.5114	13.8288	13.8410
	(50×50), 2	23409	11.9256	11.9256	12.0505	12.0588	12.7691	12.7691	13.0134	13.0134	13.4159	13.5104	13.7997	13.8099
	(60×60), 2	33489	11.9125	11.9125	12.0226	12.0309	12.7446	12.7446	13.0126	13.0126	13.4013	13.5098	13.7787	13.7886
	(60×60), 3	44652	11.6416	11.6416	11.6628	11.6694	12.3937	12.3937	12.5937	12.5937	13.0942	13.1138	13.4247	13.4250
	(60×60), 4	55815	11.4484	11.4484	11.4761	11.4852	12.2054	12.2054	12.5724	12.5724	12.8888	13.0941	13.2296	13.2409
	(60×60), 5	66978	11.3866	11.3866	11.4243	11.4337	12.1481	12.1481	12.5531	12.5531	12.8204	13.0753	13.1644	13.1761
	(60×60), 6	78141	11.3840	11.3840	11.4212	11.4307	12.1451	12.1451	12.5488	12.5488	12.8176	13.0713	13.1613	13.1730
	(60×60), 7	89304	11.3811	11.3811	11.4184	11.4279	12.1420	12.1420	12.5451	12.5451	12.8147	13.0678	13.1583	13.1699
LD	(10×10), 1	1089	12.9981	12.9981	13.4864	13.4979	13.4979	13.7764	13.8984	14.0784	14.0784	14.2160	14.2272	14.4217
	(20×20), 1	3969	12.0092	12.0092	12.3527	12.3624	13.0049	13.0049	13.0209	13.0209	13.4740	13.5105	13.8272	13.9699
	(30×30), 1	8649	11.8404	11.8404	12.0287	12.0386	12.7306	12.7306	13.0064	13.0064	13.3216	13.5038	13.7357	13.7483
	(40×40), 1	15129	11.7893	11.7893	11.9170	11.9268	12.6332	12.6332	13.0036	13.0036	13.2648	13.5015	13.6520	13.6642
	(50×50), 1	23409	11.7654	11.7654	11.8656	11.8753	12.5882	12.5882	13.0024	13.0024	13.2380	13.5004	13.6129	13.6251
	(60×60), 1	33489	11.7523	11.7523	11.8377	11.8475	12.5638	12.5638	13.0018	13.0018	13.2232	13.4997	13.5916	13.6039
	(60×60), 2	55815	11.6186	11.6186	11.6392	11.6477	12.3759	12.3759	12.5416	12.5416	13.0648	13.0753	13.3763	13.4135
	(60×60), 3	78141	11.3842	11.3842	11.4253	11.4350	12.1490	12.1490	12.5377	12.5377	12.8200	13.0608	13.1656	13.1775
	(60×60), 4	100467	11.3769	11.3769	11.4166	11.4263	12.1400	12.1400	12.5375	12.5375	12.8110	13.0606	13.1558	13.1676

Table D.20: Convergence of the frequency parameters λ for the first 12 modes of a CCCC square laminated plate with $\frac{t}{b} = 0.1$ and stacking sequence $0°/90°/0°/90°/0°$. Material 2 is used.

			mode number											
theory	$(n_x \times n_y)$, N	n_{dof}	1	2	3	4	5	6	7	8	9	10	11	12
ED	(10×10), 2	1089	2.5176	4.0306	4.4509	5.4221	6.2588	6.9416	7.1728	7.5400	8.7703	8.9258	9.5008	9.6905
	(20×20), 2	3969	2.4955	3.9428	4.3778	5.3424	5.9953	6.7213	6.9907	7.3773	8.3353	8.6263	9.0652	9.1868
	(30×30), 2	8649	2.4914	3.9266	4.3642	5.3271	5.9472	6.6805	6.9557	7.3454	8.2277	8.5938	8.9824	9.0936
	(40×40), 2	15129	2.4900	3.9210	4.3595	5.3217	5.9305	6.6663	6.9433	7.3341	8.1903	8.5821	8.9533	9.0610
	(50×50), 2	23409	2.4893	3.9184	4.3573	5.3192	5.9227	6.6597	6.9376	7.3289	8.1730	8.5766	8.9398	9.0460
	(60×60), 2	33489	2.4889	3.9170	4.3561	5.3178	5.9185	6.6561	6.9345	7.3261	8.1636	8.5736	8.9325	9.0378
	(60×60), 3	44652	2.3405	3.5024	4.1630	4.9288	5.1407	6.2155	6.3917	6.9201	6.9690	7.8077	7.8922	8.7021
	(60×60), 4	55815	2.3398	3.4998	4.1618	4.9258	5.1337	6.2080	6.3894	6.9159	6.9543	7.7923	7.8837	8.6984
	(60×60), 5	66978	2.3142	3.4388	4.1257	4.8658	5.0350	6.1153	6.3338	6.8246	6.8458	7.6702	7.7875	8.6184
	(60×60), 6	78141	2.3142	3.4386	4.1256	4.8657	5.0347	6.1150	6.3337	6.8241	6.8456	7.6697	7.7873	8.6181
	(60×60), 7	89304	2.3114	3.4354	4.1216	4.8613	5.0315	6.1107	6.3288	6.8207	6.8405	7.6655	7.7821	8.6133
LD	(10×10), 1	2178	2.3663	3.5751	4.2694	5.0178	5.3882	6.3877	6.7050	7.1493	7.5858	8.0695	8.2547	9.4064
	(20×20), 1	7938	2.3486	3.5119	4.1992	4.9544	5.1820	6.2526	6.4837	6.9897	7.0869	7.9006	7.9472	8.8898
	(30×30), 1	17298	2.3453	3.5002	4.1862	4.9420	5.1446	6.2266	6.4431	6.9587	6.9986	7.8353	7.9199	8.7954
	(40×40), 1	30258	2.3441	3.4961	4.1816	4.9377	5.1315	6.2173	6.4289	6.9476	6.9681	7.8125	7.9100	8.7625
	(50×50), 1	46818	2.3436	3.4941	4.1795	4.9356	5.1255	6.2130	6.4223	6.9421	6.9543	7.8019	7.9053	8.7473
	(60×60), 1	66978	2.3433	3.4931	4.1784	4.9345	5.1222	6.2107	6.4187	6.9388	6.9472	7.7961	7.9028	8.7390
	(60×60), 2	122793	2.3108	3.4337	4.1221	4.8609	5.0284	6.1089	6.3317	6.8160	6.8423	7.6619	7.7827	8.6207
	(60×60), 3	178608	2.3090	3.4295	4.1172	4.8546	5.0192	6.0988	6.3216	6.7994	6.8315	7.6451	7.7693	8.6028
	(60×60), 4	234423	2.3088	3.4293	4.1168	4.8542	5.0189	6.0982	6.3209	6.7988	6.8307	7.6444	7.7685	8.6015

Table D.21: Convergence of the frequency parameters λ for modes 12-24 of a CCCC square laminated plate with $\frac{t}{b} = 0.1$ and stacking sequence $0°/90°/0°/90°/0°$. Material 2 is used.

theory	$(n_x \times n_y)$, N	n_{dof}	mode number 13	14	15	16	17	18	19	20	21	22	23	24
ED	(10×10), 2	1089	10.0474	10.5941	10.8483	11.9378	12.1351	12.2617	12.6869	12.8648	12.9161	13.0083	13.3125	13.4360
	(20×20), 2	3969	9.6633	10.3499	10.6202	10.8439	11.3964	11.7368	12.0223	12.0959	12.4063	12.8405	12.9685	13.4633
	(30×30), 2	8649	9.5888	10.2926	10.5655	10.6421	11.2305	11.5582	11.9452	11.9724	12.2893	12.7295	12.9610	13.1256
	(40×40), 2	15129	9.5625	10.2718	10.5456	10.5719	11.1724	11.4959	11.8923	11.9532	12.2473	12.6895	12.9584	13.0082
	(50×50), 2	23409	9.5504	10.2620	10.5363	10.5396	11.1456	11.4672	11.8678	11.9440	12.2277	12.6708	12.9540	12.9572
	(60×60), 2	33489	9.5437	10.2567	10.5220	10.5312	11.1310	11.4515	11.8545	11.9390	12.2170	12.6606	12.9247	12.9565^s
	(60×60), 3	44652	8.8903	9.1003	9.2015	9.5718	9.8610	10.7409	10.8626	10.9373	11.0601	11.3767	11.4353	11.9928
	(60×60), 4	55815	8.8632	9.0947	9.1848	9.5440	9.8509	10.7117	10.8184	10.9191	11.0548	11.3694	11.3903	11.9810
	(60×60), 5	66978	8.7197	9.0046	9.0630	9.4063	9.7421	10.5747	10.6772	10.7894	10.9476	11.2532	11.2556	11.8533
	(60×60), 6	78141	8.7190	9.0044	9.0627	9.4057	9.7418	10.5742	10.6765	10.7891	10.9471	11.2525	11.2552	11.8530
	(60×60), 7	89304	8.7140	8.9993	9.0575	9.4001	9.7366	10.5680	10.6664	10.7839	10.9429	11.2424	11.2507	11.8483
LD	(10×10), 1	2178	9.4722	9.6554	10.1446	10.2205	10.5634	11.1575	11.3580	12.3869	12.4885	12.5266	12.7648	13.0037
	(20×20), 1	7938	9.1444	9.2539	9.2769	9.7812	9.9740	10.8947	11.0298	11.3267	11.3956	11.6666	11.8359	12.2173
	(30×30), 1	17298	8.9707	9.1777	9.2322	9.6419	9.9188	10.7991	10.9837	11.0231	11.2129	11.5101	11.5778	12.0986
	(40×40), 1	30258	8.9107	9.1510	9.2160	9.5936	9.8989	10.7651	10.9190	10.9662	11.1493	11.4554	11.4890	12.0563
	(50×50), 1	46818	8.8830	9.1386	9.2083	9.5713	9.8896	10.7492	10.8712	10.9578	11.1200	11.4301	11.4481	12.0366
	(60×60), 1	66978	8.8681	9.1318	9.2042	9.5592	9.8845	10.7405	10.8453	10.9532	11.1041	11.4163	11.4260	12.0258
	(60×60), 2	122793	8.7071	9.0059	9.0563	9.3945	9.7418	10.5647	10.6575	10.7872	10.9581	11.2348	11.2649	11.8610
	(60×60), 3	178608	8.6806	8.9876	9.0375	9.3684	9.7217	10.5376	10.6190	10.7629	10.9288	11.1973	11.2356	11.8305
	(60×60), 4	234423	8.6794	8.9864	9.0365	9.3672	9.7205	10.5362	10.6171	10.7616	10.9267	11.1953	11.2335	11.8285

Table D.22: Convergence of the frequency parameters λ for modes 25-36 of a CCCC square laminated plate with $\frac{t}{b} = 0.1$ and stacking sequence $0°/90°/0°/90°/0°$. Material 2 is used.

theory	$(n_x \times n_y)$, N	n_{dof}	mode number 25	26	27	28	29	30	31	32	33	34	35	36
ED	(10×10), 2	1089	13.5898	13.6801	13.8922	14.0800	14.8394	15.1972	15.2239	15.3468	15.5086	15.6223	15.7111	15.9021
	(20×20), 2	3969	13.6229	13.7816	13.8903	13.9739	14.3523	14.6283	14.6885	14.7063	14.9566	15.1218	15.2138	15.4510
	(30×30), 2	8649	13.5995	13.6122	13.7067	13.8999	14.0475	14.3604	14.4697	14.6817	15.0048	15.2769	15.3940	15.4450
	(40×40), 2	15129	13.4978	13.6085	13.6775	13.8710	13.9411	14.2664	14.3915	14.6731	14.9299	15.3683	15.3924	15.4759
	(50×50), 2	23409	13.4508	13.6067	13.6635	13.8571	13.8920	14.2229	14.3551	14.6692	14.8950	15.3555	15.3921	15.4465
	(60×60), 2	33489	13.4253	13.6058	13.6558	13.8494	13.8654	14.1993	14.3353	14.6670^s	14.8760	15.3465	15.3485	15.4760
	(60×60), 3	44652	12.2601	12.4318	12.8792	12.8903	12.9564^s	13.3726	13.4368	13.6057^s	13.6987	13.7644	14.0270	14.2131
	(60×60), 4	55815	12.2292	12.3851	12.8129	12.8704	12.9475^s	13.3052	13.4298	13.5972^s	13.6899	13.7159	13.9945	14.1658
	(60×60), 5	66978	12.0862	12.2476	12.6876	12.7262	12.9474^s	13.1823	13.2947	13.5505	13.5723	13.5971^s	13.8395	14.0409
	(60×60), 6	78141	12.0858	12.2470	12.6869	12.7259	12.9039^s	13.1816	13.2940	13.5499	13.5556^s	13.5719	13.8391	14.0403
	(60×60), 7	89304	12.0797	12.2369	12.6672	12.7211	12.9038^s	13.1626	13.2898	13.5454	13.5556^s	13.5623	13.8335	14.0219
LD	(10×10), 1	2178	13.1013	13.2669	13.3191	13.3843	13.5719	13.6755	13.7414	14.0744	14.3872	14.8350	15.2809	15.3607
	(20×20), 1	7938	12.3801	12.7393	12.9638	13.0525	13.6184	13.6414	13.9828	13.9862	14.0530	14.1599	14.1911	14.6160
	(30×30), 1	17298	12.3153	12.5477	12.9564	12.9704	13.1519	13.6078	13.6200	13.6718	13.8569	13.9109	14.0959	14.3899
	(40×40), 1	30258	12.2904	12.4806	12.9393	12.9537	12.9851	13.4721	13.5626	13.6040	13.8101	13.8131	14.0692	14.3098
	(50×50), 1	46818	12.2784	12.4496	12.9088	12.9245	12.9525	13.4043	13.5122	13.6023	13.7679	13.7880	14.0560	14.2684
	(60×60), 1	66978	12.2719	12.4327	12.8675	12.9164	12.9519^s	13.3677	13.4849	13.6013^s	13.7434	13.7759	14.0487	14.2387
	(60×60), 2	122793	12.0808	12.2315	12.6563	12.7318	12.8701^s	13.1529	13.3160	13.5233^s	13.5610	13.5706	13.8418	14.0145
	(60×60), 3	178608	12.0495	12.1937	12.6050	12.6981	12.8701^s	13.1028	13.2716	13.5202	13.5232^s	13.5264	13.8023	13.9646
	(60×60), 4	234423	12.0478	12.1917	12.6020	12.6960	12.8701^s	13.0999	13.2683	13.5180	13.5232	13.5232^s	13.8001	13.9617

Table D.23: Convergence of the frequency parameters λ for the first 12 modes of a CCCC square laminated plate with $\frac{t}{b} = 0.1$ and stacking sequence $45°/-45°/45°$. Material 2 is used.

theory	$(n_x \times n_y)$, N	n_{dof}	mode number 1	2	3	4	5	6	7	8	9	10	11	12
ED	(10×10), 2	1089	2.1395	3.3904	4.0227	4.7245	5.7474	6.1262	6.2311	7.1786	7.8593	8.3388	8.4812	8.9692
	(20×20), 2	3969	2.1160	3.2962	3.9423	4.5716	5.4729	5.9231	5.9730	6.8940	7.4937	7.7425	7.9777	8.4474
	(30×30), 2	8649	2.1115	3.2789	3.9272	4.5423	5.4231	5.8869	5.9240	6.8333	7.4201	7.6372	7.8947	8.3465
	(40×40), 2	15129	2.1098	3.2728	3.9219	4.5320	5.4057	5.8742	5.9068	6.8115	7.3940	7.6007	7.8664	8.3109
	(50×50), 2	23409	2.1091	3.2700	3.9194	4.5272	5.3977	5.8684	5.8988	6.8013	7.3819	7.5839	7.8534	8.2943
	(60×60), 2	33489	2.1087	3.2685	3.9181	4.5246	5.3933	5.8652	5.8944	6.7957	7.3753	7.5748	7.8464	8.2853
	(60×60), 3	44652	1.9958	3.0845	3.6874	4.2432	5.0702	5.4881	5.5126	6.3568	6.8155	7.1107	7.3869	7.7146
	(60×60), 4	55815	1.9952	3.0832	3.6859	4.2404	5.0671	5.4828	5.5097	6.3512	6.8059	7.1048	7.3821	7.7049
	(60×60), 5	66978	1.9879	3.0615	3.6726	4.1960	5.0347	5.4097	5.4882	6.2965	6.7025	7.0577	7.3489	7.6233
	(60×60), 6	78141	1.9878	3.0614	3.6725	4.1959	5.0345	5.4093	5.4881	6.2962	6.7019	7.0575	7.3487	7.6228
	(60×60), 7	89304	1.9837	3.0499	3.6653	4.1736	5.0179	5.3742	5.4771	6.2699	6.6545	7.0345	7.3330	7.5856
LD	(10×10), 1	1452	2.0555	3.2279	3.8555	4.4474	5.4741	5.8017	5.8711	6.8076	7.2577	7.9366	8.1255	8.4503
	(20×20), 1	5292	2.0339	3.1408	3.7790	4.3070	5.2122	5.5642	5.6759	6.5182	6.9131	7.3687	7.6518	7.9273
	(30×30), 1	11532	2.0298	3.1249	3.7647	4.2803	5.1649	5.5195	5.6410	6.4583	6.8455	7.2684	7.5730	7.8281
	(40×40), 1	20172	2.0284	3.1193	3.7597	4.2709	5.1484	5.5039	5.6289	6.4369	6.8217	7.2336	7.5461	7.7932
	(50×50), 1	31212	2.0277	3.1167	3.7574	4.2665	5.1408	5.4966	5.6233	6.4269	6.8106	7.2176	7.5337	7.7770
	(60×60), 1	44652	2.0273	3.1153	3.7561	4.2642	5.1366	5.4926	5.6202	6.4214	6.8046	7.2089	7.5270	7.7682
	(60×60), 2	78141	1.9902	3.0664	3.6801	4.2042	5.0469	5.4216	5.5039	6.3144	6.7187	7.0799	7.3765	7.6469
	(60×60), 3	111630	1.9812	3.0435	3.6613	4.1618	5.0095	5.3567	5.4718	6.2575	6.6319	7.0241	7.3269	7.5689
	(60×60), 4	148840	1.9810	3.0431	3.6607	4.1611	5.0085	5.3556	5.4706	6.2560	6.6304	7.0223	7.3247	7.5668

Table D.24: Convergence of the frequency parameters λ for modes 13-24 of a CCCC square laminated plate with $\frac{t}{b} = 0.1$ and stacking sequence $45°/-45°/45°$. Material 2 is used.

theory	$(n_x \times n_y)$, N	n_{dof}	mode number											
			13	14	15	16	17	18	19	20	21	22	23	24
ED	(10×10), 2	1089	9.4749	9.5723	10.5681	10.5777	11.1978	11.2398	11.3891	11.7077	11.9156	12.4413	12.8740	13.0047
	(20×20), 2	3969	9.0926	9.0939	10.0603	10.0891	10.1868	10.3408	10.7565	10.8022	11.2014	11.7208	12.3684	12.4112
	(30×30), 2	8649	8.9906	9.0110	9.8887	9.9315	10.0083	10.2882	10.6216	10.6347	11.0780	11.5527	12.1766	12.2125
	(40×40), 2	15129	8.9540	8.9805	9.8198	9.8845	9.9480	10.2683	10.5728	10.5761	11.0346	11.4912	12.0725	12.1519
	(50×50), 2	23409	8.9369	8.9661	9.7881	9.8624	9.9205	10.2587	10.5490	10.5498	11.0143	11.4623	12.0224	12.1028
	(60×60), 2	33489	8.9276	8.9582	9.7710	9.8503	9.9057	10.2534^s	10.5343	10.5373	11.0032	11.4464	11.9950	12.0748
	(60×60), 3	44652	8.1915	8.3856	9.1265	9.1859	9.3308	9.6168	9.8244	10.2533^s	10.3562	10.5597	11.0168	11.2585
	(60×60), 4	55815	8.1756	8.3767	9.1108	9.1763	9.3216	9.5934	9.8093	10.1356^s	10.3448	10.5360	10.9821	11.2360
	(60×60), 5	66978	8.0447	8.3114	9.0037	9.1135	9.2570	9.4506	9.7153	10.1356^s	10.2718	10.4076	10.8143	11.1196
	(60×60), 6	78141	8.0436	8.3110	9.0028	9.1132	9.2565	9.4492	9.7145	10.1210^s	10.2712	10.4062	10.8122	11.1184
	(60×60), 7	89304	7.9862	8.2815	8.9561	9.0840	9.2243	9.3925	9.6735	10.1210^s	10.2405	10.3524	10.7433	11.0699
LD	(10×10), 1	1452	8.8029	9.0546	9.9831	10.3412	10.5487	10.7219	10.8264	11.0930	11.4279	11.7185	12.0045	12.3410
	(20×20), 1	5292	8.3263	8.6410	9.3897	9.6165	9.6874	9.8627	10.1838	10.3236	10.7248	10.8966	11.2833	11.6583
	(30×30), 1	11532	8.2298	8.5511	9.2570	9.4248	9.5446	9.7101	10.0163	10.2715	10.5926	10.7187	11.1112	11.4712
	(40×40), 1	20172	8.1955	8.5183	9.2093	9.3589	9.4948	9.6576	9.9577	10.2517	10.5449	10.6547	11.0488	11.4017
	(50×50), 1	31212	8.1796	8.5029	9.1870	9.3286	9.4718	9.6335	9.9307	10.2422	10.5225	10.6248	11.0196	11.3688
	(60×60), 1	44652	8.1709	8.4944	9.1748	9.3122	9.4594	9.6204	9.9160	10.2370^s	10.5103	10.6084	11.0036	11.3509
	(60×60), 2	78141	8.0657	8.3432	9.0340	9.1493	9.2956	9.4796	9.7530	10.1180^s	10.3225	10.4450	10.8462	11.1665
	(60×60), 3	111630	7.9602	8.2697	8.9366	9.0729	9.2114	9.3701	9.6580	10.1180^s	10.2322	10.3319	10.7156	11.0536
	(60×60), 4	148840	7.9582	8.2670	8.9338	9.0698	9.2081	9.3671	9.6545	10.1179^s	10.2274	10.3281	10.7123	11.0489

Table D.25: Convergence of the frequency parameters λ for modes 25-36 of a CCCC square laminated plate with $\frac{t}{b} = 0.1$ and stacking sequence $45°/-45°/45°$. Material 2 is used.

			mode number											
theory	$(n_x \times n_y)$, N	n_{dof}	25	26	27	28	29	30	31	32	33	34	35	36
ED	(10×10), 2	1089	13.4411	13.5695	13.8651	13.9200	14.3491	14.5262	14.5283	14.5527	14.7703	14.8917	15.1590	15.3452
	(20×20), 2	3969	12.6022	12.6024	13.1238	13.1854	13.3671	13.4188	13.9062	14.0975	14.1682	14.5302	14.9719	15.0905
	(30×30), 2	8649	12.2680	12.3259	12.8983	12.9536	13.1370	13.2174	13.7881	13.8606	13.9712	14.3501	14.6245	14.6654
	(40×40), 2	15129	12.1546	12.2502	12.7996	12.8897	13.0612	13.1410	13.7404	13.7749	13.8959	14.2803	14.4389	14.4803
	(50×50), 2	23409	12.1228	12.2169	12.7543	12.8592	13.0269	13.1047	13.7166	13.7346	13.8600	14.2463	14.3532	14.3956
	(60×60), 2	33489	12.1067	12.1991	12.7297	12.8423	13.0085	13.0847	13.7031^s	13.7126	13.8402	14.2274	14.3069	14.3500
	(60×60), 3	44652	11.3344	11.3876	11.9264	12.0285	12.2782	12.5173	12.7134	12.8422^s	13.3442	13.4118	13.5266	13.5690
	(60×60), 4	55815	11.3189	11.3744	11.9061	11.9947	12.2587	12.4729	12.6633^s	12.6809	13.3176	13.3768	13.5064	13.5365
	(60×60), 5	66978	11.2314	11.2933	11.8023	11.8513	12.1470	12.3172	12.5467	12.6633^s	13.1975	13.2366	13.3971	13.4114
	(60×60), 6	78141	11.2310	11.2929	11.8014	11.8495	12.1454	12.3151	12.5450	12.6415^s	13.1961	13.2348	13.3966	13.4104
	(60×60), 7	89304	11.1924	11.2575	11.7576	11.7913	12.0949	12.2590	12.4906	12.6415^s	13.1477	13.1765	13.3495	13.3592
LD	(10×10), 1	1452	13.2277	13.4146	13.5126	13.5631	13.8248	13.8817	13.9247	14.1078	14.2601	14.3388	14.4183	14.7820
	(20×20), 1	5292	11.9921	12.0225	12.4639	12.5086	12.7252	12.9407	13.0948	13.2290	13.8865	13.8974	14.0044	14.3860
	(30×30), 1	11532	11.6640	11.7186	12.2231	12.2322	12.5269	12.7099	12.9270	12.9690	13.6497	13.7115	13.7797	13.9737
	(40×40), 1	20172	11.5519	11.6160	12.1247	12.1481	12.4559	12.6290	12.8640	12.8755	13.5568	13.5970	13.7321	13.8034
	(50×50), 1	31212	11.5005	11.5693	12.0794	12.1086	12.4227	12.5915	12.8317	12.8339	13.5120	13.5409	13.7084	13.7255
	(60×60), 1	44652	11.4728	11.5441	12.0549	12.0870	12.4045	12.5712	12.8078	12.8173^s	13.4872	13.5095	13.6836	13.6931
	(60×60), 2	78141	11.2824	11.3488	11.8575	11.8966	12.2039	12.3687	12.6013	12.6370^s	13.2667	13.2920	13.4675	13.4764
	(60×60), 3	111630	11.1804	11.2480	11.7453	11.7714	12.0790	12.2438	12.4746	12.6368^s	13.1380	13.1591	13.3393	13.3466
	(60×60), 4	148840	11.1755	11.2425	11.7396	11.7666	12.0734	12.2377	12.4686	12.6368^s	13.1301	13.1530	13.3316	13.3394

Table D.26: Convergence of the frequency parameters λ for the first 12 modes of CCCC square composite plate with $\frac{t}{b} = 0.1$, $\frac{t_c}{t_f} = 10$ and stack sequence $0°/90°/\text{core}/0°/90°$. Material 4 and 5 are used for faces and core respectively.

			mode number											
theory	$(n_x \times n_y)$, N	n_{dof}	1	2	3	4	5	6	7	8	9	10	11	12
ED	(10×10), 2	1089	2.3306	3.9625	3.9625	5.0910	6.1641	6.1893	6.9095	6.9095	7.5861	7.5861	8.2429	8.2846
	(20×20), 2	3969	2.3060	3.8822	3.8822	5.0110	5.9324	5.9561	6.7424	6.7424	7.5562	7.5562	8.1016	8.2056
	(30×30), 2	8649	2.3012	3.8672	3.8672	4.9954	5.8897	5.9131	6.7097	6.7097	7.5504	7.5504	8.0697	8.1099
	(40×40), 2	15129	2.2994	3.8618	3.8618	4.9898	5.8747	5.8981	6.6982	6.6982	7.5483	7.5483	8.0582	8.0766
	(50×50), 2	23409	2.2985	3.8593	3.8593	4.9872	5.8678	5.8911	6.6927	6.6927	7.5473	7.5473	8.0527	8.0611
	(60×60), 2	33489	2.2981	3.8579	3.8579	4.9857	5.8640	5.8873	6.6898	6.6898	7.5468	7.5468	8.0498	8.0527
	(60×60), 3	44652	0.5501	0.8828	0.8828	1.1286	1.2871	1.2873	1.4743	1.4743	1.7383	1.7383	1.7629	1.8893
	(60×60), 4	55815	0.5483	0.8789	0.8789	1.1225	1.2795	1.2798	1.4644	1.4644	1.7252	1.7252	1.7488	1.8736
	(60×60), 5	66978	0.2582	0.4370	0.4370	0.5737	0.6844	0.6849	0.7932	0.7932	0.9824	0.9998	0.9998	1.0903
	(60×60), 6	78141	0.2579	0.4364	0.4364	0.5729	0.6836	0.6841	0.7922	0.7922	0.9813	0.9989	0.9989	1.0894
	(60×60), 7	89304	0.2574	0.4357	0.4357	0.5720	0.6826	0.6830	0.7911	0.7911	0.9800	0.9975	0.9975	1.0879
LD	(10×10), 1	2178	0.2321	0.4129	0.4129	0.5484	0.7093	0.7100	0.8112	0.8112	1.0288	1.1797	1.1797	1.2576
	(20×20), 1	7938	0.2300	0.3996	0.3996	0.5297	0.6492	0.6498	0.7523	0.7523	0.9431	0.9874	0.9874	1.0721
	(30×30), 1	17298	0.2295	0.3970	0.3970	0.5261	0.6391	0.6397	0.7423	0.7423	0.9287	0.9585	0.9585	1.0443
	(40×40), 1	30258	0.2292	0.3960	0.3960	0.5248	0.6355	0.6361	0.7387	0.7387	0.9235	0.9486	0.9486	1.0347
	(50×50), 1	46818	0.2291	0.3955	0.3955	0.5241	0.6338	0.6344	0.7369	0.7369	0.9211	0.9440	0.9440	1.0302
	(60×60), 1	66978	0.2290	0.3953	0.3953	0.5237	0.6328	0.6334	0.7360	0.7360	0.9197	0.9415	0.9415	1.0278
	(60×60), 2	122793	0.2275	0.3922	0.3922	0.5191	0.6274	0.6280	0.7291	0.7291	0.9108	0.9335	0.9335	1.0185
	(60×60), 3	178608	0.2275	0.3921	0.3921	0.5190	0.6273	0.6279	0.7290	0.7290	0.9106	0.9332	0.9332	1.0182
	(60×60), 4	234423	0.2275	0.3921	0.3921	0.5190	0.6273	0.6279	0.7290	0.7290	0.9106	0.9332	0.9332	1.0182

Table D.27: Convergence of the frequency parameters λ for modes 13-24 of CCCC square composite plate with $\frac{t}{b} = 0.1$, $\frac{t_c}{t_f} = 10$ and stack sequence 0°/90°/core/0°/90°. Material 4 and 5 are used for faces and core respectively.

			mode number											
theory	$(n_x \times n_y)$, N	n_{dof}	13	14	15	16	17	18	19	20	21	22	23	24
ED	(10 × 10), 2	1089	8.7262	8.7262	8.7366	8.8157	9.1796	9.1924	10.0299	10.0299	10.0822	10.0822	11.4157	11.5503
	(20 × 20), 2	3969	8.2056	8.2269	8.7608	8.7906	8.8022	9.1665	9.8527	9.8527	9.8776	9.8776	10.5818	10.5884
	(30 × 30), 2	8649	8.1099	8.2161	8.7139	8.7270	8.7520	9.2499	9.7992	9.7992	9.8485	9.8485	10.4017	10.4083
	(40 × 40), 2	15129	8.0766	8.2123	8.6878	8.7005	8.7481	9.2794	9.7797	9.7797	9.8384	9.8384	10.3389	10.3455
	(50 × 50), 2	23409	8.0611	8.2105	8.6756	8.6882	8.7463	9.2931	9.7705	9.7705	9.8338	9.8338	10.3099	10.3165
	(60 × 60), 2	33489	8.0527	8.2095	8.6689	8.6815	8.7453	9.3005	9.7654	9.7654	9.8312	9.8312	10.2942	10.3008
	(60 × 60), 3	44652	1.8895	2.1340	2.1340	2.2388	2.2389	2.3663	2.3663	2.4635	2.5778	2.5784	2.7925	2.7925
	(60 × 60), 4	55815	1.8738	2.1137	2.1137	2.2183	2.2184	2.3429	2.3429	2.4368	2.5496	2.5501	2.7630	2.7630
	(60 × 60), 5	66978	1.0916	1.2552	1.2552	1.3853	1.3857	1.4656	1.4656	1.5013	1.5352^s	1.5496^s	1.5496^s	1.5700^s
	(60 × 60), 6	78141	1.0906	1.2542	1.2542	1.3845	1.3848	1.4648	1.4648	1.5005	1.5346^s	1.5485^s	1.5485^s	1.5686^s
	(60 × 60), 7	89304	1.0891	1.2526	1.2526	1.3825	1.3828	1.4627	1.4627	1.4985	1.5276^s	1.5419^s	1.5419^s	1.5623^s
LD	(10 × 10), 1	2178	1.2596	1.3333	1.3673	1.3673	1.4073	1.4326	1.4326	1.4776	1.4783	1.5259	1.5259	1.6539
	(20 × 20), 1	7938	1.0738	1.2363	1.2363	1.3329	1.3630	1.3630	1.3988	1.4275	1.4279	1.4468	1.4473	1.4904
	(30 × 30), 1	17298	1.0459	1.2063	1.2063	1.3328	1.3603	1.3607	1.3622	1.3622	1.3972	1.4367	1.4367	1.4419
	(40 × 40), 1	30258	1.0363	1.1960	1.1960	1.3328	1.3379	1.3383	1.3619	1.3619	1.3966	1.4149	1.4149	1.4402
	(50 × 50), 1	46818	1.0318	1.1911	1.1911	1.3276	1.3280	1.3328	1.3617	1.3617	1.3964	1.4049	1.4049	1.4347
	(60 × 60), 1	66978	1.0294	1.1884	1.1884	1.3220	1.3224	1.3328^s	1.3617^s	1.3617^s	1.3962^s	1.3994	1.3994	1.4309
	(60 × 60), 2	122793	1.0199	1.1771	1.1771	1.3107	1.3110	1.3268^s	1.3485^s	1.3485^s	1.3768^s	1.3867	1.3867	1.4162^s
	(60 × 60), 3	178608	1.0196	1.1767	1.1767	1.3100	1.3104	1.3257^s	1.3473^s	1.3473^s	1.3755^s	1.3861	1.3861	1.4147^s
	(60 × 60), 4	234423	1.0196	1.1767	1.1767	1.3100	1.3104	1.3257^s	1.3473^s	1.3473^s	1.3755^s	1.3861	1.3861	1.4147^s

Table D.28: Convergence of the frequency parameters λ for modes 25-36 of CCCC square composite plate with $\frac{t}{b} = 0.1$, $\frac{t_c}{t_f} = 10$ and stack sequence 0°/90°/core/0°/90°. Material 4 and 5 are used for faces and core respectively.

			mode number											
theory	$(n_x \times n_y)$, N	n_{dof}	25	26	27	28	29	30	31	32	33	34	35	36
ED	(10 × 10), 2	1089	11.5563	11.8066	11.8066	11.9481	12.0034	12.3271	12.3317	12.7278	12.7278	13.1535	13.1535	14.2770
	(20 × 20), 2	3969	11.0350	11.0350	11.3020	11.5749	11.6351	11.8611	11.8663	13.0378	13.0378	13.0444	13.0444	13.3865
	(30 × 30), 2	8649	10.8853	10.8853	11.2535	11.5062	11.5670	11.7529	11.7581	12.7354	12.7354	12.9726	12.9726	13.1240
	(40 × 40), 2	15129	10.8328	10.8328	11.2349	11.4822	11.5433	11.7139	11.7191	12.6300	12.6300	12.9447	12.9447	13.0320
	(50 × 50), 2	23409	10.8085	10.8085	11.2260	11.4711	11.5323	11.6957	11.7008	12.5813	12.5813	12.9313	12.9313	12.9894
	(60 × 60), 2	33489	10.7953	10.7953	11.2210	11.4651	11.5263	11.6857	11.6909	12.5549	12.5549	12.9239	12.9239	12.9663
	(60 × 60), 3	44652	2.8722	2.8722	2.9035	2.9038	3.0910	3.0910	3.2468	3.3554	3.3564	3.4024	3.4025	3.5015
	(60 × 60), 4	55815	2.8372	2.8372	2.8711	2.8713	3.0535	3.0535	3.2033	3.3111	3.3118	3.3636	3.3637	3.4596
	(60 × 60), 5	66978	1.6014^s	1.6022^s	1.6101	1.6122	1.6302^s	1.6302^s	1.7015^s	1.7218^s	1.7218^s	1.7580^s	1.7600^s	1.8331
	(60 × 60), 6	78141	1.5999^s	1.6008^s	1.6094	1.6113	1.6287^s	1.6287^s	1.6999^s	1.7201^s	1.7201^s	1.7562^s	1.7584^s	1.8322
	(60 × 60), 7	89304	1.5938^s	1.5947^s	1.6072	1.6091	1.6230^s	1.6230^s	1.6947^s	1.7147^s	1.7147^s	1.7511^s	1.7533^s	1.8298
LD	(10 × 10), 1	2178	1.7651	1.7651	1.7755	1.8185	1.8209	1.9401	1.9405	1.9518	1.9518	2.0037	2.0037	2.1393
	(20 × 20), 1	7938	1.4904	1.4977	1.5022	1.5022	1.5916	1.6261	1.6261	1.6430	1.6457	1.6759	1.6776	1.7858
	(30 × 30), 1	17298	1.4424	1.4558	1.4847	1.4847	1.5775	1.5801	1.5817	1.6068	1.6068	1.6558	1.6575	1.7617
	(40 × 40), 1	30258	1.4407	1.4414	1.4827	1.4827	1.5557	1.5582	1.5781	1.6004	1.6004	1.6490	1.6506	1.7535
	(50 × 50), 1	46818	1.4394	1.4399	1.4817	1.4817	1.5457	1.5481	1.5764	1.5974	1.5974	1.6459	1.6475	1.7496
	(60 × 60), 1	66978	1.4389^s	1.4394^s	1.4812^s	1.4812^s	1.5402	1.5426	1.5755^s	1.5957^s	1.5957^s	1.6441^s	1.6457^s	1.7475^s
	(60 × 60), 2	122793	1.4169	1.4170^s	1.4534^s	1.4534^s	1.5254	1.5275	1.5407^s	1.5630^s	1.5630^s	1.6069^s	1.6092^s	1.7047^s
	(60 × 60), 3	178608	1.4156^s	1.4164	1.4519^s	1.4519^s	1.5248	1.5268	1.5389^s	1.5610^s	1.5610^s	1.6048^s	1.6071^s	1.7023^s
	(60 × 60), 4	234423	1.4156^s	1.4164	1.4519^s	1.4519^s	1.5248	1.5268	1.5389^s	1.5610^s	1.5610^s	1.6048^s	1.6071^s	1.7023^s

Table D.29: Convergence of the frequency parameters λ for the first 12 modes of CCCC square composite plate with $\frac{t}{b} = 0.01$, $\frac{t_c}{t_f} = 10$ and stack sequence $0°/90°/\text{core}/0°/90°$. Material 4 and 5 are used for faces and core respectively.

			mode number											
theory	$(n_x \times n_y)$, N	n_{dof}	1	2	3	4	5	6	7	8	9	10	11	12
ED	(10×10), 2	1089	0.3542	0.7615	0.7615	1.0450	1.5156	1.5188	1.7044	1.7044	2.2047	2.7211	2.7211	2.8463
	(20×20), 2	3969	0.3459	0.7177	0.7177	0.9822	1.3420	1.3450	1.5289	1.5289	1.9594	2.2135	2.2135	2.3511
	(30×30), 2	8649	0.3443	0.7099	0.7099	0.9710	1.3134	1.3164	1.4997	1.4997	1.9185	2.1363	2.1363	2.2756
	(40×40), 2	15129	0.3437	0.7072	0.7072	0.9671	1.3035	1.3065	1.4896	1.4896	1.9043	2.1102	2.1102	2.2500
	(50×50), 2	23409	0.3434	0.7059	0.7059	0.9652	1.2990	1.3019	1.4849	1.4849	1.8978	2.0983	2.0983	2.2382
	(60×60), 2	33489	0.3432	0.7052	0.7052	0.9642	1.2965	1.2994	1.4823	1.4823	1.8942	2.0918	2.0918	2.2318
	(60×60), 3	44652	0.2876	0.5240	0.5240	0.6927	0.8424	0.8456	0.9651	0.9651	1.1817	1.2031	1.2031	1.2943
	(60×60), 4	55815	0.2876	0.5239	0.5239	0.6927	0.8423	0.8455	0.9650	0.9650	1.1815	1.2030	1.2030	1.2941
LD	(10×10), 1	2178	0.1602	0.2605	0.2605	0.3316	0.3938	0.3943	0.4409	0.4409	0.5209	0.5444	0.5444	0.5746
	(20×20), 1	7938	0.1593	0.2572	0.2572	0.3292	0.3815	0.3821	0.4337	0.4337	0.5147	0.5147	0.5161	0.5540
	(30×30), 1	17298	0.1591	0.2565	0.2565	0.3286	0.3793	0.3799	0.4323	0.4323	0.5093	0.5093	0.5150	0.5500
	(40×40), 1	30258	0.1590	0.2562	0.2562	0.3284	0.3785	0.3791	0.4317	0.4317	0.5074	0.5074	0.5145	0.5486
	(50×50), 1	46818	0.1590	0.2561	0.2561	0.3283	0.3781	0.3787	0.4315	0.4315	0.5065	0.5065	0.5143	0.5480
	(60×60), 1	66978	0.1590	0.2560	0.2560	0.3282	0.3779	0.3785	0.4313	0.4313	0.5060	0.5060	0.5141	0.5476
	(60×60), 2	122793	0.1589	0.2560	0.2560	0.3281	0.3777	0.3783	0.4311	0.4311	0.5057	0.5057	0.5139	0.5473
	(60×60), 3	178608	0.1589	0.2560	0.2560	0.3281	0.3777	0.3783	0.4311	0.4311	0.5057	0.5057	0.5139	0.5473

Table D.30: Convergence of the frequency parameters λ for modes 13-24 of CCCC square composite plate with $\frac{t}{b} = 0.01$, $\frac{t_c}{t_f} = 10$ and stack sequence $0°/90°$/core/$0°/90°$. Material 4 and 5 are used for faces and core respectively.

theory	$(n_x \times n_y)$, N	n_{dof}	mode number 13	14	15	16	17	18	19	20	21	22	23	24
ED	(10×10), 2	1089	2.8537	3.2017	3.2017	3.9780	4.5747	4.5758	4.6621	4.6621	4.8876	4.9025	5.4345	5.4345
	(20×20), 2	3969	2.3569	2.6858	2.6858	3.2881	3.3388	3.3398	3.4531	3.4531	3.7107	3.7188	4.2028	4.2028
	(30×30), 2	8649	2.2811	2.6052	2.6052	3.1682	3.1692	3.1798	3.2856	3.2856	3.5447	3.5520	4.0218	4.0218
	(40×40), 2	15129	2.2554	2.5778	2.5778	3.1116	3.1126	3.1429	3.2300	3.2300	3.4893	3.4963	3.9610	3.9610
	(50×50), 2	23409	2.2435	2.5652	2.5652	3.0858	3.0868	3.1260	3.2046	3.2046	3.4640	3.4710	3.9333	3.9333
	(60×60), 2	33489	2.2371	2.5583	2.5583	3.0719	3.0729	3.1168	3.1910	3.1910	3.4504	3.4573	3.9183	3.9183
	(60×60), 3	44652	1.2978	1.4685	1.4685	1.5820	1.5829	1.6577	1.6577	1.7105	1.7972	1.7996	1.9715	1.9715
	(60×60), 4	55815	1.2976	1.4683	1.4683	1.5817	1.5826	1.6574	1.6574	1.7102	1.7969	1.7993	1.9711	1.9711
LD	(10×10), 1	2178	0.5747	0.6290	0.6290	0.7087	0.7179	0.7180	0.7353	0.7353	0.7675	0.7676	0.8180	0.8180
	(20×20), 1	7938	0.5541	0.6192	0.6192	0.6545	0.6547	0.6853	0.6853	0.7053	0.7372	0.7373	0.8018	0.8018
	(30×30), 1	17298	0.5502	0.6167	0.6167	0.6437	0.6438	0.6766	0.6766	0.7033	0.7312	0.7313	0.7823	0.7823
	(40×40), 1	30258	0.5488	0.6158	0.6158	0.6399	0.6400	0.6735	0.6735	0.7025	0.7291	0.7291	0.7755	0.7755
	(50×50), 1	46818	0.5481	0.6154	0.6154	0.6381	0.6382	0.6721	0.6721	0.7021	0.7281	0.7281	0.7724	0.7724
	(60×60), 1	66978	0.5477	0.6151	0.6151	0.6371	0.6373	0.6713	0.6713	0.7018	0.7275	0.7275	0.7707	0.7707
	(60×60), 2	122793	0.5474	0.6147	0.6147	0.6367	0.6369	0.6708	0.6708	0.7013	0.7269	0.7270	0.7701	0.7701
	(60×60), 3	178608	0.5474	0.6147	0.6147	0.6367	0.6369	0.6708	0.6708	0.7013	0.7269	0.7270	0.7701	0.7701

Table D.31: Convergence of the frequency parameters λ for modes 25-36 of CCCC square composite plate with $\frac{t}{b} = 0.01$, $\frac{t_c}{t_f} = 10$ and stack sequence $0°/90°/core/0°/90°$. Material 4 and 5 are used for faces and core respectively.

			mode number											
theory	$(n_x \times n_y)$, N	n_{dof}	25	26	27	28	29	30	31	32	33	34	35	36
ED	(10×10), 2	1089	6.5411	7.4047	7.4047	7.4447	7.4486	7.5682	7.5682	7.6076	7.6076	7.8543	7.8890	8.2958
	(20×20), 2	3969	4.7416	4.7416	4.8357	4.8387	4.9829	5.0496	5.0496	5.4401	5.4507	6.0951	6.0951	6.4461
	(30×30), 2	8649	4.4108	4.4108	4.5100	4.5128	4.7300	4.7300	4.7488	5.1192	5.1281	5.7427	5.7427	5.8627
	(40×40), 2	15129	4.3032	4.3032	4.4040	4.4067	4.6257	4.6257	4.6703	5.0138	5.0221	5.6259	5.6259	5.6768
	(50×50), 2	23409	4.2546	4.2546	4.3561	4.3588	4.5786	4.5786	4.6344	4.9660	4.9741	5.5728	5.5728	5.5936
	(60×60), 2	33489	4.2285	4.2285	4.3304	4.3331	4.5532	4.5532	4.6150	4.9403	4.9483	5.5442	5.5442	5.5491
	(60×60), 3	44652	2.0024	2.0024	2.0343	2.0356	2.1530	2.1530	2.2573	2.3261	2.3275	2.3653	2.3656	2.4204
	(60×60), 4	55815	2.0019	2.0019	2.0338	2.0351	2.1525	2.1525	2.2567	2.3255	2.3269	2.3647	2.3650	2.4197
LD	(10×10), 1	2178	0.8929	0.9222	0.9222	0.9293	0.9294	0.9432	0.9432	0.9659	0.9672	1.0054	1.0054	1.0749
	(20×20), 1	7938	0.8086	0.8086	0.8263	0.8263	0.8681	0.8681	0.8972	0.9269	0.9269	0.9586	0.9586	0.9783
	(30×30), 1	17298	0.8048	0.8048	0.8095	0.8096	0.8553	0.8553	0.8941	0.9183	0.9183	0.9260	0.9260	0.9490
	(40×40), 1	30258	0.8034	0.8034	0.8037	0.8038	0.8508	0.8508	0.8927	0.9149	0.9149	0.9151	0.9151	0.9391
	(50×50), 1	46818	0.8010	0.8011	0.8026	0.8026	0.8487	0.8487	0.8920	0.9098	0.9099	0.9136	0.9136	0.9346
	(60×60), 1	66978	0.7996	0.7996	0.8022	0.8022	0.8476	0.8476	0.8915	0.9071	0.9071	0.9127	0.9127	0.9321
	(60×60), 2	122793	0.7989	0.7989	0.8015	0.8015	0.8468	0.8468	0.8907	0.9062	0.9062	0.9118	0.9118	0.9311
	(60×60), 3	178608	0.7989	0.7989	0.8015	0.8015	0.8468	0.8468	0.8907	0.9062	0.9062	0.9118	0.9118	0.9311

Table D.32: Convergence of the frequency parameters λ for the first 12 modes of CCCC square composite plate with $\frac{t}{b} = 0.1$, $\frac{t_c}{t_f} = 50$ and stack sequence $0°/90°/\text{core}/0°/90°$. Material 4 and 5 are used for faces and core respectively.

theory	$(n_x \times n_y)$, N	n_{dof}	mode number 1	2	3	4	5	6	7	8	9	10	11	12
ED	(10×10), 2	1089	1.7365	2.9263	2.9263	3.7501	4.5228	4.5398	5.0648	5.0648	5.2895	5.2895	5.4506	5.4506
	(20×20), 2	3969	1.7194	2.8705	2.8705	3.6962	4.3601	4.3763	4.9507	4.9507	5.4304	5.4304	5.9151	5.9314
	(30×30), 2	8649	1.7161	2.8601	2.8601	3.6856	4.3301	4.3461	4.9283	4.9283	5.4263	5.4263	5.9075	5.9102
	(40×40), 2	15129	1.7148	2.8564	2.8564	3.6819	4.3196	4.3355	4.9204	4.9204	5.4248	5.4248	5.9024	5.9048
	(50×50), 2	23409	1.7142	2.8546	2.8546	3.6801	4.3147	4.3306	4.9167	4.9167	5.4241	5.4241	5.8941	5.8941
	(60×60), 2	33489	1.7139	2.8537	2.8537	3.6791	4.3120	4.3279	4.9147	4.9147	5.4237	5.4237	5.8882	5.8882
	(60×60), 3	44652	0.3006	0.4761	0.4761	0.6036	0.6782	0.6783	0.7737	0.7737	0.8903	0.8903	0.9133	0.9658
	(60×60), 4	55815	0.2990	0.4732	0.4732	0.5995	0.6733	0.6734	0.7676	0.7676	0.8825	0.8825	0.9050	0.9566
	(60×60), 5	66978	0.2987	0.4726	0.4726	0.5988	0.6725	0.6725	0.7666	0.7666	0.8813	0.8813	0.9038	0.9553
	(60×60), 6	78141	0.2986	0.4725	0.4725	0.5987	0.6723	0.6724	0.7664	0.7664	0.8811	0.8811	0.9036	0.9551
	(60×60), 7	89304	0.2847	0.4505	0.4505	0.5706	0.6407	0.6407	0.7302	0.7302	0.8393	0.8393	0.8606	0.9096
LD	(10×10), 1	2178	0.2675	0.4269	0.4269	0.5368	0.6211	0.6211	0.6944	0.6944	0.8117	0.8416	0.8416	0.8890
	(20×20), 1	7938	0.2672	0.4238	0.4238	0.5361	0.6060	0.6060	0.6881	0.6881	0.8006	0.8006	0.8101	0.8631
	(30×30), 1	17298	0.2671	0.4232	0.4232	0.5359	0.6032	0.6033	0.6867	0.6867	0.7933	0.7933	0.8094	0.8582
	(40×40), 1	30258	0.2671	0.4229	0.4229	0.5357	0.6022	0.6023	0.6862	0.6862	0.7907	0.7907	0.8091	0.8565
	(50×50), 1	46818	0.2670	0.4228	0.4228	0.5357	0.6018	0.6018	0.6860	0.6860	0.7895	0.7895	0.8089	0.8556
	(60×60), 1	66978	0.2670	0.4227	0.4227	0.5356	0.6015	0.6015	0.6858	0.6858	0.7888	0.7888	0.8088	0.8552
	(60×60), 2	122793	0.2657	0.4203	0.4203	0.5321	0.5972	0.5972	0.6804	0.6804	0.7818	0.7818	0.8014	0.8470
	(60×60), 3	178608	0.2656	0.4202	0.4202	0.5320	0.5971	0.5972	0.6803	0.6803	0.7817	0.7817	0.8013	0.8468
	(60×60), 4	234423	0.2656	0.4202	0.4202	0.5320	0.5971	0.5971	0.6803	0.6803	0.7816	0.7816	0.8012	0.8468

Table D.33: Convergence of the frequency parameters λ for modes 13-24 of CCCC square composite plate with $\frac{t}{b} = 0.1$, $\frac{t_c}{t_f} = 50$ and stack sequence $0°/90°/\text{core}/0°/90°$. Material 4 and 5 are used for faces and core respectively.

			mode number											
theory	$(n_x \times n_y)$, N	n_{dof}	13	14	15	16	17	18	19	20	21	22	23	24
ED	(10×10), 2	1089	5.9544	6.0026	6.0237	6.3148	6.3199	6.3266	6.3412	6.3626	6.3626	6.4356	6.6911	6.6993
	(20×20), 2	3969	5.9960	5.9960	6.2864	6.4210	6.4290	6.6302	7.0833	7.0833	7.1840	7.1840	7.2090	7.2090
	(30×30), 2	8649	5.9286	5.9286	6.2795	6.3689	6.3768	6.6901	7.0641	7.0641	7.1476	7.1476	7.5663	7.5706
	(40×40), 2	15129	5.9050	5.9050	6.2770	6.3505	6.3584	6.7113	7.0573	7.0573	7.1344	7.1344	7.5220	7.5263
	(50×50), 2	23409	5.8988	5.9036	6.2758	6.3420	6.3498	6.7211	7.0542	7.0542	7.1281	7.1281	7.5016	7.5059
	(60×60), 2	33489	5.8968	5.9029	6.2751	6.3373	6.3452	6.7265	7.0524	7.0524	7.1247	7.1247	7.4905	7.4948
	(60×60), 3	44652	0.9658	1.0818	1.0818	1.1098	1.1098	1.1719	1.1719	1.2285	1.2702	1.2702	1.3359	1.3359
	(60×60), 4	55815	0.9566	1.0703	1.0703	1.0978	1.0978	1.1585	1.1585	1.2136	1.2543	1.2543	1.3185	1.3185
	(60×60), 5	66978	0.9554	1.0688	1.0688	1.0963	1.0963	1.1569	1.1569	1.2119	1.2525	1.2525	1.3166	1.3166
	(60×60), 6	78141	0.9551	1.0685	1.0685	1.0960	1.0960	1.1566	1.1566	1.2116	1.2521	1.2522	1.3162	1.3162
	(60×60), 7	89304	0.9097	1.0173	1.0173	1.0436	1.0436	1.1011	1.1011	1.1531	1.1917	1.1917	1.2528	1.2528
LD	(10×10), 1	2178	0.8891	0.9700	0.9700	1.0876	1.0990	1.0991	1.1264	1.1264	1.1749	1.1753	1.2508	1.2508
	(20×20), 1	7938	0.8631	0.9611	0.9611	1.0070	1.0070	1.0558	1.0558	1.0886	1.1349	1.1349	1.2266	1.2266
	(30×30), 1	17298	0.8582	0.9587	0.9587	0.9914	0.9914	1.0438	1.0438	1.0870	1.1272	1.1272	1.1977	1.1977
	(40×40), 1	30258	0.8565	0.9577	0.9577	0.9860	0.9860	1.0395	1.0395	1.0862	1.1244	1.1244	1.1878	1.1878
	(50×50), 1	46818	0.8556	0.9572	0.9572	0.9835	0.9835	1.0375	1.0375	1.0858	1.1231	1.1231	1.1832	1.1832
	(60×60), 1	66978	0.8552	0.9569	0.9569	0.9821	0.9821	1.0364	1.0364	1.0855	1.1223	1.1223	1.1807	1.1807
	(60×60), 2	122793	0.8470	0.9467	0.9467	0.9714	0.9714	1.0245	1.0245	1.0722	1.1081	1.1081	1.1652	1.1652
	(60×60), 3	178608	0.8468	0.9465	0.9465	0.9712	0.9712	1.0243	1.0243	1.0719	1.1078	1.1079	1.1649	1.1649
	(60×60), 4	234423	0.8468	0.9464	0.9464	0.9711	0.9711	1.0242	1.0242	1.0719	1.1077	1.1078	1.1648	1.1648

Table D.34: Convergence of the frequency parameters λ for modes 25-36 of CCCC square composite plate with $\frac{t}{b} = 0.1$, $\frac{t_c}{t_f} = 50$ and stack sequence $0°/90°/\text{core}/0°/90°$. Material 4 and 5 are used for faces and core respectively.

			mode number											
theory	$(n_x \times n_y)$, N	n_{dof}	25	26	27	28	29	30	31	32	33	34	35	36
ED	(10×10), 2	1089	6.7999	6.7999	7.1295	7.1787	7.1787	7.2720	7.3346	7.3346	7.3602	7.3602	7.3826	7.3826
	(20×20), 2	3969	7.2316	7.2316	7.2684	7.2684	7.3187	7.3187	7.3821	7.3821	7.4589	7.4590	7.5502	7.5502
	(30×30), 2	8649	7.9156	7.9156	8.1820	8.2324	8.2723	8.5340	8.5375	8.6708	8.6708	8.6957	8.6957	8.7368
	(40×40), 2	15129	7.8789	7.8789	8.1697	8.2163	8.2564	8.5073	8.5107	9.1479	9.1479	9.3771	9.3771	9.4362
	(50×50), 2	23409	7.8619	7.8619	8.1638	8.2089	8.2491	8.4947	8.4982	9.1137	9.1137	9.3682	9.3682	9.4064
	(60×60), 2	33489	7.8526	7.8526	8.1606	8.2048	8.2451	8.4879	8.4914	9.0951	9.0951	9.3632	9.3632	9.3903
	(60×60), 3	44652	1.3887	1.3887	1.3986	1.3986	1.4737	1.4737	1.5516	1.5691	1.5691	1.5870	1.5870	1.6150
	(60×60), 4	55815	1.3697	1.3698	1.3791	1.3791	1.4521	1.4521	1.5274	1.5451	1.5451	1.5618	1.5619	1.5894
	(60×60), 5	66978	1.3677	1.3677	1.3771	1.3771	1.4499	1.4499	1.5250	1.5426	1.5426	1.5593	1.5594	1.5868
	(60×60), 6	78141	1.3673	1.3673	1.3767	1.3767	1.4495	1.4495	1.5246	1.5421	1.5421	1.5588	1.5589	1.5863
	(60×60), 7	89304	1.3012	1.3012	1.3096	1.3096	1.3789	1.3789	1.4497	1.4672	1.4672	1.4823	1.4823	1.5089
LD	(10×10), 1	2178	1.3646	1.4107	1.4107	1.4221	1.4224	1.4437	1.4437	1.4788	1.4811	1.5413	1.5413	1.6559
	(20×20), 1	7938	1.2416	1.2416	1.2654	1.2654	1.3296	1.3296	1.3740	1.4183	1.4183	1.4628	1.4628	1.4938
	(30×30), 1	17298	1.2374	1.2374	1.2410	1.2410	1.3114	1.3114	1.3706	1.4064	1.4065	1.4134	1.4134	1.4500
	(40×40), 1	30258	1.2327	1.2327	1.2357	1.2357	1.3051	1.3051	1.3690	1.3968	1.3968	1.4021	1.4021	1.4352
	(50×50), 1	46818	1.2288	1.2288	1.2348	1.2348	1.3021	1.3021	1.3681	1.3892	1.3892	1.4000	1.4000	1.4284
	(60×60), 1	66978	1.2266	1.2266	1.2343	1.2343	1.3005	1.3005	1.3676	1.3851	1.3851	1.3989	1.3989	1.4247
	(60×60), 2	122793	1.2098	1.2098	1.2169	1.2169	1.2812	1.2812	1.3459	1.3637	1.3637	1.3762	1.3763	1.4019
	(60×60), 3	178608	1.2093	1.2093	1.2165	1.2165	1.2808	1.2808	1.3454	1.3632	1.3632	1.3755	1.3756	1.4013
	(60×60), 4	234423	1.2093	1.2093	1.2164	1.2164	1.2807	1.2807	1.3453	1.3630	1.3630	1.3755	1.3756	1.4012

Table D.35: Convergence of the frequency parameters λ for the first 10 modes of a SSSS square laminated plate in OC configuration with $\frac{t}{b} = 0.02$ ($\frac{t_m}{t} = \frac{11}{45}$, $\frac{t_p}{t} = \frac{2}{15}$) and stacking sequence PZT-4/0°/90°/0°/PZT-4. Material 2 is used.

			mode number									
theory	$(n_x \times n_y)$, N	n_{dof}	1	2	3	4	5	6	7	8	9	10
ED	(10×10), 2	2178	249.8234	587.6812	733.9164	1026.2299	1233.4125	1622.0382	1628.4465	1886.6525	2291.7155	2412.0327
	(20×20), 2	7938	247.6534	569.3481	709.2811	991.1413	1135.6307	1498.7293	1518.3593	1754.1383	1955.3309	2231.7959
	(30×30), 2	17298	247.2547	566.0729	704.8763	984.8435	1119.0054	1476.5650	1500.4837	1731.3244	1901.8979	2200.5886
	(40×40), 2	30258	247.1154	564.9351	703.3458	982.6537	1113.2879	1468.9351	1494.3181	1723.4585	1883.7683	2189.8177
	(50×50), 2	46818	247.0510	564.4100	702.6394	981.6426	1110.6590	1465.4256	1491.4800	1719.8383	1875.4744	2184.8587
	(60×60), 2	66978	247.0160	564.1251	702.2562	981.0940	1109.2356	1463.5250	1489.9425	1717.8772	1870.9947	2182.1718
	(30×30), 3	26908	246.4327	562.7952	696.3089	972.0996	1106.9028	1437.5473	1476.1638	1685.4886	1867.8400	2139.2431
	(30×30), 4	34596	246.3982	562.7665	696.1291	971.9387	1106.8626	1437.0805	1476.0010	1685.0380	1867.7622	2138.7915
LD	(10×10), 1	2904	249.1560	584.1443	724.0922	1010.9604	1215.6781	1576.3503	1587.7951	1824.1113	2225.7965	2321.9932
	(20×20), 1	10584	247.0111	566.1745	700.3596	977.5683	1121.6448	1456.3968	1490.4677	1703.7313	1912.0941	2161.8507
	(30×30), 1	23064	246.6170	562.9616	696.1102	971.5580	1105.6018	1435.7740	1473.5896	1682.8223	1861.7239	2133.7076
	(40×40), 1	40344	246.4793	561.8453	694.6333	969.4669	1100.0810	1428.6664	1467.7618	1675.6011	1844.6016	2123.9680
	(50×50), 1	62424	246.4156	561.3300	693.9515	968.5012	1097.5419	1425.3957	1465.0781	1672.2756	1836.7632	2119.4793
	(60×60), 1	89304	246.3810	561.0505	693.5816	967.9772	1096.1669	1423.6240	1463.6239	1670.4736	1832.5281	2117.0462
	(30×30), 2	42284	246.2520	561.9550	695.1006	969.9622	1103.5655	1433.0408	1470.9969	1679.6405	1858.3014	2129.7030
	(30×30), 3	61504	246.2515	561.9515	695.0954	969.9560	1103.5472	1433.0145	1470.9795	1679.6157	1858.2434	2129.6729

Table D.36: Convergence of the frequency parameters λ for the first 10 modes of a SSSS square laminated plate in SC configuration with $\frac{t}{b} = 0.02$ ($\frac{t_m}{t} = \frac{11}{45}$, $\frac{t_p}{t} = \frac{2}{15}$) and stacking sequence PZT-4/0°/90°/0°/PZT-4. Material 2 is used.

			mode number									
theory	$(n_x \times n_y)$, N	n_{dof}	1	2	3	4	5	6	7	8	9	10
ED	(10×10), 2	2178	249.6910	586.9856	732.5894	1023.8809	1230.2645	1616.2488	1621.4544	1877.7914	2280.3254	2397.8324
	(20×20), 2	7938	247.5252	568.7181	708.0802	989.0838	1133.1341	1493.1213	1513.7825	1747.1660	1947.9200	2221.3193
	(30×30), 2	17298	247.1273	565.4541	703.6969	982.8347	1116.6093	1471.1732	1496.0929	1724.6430	1895.0153	2190.6561
	(40×40), 2	30258	246.9883	564.3202	702.1739	980.6615	1110.9257	1463.6163	1489.9900	1716.8752	1877.0589	2180.0668
	(50×50), 2	46818	246.9240	563.7969	701.4709	979.6581	1108.3123	1460.1402	1487.1805	1713.2997	1868.8433	2175.1904
	(60×60), 2	66978	246.8891	563.5130	701.0895	979.1137	1106.8972	1458.2576	1485.6584	1711.3628	1864.4056	2172.5480
	(30×30), 3	26908	246.4286	562.7573	696.2950	972.0351	1106.7391	1437.5053	1475.9428	1685.3725	1867.3590	2138.9293
	(30×30), 4	34596	246.3942	562.7290	696.1157	971.8756	1106.7001	1437.0406	1475.7832	1684.9258	1867.2850	2138.4852
LD	(10×10), 1	2904	249.1550	584.1367	724.0862	1010.9424	1215.6411	1576.3238	1587.7363	1824.0624	2225.6553	2321.8825
	(20×20), 1	10584	247.0102	566.1678	700.3544	977.5530	1121.6175	1456.3770	1490.4242	1703.6947	1912.0125	2161.7743
	(30×30), 1	23064	246.6161	562.9551	696.1051	971.5431	1105.5759	1435.7552	1473.5484	1682.7875	1861.6497	2133.6360
	(40×40), 1	40344	246.4784	561.8389	694.6282	969.4522	1100.0555	1428.6479	1467.7213	1675.5670	1844.5298	2123.8981
	(50×50), 1	62424	246.4147	561.3236	693.9465	968.4866	1097.5166	1425.3774	1465.0380	1672.2417	1836.6926	2119.4101
	(60×60), 1	89304	246.3801	561.0441	693.5766	967.9627	1096.1418	1423.6058	1463.5840	1670.4398	1832.4580	2116.9773
	(30×30), 2	42284	246.2511	561.9490	695.0959	969.9486	1103.5416	1433.0236	1470.9589	1679.6086	1858.2332	2129.6373
	(30×30), 3	61504	246.2507	561.9455	695.0907	969.9423	1103.5233	1432.9972	1470.9415	1679.5838	1858.1752	2129.6072

Bibliography

[1] *PETSc Users Manual - Revision 3.1.*

[2] *SLEPc Users Manual: Scalable Library for Eigenvalue Problem Computations.*

[3] *SPARSKIT: a basic tool kit for sparse matrix computations.*

[4] N. Atalla and R.J. Bernhard. Review of numerical solutions for low-frequency structural-acoustic problems. *Applied Acoustics*, 43(3):271 – 294, 1994. Structural Acoustics and Vibrations.

[5] Klaus-Jurgen Bathe. *Finite Element Procedures.* Prentice Hall, 6$^{\text{th}}$ edition, 1996.

[6] R.E. Bellman and J. Casti. Differential quadrature and long-term integration. *Journal of Mathematical Analysis and Applications*, 34:235–238, 1971.

[7] A. Benjeddou. Advances in piezoelectric finite element modeling of adaptive structural elements: a survey. *Computers and Structures*, 76(1-3):347 – 363, 2000.

[8] A. Benjeddou, J. F. De, and S. Letombe. Free vibrations of simply-supported piezoelectric adaptive plates: an exact sandwich formulation. *Thin-Walled Structures*, 40(7-8):573 – 593, 2002.

[9] R. J. Bernhard and Jr. J. E. Huff. Structural-acoustic design at high frequency using the energy finite element method. *Journal of Vibration and Acoustics*, 121(3):295–301, 1999.

[10] S. Brischetto and E. Carrera. Importance of higher order modes and refined theories in free vibration analysis of composite plates. *Journal of Applied Mechanics*, 77(1):011013, 2010.

[11] S. Brischetto, E. Carrera, and L. Demasi. Improved response of unsymmetrically laminated sandwich plates by using zig-zag functions. *Journal of Sandwich Structures and Materials*, 11(2-3):257–267, March/May 2009.

[12] L. Brusa, R. Ciacci, and A. Greco. Vibration analysis of coupled fluid-structure systems: A convenient computational approach. *Nuclear Engineering and Design*, 70(1):101 – 106, 1982.

[13] E. Carrera. Multilayered shell theories that account for a layer-wise mixed description. part i. governing equations. *AIAA Journal*, 37:69–78, 1999.

[14] E. Carrera. Multilayered shell theories that account for a layer-wise mixed description. part i. numerical evaluations. *AIAA Journal*, 37:1117–1124, 1999.

[15] E. Carrera. A reissner's mixed variational theorem applied to vibration analysis of multilayered shell. *Journal of Applied Mechanics*, 66(1):69–78, 1999.

[16] E. Carrera. A study of transverse normal stress effect on vibration of multilayered plates and shell. *Journal of Sound and Vibration*, 225(5):803 – 829, 1999.

[17] E. Carrera. Transverse normal stress effects in multilayered plates. *Journal of Applied Mechanics*, 66:1004–1012, 1999.

[18] E. Carrera. Single-layer vs multi-layers plate modelings on the basis of reissner's mixed theorem. *AIAA Journal*, 38:342–352, 2000.

[19] Erasmo Carrera. c_z^0 requirements–models for the two dimensional analysis of multilayered structures. *Composite Structures*, 37(3-4):373 – 383, 1997.

[20] Erasmo Carrera. Developments, ideas, and evaluations based upon reissner's mixed variational theorem in the modeling of multilayered plates and shells. *Applied Mechanics Reviews*, 54(4):301–329, 2001.

[21] Erasmo Carrera and Salvatore Brischetto. Analysis of thickness locking in classical, refined and mixed multilayered plate theories. *Composite Structures*, 82(4):549 – 562, 2008.

[22] Filippo Casadei, Lorenzo Dozio, Massimo Ruzzene, and Kenneth A. Cunefare. Periodic shunted arrays for the control of noise radiation in an enclosure. *Journal of Sound and Vibration*, 329(18):3632 – 3646, 2010.

[23] W. Q. Chen and C. F. Lu. 3d free vibration analysis of cross-ply laminated plates with one pair of opposite edges simply supported. *Composite Structures*, 69(1):77 – 87, 2005.

[24] L. Demasi. An invariant finite element model for composite structures: the generalized unified formulation. *AIAA Journal*, 18(8):1602–1619, 2010.

[25] W. Desmet. Mid-frequency vibro-acoustic modelling: Challenges and potential solutions. pages 835–862, 2002. cited By (since 1996) 7.

[26] Wim Desmet. *A wave based prediction technique for coupled vibro-acoustic analysis*. PhD thesis, Katholieke Universiteit Leuven, 1995.

[27] J.-F. De, W. Larbi, and R. Ohayon. Piezoelectric structural acoustic problems: Symmetric variational formulations and finite element results. *Computer Methods in Applied Mechanics and Engineering*, 197(19-20):1715 – 1724, 2008. Computational Methods in Fluid-Structure Interaction.

[28] Carrera E. A class of two-dimensional theories for anisotropic multilayered plates analysis. *ATTI DELLA ACCADEMIA DELLE SCIENZE DI TORINO. CLASSE DI SCIENZE FISICHE MATEMATICHE E NATURALI*, 19-20:1–39, 1995.

[29] Demasi L. E. Carrera. Two benchmarks to assess two-dimensional theories of sandwich, composite plates. *AIAA Journal*, 41:1356–362, 2003.

[30] P. Nali E. Carrera, S. Brischetto. Variational statements and computational models for multifield problems and multilayered structures. *Mechanics of Advanced Materials and Structures*, 15(3):182 – 198, 2008.

[31] P. Gardonio F. Fahy. *Sound and structural vibration: radiation, transmission and response*. Elsevier, 2nd edition, 2007.

[32] Jos Caas F. Pars. *Boundary element method: fundamentals and applications*. Oxford University Press, 1997.

[33] C.A. Felippa and R. Ohayon. Mixed variational formulation of finite element analysis of acoustoelastic/slosh fluid-structure interaction. *Journal of Fluids and Structures*, 4(1):35 – 57, 1990.

[34] Bert Van Genechten, Dirk Vandepitte, and Wim Desmet. A direct hybrid finite element - wave based modelling technique for efficient coupled vibro-acoustic analysis. *Computer Methods in Applied Mechanics and Engineering*, In Press, Accepted Manuscript:–, 2010.

[35] Paul Heyliger and D. A. Saravanos. Exact free-vibration analysis of laminated plates with embedded piezoelectric layers. *The Journal of the Acoustical Society of America*, 98(3):1547–1557, 1995.

[36] Fredrik Holmstrom. Structure-acoustic analysis usinf fem/bem; implementation in matlab. Master's thesis, Lund University, 2001.

[37] Takuro Ikeda. *Fundamental of piezoelectricity*. Oxford Science Publications, 1996.

[38] T. Kant and K. Swaminathan. Estimation of transverse/interlaminar stresses in laminated composites - a selective review and survey of current developments. *Composite Structures*, 49(1):65 – 75, 2000.

[39] S. M. Kim and M. J. Brennan. A compact matrix formulation using the impedance and mobility approach for the analysis of structural-acoustic systems. *Journal of Sound and Vibration*, 223(1):97 – 113, 1999.

[40] W. T. Koiter. A consistent first approximation in the general theory of elastic shells. In *Proceedings of Symposium on the Theory of Thin Elastic Shell*, number 12-23, 1959.

[41] A.W. Leissa. The historical bases of the rayleigh and ritz methods. *Journal of Sound and Vibration*, 287(4-5):961 – 978, 2005.

[42] K. M. Liew, T. Y. Ng, and Jordan Z. Zhang. Differential quadrature-layerwise modeling technique for three-dimensional analysis of cross-ply laminated plates of various edge-supports. *Computer Methods in Applied Mechanics and Engineering*, 191(35):3811 – 3832, 2002.

[43] K. M. Liew and T. M. Teo. Modeling via differential quadrature method: Three-dimensional solutions for rectangular plates. *Computer Methods in Applied Mechanics and Engineering*, 159(3-4):369 – 381, 1998.

[44] K.M. Liew, K.C. Hung, and M.K. Lim. A continuum three-dimensional vibration analysis of thick rectangular plates. *International Journal of Solids and Structures*, 30(24):3357 – 3379, 1993.

[45] James Lighthill. *Waves in fluids*. Cambridge University Press, 1978.

[46] Marcus Wagner Lothar Gaul, Martin Kgl. *Boundary element methods for engineers and scientists: an introductory course with advance topics*. Springer, 2003.

[47] R. H. Lyon and R. G. Dejong. *Theory and application of Statistical Energy Analysis*. Butterworth-Heineman, 1995.

[48] C.F. L, W.Q. Chen, and J.W. Shao. Semi-analytical three-dimensional elasticity solutions for generally laminated composite plates. *European Journal of Mechanics - A/Solids*, 27(5):899 – 917, 2008.

[49] Zhen-Dong Ma and Ichiro Hagiwara. Development of a new mode-superposition technique for modal frequency response analysis of coupled acoustic-structural systems. *Finite Elements in Analysis and Design*, 14(2-3):209 – 223, 1993. Special Issue Optimum Design in Japan.

[50] S. Marburg and B. Nolte. *Computational Acoustics of Noise Propagation in Fluids Finite and Boundary Element Methods*, chapter 9. Springer, 2008.

[51] Raville ME. Determination of natural frequencies of vibration of a sandwich plate. *Exp Mech*, 1967.

[52] A.K. Noor and W.S. Burton. Assessment of shear deformation theories for multilayered composite plates. *Appl Mech Rev*, 42(1):1 13, 1989.

[53] R. L. Taylor O. C. Zienkiewicz. *The Finite Element Method*. Elsevier, 6^{th} edition, 2005.

[54] N.J. Pagano. Exact solutions for rectangular bidirectional composites and sandwich plates. *Journal of Composite Materials*, 4(1):20–34, 1970.

[55] Jie Pan and David Alan Bies. The effect of fluid–structural coupling on sound waves in an enclosure—experimental part. *The Journal of the Acoustical Society of America*, 87(2):708–717, 1990.

[56] Jie Pan and David Alan Bies. The effect of fluid–structural coupling on sound waves in an enclosure—theoretical part. *The Journal of the Acoustical Society of America*, 87(2):691–707, 1990.

[57] Allan D. Pierce. *Acoustics: an introduction to its physical principles and applications*. Acoustical Society of America, 1991.

[58] R. Srinivasan Puri. *Krylov subspace based direct projection techniques for low frequency, fully Coupled, structural acoustic analysis and optimization*. PhD thesis, Oxford Brookes University, 2008.

[59] H. J-P Morand R. Ohayon. *Fluid Structure Interaction: applied numerical methods*. Wiley, 1995.

[60] M. K. Rao and Y. M. Desai. Analytical solutions for vibrations of laminated and sandwich plates using mixed theory. *Composite Structures*, 63(3-4):361 – 373, 2004.

[61] J. N. Reddy. A simple higher-order theory for laminated composite plates. *Journal of Applied Mechanics*, 51(4):745–752, 1984.

[62] J. N. Reddy. On refined computational models of composite laminates. *Int. J. Numer. Meth. Engng.*, 27(2):361 – 382, 1989.

[63] J.N. Reddy. *Mechanics of laminated composite plates and shell-theory and analysis*. CRC Press, 2004.

[64] E. Reissner. On a certain mixed variational theory and proposed applications. *International Journal of Numerical Methods in Engineering*, 20:1366 – 1368, 1984.

[65] E. Reissner. On a mixed variational theorem and on shear deformable plate theory. *International Journal of Numerical Methods in Engineering*, 23:193 – 198, 1986.

[66] P. Bremner R.S. Langley. A hybrid method for the vibration analysis of complex structural- acoustic systems. *Journal of the Acoustical Society of America*, 105(3):1657–1671, 1999. cited By (since 1996) 77.

[67] Y. Saad. *Numerical Methods for Large Eigenvalue Problems: Theory and Algorithms*. John Wiley and Sons, 1992.

[68] Gran Sandberg. A new strategy for solving fluid-structure problems. *International Journal for Numerical Methods in Engineering*, 38(3):357–370, 1995.

[69] Vijay K. Varadan Senthil V. Gopinathan, Vasundara V. Varadan. A review and critique of theories for piezoelectric laminates. *Smart Materials and Structures*, 9(1):24, 2000.

[70] Andrew J. Fleming S.O. Reza Moheimani. *Piezoelectric transducers for vibration control and damping*. Springer, 2006.

[71] S. Srinivas and A.K. Rao. Bending, vibration and buckling of simply supported thick orthotropic rectangular plates and laminates. *International Journal of Solids and Structures*, 6(11):1463 – 1481, 1970.

[72] S. Srinivas, C.V. Joga Rao, and A.K. Rao. An exact analysis for vibration of simply-supported homogeneous and laminated thick rectangular plates. *Journal of Sound and Vibration*, 12(2):187 – 199, 1970.

[73] Michel Tournour and Noureddine Atalla. Pseudostatic corrections for the forced vibroacoustic response of a structure-cavity system. *The Journal of the Acoustical Society of America*, 107(5):2379–2386, 2000.

[74] Tongan Wang, Vladimir Sokolinsky, Shankar Rajaram, and Steven R. Nutt. Consistent higher-order free vibration analysis of composite sandwich plates. *Composite Structures*, 82(4):609 – 621, 2008.

[75] Wu Zhen, Chen Wanji, and Ren Xiaohui. An accurate higher-order theory and c^0 finite element for free vibration analysis of laminated composite and sandwich plates. *Composite Structures*, 92(6):1299 – 1307, 2010.

[76] D. Zhou, Y. K. Cheung, F. T. K. Au, and S. H. Lo. Three-dimensional vibration analysis of thick rectangular plates using chebyshev polynomial and ritz method. *International Journal of Solids and Structures*, 39(26):6339 – 6353, 2002.